NASA CR-2001-210265

2001 RESEARCH REPORTS

NASA/ASEE SUMMER FACULTY FELLOWSHIP PROGRAM

JOHN F. KENNEDY SPACE CENTER
AND
UNIVERSITY OF CENTRAL FLORIDA

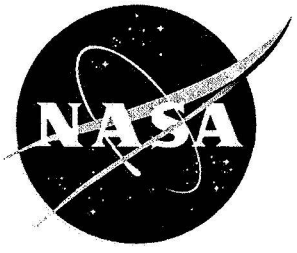

2001 RESEARCH REPORTS

NASA/ASEE SUMMER FACULTY FELLOWSHIP PROGRAM
JOHN F. KENNEDY SPACE CENTER
UNIVERSITY OF CENTRAL FLORIDA

EDITORS:

Dr. E. Ramon Hosler, University Program Director
Department of Mechanical, Materials and Aerospace Engineering
College of Engineering
University of Central Florida

Ms. Cassandra Black, NASA/KSC Program Director
University Programs Office
John F. Kennedy Space Center

NASA Grant No. NAG10-299

Contractor Report No. CR-2001-210265

October 2001

PREFACE

This document is a collection of technical reports on research conducted by the participants in the 2001 NASA/ASEE Summer Faculty Fellowship Program at the John F. Kennedy Space Center (KSC). This was the seventeenth year that a NASA/ASEE program has been conducted at KSC. The 2001 program was administered by the University of Central Florida (UCF) in cooperation with KSC. The program was operated under the auspices of the American Society for Engineering Education (ASEE) and the Education Division, NASA Headquarters, Washington, D.C. The KSC program was one of nine such Aeronautics and Space Research Programs funded by NASA Headquarters in 2001.

The basic common objectives of the NASA/ASEE Summer Faculty Fellowship Program are:

a. To further the professional knowledge of qualified engineering and science faculty members;
b. To stimulate an exchange of ideas between teaching participants and employees of NASA;
c. To enrich and refresh the research and teaching activities of participants institutions; and,
d. To contribute to the research objectives of the NASA center.

The KSC Faculty Fellows spent ten weeks (May 21 through July 27, 2001) working with NASA scientists and engineers on research of mutual interest to the university faculty member and the NASA colleague. The editors of this document were responsible for selecting appropriately qualified faculty to address some of the many research areas of current interest to NASA/KSC. A separate document reports on the administrative aspects of the 2001 program. The NASA/ASEE program is intended to be a two-year program to allow in-depth research by the university faculty member. In many cases a faculty member has developed a close working relationship with a particular NASA group that had provided funding beyond the two-year limit.

TABLE OF CONTENTS

2001 NASA/ASEE SUMMER FACULTY FELLOWSHIP PROGRAM

JOHN F. KENNEDY SPACE CENTER
UNIVERSITY OF CENTRAL FLORIDA

GUIDELINES FOR PROJECT MANAGEMENT

David Ben-Arieh
Associate Professor
Department of Industrial & Manufacturing Systems Engineering
Kansas State University

And
Kim Jenkins
Process Management Division

ABSTRACT

Project management is an important part of the professional activities at Kennedy Space Center (KSC). Project management is the means by which many of the operations at KSC take shape. Moreover, projects at KSC are implemented in a variety of ways in different organizations. The official guidelines for project management are provided by NASA headquarters and are quite general.

The project reported herein deals with developing practical and detailed project management guidelines in support of the project managers. This report summarizes the current project management effort in the Process Management Division and presents a new modeling approach of project management developed by the author. The report also presents the Project Management Guidelines developed during the summer.

GUIDELINES FOR PROJECT MANAGEMENT

David Ben-Arieh

1. Introduction

Kennedy Space Center has developed the mission of being the Spaceport Center of the nation. As such it is the recognized authority within NASA on Spaceport technologies, which include all the technologies required to prepare and launch space vehicles.

Many of the operations with a focus on Spaceport technologies are project oriented. These operations include developing the ground facilities and infrastructure, and maintaining, modifying, loading and launching the space vehicles. Many of these activities are project oriented in the sense that they are one-time improvement projects, consisting of many activities with a definite start time and due date, and a given budget.

Thus project management becomes a crucial skill in KSC professional activities, essential for on time and on budget delivery of quality projects.

Agency wide guidelines for project management are available in the form of a NASA Procedures and Guidelines (NPG) document developed at the headquarter level. As such it is a high level document covering the broad concept of project and program management within NASA. The document does not provide detailed, implementation-oriented guidelines that can assist the project managers in their task. Thus, this summer project intends to satisfy the need for detailed project management guidelines.

This report presents the current methodology developed in the Process Management Division and then present the author's approach towards modeling the project Management Process and the guidelines developed for that process.

2. Current Modeling Approach

The current modeling approach developed by Kim Jenkins represent the Project Management activities as a process. This process is defined and supported by several NASA documents including the following (the nature and types of NASA documentation is not discussed in this report):

KDP-KSC-P-2754
KDP-KSC-P-2600
KDP-KSC-P-2603
NPG 7120.5A
KDP-KSC-M-1000 (Business Management System Manual)
KSC-SMO Operational Plan (Draft)
KMI 8070.6 (KSC Technical Specs and Standards Manual).
Executive Order EO12862 (Setting Customer Service Standards)

An example for the modeling approach is presented in Figure 1 below. This Figure describes the process of Project Formulation as defined by NPG 7120.5.

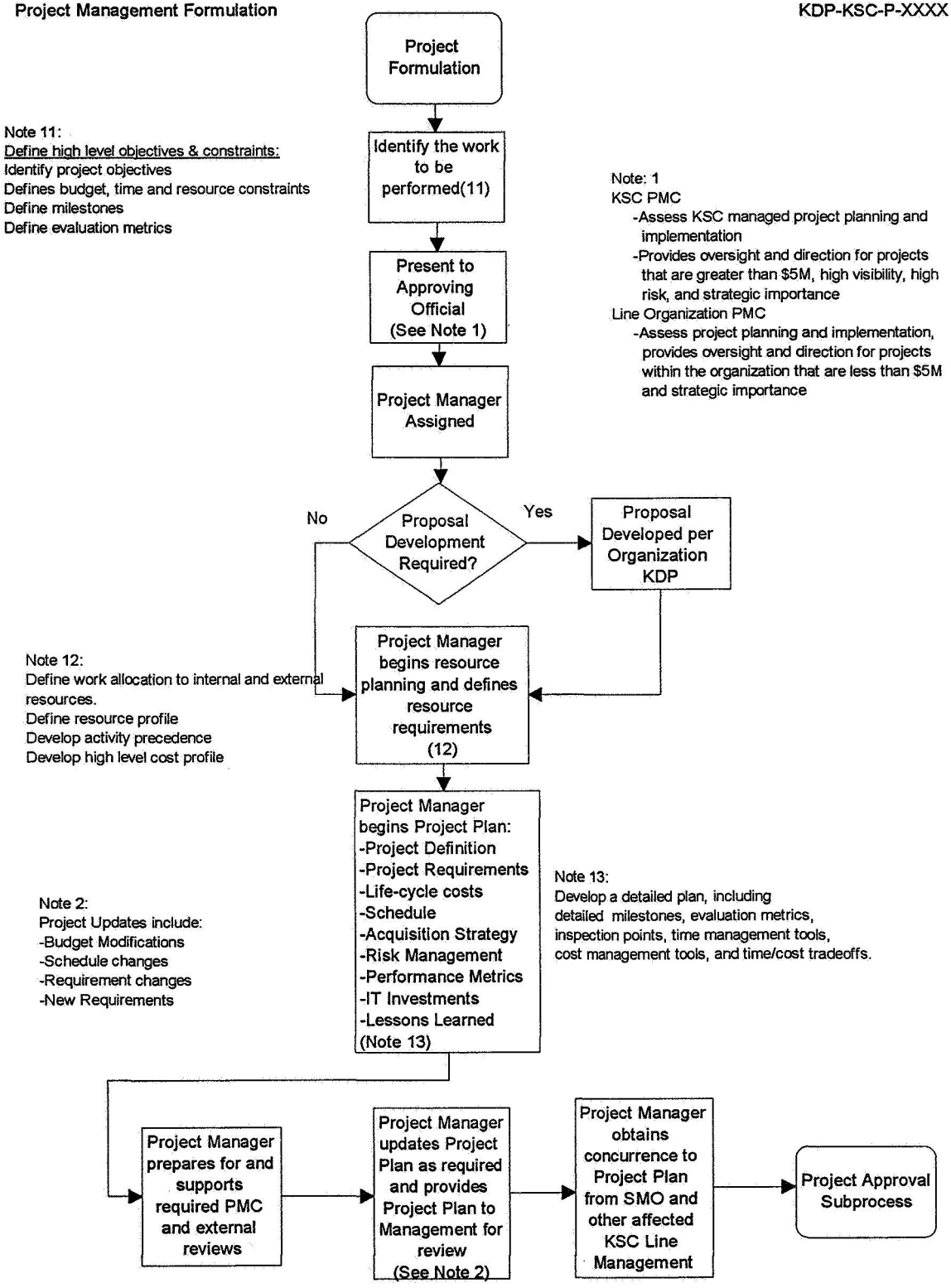

Figure 1: Process Flow Description of the Project Formulation Process

The analysis of the current modeling approach revealed some of its shortcomings in identifying the information required by each activity and the desired output of each such activity. In order to compensate for this handicap, the author with his KSC colleague developed an information based modeling approach for Project Management. This approach is demonstrated in Figure 2.

3. Project Management Guidelines

The next step of this project was to interview project managers within a variety of organizations at KSC, and to try and derive guidelines that are meaningful to the project managers. In order to define these guidelines, the following objectives were identifies:

1. Standardization of project planning and management.
   By standardization the organization can achieve a uniformly high level of performance, a known set of expectations from project leaders, and a known set of requirements from the support personnel (such as cost estimators, risk analyzers, and forecasters).

2. Capture knowledge from experience project managers.
   Some project managers have a vast intangible experience accumulated over many years of practice (with successes as well as failures). This valuable resource can be formulated into the Project Management Guidelines.

3. Provide assistance to project managers.
   Many times, project managers are being absorbed by the projects details and may be unable to remove themselves into an objective standpoint. The Project Management Guidelines will help all project managers with all levels of experience to exercise an impartial and professional management of the project. In addition, the guidelines will define a firm set of support activities and documentations that will be prepared by staff functions in support of the project manger.

4. Institutionalize best practices and affect agency culture.
   This last objective will help establish highly professional level of performance at NASA. Hopefully, this practice will penetrate all levels and functions of the organization and will improve the overall quality, accountability, and cost and risk management in all avenues of the organization.

The objectives of the Project Management Guidelines led to the development of guidelines for two processes: Project Preparation and Project Planning, but due to space limitations only the Preparation stage is presented in this report. The reader is reminded that the scope of Project Management is much broader, and additional guidelines need to be developed in order to cover the entire process completely. This additional work is planned for the future.

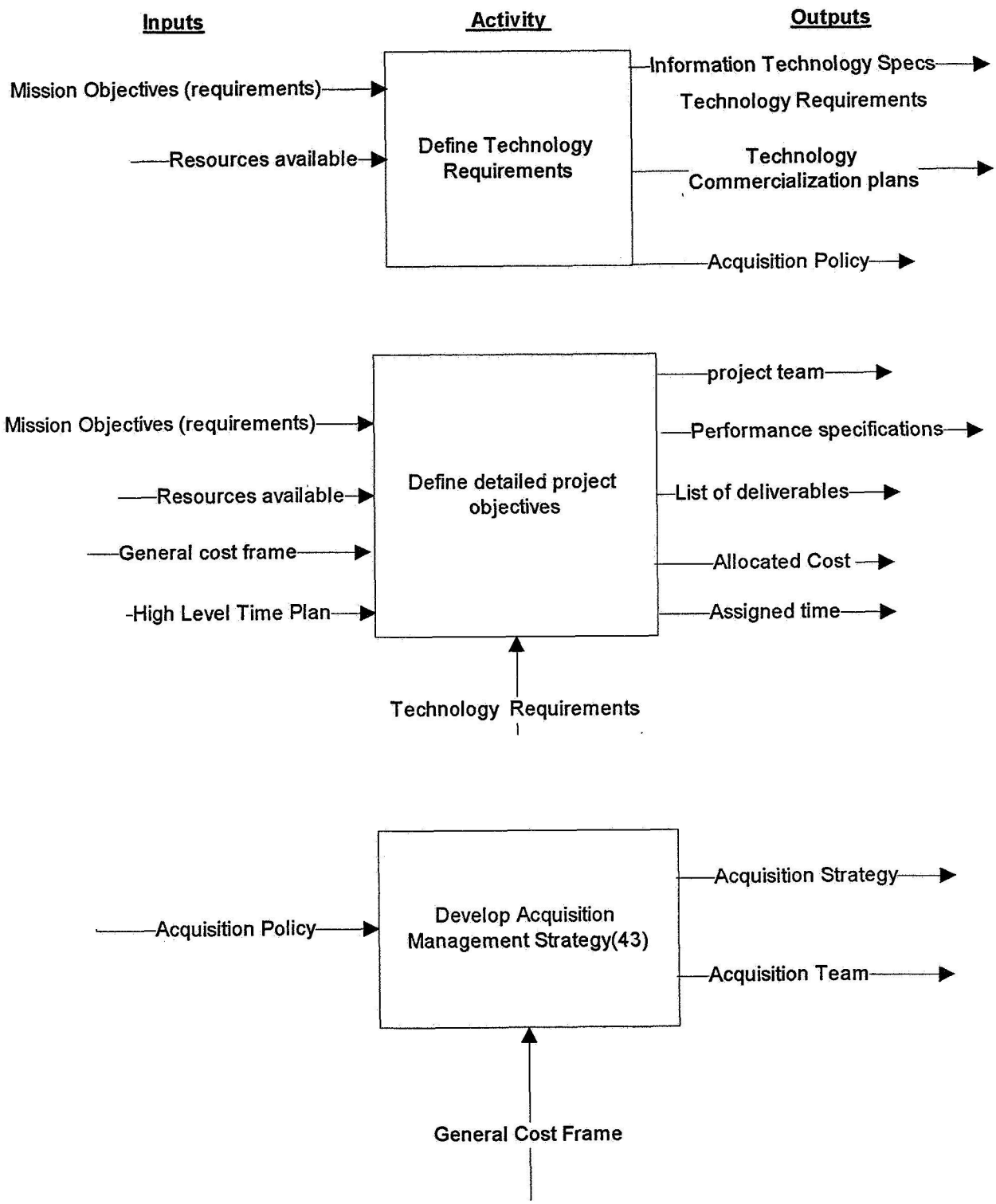

Figure 2: Information Flow Approach to Modeling Project Management

3.1 Guidelines for the Preparatory Stage (Part I of Formulation)

A. Defining Customer Requirements

1. Identify project motivation:
   - Market demand.
   - Business need.
   - Customer request.
   - Technological advance.
   - Legal requirement.
   - Social need. Etc.

2. Identify the customer:
   - The system operators.
   - Maintainers.
   - Sustainers, etc.
   - Resolve *permission* issues.

3. Develop a communication protocol with the customer.
   - Understand who the customer is (the organization, mission, etc.)
   - Develop vocabulary and common terms, units, and modeling approach (if any).

4. Understand the context of the implementation:
   - Define and describe the required behavior and performance.
   - Define the expected project life cycle: *planning, implementation, operation* and *disposal.*
   - Define the project release mode: *evolutionary, single delivery* or *incremental delivery.*
   - Identify and manage constraints and assumptions.
   - Identify interfaces with other (existing) systems.
   - Identify existing or planned support systems.
   - For service requirements develop a clear and concise definition.

5. Define high-level requirements and constraints:
   - Review related documentation.
   - Define *essential* and *desired* requirements.
   - Consider *Safety* and *Environmental* issues.
   - Prioritize the requirements.

   Methods:
   - Interview the customer.
   - Create a focus group consisting of customer representatives and project management reps.

Notes:
To minimize requirements changes:

- Document the reqs formally.
- Develop reqs accountability and traceability.
- Declare "Time Fences" with customer agreement.

6. Break down the requirements in hierarchical levels.
   - Allow traceability
   - Ensure consistency.
   - Allows complete change impact analysis

7. Define verification method for each requirement and for the entire project.
   - Interact with requirements when developing the verification methods. Saves time and cost.
   - Organize requirements by verification method. Ensure that all reqs are covered.
   - Communicate with the customer.

8. Develop evaluation criteria for each requirement.
   - Define the Go/No-Go properties.
   - Defined the desired properties in quantifiable terms (if possible) (this is termed "performance indicators" in 7120.5B (pg. 100)).
   - Define and communicate acceptable and unacceptable levels.

9. Develop Project Requirements Traceability and Accountability
   - Develop hierarchical breakdown of requirements (from high level to lower levels).
   - Develop a verification plan for these requirements.
   - Identify and manage TBD and TBR requirements.

10. Develop a Risk Philosophy that will drive the risk management.
    - Identify the risk sources.
    - Identify opportunities.

11. Develop Project Objectives Document/Agreement (aka "Statement of Work" in NASA) with the customer. Watch for:
    - Mixing tasks, specifications, approvals and special instructions.
    - Imprecise language.
    - No pattern, structure of chronological order.
    - Wide variation of tasks' sizes.
    - Wide variation in how-to description of tasks.
    - Impossible tasks.
    - Missing tasks.
    - Failure to get third party review of customer agreement.

- Client supplied information failure.

12. Develop a candidate physical or logical solution.

Notes:
Requirements mandatory characteristics:

- Needed.
- Verifiable.
- Attainable:
  - Technically.
  - Cost.
  - Schedule.

Other characteristics

- Improve communications:
  - One thought.
  - Concise.
  - Simple.
  - Stated positively.
  - Grammatically correct.
  - Unambiguous – can only be understood one way.

Requirements Should State

- What shall be done.
- Who is responsible: system, software, structure, etc.

All requirements should be accompanies by a rationale:

1. Why is the system needed.
2. What assumptions are made.
3. What design effort is driven by the requirements.
4. Other data that will be needed to maintain the requirement over time.

B. Define the organization that will implement the project

1 Choose among the following organization styles: pure support (functional) skill based organization, pure support – product based organization, pure project organization, conventional matrix organization, or compound matrix organization.

2 Identify the Management Team.

3 Identify support teams (risk, cost, technical assistance, etc.)

4 Identify all related offices.

5 Identify the main facilities that will be used for the project.

6 Search for partnerships or business opportunities. (7120.5B pg. 42).

C. Identify the project team

1. Define the project manager roles, responsibilities and authority.
2. Select and identify the project team – direct and support stuff.
3. Identify and manage the major interfaces and inter-relationships.
4. Develop a common code of conduct.
   4.1. Responsibilities, authorities, reporting, behavior, expectations, etc.
   4.2. Plan shared reward for project teams.

Tools:

- Task/Responsibility Matrix or Task-Responsibility Identification (cross of org. chart and WBS)
- Linear Responsibility Chart (Matrix of position/titles/people vs. activities – show degree of authority, responsibility, etc).

4. CONCLUSIONS

Project management is an essential part of NASA in general and KSC in particular. Currently, project managers get little assistance from agency documentation, and there are no center-wide recommended practices for project management. This project complemented the work performed in the Process Management Division and developed detailed guidelines for the project managers. The guidelines are accompanied by two main recommendations:

1. Modify the NPG 7120.5 recommendation regarding the structure of a project, and break a project life cycle into the following stages: Preparation, Planning, Approval and Implementation. Project "evaluation" should be exercised as project control activities concurrently with all these four stages.
2. Separate Project Management from Program Management as a distinct and different methodology (even though a program can be viewed as a collection of projects). Program Management should consist of a more strategic approach compared to Project Management that is more tactical in nature.

REFERENCES:

1. NASA's Project Management, March 26 –April 6, 2001, APPL course notes, Management Education Center, Wallops Flight Facility, Wallops Island VA.
2. NASA's Advanced Project Management, June 4-Jun 14, 2001, APPL course notes, Management Education Center, Wallops Flight Facility, Wallops Island VA.
3. *Visualizing Project Management, A Model for Business and technical Success*, 2cd Edition, by Forsberg K., Mooz, H., and Cotterman, H., John Wiley & Sons, 2000.

2001 NASA/ASEE Summer Faculty Fellowship Program
John F. Kennedy Space Center
University of Central Florida

Improved Quick Disconnect (QD) Interface Through Fail Safe Parts Identification

Evelyn Blanch-Payne, Ph. D., Associate Professor
Psychology Department
Oakwood College
7000 Adventist Blvd.
Huntsville, Al 35896

KSC Colleagues, Deborah Carstens, Ph.D. and Damon Stambolian
Spaceport Engineering & Technology Directorate/YA-D4

Improved Quick Disconnect (QD) Interface Through Fail Safe Parts Identification

Evelyn Blanch-Payne, Ph.D.

Abstract

An extensive review of existing Quick Disconnects (QDs) mating and demating operations was performed to determine which shuttle part interface identifications and procedures contribute to human factor errors. The research methods used consisted of interviews with engineers and technicians, examination of incident reports, critiques of video and audio tapes of QD operations, and attendance of a Hyper QD operational course. The data strongly suggests that there are inherit human factor errors involved in QD operations. To promote fail-safe operations, QD interface problem areas and recommendations were outlined and reviewed. It is suggested that dialogue, investigations and recommendations continue.

Introduction

Kennedy Space Center's Space Shuttle Program is engaged in a large scale effort to systematically analyze, understand and mitigate safety risks induced by human factor errors. The Industrial Engineering for Safety (IES) program is given the responsibility of designing safety upgrades as well as verifying the safety of large and complex systems. Historically, the focus on safety was primarily on improving flight safety by changing flight hardware. Currently, the focus is on reliability of flight hardware and the reduction of catastrophic failures due to flight hardware critical failure modes, accepted risk hazards, flight and ground safety risks caused by human error during processing, and handling and manufacturing of flight hardware.

The reliability and safety of flight systems is dependent upon human characteristics and the dynamic interactive factors involved in man-machine interface. The consequences of human errors are very diverse and can range from damage to equipment and property, injury to personnel, fatalities, and disruption of scheduled system operation. All represent a significant cost to the space program. To minimize human error, we must seek to reduce the frequency of occurrences and diminish the impact of such occurrences. To accomplish this, we can implement new and better measures to prevent repetitive occurrences.

The focus of this paper is on improved hardware interface with quick disconnects through fail-safe parts identification. The frequency and types of problems encountered with quick disconnect mismates will be provided. Finally, this paper will provide recommendations for the improvement and fail-safe of quick disconnects.

Background

Past experience revealed that the task of mating and demating quick disconnects (QD) resulted in incidents due to numerous human factor errors and the poor interconnection of environmental conditions (i.e., industrial design, workspace design, and display design). For example, there have been a number of occurrences in which technicians inadvertently mated ground half coupling (GHC) QDs to the wrong air half coupling (AHC). Furthermore, technicians are consistently required to perform a series of QD mates and demates involving similar nomenclature identification and have mentally transposed the system code and mismated the QD.

Apparently, there is a need to improve QD mate/demate operations under the current industrial designs. A major accident has not occurred, however, the potential does exist for both human injury and flight hardware damage to the Orbiter. Consequently, with the recent rise in the occurrence of incident rates, this research project focused on identifying the root causes of error in parts identification and providing recommendations for corrective action to resolve human factor errors.

This project involved an extensive review of existing QD operations as well as pre-existing problems that have been documented from 1995 to the present. For this reason, the following objectives were established to investigate QD mate/demate procedures and to evaluate current practices relating to Orbiter Maneuvering System Reaction Control System (OMS RCS) QD operations.

Study Objectives were to:

1) **Determine which shuttle processing interfaces QD can be improved by the fail-safe concept.**
2) **Provide recommendations on how to improve the QD interfaces. Recommendations will not violate policy and procedures regarding Safety, Environmental, Current Union Agreements, and NASA regulatory requirements. Recommendations will support existing shuttle processing contracts and guidelines established in support of Orbiter/GSE processing.**

This ten week effort concentrated solely on the above objectives, however, continual dialogue through investigations and recommendations will continue.

Methodology

The methodology used in this project included: an investigation of QD operational procedures, interviews with engineers and technicians, examination of incident reports, observation of video and audio tapes and attendance of a Hyper QD class. Each of these methods is presented in more detail in the following section. Given the limited time to accomplish the objectives of this project, the research techniques utilized were designed to obtain results in a timely manner.

Methods used to identify QD problem areas were:

1) **Interviews focusing on identifying recurring problems associated with QD mates. Questions were posed to technicians and engineers involved with QD operations at Kennedy Space Center, and the respondents included teams from NASA-KSC engineers and technicians, and USA Industrial Engineers and Human Factors personnel.**

Questions were designed to assess the impact of environmental factors on human factor error in part identification of QD mates during processing and maintenance of the Orbiter. Knowledge gained from such interviews was used to confirm and clarify data from the following sources.

1) **Incident reports (White Paper Reports) generated by USA ground operations safety reporting.**

2) **Documentation of PR and OASIS reports with close call consequence ratings for potential damage to major essential flight elements.**

3) **Video and audio taping of actual QD operations.**

4) **QD operations during the course LSC 590 Hyper QD installation.**

These research methods provided insight into incidents within QD operations. Problems and recommendations are categorized into the following areas:

1. **Industrial Design**
2. **Display Design**
3. **Task Design**
4. **Team Communication**
5. **Distractions**
6. **Cognitive Processing Errors**

Results

The primary findings from interviews and incident reports reveal that numerous errors are encountered with QD during operations. Interview data is summarized in the conclusions and recommendations section and is presented in the format of problems (P) and recommendations (R). Inspection of the data from incident reports dating from 1995 to 2001 supports the interview data that

human factor errors do occur while mating and demating QDs. The chart provides a summary of documented errors with the frequency and facility location.

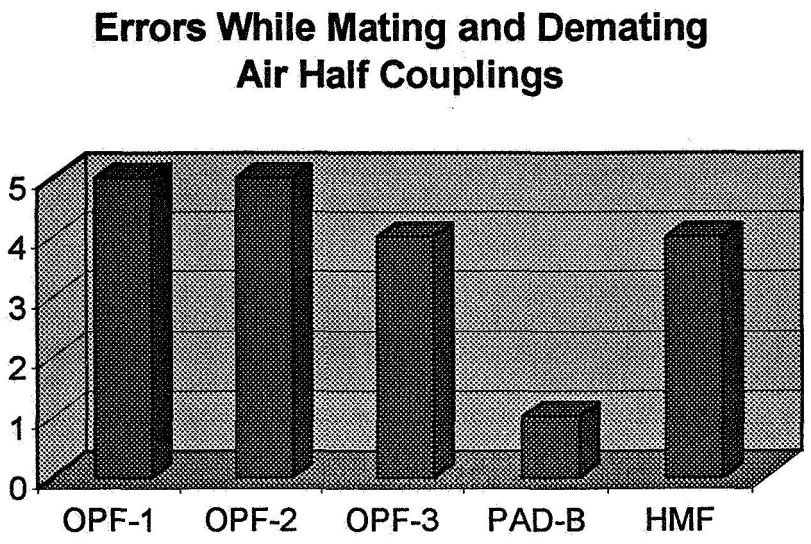

Conclusions and Recommendations

Summary of Human Factor Problems/Errors Contributing to QD Mismate Interface and Suggested Recommendations

P – problem
R – recommendation

- **Industrial Design**

Poor visual indicators and numerical markings

- **Although Rockwell documented in 1981 that the existing QD numbering system was easy to confuse, we are still experiencing the following problems associated with QD numbers:**

P – 1 Size of lettering in numbering system is too small.

R – 1 Numbers must be large enough and visually clear on door panels and QDs.

P – 2 Some numbers are erased or faint as a result of fuel leakage

R – 1 Improve the current maintenance program

P – 3 Engraved numbers are not visually clear on door panels and at times, depending on the set up, can be difficult to read.

R – 3 Collect data of each panel and analyze

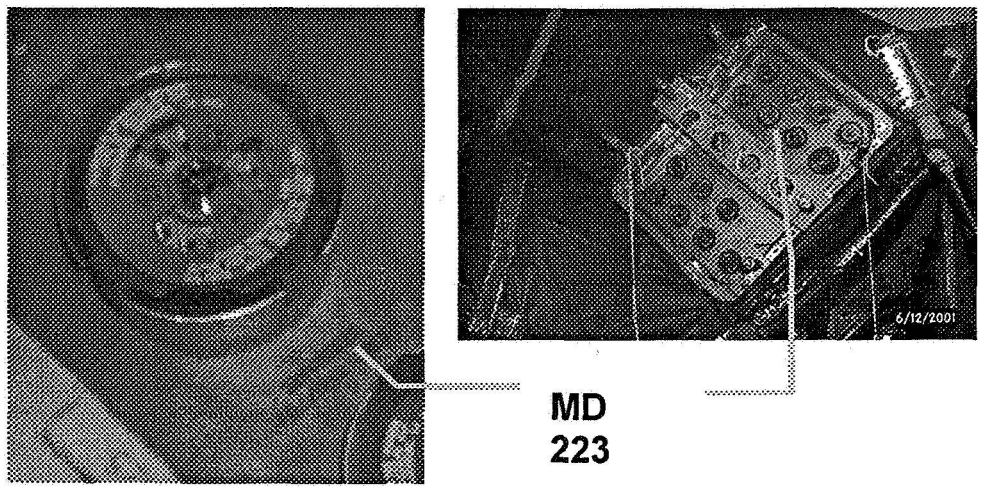

P – 4 Numbers are not consistently stationed at the same location (i.e., sometimes numbers are above the QD, sometimes below the QD).

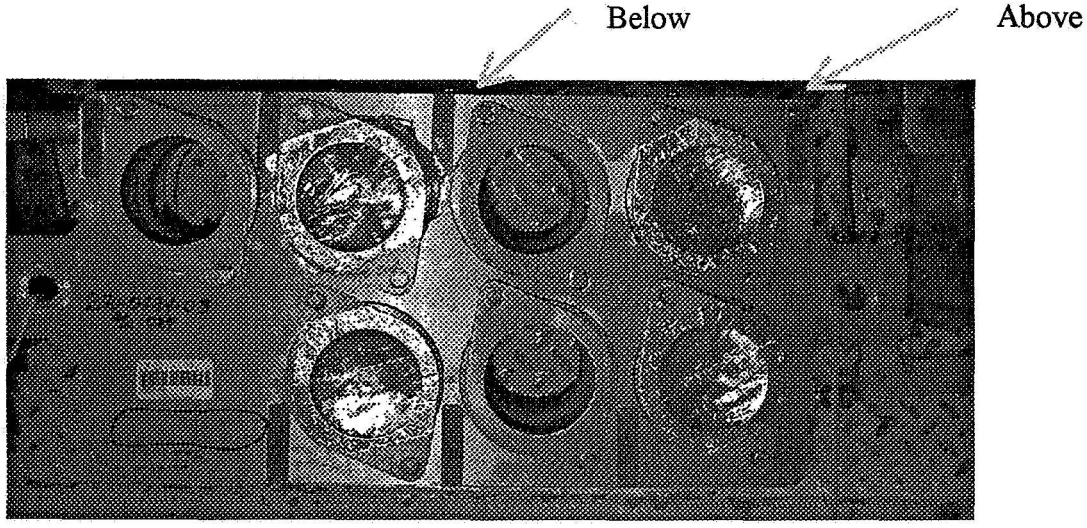

R – 4 Evaluate and standardize, with consideration of horizontal and vertical processing

P – 5 Poor illumination during some QD positioning

R - 5 It is essential that appropriate illumination during all QD operations and positionings be maintained. Perhaps head mounted telescopic lighting would provide more direct illumination.

P – 6 Scupper Identifications are at times missing or not available and are not clearly marked. The following picture shows the QD numbers being marked with a marker.

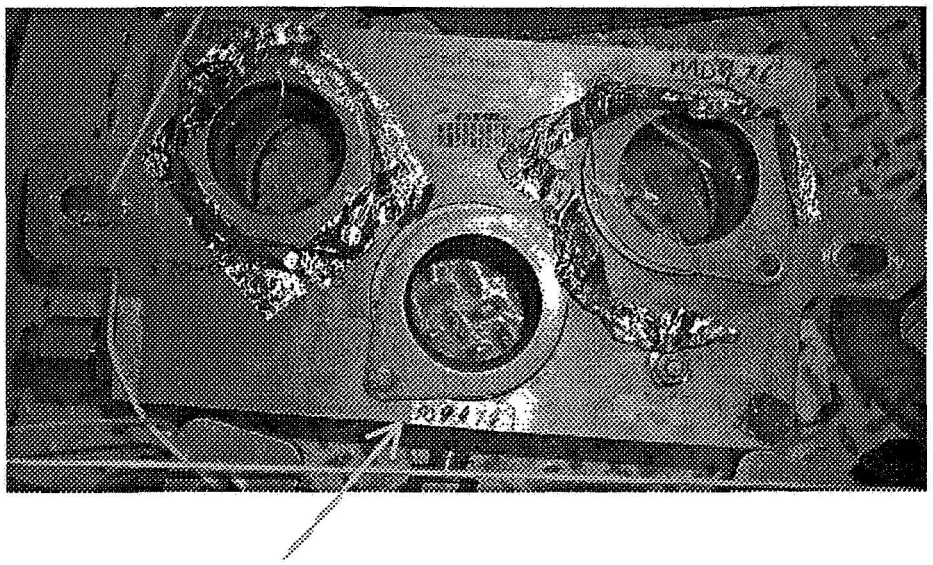

R – 6 Appropriate Scupper identification must be provided and maintained. Engineers should conduct a pre-task walk down to verify and insure that all scuppers are appropriately identified.

P – 7 Before installing the GHC, the technician needs to confirm the AHC number with the scupper number, usually with a flash light. Scupper numbers have different layouts and if the technician does not confirm with the AHC this could lead to a mismate.

R- 7 Standardize the layout of scupper tagging to reduce the confusion to a minimum.

P – 8 Obstructions to installing the QD, (example: lanyard in way).

R – 8 Obstructions towards the installation of QD's should be designed out of the system.

Some workspace positions have inherited poor illumination and at the same time may be difficult to reach. Note picture illustration:

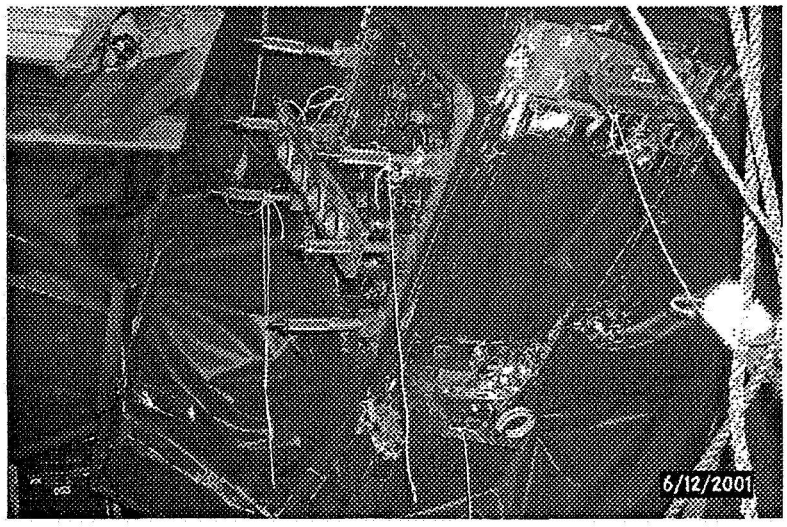

P – 1 The SCAPE suit inhibits visual perception as well as normal tactical and dexterity operations.

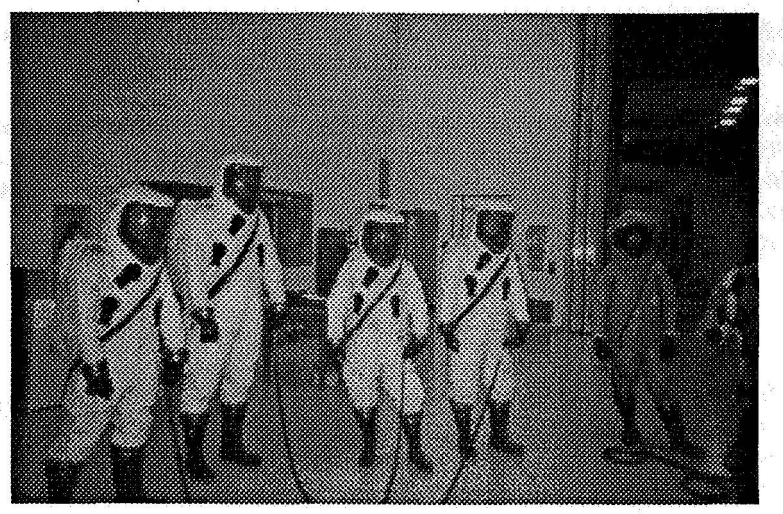

R – 1 Pre-task walk down and labeling should reduce the chance for making mistakes.

➢ <u>Display Design</u>

Dual coding system often causes Technicians to inadvertently perform mismates. The following GHC QDs, located at the designated purge header panel, are a dual purpose QD and promote human error during interface connections with the Orbiter: The majority of these dual purpose QDs are mated to the AHC at the same Orbiter door.

Purge Header Panel	Dual Purpose QD	Orbiter Door
Panel S70-0865-22	MD311/511 MD307/507 MD309/509 MD313/513	56-34/56-36 59-22 59-22 59-22
Panel S70-0865-24	MD212/412 MD208/408 MD214/414	56-09/56-13 59-21 59-21
Panel S70-0865-26	MD213/413 MD209/409 MD211/411	59-21 59-21 56-33/56-35

R - 1 Initiate practical means of change to re-identify the AHC and GHC QDs that will be fail-safe.

R - 2 Ideally, visual cue in the form of color-coded tags and/or symbols to facilitate QD identification when dual coding systems are being used.

- ***A colored tie wrap, or some other method of tagging, could be used to alert the Technician of dual purpose QDs. This extra cautious measure will aid the technician toward preventing a mismate.***

- ***The engineer should read only the designated QD number that is to be mated, and caution! the Technician of the likelihood of a mismate.***

R - 3 For operations involving dual purpose QDs the OMI instructional manual should be modified to read only the intended QD. Change the procedures to list only the QD number that is connected to the work step. This change will limit the possibility of the wrong QD number being called out when connecting to the vehicle.

Sequence steps should read as follows for example:
"verify GHC MD 215 to AHC MD 215"
instead of:
"verify GHC MD 223/215 to AHC MD 215"

R - 4 Cover all flight caps if not in use during the ongoing operations. Currently tape is widely used to cover unused holes, possibly there could be a better design rather than tape to accomplish this. Also notice that the Door number 59-10 is marked with a marker and is not permanently tagged.

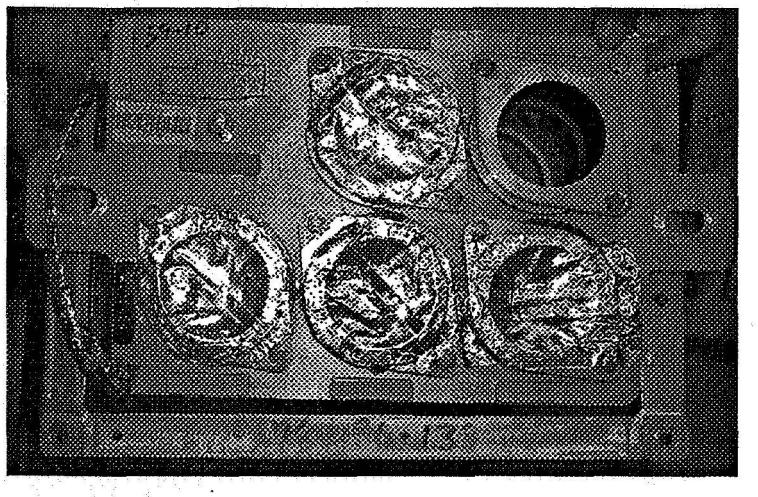

Similarity in the QD nomenclature has caused and contributed to human errors.

P - Technicians transpose similar ID numbers. To mention a few examples:

a) Technician vented GN2 into the test cell MD-707, should have vented through outside scrubber system MD-107.

b) Technician inadvertently demated and mated to the wrong purge header. Tech was requested to demate MD164 from AHC164. The Tech inadvertently demated MD124 from the vehicle.

Note: See Result Section for full list of documented mismates recorded for the past 10 years.

R - Engineer should do pre-task operations and designate those QDs to be mated/de-mated.

R - Engineer must require Technician to repeat, more than once, and verify QD operations. Should reinforced at the OIS Discipline Course/Training.

R - Perhaps a second designator such as a letter or symbol can be used along with the ID number.

➢ **Task Design**

Technicians often are required to leave one floor level to mate a QD after receiving commands from the System Engineer at a different floor location.

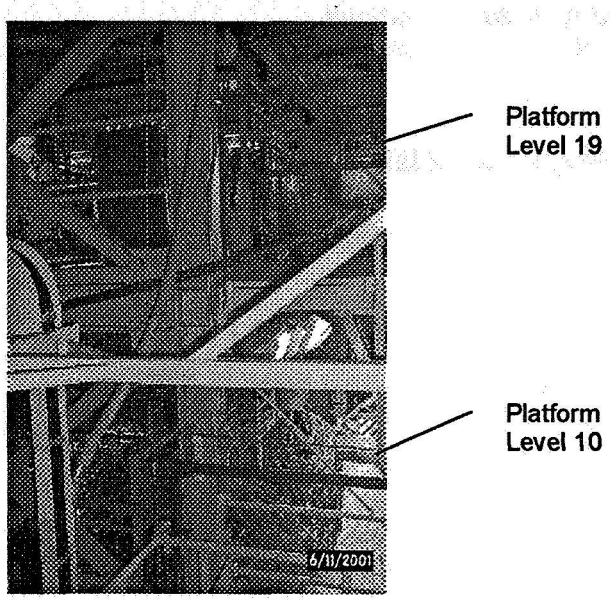

P - 1 Hearing commands information and having to walk to another level to perform the operation increases human error.

R –1 Engineers must call commands in appropriate sequence with the panel and floor level in consideration. By performing a walk down before the actual operation, the engineer would have a better understanding of the floor levels where the operation is taking place.

P - 2 Interruptions between a given command and performing the task increases human error.

R – 2 All Technicians working the QD operations must verify the QD operations.

➢ **Team Communication**

Lack of Task Team Pre-Briefing

P - 1 Engineer often do not perform a thorough walk down to check and verify the configuration sight prior to QD operations

R - 1 Engineer must conduct a walk down of the area to survey QD numbers, Orbiter door locations blanking plate requirements, and platform levels prior to the operation and make appropriate designations necessary.

P - 2 Engineer may not review OMI prior to the QD operations to ensure that all steps are feasible

R – 2 Engineer should take the time to read the command operations prior to pre-briefing.

P – 3 Engineer may or may not perform a pre-task briefing to insure that Technicians understand the nature of operation and understand the "big picture"

R - 3 Provide pre and post-briefing sessions. The bottom line is to improve communication between the Engineer and the Technicians.

- ***Engineer must conduct a pretest briefing session prior to the Technician performing the QD operations. A general-purpose statement at the beginning of each sequence to describe the task is warranted. In addition, during the pretest briefing, visual reinforcement of the operation would further improve the understanding of the operations.***
- ***Utilize morning safety briefing as a forum for incident/error prevention discussions.***

➢ <u>Team Communication less than adequate:</u>

P - 1 Technicians may not acknowledge System Engineer commands by performing call back verification

R - 1 Require Technicians to verify operations. (OIS Discipline)

P - 2 Door designation may not be called out between operations (i.e., tech during the mating operations may assume an incorrect QD designation)

R - 2 Engineer should not precede to the next command until QD operation is verified/ affirmed by the Technician.

P - 3 Head set may filtered in background nose from the high bay

R - 3 Assemble Engineers and Technicians for team discussion to critique their QD operations. Discuss and listen to the OIS tape of the task.

P - 4 Engineer may read the work instructions a little too rapidly at times

R - 4 Technicians should not hesitate to ask for instructions to be read slower or repeated for clarity.

P - 5 Engineer may not communicate all the necessary information needed for the Technician to make the right decision on which QDs are to be connected. (Note also the confusion created due to the dual use of QDs)

R - 5 Utilize lessons learned sessions to communicate to the workforce the necessity for good test discipline at all times. It is apparent that there is a need for the Engineer to check panels prior to QD operation and conduct a walk down before conducting pretest briefing procedures with Technicians.

P - 6 Work steps are not written clearly.

R - 6 Insure that all work steps are written clearly.

➢ **Operational Team Support May Lead to Human Error**

P - 1 In the crotch area of the OMS pod, when another technician is assisting and wearing the headset, call out steps from the platform may not be all inclusive for the technician performing the QD operation.

R - 1 When Technicians are out of the range for connected headphone, wireless headphone must be provided. Engineer must give door location along with crotch area description.

P - 2 Technicians may be relieved to take a break while the two new technicians may not receive sufficient pre-briefing.

R - 2 Try to schedule break with shift change. Technicians are to complete the task prior to change of shift. Allow for shift overlap to brief oncoming Technicians of the current task.

- ***Improved task team discipline***
- ***Face to face Hand-offs tie-ins are a must.***

➢ **Distractions**

Technician can be interrupted during QD command operations. To mention some examples:

P - 1 Outside background bay noise

R - 1 All outside bay noise must be eliminated where possible. Engineer must brief all personnel involved in QD operations to reduce as much as possible any confusion or interference that may be attributed to outside noise.

P - 2 Working on several tasks simultaneously

R - Technicians are to work on operations in sequential order and verify all operations.

P - 3 Interruptions from other technicians needing the work area or asking questions concerning another QD operation.

R - 3 Get rid of all distractions and interruptions. QD operations are too critical for distractions to interfere with operations

P - 4 Working steps out of sequence:

- **Working more than one QD installation with same suit set up**
- **Working series of single steps with out verifying QD operations**

R - 4 Technicians are to work on operations in sequential order and verify operations. Simultaneously working on several QDs operations should not be permitted. Such activity causes attention to focus away from the immediate task.

➢ **Cognitive Decision Processing Error**

Similar ID numbers (GHC MD 711, GHC MD 707, AHC MD 111, AHC MD107 and GHC MD 107) on QD are often transposed when making the QD mate. These particular QDs nomenclature have lead to numerous incidents and have contributed to a majority of the incidents/accidents occurrence. Previous citations by USA (1996) QD Mate/Demate Accuracy Team and an outside Human Factors consulting group hired by Rockwell International (1981) have previously

confirmed this as a contributing cause. The following is a list of GHC OMS QDs that are often identified as having similar nomenclature:

Purge Header Panel	Dual Purpose QD	Orbiter Door
Panel S70-0865-02	MD117 MD711 MD111 MD147 MD157 MD127 MD137	28-13....
Panel S70-0865-04	MD106 MD126 MD128 MD138 MD148 MD158	28-00 28-12....
Panel S70-0865-20	MD314/514 MD310/510 MD308/508	59-22....

P - 1 Technicians may check designations and look away from the reference point and still transpose numbers wrong (i.e., seeing the number 3 instead of the number 5). Tabulation of these QD incident provide insight into the types of occurrence and the frequency of the occurrence which is illustrated in the preceding result section.

R - 1 Technicians must maintain focus

P - 2 Technician may not work specific task and may not be knowledgeable of the specific QD operation.

R - 2 When similar nomenclature ID numbers are being mated and demated, the Engineer should perform pre-task operations by marking the appropriate the QDs and panels to be used.

Summary

Human errors and the catastrophic failures produced by them will continue as long as there are human-machine interactions and as long as we fail to understand the psychology behind human failures. It's a nontrivial task, one that involves understanding how humans learn, how we deal with process sensory inputs among numerous others. The cognitive processes that enable unique human capabilities also make humans vulnerable to certain forms of errors. The good news is that error rates can be reduced by redesigning external factors to reduce vulnerability to error and by designing systems and procedures to assist recovery from error.

USING WEARABLE COMPUTERS IN SHUTTLE PROCESSING: A FEASIBILITY STUDY[1]

Martha A. Centeno
Industrial and Systems Engineering
Florida International University
Miami, Fl 33199

Daisy Correa
Marcia Groh-Hammond
Shuttle Process Integration - PH-M1-B
Kennedy Space Center, Fl 32899

1. INTRODUCTION

Shuttle processing operations are performed following prescribed instructions compiled in a Work Authorization Document (WAD). Until very recently, WADs were printed so that they could be properly executed, including the buy off of each and every step by the appropriate authorizing agent. However, with the development of EPICs, Maximo, and PeopleSoft applications, some of these documents are now available in electronic format; hence, it is possible for technicians and engineers to access them on line and buy off the steps electronically. To take full advantage of these developments, technicians need access to such documents at the point of job execution. Body wearable computers present an opportunity to develop a WAD delivery system that enables access while preserving technician's mobility, safety levels, and quality of work done.

The primary objectives of this project were to determine if body wearable computers are a feasible delivery system for WADs. More specifically, identify and recommend specific brands of body wearable computers readily available on the market. Thus, this effort has field-tested this technology in two areas of shuttle processing, and it has examined the usability of the technology. Results of two field tests and a Human Factors Usability Test are presented. Section 2 provides a description of the body wearable computer technology. Section 3 presents the test at the Space Shuttle Main Engine (SSME) Shop. Section 4 presents the results of the integration test at the Solid Rocket Boosters Assembly and Refurbishing Facility (SRBARF). Section 5 presents the results of the usability test done at the Operations Support Building (OSB).

2. WEARABLE COMPUTERS TECHNOLOGY

Wearable computers are small size PC's that differ from Pocket PCs at the hardware as well as the operating system level. Wearable computers are just like any desktop PC or Laptop. As such, they use the same operating system as a PC, whether it is Windows, Windows NT, or Linux. Hence, they can run any application that a regular PC can run. Wearable computers may have the elements described in Table 1. Exactly which combination of elements is required depends on the type of job to be done and the software to be used for it.

The processor for wearable computers will continue to evolve paralleling that of processors for regular PCs. At present, the chip and motherboard size are a lot smaller than the one used in regular PC; hence, the technology is moving about one step behind that of a regular PC. This means that available speeds on a wearable unit will be slower than that of current PCs or laptops. In regards to display devices, wearable units normally come with a flat panel with a built-in touch screen, but they can also be fitted a Heads Up Display Device (HUD). The flat panel size is as big as 9 inches. Larger panel are possible but are unlikely to appear on the market, as they would defeat the goal of the unit being wearable. Smaller panels are also possible; however, the functionality of it on the workplace may be diminished. Smaller panels may be functional for text-based output only. If the output is graphics-based, however, a large screen may be required to avoid continuous scrolling of the screen to see the information needed.

An alternative to the flat panel is the heads up display (HUD) device (Figure 1). Typically, the manufacturer of the wearable unit is not the manufacturer of the HUD. They simply partner with someone who produces the HUD and fit it to their unit. There are two basic types of HUDs: 1) binocular and 2) monocular. Binocular HUDs are good for training and virtual reality work. The user receives all the information via the HUD, and he or she is not

[1] This effort was funded under NASA grant NAG10-292 and a NASA/A.S.E.E. Fellowship.

required to move around. Monocular HUDs come either as "see-through" or "see-around" displays. This type of HUD is good when the user has to move around, and he or she is required to read additional information outside the HUD. Current HUDs are either color or monochrome displays. The resolution of the display is restricted to a maximum of a 640x800 resolution. The technology is also advancing to allow for depth of display adjustment, so that it can simulate projection at 2, 4, or 8 feet. Some prototype models of HUDs allow for the display element to be moved away from the plane of sight as needed.

CPU	o Pentium Based Chip. o Chip speeds of 233 MHz and up; latest model are running 800 MHz. o Hard disk of 6 GB and up. Some of the smallest model may have smaller drives of only 3 GB. o RAM memory of 64 MB and up. The current limit is 512 MB. o USB port. o Customized port to plug in a port replicator. Out of the port replicator it is possible to have serial ports, mouse and keyboard ports, and video ports. o Some of the CPUs have an integrated mouse.
DATA DISPLAY	o Flat Panel (6 or 9 inches of viewable screen). o Heads up display. Depending on the manufacturer, the HUD could be a monocular, see through or see around display; or it could be a binocular semi or full immersion HUD.
DATA ENTRY	o Flat Panel Touch screen. o Mini keyboard. o External handheld mouse. o Head set with microphone.
NETWORKING	o PCMCIA cards for hardwire connectivity as well as for wireless connectivity.
OTHER ACCESSORIES	o PCMCIA based CD drive. o Mini keyboard through additional ports. o Docking station, with multiple ports for floppy diskettes and similar devices.

Table 1: Elements of a Wearable Computer

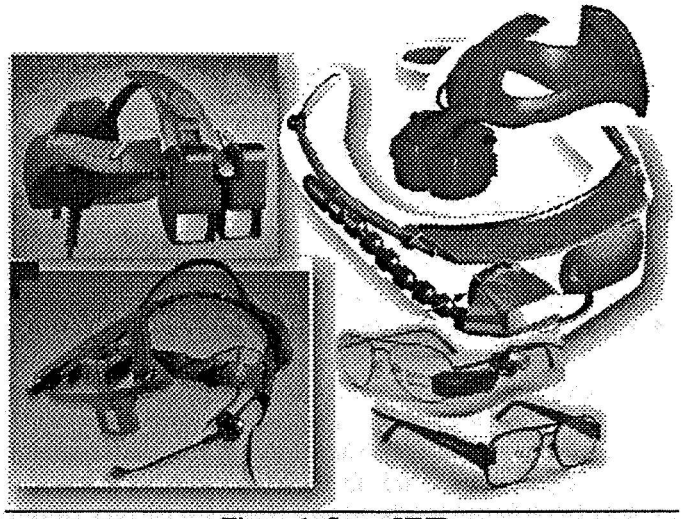

Figure 1: Some HUDs

When fitted with a HUD, the user has the option of a mini keyboard or voice command for data entry. Screen navigation can be done via voice command or via mouse. Voice command requires the acquisition of a voice recognition program, such as ViaVoice from IBM. The technology for voice recognition has made significant progress, but it is still a bit difficult to use, as it requires individual voice recognition training. Furthermore, it does not work well when the work environment is a bit noisy, even in low-level noise. Nonetheless, significant progress is expected in the next few years.

In regards to networking capabilities, a wearable computer has the same capabilities as a regular PC. The units require the use of a PCMCIA type of card to connect to a network in either a wired or wireless form. Using a

wearable computer in a wired or wireless network is totally dependent on how the user is supposed to be working. There is one concern in regards to the use of this technology in a wireless environment, and that is that the card communicates with the wireless network via RF signals. In environments where explosive are handled, this option may not be advisable. The lack of wireless connectivity does not prohibit the use of the wearable computers technology as the information regarding WADs could be preloaded, and the data entered by the user could then be uploaded to the network via a wired connection.

Commercially, there are three main players: Xybernaut, VIA, and Perkins Engineering. Xybernaut is the leader on the market. They have been manufacturing wearable computers for several years. Figure 2 shows their Mobile Assistant IV (MA IV) model. Their latest model, the Mobile Assistant V (MA V) is the product of a partnership with IBM. The MA V was released to the market during the summer 2001. Figure 3 shows the unit from Via. It is very light and seats on a regular belt. The CPU wraps around the back of the user. Figure 4 shows the Perkins Engineering's unit called Mid-Riff Brain (MRB). The unit is just as robust as the MA IV. One advantage of the MRB is the belt upon which the unit is carried. The MRB's belt is fully adjustable and very light, and it has an articulating arm that holds the flat panel display.

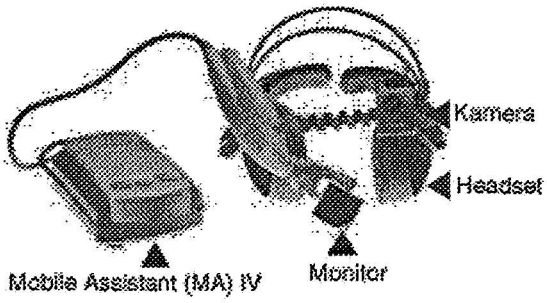

Figure 2: Xybernaut's Wearable Unit

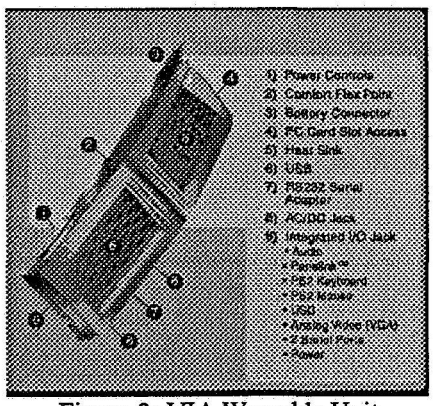
Figure 3: VIA Wearable Unit

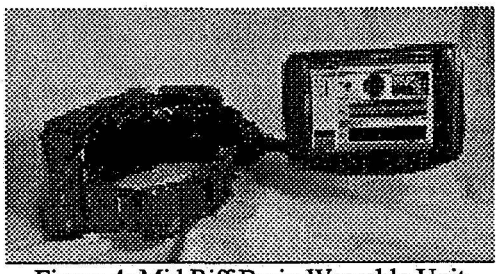
Figure 4: Mid Riff Brain Wearable Unit

3. WEARABLE COMPUTERS FOR SSME RECEIVING INSPECTION

The primary goal of this test was to establish the benefits of using a wearable computer to process the WAD V6033 N: SSME Receiving Inspection. The test was done in the SSME shop, located in the OPF 3 Annex. This was a first trial on field-testing the MA IV as well as on the test procedure itself. Technicians were given little or no training. The number of technicians that participated in the test was five. The test required the use of a laptop, wearable unit, and paper based to engage in parallel processing of the WAD for comparison purposes. The real buying was done on the paper version. Rocketdyne developed the software used for the electronic buys. Acceptance by the user was measured via direct observations and post-trial questionnaires addressing two distinct processes: 1) *Assembling the unit*, and 2) *Interaction with the Unit*. For the interaction with the unit, four aspects

were studied: Physical, Mobility, Data Entry, and Data Display.

Only three of the five technicians that were somehow involved in the test actually used the wearable computer. From an overall point of view, there was great variation in their responses (Table 2). 10.53% found at least one aspect of the unit highly difficult to interact with. A large 38.60% were dubious about how easy it is to work with this unit. Only 50.8% thought it was relatively easy to work with the unit. A closer look to the responses to each aspect reveals that it seems that the overall weight of the wearable computer is OK. The only instance in which there may be a problem is in the continuous use of the touch screen on the arm; after awhile, the weight of the touch screen becomes too much. Furthermore, constant use of the touch screen on the arm limits technicians' ability to reach where they need to reach. A percentage-based analysis reveals that the *data display aspect* received a very low ranking, getting no positive ranking whatsoever, and an 80% of ambivalent Reponses. On the other hand, the *data entry aspect* received 75% high rankings, and it only got 12.5% negative responses. For the other aspects, the ambivalent posture was significant, but the negative rating was low. Thus, the display was the one that disenchanted the technicians.

In general, technicians seem to like the idea of using a wearable computer to do their job, but not necessarily in the SSME shop and not necessarily for this WAD. Their main concern seems to be the effect of any radiated energy. This needs to be addressed. Use of the wireless network is the main source of radiation.

	Negative	Ambivalent	Positive
Overall	10.53%	38.60%	50.88%
Display	20.00%	80.00%	- -
Data Entry	12.50%	12.50%	75.00%
Mobility	8.33%	50.00%	41.67%
Physical	8.33%	41.67	50.00%

Table 2: Frequency of Responses – Interaction

4. Wearable Computer Usage for TPS Automated Thickness Measurement

The primary goal of this test was to establish the benefits of using a wearable computer as part of an integrated system that fully automates the TPS Thickness Measurement Activity. Full scale integration of wearable computers required a two-phase approach: 1) evaluate and test the integration of the hardware and 2) test the integrated system with the help of the technicians. The current system (Figure 5) has been performing well; however, it has gotten obsolete, and it fails to take advantage of current data analysis packages. Under the current system, technicians write the value read from the KUDA sensor on a paper map of the corresponding SRB structure (Figure 6). Since the data resides on paper, it only gets analyze on a reactive mode. Hence, it needs to be replaced with a system that allows on-line data collection and proactive data analysis. Figure 7 shows a conceptual proposed system using the wearable unit from Xybernaut (MA IV). Our test proved that such integration is feasible.

The new KUDA sensor was tested for accuracy and for compatibility with a wearable unit. To achieve this, a software application was developed by a USA SRBARF team, using RSView32. The hypotheses being tested are given in Table 3. The tests of hypothesis revealed that there is no statistical difference in readings between the sensors when doing it under calibration. However, Table 4 shows that there may be a minor hidden difference on the reading of 1 unit (mean value = -1). It appears that the new sensor is consistently reading one unit higher than the current sensor (85% of the time). This is visible from the position of the confidence interval on the horizontal axis. The good thing is that such variation is consistent across all readings as they have a perfect positive correlation ($\rho = 1$, Figure 8).

The tests of hypothesis for actual readings revealed that ***there is*** a statistical difference in readings between the sensors (Table 4). However, this table also shows that once again, it appears that the new sensor is consistently reading 2 units higher than the current sensor (mean value = -2.04), and that the confidence interval's upper limit is very close to 0. Once again, the good thing is that such variation is consistent across all readings as they have a strong positive correlation ($\rho = .982$, Figure 9). Hence, although the test says that there is a statistically

significant difference, we know that the difference is on the new sensor giving higher readings by 2 units on the average. This can be removed by recalibrating the sensor, i.e. by offsetting its zero point. This can be done with 95% confidence and with the assurance that indeed the two sensors are paralleling their behavior as shown in Figure 10 and Figure 11.

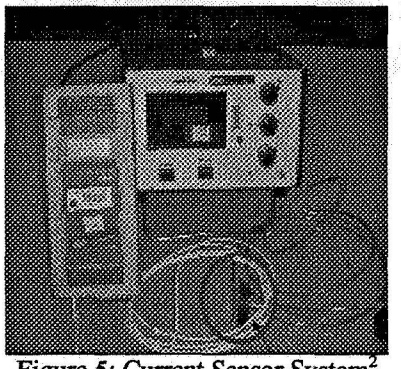

Figure 5: Current Sensor System[2]

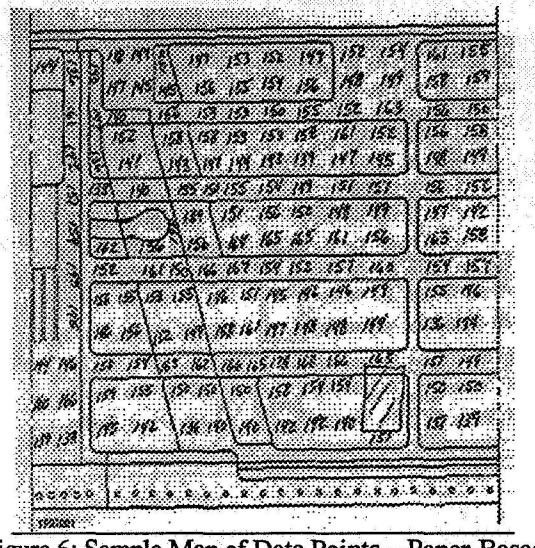

Figure 6: Sample Map of Data Points – Paper-Based

- **Proposed Replacement**
  - Kaman Instrumentation
    - Standard KuDA Series 38U Probe
      - State of the ART
      - Full Manufactures Support
      - Eddy Current Measurement
      - Comparable to Existing System
      - RS-232 Communications
  - Xybernaut Mobile Computer
    - Model MA4-00213
    - RSView32 Software
      - Fully Programmable Graphical Interface
      - Automated Data Collection
      - USA / NASA Lan Connectable
      - Compatible w / Proposed Spray System upgrade

Figure 7: New KUDA System – Proposed

Hypothesis 1:	**Hypothesis 2:**
$H_0 : \mu_{cc} = \mu_{nc}$ Converted to → $H_0 : \delta_1 = 0$	$H_0 : \mu_{ca} = \mu_{na}$ Converted to → $H_0 : \delta_2 = 0$
$H_1 : \mu_{cc} \neq \mu_{nc}$ $H_1 : \delta_1 \neq 0$	$H_1 : \mu_{ca} \neq \mu_{na}$ $H_1 : \delta_2 \neq 0$
δ_1 = Difference between population means (current – new)	δ_2 = Difference between population means (current – new)
μ_{cc} = Average readings with the current sensor - calibration.	μ_{ca} = Average readings with the current sensor – actual.
μ_{nc} = Average readings with the new sensor - calibration.	μ_{na} = Average readings with the new sensor - actual.

[2] Figure 5 to Figure 7 were taken from a PowerPoint Presentation developed by USA SRBARF personnel

Table 3: Hypotheses tested – SRBARF

	MEAN	STD. DEVIATION	STD. ERROR MEAN	CI LOWER	CI UPPER
CURRCALI - NEWCALI	-1.0000	1.5275	.5774	-2.4127	.4127
CURRCALI	299.143	216.4882	81.8249	**CORRELATION**	ρ
NEWCALI	300.143	215.9517	81.6221	CurrCali & NewCali	1.00
CURRENT - NEWKUDA	-2.0476	1.7169	.3747	-2.8291	-1.2661
CURRENT	190.9048	8.9661	1.9566	**CORRELATION**	ρ
NEWKUDA	192.9524	8.9525	1.9536	Current & New	0.982

Table 4: Test and Descriptive Statistics – KUDA

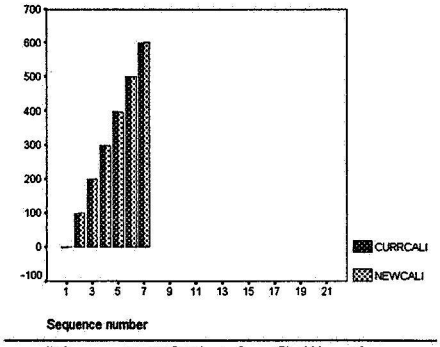

Figure 8: TSPlot for Calibration

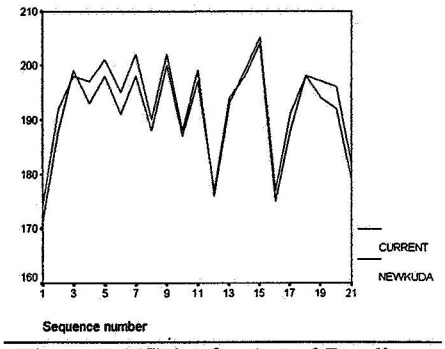

Figure 9: TSPlot for Actual Readings

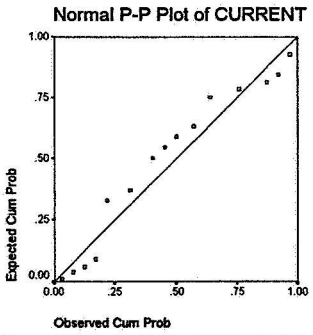

Figure 10: Normal P-P Plot – Current

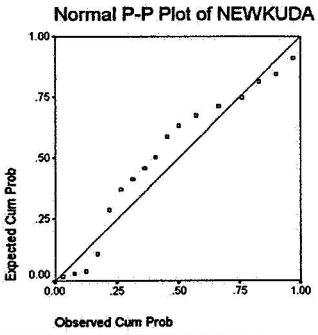

Figure 11: Normal P-P Plot – New KUDA

The software was tested and works excellently. Once the sensor does the reading, the new application software stores the reading in an Excel file. All data pertinent to structure and coordinate of the reading is also captured. But, what happens once the data is collected? At the moment, not much happens with the collected data because the data goes to a piece of paper. But now that we have established communication between the KUDA and the CPU, the data goes directly to the computer (an Excel file). Thus, with the wearable-based system, data analysis can be done on a more continuous basis provided that the right analysis tool is available. We tested the use of PIExpert, which is a program for process improvement. Full discussion of this test is found in another report submitted to PH-M1-B. The success of this experiment represents a great improvement in data collection, data analysis, and process control and monitoring because it will enable proactive analysis and control instead of reactive analysis (Figure 12). The test showed that the integration of the KUDA sensor is feasible. This new system will significantly reduce the time needed to capture the readings and to store them in an Excel file because it avoid the manual data entry step. In addition, the use of PIExpert may lead to a reduction in the number of observations needed. It has been estimated that in addition to the elimination of data entry, there may be a reduction in the actual data collection time of about 26 hours per flow.

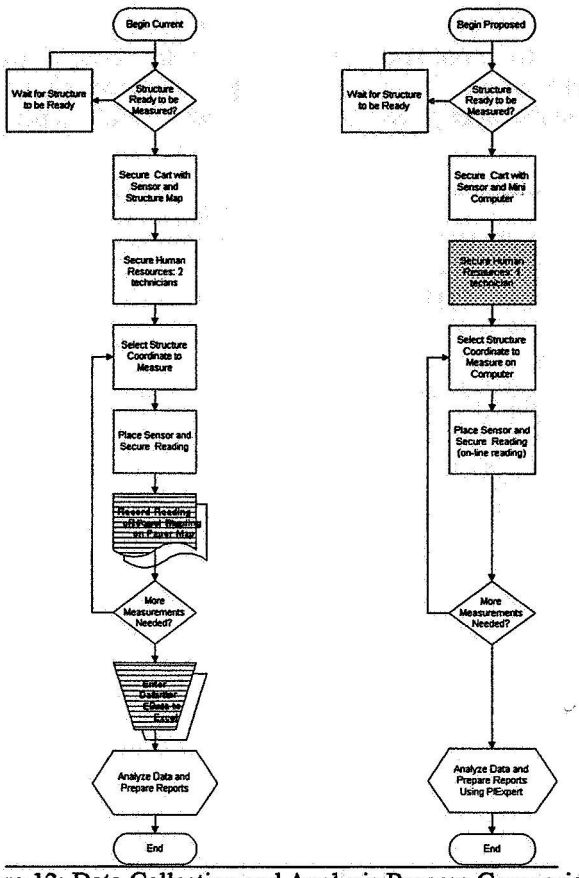

Figure 12: Data Collection and Analysis Process Comparison

Specific recommendations are that:

1. USA SRBARF acquires a wearable unit. Mid Riff Brain seems to be a more robust CPU; however, the MA V model has become available and it is lighter than Mid Riff Brain.

2. USA SRBARF acquires a copy of the PIExpert software. This will enable on-line process control, data analysis, and reporting.

3. Request a demonstration unit from Perkins Engineering (Mid Riff Brain) and VIA to do a test, including the usability test (Phase 1 and Phase 2).

4. Conduct usability test with the technicians using existing MA IV unit (Phase 2). Questionnaire in the Test Plan may need some modifications.

5. OSB USABILITY TEST

The primary goal of this test was to establish the usability of wearable computers when carrying out normal computer functions such as reading text, graphics, schematics, and entering data. The unit used for this test was the Xybernaut's MA IV unit. Other units such as the VIA and MRB need to be tested as well.

The usability test was done in the Operations Support Building (OSB) where a temporary wireless network was set up. The test required the development of two web pages and the use of the Shuttle simulator linked from the KSC main web page. The test called for two different modalities of interaction: 1) For data display → touch screen

and heads up display, and 2) For data entry → touch screen using JOT software and super mini keyboard. Hence, two groups were formed, and the order was swapped to reduce learning bias. Acceptance by the users was measured via direct observations and post-test questionnaire addressing four aspects: physical, mobility, data entry, and data display. The actual questions in the order given are shown in Table 5. All the participants were knowledgeable user of a regular PC.

Q#	Statements
1	The text displayed on the touch screen panel was easy to read.
2	The video shown on the touch screen was easy to see.
3	The schematics / drawing displayed on the touch screen panel were easy to see and understand.
4	Sounds coming out the touch screen speakers were easy to hear.
5	Typing on the wrist keyboard was easy.
6	Interacting with the touch screen panel with the stylus was easy.
7	The text display on the HUD device was easy to read.
8	The video shown on the HUD was easy to see.
9	The schematics / drawings displayed on the HUD were easy to see and understand.
10	Sounds coming out the HUD speakers were easy to hear.
11	Typing on the wrist keyboard while wearing the HUD was easy.
12	Interacting with the mouse was easy.
13	Reading instructions on paper while wearing the HUD was easy.
14	Entering Text using the wrist keyboard was easy
15	Entering text using the JOT program was easy
16	Scrolling on the touch screen was easy.
17	Overall Interaction with the wearable computer was easy
18	My lower back was comfortable while using the wearable computer.
19	My hip area was comfortable while using the wearable computer.
20	My arm was comfortable while wearing the touch screen on it.
21	The overall weight of the wearable was OK.
22	I was able to comfortably walk, while using the wearable computer.
23	I was able to comfortably climb, while using the wearable computer.
24	I was able to comfortably bend while using the wearable computer.
25	I was able to reach wherever I needed to while I was using the touch screen on my arm.
26	My eyes were comfortable when I read schematics from the touch screen.
27	My eyes were comfortable when I read text from the touch screen.
28	My neck was comfortable while using the touch screen.
29	My eyes were comfortably when I read schematics from the HUD.
30	My eyes were comfortably when I read text from the HUD.
31	My neck was comfortable while using the HUD
32	Overall, I was physically comfortable after using the wearable computer.

Table 5: Ordered Questions

Table 6 shows the frequency of responses for all questions. Overall, it can be seen that 62.32% of the responses were either ***agree*** or ***strongly agree***. Only 8.12% of the responses were either ***disagree*** or ***strongly disagree***. A significant 29.57% of the responses were in the ambivalent area (***somewhat agree, somewhat disagree***) The analysis per aspect will show the areas that caused this ambivalence. From these responses, it can be concluded that overall there is a strong inclination to using this technology, provided that some issues are resolved.

A couple of questions we had from the beginning were whether the responses would be correlated to the participant's weight or gender. It was necessary to establish an answer to these questions because if the technology is adopted, users selection as well as training required must take into account any difference that there might be. Thus, we ran several tests of hypothesis comparing responses across gender as well as weight. Results of these tests are given in Table 7, Table 7: Comparison Based on Weight and Gender

, and Table 8. The actual *paired-t* tests were done on the difference $\delta = \mu_1 - \mu_2$, postulating that there is no difference ($\delta = 0$) as the null hypothesis. The tables show a 95% confidence interval around the mean value of δ;

hence, if the confidence interval contains the value zero, the null hypothesis cannot be rejected. Failing to reject the null hypothesis implies no evidence of a difference between the two population mean responses.

	Negative	Ambivalent	Positive
All Questions	8.12%	29.57%	62.32%
Data Display	7.50%	32.50%	60.00%
Data Entry	6.38%	37.23%	56.38%
Mobility	9.09%	9.09%	81.82%
Physical	7.69%	27.35%	64.96%

Table 6: Frequency of Answers - All questions

With respect to weight, we found no significant difference, except in the mobility aspect (Table 7). People with less weight rated the unit in the *disagree* level, whereas the heavier individuals were a lot more incline to say that the unit allow for great mobility. However, even in mobility, the level of difference is not conclusive since the upper limit of the confidence interval is very close to 0 ($-4.26 \le \delta \le -0.07$). The latter is mildly corroborated when we looked at the correlation factor between weight and average response, which shows that there is only a ***weak positive correlation*** ($\rho = 0.275$); i.e. the higher the weight of the user, the higher the ranking of the unit (highest value is the most positive) (Table 8). This result *was expected* because despite the low weight of the unit used, it still looks bulky on thinner individuals. Technology will continue to evolve to a point in which perhaps this will not be an issue any longer. With respect to gender, there is no significance difference either (Table 7: Comparison Based on Weight and Gender

); the correlation analysis also shows that there is only an indication of a ***weak, positive correlation*** ($\rho = 0.240$).

Question 17 requested a perceived easy of interaction, and Question 32 requested a perceived comfort. In these two perceptions, we also investigated if there was a correlation based on gender. From Table 7: Comparison Based on Weight and Gender

, it can also be seen that there was *no difference* on the perceived level of ease of interaction or comfort. However, the width of the 95% confidence interval [4.442 and 5.72 in a (-6,6) range] as well as the correlation factor [0.4 (moderate) with a significance of 0.1] indicate that there ***may be*** some difference, trending towards male users being more inclined to perceive the unit as easy to use and comfortable. Confirming if such difference really exists is important when deciding which technician will use the unit. *Small, medium, large body frame? Male or female? What kind of training should the user be given?* It is recommended that if the technology is implemented, training for small-framed users as well as for female users take into account the slight difference.

Hypothesis Being Tested: $H_0 : \mu_1 = \mu_2$, $H_1 : \mu_1 \neq \mu_2$ Converted to → $H_0 : \delta_1 = 0$, $H_1 : \delta_1 \neq 0$

where δ = Difference between population means and μ_1 = Average of population below or at 140 lbs. And μ_2 = Average of population above 140 lbs.

ASPECT	MEAN	STD. DEVIATION	STD. ERROR	CI-LOWER	CI-UPPER
Overall	-.4533	1.0248	.4184	-1.5288	.6222
Physical	-.3833	1.4204	.5799	-1.8740	1.1073
Data Entry	-.3700	1.1362	.4639	-1.5624	.8224
Data Display	-.1633	1.1583	.4729	-1.3789	1.0522
Mobility	-2.1667	1.9916	.8131	-4.2568	-7.6359E-02

Hypothesis Being Tested: $H_0 : \mu_1 = \mu_2$, $H_1 : \mu_1 \neq \mu_2$ Converted to → $H_0 : \delta_1 = 0$, $H_1 : \delta_1 \neq 0$

where δ = Difference between population means and μ_1 = Average of Female population and μ_2 = Average of Male population

ASPECT	MEAN	STD. DEVIATION	STD. ERROR	CI-LOWER	CI-UPPER
Gender	-.5780	.8484	.3794	-1.6315	.4755
Q17	0.800	1.7889	.8000	-1.4212	3.0212
Q32	-2.4000	2.3022	1.0296	-5.2585	.4585

Table 7: Comparison Based on Weight and Gender

	WEIGHT		GENDER	
	ρ FACTOR	SIG. (2 TAILED)	ρ FACTOR	SIG. (2 TAILED)
Overall Average	0.275	0.387	0.240	0.453
Q17	--	--	-0.316	0.317
Q32	--	--	0.493	0.103

Table 8: Correlation Average Response - Pearson Correlation

6. SUMMARY

This effort has explored the state of the art of wearable computers technology, and it has explore its introduction in some areas of shuttle assembly. The tests clearly show that the technology is indeed appropriate for some areas but not for others. It also revealed the strengths and weaknesses of existing commercial units. The use of HUDs is not recommended at this point in time. HUD technology will continue to mature and medical concerns will be addressed.

It is recommended that wearable computers be used at the SRBARF for TPS Thickness measurement, but in a batch mode, so that there is no need to set up a wireless network in an area where explosives are used. Exploring other areas to use this technology is also recommended. Tile water reproofing may be an excellent candidate to fully test next.

Full report of each test presented here has been submitted to the PH-M1-B organization.

ACKNOWLEDGMENTS

Special thanks are due to all technicians and engineers who facilitated and participated in this study. Among these are: Jason Armour, Merle Japp, and David Mandernack from Rocketdyne; Carrie Oyler from IE/HFE USA; David Eckols, Leonard Hutto, Sue Kohl, Leif Morton, Don Noah, and Anil Patel from SRBARF USA; Daisy Correa, Marcia Groh-Hammond, Angel Lopez, Alicia Mendoza, Darcy Miller, Jessica Mock, Luis Saucedo, Kimberly Shanks, Damon Stambolian from NASA. Deep gratitude to the mangers and technicians from OPF 1, 2, and 3 for their support with this effort.

2001 NASA/ASEE SUMMER FACULTY FELLOWSHIP PROGRAM

JOHN F. KENNEDY SPACE CENTER
UNIVERSITY OF CENTRAL FLORIDA

Assessing the Rayleigh Intensity Remote Leak Detection Technique

Dr. Sandra Clements
Visiting Assistant Professor
Physics and Space Sciences
Florida Institute of Technology
Christopher Davis

ABSTRACT

Remote sensing technologies are being considered for efficient, low cost gas leak detection. An exploratory project to identify and evaluate remote sensing technologies for application to gas leak detection is underway. During Phase 1 of the project, completed last year, eleven specific techniques were identified for further study. One of these, the Rayleigh Intensity technique, would make use of changes in the light scattered off of gas molecules to detect and locate a leak. During the 10-week Summer Faculty Fellowship Program, the scatter of light off of gas molecules was investigated. The influence of light scattered off of aerosols suspended in the atmosphere was also examined to determine if this would adversely affect leak detection. Results of this study indicate that in unconditioned air, it will be difficult, though perhaps not impossible, to distinguish between a gas leak and natural variations in the aerosol content of the air. Because information about the particle size distribution in clean room environments is incomplete, the applicability in clean rooms is uncertain though more promising than in unconditioned environments. It is suggested that problems caused by aerosols may be overcome by using the Rayleigh Intensity technique in combination with another remote sensing technique, the Rayleigh Doppler technique.

Sandra Clements

1. INTRODUCTION

Detecting and locating gas leaks is a costly endeavor critical to the safety and success of launching vehicles into space. Remote sensing technologies are being considered as replacement for in situ techniques with the goal of dramatically reducing the cost of detecting gas leaks by an order of magnitude or more. During Phase 1 of the Remote Leak Detection project, eleven remote sensing technologies were identified for further study (private communication from Glenn Sellars and Danli Wang, Florida Space Institute, Kennedy Space Center, Florida). The level of theoretical and experimental development of each technology was assessed for its applicability to remote leak detection. The specific goal of the Remote Leak Detection project is to identify remote sensing techniques that will locate hydrogen and helium leaks into air. The two gases, hydrogen and helium, were chosen because of their importance in verification and normal operations of launch systems. These gases are also among the most challenging to detect.

One of the eleven possible remote leak detection techniques, the Rayleigh Intensity technique, was investigated during the 10-week Summer Faculty Fellowship Program. The results of that investigation are described here.

2. THE RAYLEIGH INTENSITY TECHNIQUE

With the Rayleigh Intensity technique, a laser would be directed toward the site being monitored for gas leaks. The laser light would scatter off of air molecules (and particulates) and this scattered light would be detected. In order for this technique to be viable for leak detection, the intensity of scattered light with and without a leak would need to differ. Because this technique involves the scatter of electromagnetic radiation off of small particles, a theory describing such scatter will be examined.

2.1. Mie Theory and the Scatter of Electromagnetic Radiation

Mie theory [1] was developed to describe the scattering of electromagnetic radiation by spherical particles. The derivation of Mie scattering theory involves finding the solutions of Maxwell's equations that describe the electromagnetic field resulting when a plane, monochromatic wave is incident on a spherical particle immersed in a homogeneous, isotropic medium. Because the solution consists of an infinite, though converging, sum of complicated terms involving Legendre functions and Bessel functions [2], computer programs are used to solve it numerically.

When the particle radius (a) is small compared to the wavelength (λ) of incident radiation ($a \lesssim \sim 0.1\lambda$) the intensity ($I$) of scattered light satisfies Rayleigh's Law ($I \propto 1/\lambda^4$). For larger radii, the scattered intensity has a flatter dependence on wavelength ($I \propto 1/\lambda^{0\text{-}2}$). In the visible region of the spectrum, Rayleigh scattering occurs from air molecules and small aerosol particles (sea salt and atmospheric dust condensation nuclei, etc.) whereas Mie scattering occurs from larger aerosol particles (dust, pollen, water droplets, etc.).

Rayleigh's Law, given below, describes the scattered intensity in the small particle limit [3].

$$I = I_0 \frac{8\pi^2 a^6}{r^2 \lambda^4} \left(\frac{(n^2 - 1)}{(n^2 + 2)} \right)^2 \left(1 + \cos^2 \theta\right) \qquad \text{Rayleigh's Law}$$

The functional dependence of the scattered intensity on the particle's refractive index n, the wavelength □ of the incident radiation, the scattering angle □, and the particle size a will be examined in turn.

2.2. Index of Refraction

It is because the intensity is proportional to $((n^2 - 1)/(n^2 + 2))^2$ and the three gases of interest have very different values for this quantity that the Rayleigh Intensity method is considered a possible leak detection technique. The values for n and $((n^2 - 1)/(n^2 + 2))^2$ for the three gases of interest are given in the table below. Note that the intensity due to Rayleigh scattering in air is expected to be about 70 times greater than the intensity due to scattering in helium given that all other conditions are the same.

Gas	n	$\left((n^2-1)/(n^2+2)\right)^2$
Air	1.000274	3.34×10^{-8}
Hydrogen	1.000122	6.61×10^{-9}
Helium	1.000033	4.84×10^{-10}

In the general theory, the index of refraction can be complex and is expressed $n = n_r + i\,n_i$. The real term is the familiar $n_r = c/v$ where c is the speed of electromagnetic radiation in vacuum and v is its speed in the medium of interest. The imaginary term n_i is non-zero for absorbing materials. Values for the index of refraction of aerosols typically found in the atmosphere [4, 5] are given below.

Medium	Index of refraction
Water	1.333
Inorganic materials	1.45 – 1.6
Crystalline aerosols	1.48 – 1.64
Soot aggregates	1.56 + 0.47i

2.3. Wavelength

In the Rayleigh regime, the intensity of scattered radiation from small particles falls off like $1/\lambda^4$. Thus short wavelength radiation is scattered more efficiently than long wavelength radiation. In the Mie regime, the wavelength dependence is flatter.

The influence of particle size on the type of scattering that occurs is illustrated beautifully in nature every day. Sunlight consists of all the colors of the rainbow – red, orange, yellow, green, blue, and violet. Viewed together, these different colors are perceived as white light. When the sun's light travels through the atmosphere, it scatters off of molecules and aerosols. Because air molecules are very tiny ($a \sim 0.00015\mu m$), they scatter the shorter wavelength blue light ($\lambda \sim 0.4\mu m$) more readily than the longer wavelength red light ($\lambda \sim 0.7\mu m$). Thus when you look at the clear sky in a direction other than toward the sun, you are observing blue light that originated with the sun but that was scattered toward you by air molecules.

Clouds contain water droplets that are large relative to the wavelength of visible light. The water droplets scatter all wavelengths of the incident sunlight approximately equally. When you look at a cloud, you see the combined scattered light from many water molecules. This scattered light consists of approximately equal quantities of all the different colors of light and thus our mind perceives the cloud to be white. The same is true of fog and smoke.

The sun appears redder when it is near the horizon than it does when it is higher in the sky. This is because when the sun is low on the horizon, its light must travel through a longer path length of atmosphere than when it is higher in the sky. By the time the sun's light reached the observer, the shorter wavelengths (violet, blue, green) of light have been scattered out, leaving only the longer wavelengths (reds, oranges, yellow).

2.4. Scattering Angle and Particle Size

Rayleigh scattering varies with scattering angle, $I \propto 1 + \cos^2\theta$. Thus, the scattered radiation has its greatest intensity in the forward ($\theta = 0°$) and backward ($\theta = 180°$) directions. The forward direction is the

direction of propagation of the incident wave. The minimum intensity is found perpendicular to the direction the incident wave was traveling. This scattered radiation is polarized with the greatest polarization also occurring perpendicular to the direction of propagation of the incident wave.

Mie scattering is a more complicated function of scattering angle. The scattered intensity becomes more and more strongly forward scattered as the particle size increases. Furthermore, the angular dependence of the scattering pattern varies as the particle size varies. The dependence of polarization on angle also changes with particle size. Thus the scattered intensity from an ensemble of aerosol particles of varying sizes will be less polarized than the scattered intensity from molecules of air. If you put on Polaroid sunglasses that block out the light polarized in one direction, the intensity of the blue sky will diminish more than the intensity of the white clouds.

3. INSIGHTS FROM RUNS OF A MIE SCATTERING CODE

The simulated results in this section were obtained by running the Mie scattering code of Barber and Hill [6] for spherical particles. This Mie code was used to compute the intensity as a function of size parameter $q = 2\pi a/\lambda$ for the case of backscattering $\theta = 180°$ and parallel incident polarization. In the case of backscattering, the results are the same for the perpendicular incident polarization as for parallel incident polarization. From these results, the relationship between backscattered intensity and wavelength can be computed for any particle size. Figure 1 shows this relationship for a particle of radius $a = 0.0001\square m$, approximately the size of an air molecule.

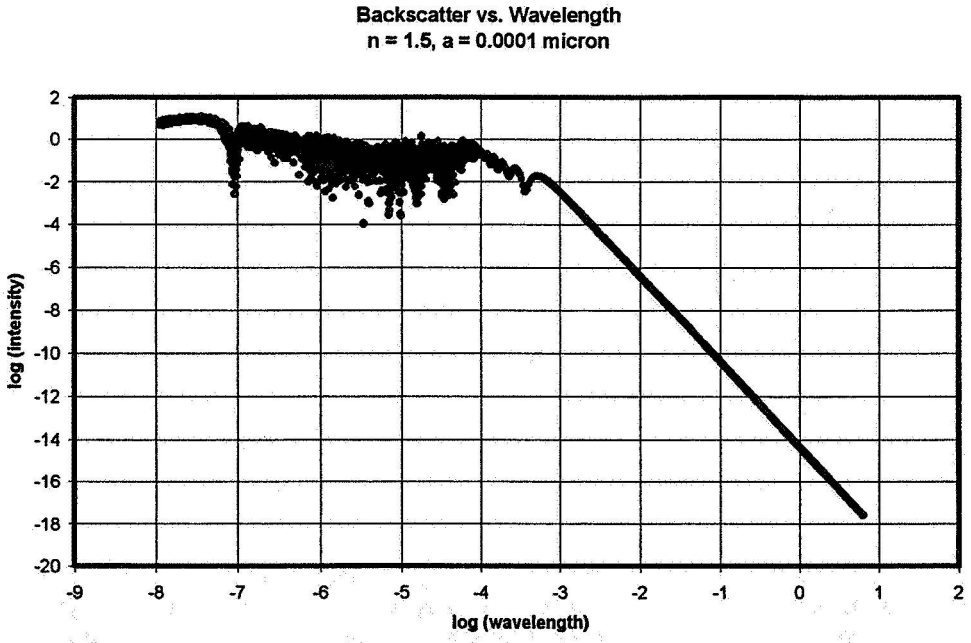

Figure 1: Backscatter as a function of wavelength for a particle with radius a = 0.0001□m.

In Figure 1, the intensity follows the Rayleigh relationship ($I \propto \lambda^{-4}$) when the wavelength is large compared to the radius of the particle or, equivalently, the radius small relative to the wavelength ($a < \sim 0.1\lambda$, $\log q < 0$ or q < 1). For larger particles ($a > \sim 0.1\lambda$, $\log q > 0$ or q > 1), the intensity-wavelength relationship is much flatter as expected for Mie scatter. For an air molecule with a radius of ~0.0001 □m, the intensity follows Rayleigh's Law in the visible part of the spectrum ($0.40\mu m < \lambda < 0.70\mu m$, $-0.40 < \log\lambda < -0.15$), scattering blue light much more readily than red light.

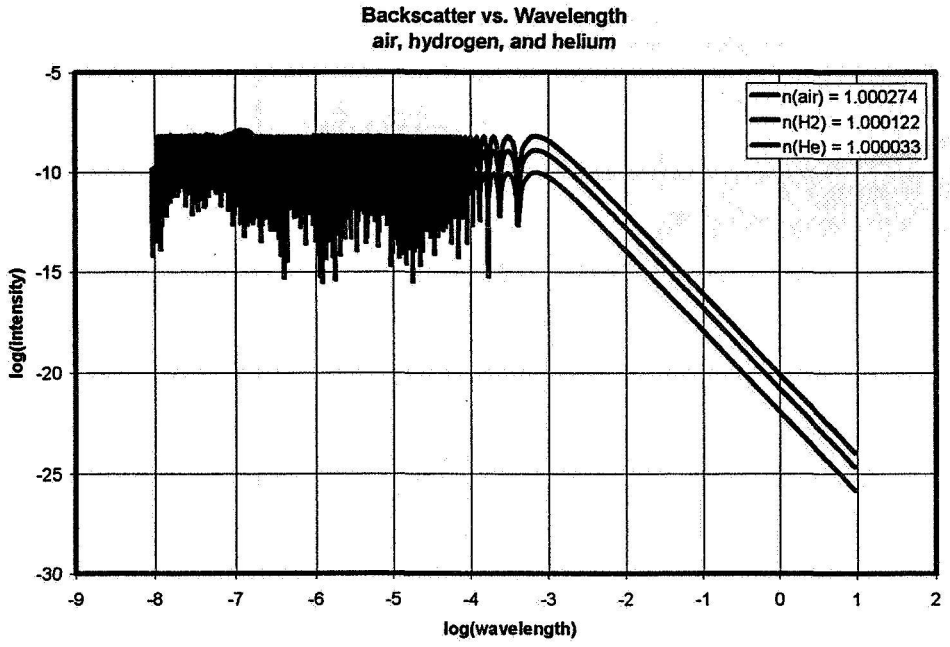

Figure 2: Backscattered intensity as a function of wavelength for air, hydrogen, and helium.

Shown in Figure 2 are the results from the Mie scattering code using the refractive indices for air, hydrogen, and helium. Note that in the visible part of the spectrum, the intensity indeed increases with increasing index of refraction as expected from the relationship $I \propto ((n^2-1)/(n^2+2))^2$. Comparing the intensity for air and the intensity for helium using this relationship gives the following.

$$\frac{I(n_{air}=1.000274)}{I(n_{He}=1.000033)}=\left(\frac{(n_{air}^2-1)/(n_{air}^2+2)}{(n_{He}^2-1)/(n_{He}^2+2)}\right)^2=\left(\frac{(1.000274^2-1)/(1.000274^2+2)}{(1.000033^2-1)/(1.000033^2+2)}\right)^2=68.9$$

The Mie scattering code gives the same ratio in the Rayleigh regime. For example, at $\lambda = 0.550\mu m$, the code gives the following simulated result.

$$\frac{I(n_{air}=1.000274)}{I(n_{He}=1.000033)}=\left(\frac{9.44976\times10^{-20}}{1.37126\times10^{-21}}\right)=68.9$$

In Figure 3, the results from the Mie scattering code for various aerosol refractive indices are shown. The five curves in this figure are for $n = 1.33$, 1.5, 1.7, $1.5+0.1i$, and $1.5+0.5i$. These five refractive indices cover the range of values expected for aerosol particles in the atmosphere [4, 5]. The first value ($n = 1.33$) is appropriate for water droplets in clouds and fog. The value $n = 1.5$ is commonly used in simulations for aerosol particles.

Comparing the curves for the real refractive indices reveals that the larger the refractive index, the steeper the slope in the Mie regime. Thus particulates with larger indices of refraction will scatter blue light slightly more readily than red light even in the Mie regime. Clouds composed of water molecules with small refractive indices ($n = 1.33$) scatter rather independently of wavelength in the Mie regime. Clouds therefore appear white.

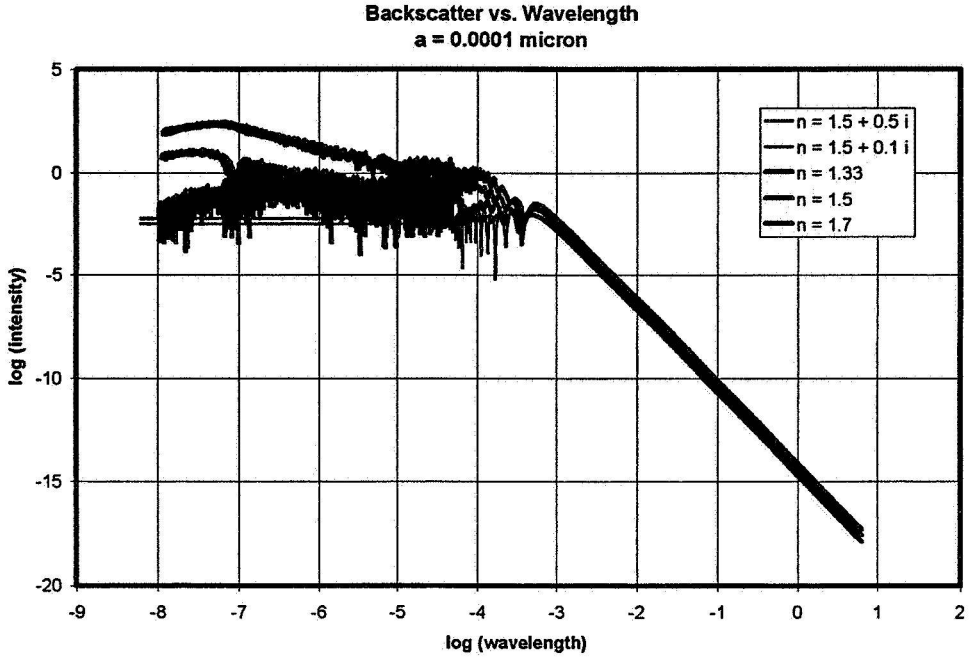

Figure 3: Relationship between backscattered intensity and wavelength for particles of various refractive indices.

4. PARTICLE SIZE DISTRIBUTION

Increasing the particle size by a factor of ten has the effect of shifting the curve horizontally toward higher wavelengths by a factor of ten. Particles smaller than ~0.1μm contribute to Rayleigh scattering in the visible part of the spectrum (*-0.40 < log λ < -0.15*), whereas those with larger radii contribute to Mie scattering. The particle size distribution for the medium through which the radiation is traveling is required in order to determine the total backscattered intensity

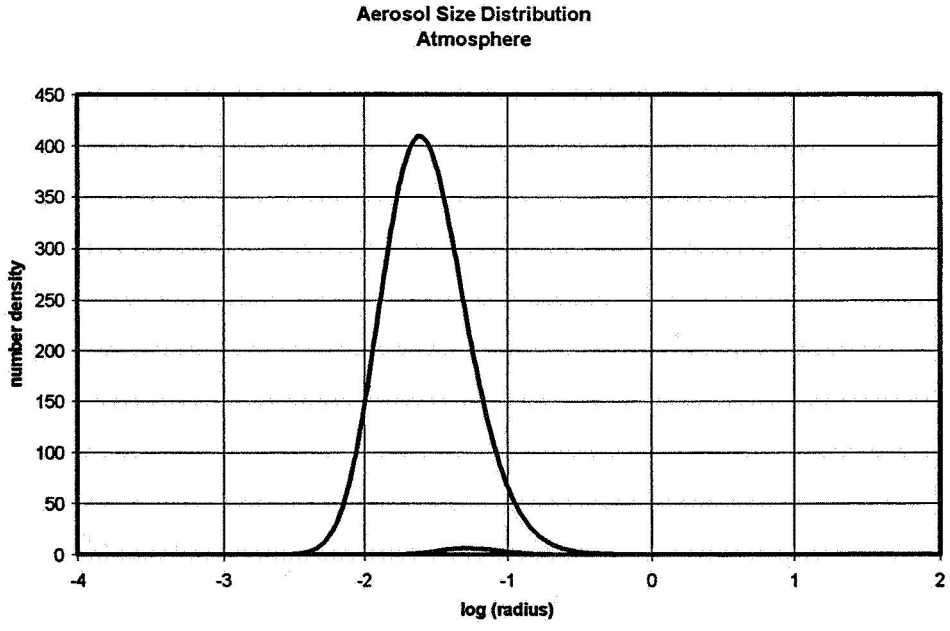

fr om an ensemble of particles of various sizes.

Figure 4: Particle Size Distribution for Continental Aerosols.
The particle size distribution is the number density of particles within a given range of sizes. This is a difficult entity to pin down. For outdoor applications, the particle size distribution will change due to the influence of weather, human activity (fires, for example), and season (springtime pollen, for example). For clean room environments, it is controlled within a range of particle sizes though not fully defined for all particle sizes.

Figure 4 shows the particle size distribution for continental aerosols [7]. This particle size distribution was used to compute the relationship between backscattered intensity and wavelength for the ensemble of particles in the air shown in Figure 5. Similar simulations were run using the particle size distribution in maritime [5] and clean room [8] conditions. The distributions for these latter two cases lack information about the number density of small particles and thus results based on these distributions are uncertain.

5. SIMULATIONS OF THE BACKSCATTERED INTENSITY FROM AN ENSEMBLE OF PARTICLES

To determine the backscattered intensity from an ensemble of particles, the backscattered intensity as a function of wavelength is determined for each particle size. Each of these is multiplied by the number density of particles having that size. At each wavelength, the total intensity contributed by all particles of each size is then summed to give the ensemble, backscattered intensity as a function of wavelength.

The ensemble result for unconditioned air having the continental aerosol content of Figure 4 is shown in Figure 5. It was obtained by summing the contribution from 600 particle sizes ranging over 6 orders of magnitude from $a = 0.0001\mu m$ to $a = 100\mu m$. The ensemble result was computed to be valid only for wavelengths within the range $-2 < \log \lambda < 1$. Only this wavelength range is shown in Figure 5. In this wavelength range, there is a contribution to the backscattered intensity from all particles sizes. The visible part of the spectrum ($-0.4 < \log \lambda < -0.15$) is included in the valid range.

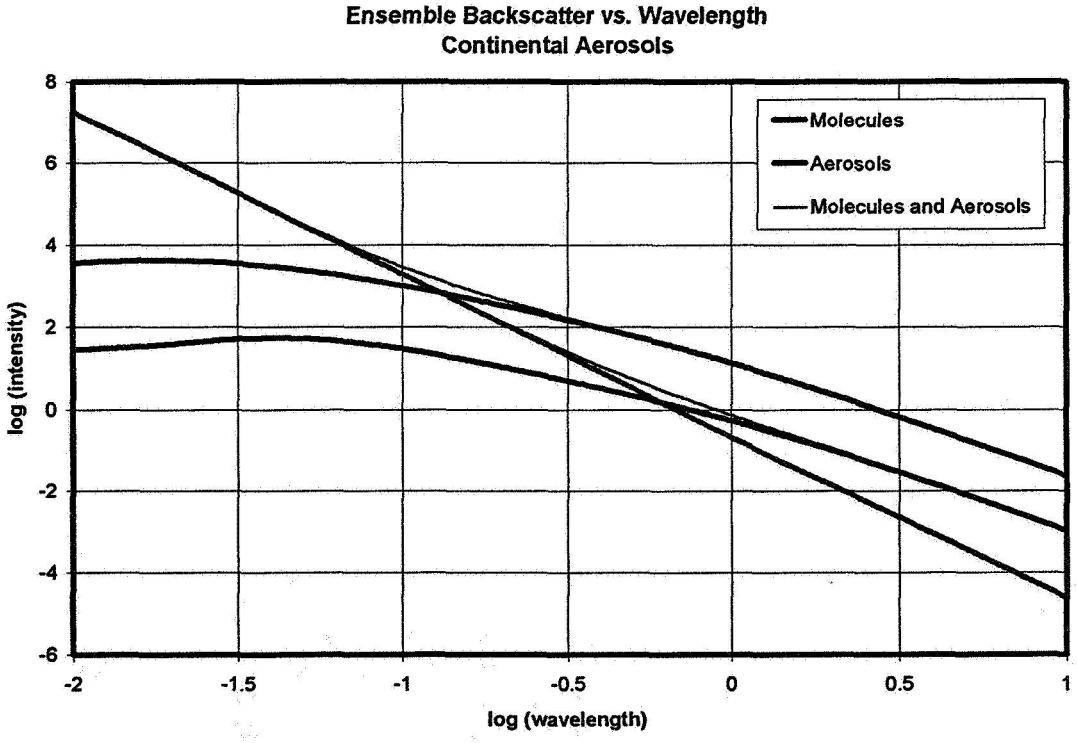

Figure 5: The backscattered intensity as a function of wavelength computed using the continental aerosol particle size distribution.

The thick black curve shows the contribution from the air molecules alone, without aerosol particles. A radius of 0.00015□m was used for the size of an air molecule and a number density of 2.5×10^{19} molecules/cm^3 was used for the density of air molecules in the atmosphere. The molecules exhibit Rayleigh scatter ($I \propto \lambda^{-4}$) over the valid wavelength range.

The gray curves show the contribution from the aerosol particles in the continental atmosphere. The upper curve represents the result when the atmospheric aerosol content is high and the lower curve represents the result when the aerosol content is low. The thin black curves represent the ensemble results for which both molecules and aerosol particles contribute.

When the aerosol content is low, the Rayleigh backscatter from molecules equals the backscatter from aerosols at a wavelength of ~0.6□m (*log* $\lambda \sim -0.22$) in the visible part of the spectrum. Furthermore, the total backscatter from molecules and aerosols (the lower thin black curve) is dominated by Rayleigh scatter from molecules for wavelengths less than ~0.288□m (*log* $\lambda \sim -0.54$). Unfortunately, this is in the ultraviolet, not visible, part of the spectrum.

When the aerosol content is high, Rayleigh backscatter from molecules equals the backscatter from aerosols at the ultraviolet wavelength of ~0.132□m (*log* $\lambda \sim -0.88$). The total backscatter from molecules and aerosols (the upper thin black curve) is dominated by Rayleigh scatter from molecules for wavelengths less than ~0.1□m (*log* $\lambda \sim -1$). At all visible wavelengths, the total backscatter is dominated by the scatter off of aerosol particles.

Note that for wavelengths less than ~0.1□m, variations in aerosol content have no significant effect on the total backscattered radiation. Unfortunately, the atmosphere is not transparent to these wavelengths and thus the Rayleigh Intensity technique would not work for detecting gas leaks in air.

Because the contribution from aerosols dominates the backscattered intensity when the aerosol content is high, a change in the backscattered intensity due to the addition of a leaking gas is unlikely to result in a significant variation in the backscattered intensity. It may be possible, however, to detect a significant variation in the backscattered intensity if the leaking gas causes a significant displacement of aerosols near the site of the leak. It will be difficult to distinguish between variations due to leaks and variations due to naturally changing aerosol content however. Figure 5 shows that the expected variations in the aerosol content of continental air would result in an order of magnitude variation in the total backscattered radiation from a laser operating in the visible part of the spectrum. Such variations in the aerosol content may mask variations due to hydrogen or helium leaks. A possible solution may be to scan the laser over a region and look for localized reductions in the backscattered intensity.

Because KSC and CCAFS are on the coast, simulations were run using the particle size distribution for maritime aerosols. Unfortunately, the lack of information on the small particle size distribution leads to uncertain results for the backscattered intensity. If one makes the assumption that the size distribution for the smaller particles is similar to that for continental air, the conclusions found for continental air would hold for maritime air as well.

Finally, simulations were run using the particle size distribution for clean room conditions. Again, the particle size distribution for these conditions is incomplete, failing to show the number density of the smaller particles. The results for clean room conditions are therefore uncertain. According to Stowers [8], the filters that condition the air for clean rooms have a harder time filtering particles with radii ~0.25□m than either larger or smaller particles. Thus, it may be that the number density of smaller particles is lower than for the same sized particles in unconditioned air. If the particle size distribution of Stowers [8] can be extrapolated to particles with radius $a = 0.01$□m, simulations indicate the backscattered intensity for Class 1 – 1000 clean rooms would be dominated by scatter off of molecules at visible wavelengths and thus the Rayleigh Intensity technique might be viable in those conditions. It might even be viable in Class 10,000 clean rooms, since the molecular contribution to the backscatter is significant in those conditions as well.

6. COMBINED RAYLEIGH INTENSITY AND RAYLEIGH DOPPLER TECHNIQUES

Even if the backscattered intensity is dominated by scattering off of aerosols, it should be possible to determine the contribution from Rayleigh scattering off of molecules using the Rayleigh Doppler technique. A high technology company, Ophir Corporation, is developing what it calls a Rayleigh/Mie Lidar system to replace the pitot tubes on aircraft and thus reduce their radar cross-sections. This technique makes use of the backscattered intensity from a laser that samples the air to determine things such as airspeed, pressure, and temperature. Both the backscattered Rayleigh signal from molecules and the backscattered signal from aerosols are detected.

In an experiment carried out in a Denver, Colorado laboratory (altitude ~5300ft), a laser with a wavelength of 852nm (0.852μm) was used to produce the Ophir Corporation's experimental results shown in Figure 6 (private communication from Martin O'Brien, Ophir Corporation, Denver, CO). This wavelength is in the infrared part of the spectrum. The random motion of the molecules Doppler shifts the backscattered radiation, thus spreading the signal out over a range of frequencies centered on the frequency of the laser. The greater the average speed of the particles, the broader the peak will be.

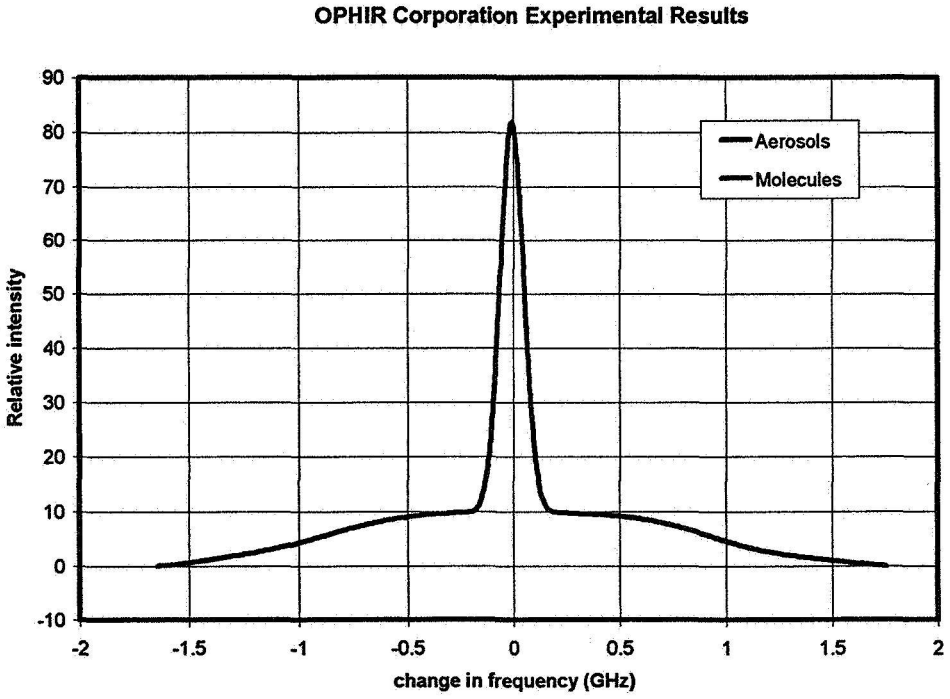

Figure 6: Results from an Ophir Corporation experiment for their Rayleigh/Mie Lidar system. (See http://www.ophir.com/rayleigh_mie_optical_data.htm for more information)

Figure 6 shows the backscattered intensity as a function of the shift in frequency. The curve has two components. The sharp, narrow peak is due to backscatter off of the larger, slower aerosol particles. The shallow, broad peak is due to backscatter off of the smaller, faster air molecules. Thus, despite the apparent strength of the aerosol component, the Rayleigh component can be identified. Integrating under the two peaks gives the backscattered intensity due to each component. When this is done, it turns out that the Rayleigh backscattered intensity from molecules is about twice the backscattered intensity from aerosols. It is interesting that at infrared wavelengths, the integrated Rayleigh signal from molecules is stronger than the integrated signal from aerosols. Extrapolating to half the experimental wavelength indicates that at 0.426□m, the backscattered intensity due to molecules would be anywhere from 4 – 16 times the backscattered intensity due to aerosols. The Ophir Corporation experimental results indicate that it is possible to distinguish between molecular and aerosol backscatter and thus it may be possible to monitor the molecular backscatter for changes due to gas leaks even when there is strong aerosol backscatter.

7. CONCLUSIONS

Application of the Rayleigh Intensity technique toward detection of hydrogen and helium leaks will be problematic in unconditioned (outdoor) air. When the aerosol content in the atmosphere is high, the leaking gas itself will not result in significant variations in the backscattered radiation since the backscattered radiation is dominated by scattering from aerosol particles. However, the leaking gas may displace aerosol particles near the leak and thus result in a decrease in the backscattered intensity. The normal variation of aerosol content in the atmosphere will also result in significant variations in the backscattered intensity of light. To distinguish this normal variation from that due to a leak will be challenging. Perhaps scanning the laser over an area and noting localized decreases in the backscattered radiation would make it possible to locate a leak.

Because the particle size distribution for clean room conditions is incomplete, it is unclear whether the Rayleigh Intensity technique would be a viable technique in those conditions. If the particle size distribution of smaller particles can be considered an extrapolation of the large particle distribution to a radius of 0.01□m, simulations indicate the technique will be viable for Class 1 – 1000 clean rooms at all visible wavelengths and for Class 10,000 clean rooms for wavelengths shorter than ~0.5□m. If the particle size distribution of smaller particles is the same as for unconditioned air, then the conclusions for unconditioned air apply. Further work to pin down the particle size distribution for small particles is indicated to eliminate uncertainties caused by the incomplete data available.

Experimental evidence has been presented indicating that it is possible to isolate the molecular contribution to the backscattered intensity from the aerosol contribution using another remote sensing technique, the Rayleigh Doppler technique. The variation in the Rayleigh scatter by molecules could then be monitored for changes due to leaks. It would be beneficial to determine the range of ratios of $I_{Rayleigh}/I_{Mie}$ over which it would be possible to distinguish between the molecular and aerosol components.

REFERENCES

[1] Mie, G, *Ann. d. Physik (4)*, 25, (1908), 377

[2] Born, Max and Wolf, Emil, *Principles of Optics. Electromagnetic Theory of Propagation, Interference and Diffraction of Light, 5th edition*, Pergamon Press, Oxford, (1975)

[3] Lang, Kenneth R., *Astrophysical Formulae*, Springer-Verlag, New York, (1980)

[4] Mészáros, Ern□, *Fundamentals of Atmospheric Aerosol Chemistry*, Akadémiai Kiadó, Budapest, (1999)

[5] McCartney, Earl J., *Optics of the Atmosphere. Scattering by Molecules and Particles*, John Wiley & Sons, New York. (1976)

[6] Barber, P. W. and Hill, S. C., *Light Scattering by Particles. Computational Methods*, World Scientific, New Jersey, (1990)

[7] Israël, H. and Israël, G. W., *Trace Elements in the Atmosphere*, Ann Arbor Science Publishers, Inc., Ann Arbor, Michigan, (1974)

[8] Stowers, Irving F., *SPIE*, 3782, (1999), 525-530

2001 NASA/ASEE SUMMER FACULTY FELLOWSHIP PROGRAM

JOHN F. KENNEDY SPACE CENTER
UNIVERSITY OF CENTRAL FLORIDA

KSC HISTORY PROJECT

Henry C. Dethloff
Professor Emeritus
Department of History
Texas A&M University
KSC Colleague: C. Shannon Roberts, Ph.D.

ABSTRACT

The KSC History Project focuses on archival research and oral history interviews on the history of Kennedy Space Center (KSC). Related projects include the preparation of a precis and chapter outline for a proposed book-length narrative history, a bibliography of key primary and secondary resources, a brief monograph overview of the history of KSC, and a monograph on the history of safety at the Center. Finally, there is work on the development of a web page and a personal history data base associated with the oral history project. The KSC History Project has been a joint endeavor between Henry C. Dethloff and Dr. Noble Lee Snaples, Jr.

KSC HISTORY PROJECT

Henry C. Dethloff

Introduction

John F. Kennedy Space Center, organized as an independent National Aeronautics and Space Administration (NASA) Launch Operations Center on March 7, 1962, is strategically situated at the apex of NASA's programs for the exploration and development of space. *Liftoff* at KSC is the most important and visible milestone in NASA space program development. Because Kennedy Space Center has been so omnipresent in the total story of NASA and space exploration, it, perhaps more so than other NASA Centers has been in the focus of the national (and global) media and press. A public presence has affected its history more so than that of other NASA facilities. External and public relations, a stress on safety, and on accommodating and educating the media, NASA's customers, and the general public have been an integral part of KSC's history.

KSC has been on the verge of NASA's interface with other NASA Centers. KSC has an historical interface with the Air Force and other government agencies and has pioneered in creating an integrated space community. KSC also has been on the leading edge of NASA's interrelationships with international partners and associates, and with the broader global community. And KSC has pioneered in NASA's changing relationships with its contractors, and with the private sector and NASA payload and launch customers.

John F. Kennedy Space Center has a very rich and complex history which considerably predates its founding, and which, in many ways is integral to the historic role of Cape Canaveral as a milepost and way station by which Western civilization came to the New World. As Cape Canaveral became a milepost and a way station in the European exploration of the New World five hundred years earlier, Cape Canaveral's Kennedy Space Center has become Earth's stepping stone and way station to space.

An Historical Overview

Cape Canaveral, a protrusion of land from the Florida peninsula into the Atlantic first encountered by European explorers about 1500, became a milepost and a way station for the European discovery and exploration of the New World. Half a century later the Cape resumed that role as a milepost and a way station in the new age of Off-World planetary discoveries and the exploration of space. "Space," commented Kennedy space Center's first center Director, Kurt Debus, perhaps reflecting on the common heritage of the New World explorers and those engaged in space and planetary exploration, "is not something new. It's part of the total environment, and we've been looking for the total environment ever since we looked out of caves at the stars." Ponce de Leon, who explored the area around Cape Canaveral in 1513, and multitudes of aerospace engineers, scientists, technicians, administrators, businesses, and their associates throughout the old world and the new, through NASA, the National Aeronautics and Space Administration, share a common bond in the continuing exploration of the total human environment.

First organized in December 1959, as the Launch Operations Directorate under the authority of the Marshall Space Flight Center located in Huntsville, Alabama, NASA's John F. Kennedy Space Center became the Launch Operations Center at Cape Canaveral on March 7, 1962. Twelve years earlier, in July 1950, an Army rocket team launched the first long-range missile, utilizing a refined version of a German World War II era V-2 rocket and a second-stage American WAC (Without Any Control)-Corporal rocket from Cape Canaveral. By the close of the decade American space vehicles, fired from the Cape, had taken the United States through the threshold of space. Just as Cape Canaveral was geographically situated to mark the way for the European exploration of the Americas, so the Kennedy Space Center is strategically situated at the apex of NASA's programs for the exploration and development of space. Earth and Space sciences and aero-space technology, new ideas, and new products, are incubated in the intricately-meshed management teams of NASA Centers and Laboratories, and in the laboratories and offices of their contractors from industry and academia. Those ideas, the space flight vehicles and missions, the Earth and Space science laboratories, and their accompanying designs, innovations, and inventions are then "hatched" or tried and tested, as it were,

under the management and direction of Kennedy Space Center. "Liftoff," at KSC is the most important and visible milestone in NASA space program development.

The history of Kennedy Space Center revisits the story of the inception of an American space program and the creation of NASA, and provides a new understanding of those remarkable events. It examines for the first time the unique relationship between KSC and the other NASA centers, and between KSC and other agencies engaged in space related activities, including the Department of Defense, the Army, the Air Force, and the Navy. This is the story, for the most part, of the men and women who managed the fantastically complicated send-offs of the launch vehicles and payloads designed and manufactured by American, and indeed, by the developing international aero-space, science, engineering, and space exploration community-and made them work.

It is the story of the Atlantic Missile Range and early experiments with long-range missiles, and of American successes and failures in early piloted flight. It is the history of Apollo and the lunar landings, now more than a quarter-century past. Including Apollo 7 and 8, there were eleven piloted Apollo missions. Nine of those went to the vicinity of the Moon. Six of those landed astronauts on the Moon. The Kennedy Space Center's role and mission in those endeavors had to do with assembling, testing, and validating the flight ready status of each of the diverse components of the Apollo systems: the three-stage rocket boosters, command module, service module, lunar module, communications systems, fuel systems, and the crew. As one of the engineers explained: "We had to take it all and put it together and make it work." That is what Kennedy Space Center was all about.

The narrative focuses heavily on the new, post-Apollo, Space Transportation System which, since the first flight of the Shuttle in April 1981, by the turn of the 21st Century had flown over 100 missions in space. Over the next two decades NASA launched over one-hundred Space Shuttle missions, each originating from KSC's Launch Complex 39, and each extending our information and knowledge of Earth's environment, and extending the human presence in space. There were, to be sure, some missions that were more notable and memorable than others. STS-7, which left Kennedy on June 18, 1983, carried Sally Ride, the first American woman in space. STS-9, launched in November 1983, carried aboard the first European-built Spacelab containing seventy-one experiments, and a West

German physicist—the first non-U.S. citizen to fly aboard an American spacecraft. STS 41-C performed the first space satellite repair. The first seven-member crew flew in October 1984. The Shuttle enabled the delivery of more communications satellites into orbit. More space walks (EVAs or extravehicular activities) became the norm. The Shuttle began a series of Spacelab flights in 1983, focusing on the conduct of multi-disciplinary Earth-science experiments by scientists and payload specialists from the United States, Great Britain, and Germany. The frequency of Shuttle flights rose. And then, on January 28, 1986, after twenty-four safe and successful Shuttle launches, *Challenger* exploded seventy-three seconds after liftoff. The entire crew, including Francis R. Scobee, Michael J. Smith, Ellison S. Onizuka, Judith A. Resnik, Ronald E. McNair, Gregory Jarvis, and Christa McAuliffe died. It was one of Kennedy Space Center's, NASA's, and the nation's "worst days." Throughout the organizaton there were studies, investigations, and reviews. KSC began a rebuilding, and a restoration. The Center reconstituted its tests and check-points to improve already tough quality controls, and to provide greater assurance and safety. *Challenger* was both an agonizing, and a learning experience.

Finally, almost three years after the *Challenger* explosion, on September 29, 1988, the twenty-sixth Shuttle flight, now appropriately designated STS-26, left the Cape on a mission to prove the safety of the redesigned Solid Rocket Boosters, and to launch a TDRS (Tracking and Data Relay) satellite. The American public, and the world watched carefully this "return to flight." Over 2,000 media representatives were on hand for the launch, as compared to the 2-300 who had been present for the *Challenger* launch. NASA's focus, and that of the media and the public, remained on the Shuttle and on Kennedy Space Center. In June 1995, NASA celebrated the 100th U.S. human space flight with the launch of *Atlantis* (STS-71). Perhaps even more significantly, *Atlantis* docked for five days with the Russian space station *Mir,* marking the extension of international cooperation in the exploration and utilization of space that had begun earlier under Skylab, Apollo-Soyuz, and Spacelab programs. In October 2000, Space shuttle *Discovery* flew the 100th Shuttle mission, all substantially expanding human understanding of space, the Solar System, and most especially knowledge of planet Earth and its

environment. Space, as Dr. Kurt H. Debus, Kennedy Space Center's first director pointed out, is but a part of the total human environment.

The assembly of an International Space Station, beginning with the delivery of a 20-ton Russian Zarya module in June 1998, followed by the STS-88 delivery in December of a Unity connecting module marked the inception of a sustained international program for living and working in space. Over the next few years, the International Space Station began to assume form and content. The addition of a joint air-lock module by STS-104 in July 2001, enabled station inhabitants to conduct space walks and to function independently over an extended time without the supplementation of the Space Shuttle. KSC is integral to the inception and development of the International Space Station, which promises to give not just Americans but the people of Earth a more permanent presence in space–that "extended environment of Earth"–well into the new millennium. In addition, KSC is NASA's lead center for the acquisition and management of Expendable Launch Vehicle launch services, so essential to the maintenance of a continuing off-world presence. Living and working in space had become a part of the human experience in the 21st Century.

And because Kennedy Space Center has been so omnipresent in the total story of NASA and space exploration, it, perhaps more so than other NASA Centers has been in the focus of the national (and global) media and press. That has created unique management problems, situations, and opportunities at KSC. A "public" presence has affected its history more so than that of other NASA facilities. External and public relations, a stress on safety, and on accommodating and educating the media, NASA's "customers," and the general public, have been an integral part of KSC's history. As Cape Canaveral became a milepost, a way station in the European exploration of the New World five hundred years earlier, Cape Canaveral's Kennedy Space Center has become within the past half-century our stepping stone, a literal launch pad, a way station in the exploration of space. Liftoff is the most critical event in the history of space exploration.

Chapter Outline: 3,2,1...Liftoff: A History of Kennedy Space Center

Dethloff and Snaples prepared a brief outline for a proposed narrative history of Kennedy Space Center which would produce a manuscript of thirteen chapters and approximately 520 pages of text plus front and end matter (bibliography and appendices), that would emphasize and develop the themes described in the historical overview. The only published histories of Kennedy Space Center include a text by Charles D. Benson and William B. Faherty entitled *Moonport: A History of Apollo Launch Facilities and Operations* (NASA SP-4204) published in 1978, and closely tied to the Apollo/Saturn lunar program. The book has recently been republished in two volumes by the University Press of Florida, without revision or update. The second publication is the NASA Public Affairs title: *The Kennedy Space Center Story*, published in 1991. A comprehensive, readable, narrative history designed for a general public audience, and technically credible and accurate is believed to be a critical requirement as KSC completes is first four decades of operation. Such a book, it is believed, will provide a useful management tool for NASA scientists, engineers, and managers, and help significantly in the education and edification of the American and global public regarding NASA, Kennedy Space Center, and space exploration.

***

3,2,1...Liftoff: A History of Kennedy Space Center

CONTENTS

C. New Construction/Expansion
D. Designing for Lunar Launch
1. Overview: KSC and Launch Complex 34, 37, and 39

Chapter IV. The Flight of Apollo
A. Apollo Missions to Apollo 17 (1972): Overview
B. KSC and Center Interface/interactions
C. AS 204/ Safety and the Human Factor
D. Focus: KSC and Apollo 8, 10, 11, 17

Chapter V. Post Apollo
A. Skylab
B. Apollo-Soyuz
C. Lee R. Scherer: Review/Redirection/KSC Plans and Programs
D. KSC And the Changing Dimensions of Space Exploration

Chapter VI. A Space Transportation System
A. The Case for a Reusable Space Vehicle
1. The ELV and the Shuttle
B. Shuttle Design and Development
C. Re-Engineering KSC's Launch facilities and operations
1. Richard G. Smith
D. Conversion: Launch Complex 39
1. VAB/Crawler/Mobile Launcher
2. Orbiter Processing Facility/Shuttle Landing Facility
3. Launch Processing System

Chapter VII. The Shuttle Takes Flight
A..STS-1 through STS-51L: Overview of STS History to 1990
1. Focus on: STS-1, STS-5, STS-41
B. Challenger (STS-51L)
C. In the Aftermath of Challenger
1. Forrest S. McCartney/KSC Reforms and Reorganization
2. The Safety Factor
D. A NASA Reappraisal/RIFs
1. The KSC/Canaveral Community

Chapter VIII. Living and Working in Space
A. Earth and Planetary Sciences and Investigations
1. Payloads and Payload Specialists
B. STS-26>35
C. Hubble/Remote Manipulation Arm/Spacelab Module
D. The Growing Public Presence at KSC
1. KSC/NASA/Public Education and the Media

Chapter IX. Countdown
A. KSC/STS in the Nineties [Overview of 50 flights]
B. A Changing Dynamics in Space
1. Capt. Robert L. Crippen, 1992-1995
2. Jay Honeycutt, 1995-1997
C. Earth and Planetary Science Missions
1. Focus on STS-41; STS-71
D. Mir Missions/ESA/Japan/Canada

Chapter X. KSC and The Internationalization of Space Exploration
- A. Reflections on the Cold War
- B. Global Communications Systems
- C. MIR Missions
- D. European Space Agency/ESA/Japan/Italy/Canada/China/The Americas

Chapter XI. The International Space Station
- A. Conceptual Development
- B. Political and Financial Evaluations
- C. The Contractors'Payloads/Assembly
- D. Mission Plans and Projections

Chapter XII. . The Role of the Expendable Launch Vehicle
- A. A Brief History of ELV Since 1960
- B. Reusable vs. Expendable
  - 1. Cost considerations and evaluations
- C. NASA Plans and Projects for the ELV
- D. KSC: Lead Center for ELV Launch and Payload Processing

Chapter XIII. Into the 21st Century
- A. Space Spinoffs/Technology/Inventions
  - 1. KSC and Privatized/Commercial Space Initiatives
- B. KSC and the Space Congresses
- C. Roy Bridges/KSC Spaceport Master Plan
  - 1. STS 20th Anniversary/Reflections
  - 2. Space Experiment Research and Processing Laboratory
- D. KSC: A Roadmap to Space Exploration

Oral History Program

In cooperation with Dr. Roger D. Launius, Lisa Malone, Elaine Liston and others, Inteviews of approximately 1-1.5 hours have been completed with each of the following:

Bridges, Roy D., Jr.
Bruckner, Bobby G.
Greenfield, Terry
Harris, Hugh W.
Malone, Lisa A.
Morgan, JoAnn
McCartney, Forrest S.
Page, George F.
Parrish, Alan J.
Rigell, I.A. "Ike"
Sieck, Robert B.
Smith, Richard G.
Solid, L.D. "Lee"
Straiton, John
Thomas, James A. (Gene)

Transcripts of the interviews, and as applicable, video tapes are being supplied by Dynacs, Inc. Copies of the transcriptions will be deposited in the KSC Archives, and in the NASA Historical Records Collections at NASA Headquarters.

KSC and Safety

Dr. Lee Snaples has prepared a brief monograph on the history of Safety at KSC, which explores the development of safety policy and procedures at Kennedy Space Center over the course of its forty-year history. The most remembered space flight accidents, Apollo 1, Apollo 13, and Challenger, are irrevocably linked to KSC in the nation's collective memory. Each of these accidents had led directly to changes in policy, procedure, and organizational structures at KSC. Safety remains a prime consideration in all design, launch, and operations work. In 1997, the Center adopted the DuPont Safety Standards for a universal code of safety.

Database and Web Page

The historians have provided assistances to the KSC Archives in the development of a database and web page that can help in the preservation and dissemination of Kennedy Space Center history. Based on the design of the Ellis Island web page, former KSC employees and those nearing retirement are encouraged to enter pertinent biographical and contact information in an electronic data base, and to recount their favorite or most memorable moments at KSC.

Conclusion

Henry C. Dethloff, with Noble Lee Snaples, Jr. have, under the auspices of the 2001 NASA/ASEE Summer Fellowship, conducted substantive research in the archives and manuscript collections of Kennedy Space Center. They have completed or assisted in the completion of sixteen oral history interviews associated with the KSC History Project. They completed a proposed chapter outline for a comprehensive, readable, and informative narrative history of Kennedy Space Center. Dr. Snaples prepared a brief monograph on the history of safety at KSC, and Dethloff prepared a 50-plus page monograph providing a brief historical overview of the Center that may have use and application in association with KSC's fortieth anniversary which is being celebrated in 2002.

2001 NASA/ASEE SUMMER FACULTY FELLOWSHIP PROGRAM

JOHN F. KENNEDY SPACE CENTER
UNIVERSITY OF CENTRAL FLORIDA

EVALUATION OF DESIGN CONCEPTS FOR COLLAPSIBLE CRYOGENIC STORAGE VESSELS

David C. Fleming
Assistant Professor
Department of Mechanical & Aerospace Engineering
Florida Institute of Technology

Eric A. Thaxton
NASA KSC Colleague

ABSTRACT

Future long-duration missions to Mars using in situ resource production to obtain oxygen from the Martian atmosphere for use as a propellant or for life support will require long term oxygen storage facilities. This report describes preliminary analysis of design concepts for lightweight, collapsible liquid oxygen storage tanks to be used on the surface of Mars. With storage at relatively low pressures, an inflatable tank concept in which the cryogen is stored within a fiber-reinforced Teflon FEP bladder is an efficient approach. The technology required for such a tank is well-developed through similar previous applications in positive expulsion bladders for zero-*g* liquid fuel rocket tanks and inflatable space habitat technology, though the liquid oxygen environment presents unique challenges. The weight of the proposed structure is largely dominated by the support structure needed to hold the tank off the ground and permit a vacuum insulation space to be maintained around the tank. In addition to the inflatable tank concept, telescoping tank concepts are studied. For a telescoping tank, the greatest difficulty is in making effective joints and seals. The use of shape memory alloy to produce a passive clamping ring is evaluated. Although the telescoping tank concepts are a viable option, it appears that inflatable tank concepts will be more efficient and are recommended.

1 INTRODUCTION

Plans for future Mars missions propose using "in situ resource production" (ISRP) plants to obtain oxygen from the atmosphere for use as a rocket propellant and, in the case of manned missions, for life support [1]. Particularly if an extended program of human missions to Mars is begun, it will be necessary to develop oxygen storage facilities on the surface of Mars. For launch from Earth, such storage tanks must obviously be lightweight. In addition, to improve the efficiency of the launch packaging the tank should be collapsible. This report describes the preliminary analysis of various design concepts for collapsible liquid oxygen storage tanks to be used on Mars. Dr. Eric Thaxton and other personnel at NASA Kennedy Space Center developed the foundations for the design concepts. While no specific mission is followed for this design study, the capacity of the tank and other design requirements are loosely based on the oxygen requirements for a manned Mars mission as described in the NASA Reference Mission [1,2]. To the extent possible the work is presented in a general fashion to permit appropriate scaling to be conducted for missions with different requirements. Detail design must wait until a specific mission with specific requirements is planned.

2 PREVIOUS RESEARCH

While there has been a substantial amount of research on ISRP, particularly for oxygen production on Mars and the Moon, relatively little attention has been paid to storage requirements and tankage. The NASA Mars Reference mission [1,2] assumes that produced oxygen will be fed directly into flight tanks on an ascent vehicle. Mueller and Durrant [3] discuss storage issues for a proposed Mars sample return mission using this storage concept. However, if a prolonged series of Mars missions is begun, or for different mission architectures, it may be more efficient to provide long-term storage tanks on Mars separate from vehicle flight tanks. Mars oxygen storage tanks will be substantially different from conventional terrestrial storage tanks or even ordinary flight tanks. However, previous engineering experience with collapsible pressure vessels, lightweight fluid storage tanks and inflatable space structures is relevant to the design of a collapsible cryogenic storage tank for Mars and is reviewed here.

ILC Dover Inc. developed a collapsible hyperbaric chamber with an interior roughly the size of a person, designed for a burst pressure of 6 atm [4]. The design uses a "bladder layer" of urethane-coated polyester to contain the gas with a "restraint layer" made of polyester webbing/polyester fabric to resist the mechanical loads. For mobile, lightweight storage of petroleum products the military uses collapsible bladder tanks. These tanks, made of fabric-reinforced elastomers, take the form of fluid-filled pillows and are available in capacities ranging up to the hundreds of thousands of gallons [5]. Flanagan and Hopkins [6] proposed a similar concept for water storage during human missions to the Moon or Mars. This tank is a simple bladder made of parachute nylon with a plastic liner. A prototype of such a 100 gallon capacity tank weighed about 1 kg (2.2 lb_m). Inflatable space structures using similar principles for containing pressure have been developed or proposed for a variety of applications [4,7]. A recent development in inflatable space habitats is Transhab, developed at JSC and proposed for either long duration space flight or as a space station module [2,4]. Transhab uses triple redundant Kevlar reinforced membranes to form the main pressure barrier and a flexible outer layer for meteor impact protection and insulation. The net thickness of the wall is about one foot. An alternative to inflatables for collapsible space habitats and modules is telescoping rigid structures. Although this concept has not received as much attention as inflatables, at least one NASA design study [8] explored the idea. In this study a two-stage telescoping arrangement for a space station module is proposed.

3 DESIGN FUNDAMENTALS

Barron [9] describes the fundamentals of the design of conventional cryogenic storage vessels. An inner vessel supports the weight of the cryogen and the associated pressure. To insulate the vessel either a vacuum space or vacuum-filled insulation is provided around the inner vessel. An outer pressure vessel contains the vacuum. A suspension system must be provided to hold the inner vessel within the outer vessel while minimizing the heat loss through the insulation space. Supports must be provided to hold the vessel. Finally, the necessary piping and fill lines must be included. Each of these basic tank components must be provided in the Mars liquid oxygen tank. Due to the mission requirements, however, the nature of these components may differ considerably from those of a conventional earth tank. Design requirements for a Mars liquid oxygen storage tank were chosen to provide a basis for evaluation. The tank must be capable of continuous operation for several Earth years and is sized to carry a mass

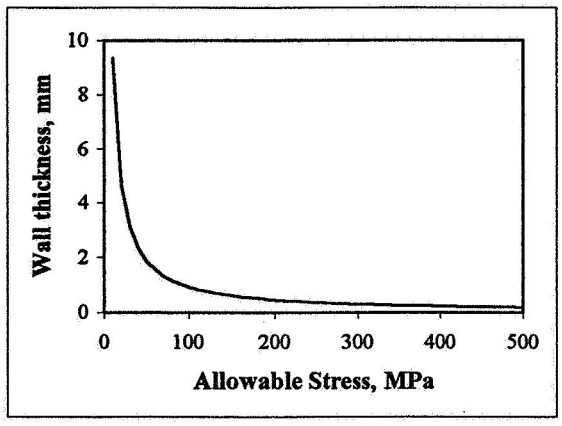

Figure 1 Minimum wall thickness for the inner vessel as a function of the allowable stress

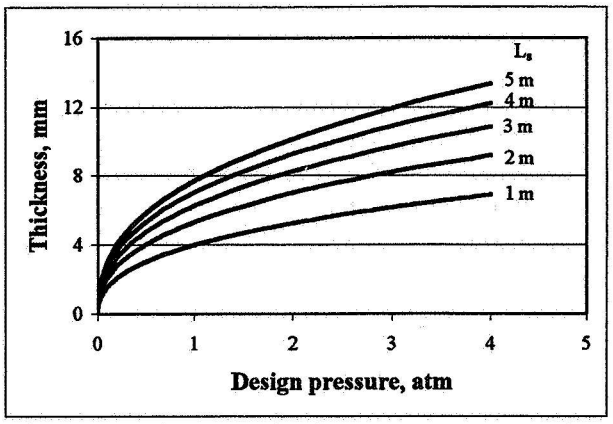

Figure 2 Minimum wall thickness for the outea rigid outer vessel as a function of thee design pressure for various unsupported lengths

of 50,000 kg (110,000 lb_m) of liquid oxygen. The tank will hold a saturated liquid at 79 K (142 R) and 276 millibar (4 psia) ullage pressure. For launch packaging it is assumed an inside diameter for the tank of nominally 10 ft (3m) will be acceptable.

The pressure tank ("inner vessel") will operate under the pressure of the oxygen vapor and the weight of the liquid oxygen. The head pressure of the liquid oxygen is 44.5 millibar per meter (0.197 psi per foot), considering the density at the operating temperature and the reduced gravity of Mars. For typical tank geometries achieving the required volume, the limit pressure is under 700 millibar (10 psi). This relatively low operating pressure of the tank will be a fundamental driver of the designs considered here. Equation 1 is the minimum thickness, t_{min}, based on static strength required by the ASME code [12]. p is the design pressure, D is the diameter of the shell, s_a is the allowable stress and e_w is the joint efficiency (assuming welded joints). Figure 1 shows the required wall thickness

$$t_{\min} = \frac{pD}{2s_a e_w - 1.2p} \tag{1}$$

as a function of the allowable stress for the assumed loading and cylindrical geometry and assuming a perfect joint efficiency. For typical engineering materials the required wall thickness is small, 1 mm (4 mils) or less. These small wall thicknesses are similar to those of flight tanks in early spacecraft, such as the pressure stabilized Atlas vehicle [10]. If the Mars storage tank is built to minimum dimensions it, too, must act as a pressure-stabilized structure, ineffective in supporting out-of-plane stresses that might be experienced while unpressurized. However, since considerable lateral loads may be anticipated during launch and landing it is likely that a rigid walled structure would require additional reinforcement. This would make its weight greater than would be required from the pressure loading alone. A flexible inflatable tank wall avoids this problem and can therefore be designed closer to its optimum weight.

Although the Mars atmosphere exists in a condition that is categorized as "Medium Vacuum" [9], this level of vacuum is insufficient from an insulation standpoint [3,11], and thus high vacuum must be drawn in the insulation space. If this vacuum is drawn on Earth (which would offer significant simplifications in the design of the vacuum system) a rigid outer vessel must support 1 atm of pressure. If vacuum is drawn in space (by venting of the insulation during flight [3]) or on Mars, then only the pressure of the Mars atmosphere (about 12 millibar or 0.2 psi, depending on the location on Mars [12]) must be supported. Required thickness for an assumed cylindrical rigid outer vessel is based on the short cylinder collapse formula shown in Equation 2 [9]. p_c is the collapse pressure, E and ν are the modulus and Poisson's ratio for the assumed isotropic shell, D is the diameter, L is the unsupported length of the cylinder, and t is the wall thickness. For a modulus of 200 GPa (steel), the required thickness is plotted in Figure 2 as a function of the design pressure for various unsupported lengths, L. The required shell thickness to

$$p_c = \frac{2.42E(t/D)^{5/2}}{(1-\nu^2)^{3/4}[(L/D)-0.45(t/D)^{1/2}]} \quad (2)$$

support Earth's atmosphere is over 5 mm for reasonable values of unsupported length and factor of safety. Because the required wall thickness scales approximately as $p^{2/5}$ designing the outer shell to resist only the pressure of Mars results in a factor of 6 improvement in thickness (and therefore weight) of a rigid outer shell with equal unsupported length, L. However, even considering the low surface pressures, a rigid pressure wall for the outer shell is not the most effective design. If the insulating material can react either the full atmospheric pressure of Earth or the slight atmospheric pressure on Mars without damage or reduction in its thermal properties, then the outer wall may be made from a flexible material or a thin foil [3,11]. Not only is this approach very lightweight, it is also very well aligned with the objective of making a collapsible vessel.

Flynn [13] discusses materials for suspension system components. Glass/epoxy composites offer about a factor of 20 improvement over stainless steel in conductivity to strength and about a factor of 4 improvement over stainless steel in conductivity to stiffness. Several applications of composite supports in cryogenic space vehicle tanks are summarized in References 14 and 15. There are two primary configurations for composite supports: struts and straps. Strut supports connect the inner tank to the outer support through pin-ended axial members that can support tension or compression loads. Strap supports operate exclusively in tension. A typical strap design uses two sets of 6 straps pulling in opposing directions. Pretension is included in the straps on installation such that all straps maintain tension throughout the full range of loading. For the collapsible tank concepts studied here maintenance of pretension in the straps is difficult. Also, the need for significant separation between the sets of straps would require excess mass in the support structure. Hence struts are considered exclusively in the designs that follow. Launch and landing loads may be a limiting factor for the suspension system. Lateral loads and g-loading in the vertical direction will be largest during launch or landing. Because of the nature of this study, there is no particular launch vehicle to be considered for the design, nor is the landing method specified. Therefore, launch and landing loads are not specifically addressed. To constrain the tank structure during flight without requiring additional mass in the suspension system, external attachment to the piping structure in the rigid end cap should be used. It is assumed that the tank piping is not connected during flight and adding a temporary mechanical attachment through the piping should not present any serious obstacles. Stabilizing the empty and collapsed structure against damage due to vibration during flight is also a significant concern for launch packaging.

Unfortunately, the tank cannot rest directly on the ground, as do the pillow bladder collapsible fuel storage tanks [5]. Most of the structural mass of the proposed Mars tank designs is associated with the support structure. The support structure must hold the effective weight of the cryogen (190 kN, or 42 kip) above the Martian surface and permit attachment with the suspension system. Installing the tank in a vertical orientation eliminates the bending moments that would be associated with a horizontal orientation and the use of cradle supports. Contact with the surface will be made through leg structures. The use of skirt supports or other vertical tank supports commonly used on Earth is impractical due to the fact that the tank must be placed on an unprepared, rocky surface. Design of the legs is assumed to be essentially similar for all tank concepts and is not addressed in detail. Wind and seismic loads should be considered in the design of support structure for a storage tank design. Although the winds on Mars can be severe, the low density of the atmosphere keeps the dynamic pressure small. A conservative calculation results in a maximum drag on the entire tank of about 900 N (200lb_f). Dynamic effects due to wind loading may be relevant, considering the pressure-stabilized, flexible nature of several of the structural concepts. In the unfilled or partially-filled state wind loading could produce a rippling effect that may degrade flexible materials at cryogenic temperatures. Current scientific belief is that there is some seismic activity on Mars, perhaps more than on the moon but less than on the Earth [12]. Seismic loading is not addressed further in this design study, though future detailed design will need to consider seismic effects.

Two primary concerns relating to material selection for the tank are oxygen compatibility and performance at cryogenic temperatures. Oxygen compatibility is discussed in NSS-1740.15 [16]. Collapsible tank concepts suggest the need to use nonmetallic materials. Although the choices for oxygen compatible nonmetallic materials are

somewhat limited fluorinated polymers, such as Teflon FEP, are acceptable. Ceramics and glasses are considered inert in the oxygen environment. The use of composite materials for liquid oxygen tankage seems problematical because the polymeric materials typically used as matrix materials are flammable and likely sensitive to impact in a liquid oxygen environment. However, there have been some successful developments in the use of composite materials for liquid oxygen tanks either using coatings [17] or proprietary oxygen compatible matrix materials [18]. Typically, the ultimate tensile strength of a solid material increases with reduction in temperature [13]. This trend applies as well to composite materials. Some plastic materials retain ductility at cryogenic temperatures. Among these are several grades of Teflon, including FEP, though their elongation at cryogenic temperatures is nowhere near their room temperature properties. For materials used as a membrane for containing the liquid oxygen or for the vacuum insulation shell, permeability is another important property. Among the fluorinated polymer grades, FEP is recognized as having superior impermeability [19,20]. The inclusion of metallic films in Teflon membranes can improve their permeability [20].

4 INFLATABLE TANK DESIGN

The basic inflatable design concept is illustrated in Figure 3. A pressure membrane with flexible reinforcement contains the liquid oxygen. A flexible vacuum jacket containing insulation covers the outer wall of the pressure membrane. To facilitate piping and to support the weight of the stored contents, a rigid structural floor supports the lower portion of the pressure membrane. A suspension system support the weight of the tank through connection between this structural floor and an external support structure. Legs support the external support structure. Preliminary design of each of the tank components follows.

The pressure membrane serves the dual role of containing the cryogen and resisting the pressure loading. Fluorinated polymers, such as Teflon FEP, are perhaps the only suitable engineering materials for containing the cryogen. However, the strength of Teflon FEP alone is relatively small. The specific strength of FEP film at the required temperature is two orders of magnitude below what can be achieved with high strength materials such as Kevlar. The pressure membrane will thus be comprised of two parts, the "bladder" which must contain the cryogen and limit leakage and permeation, and the "reinforcement" which supports the mechanical loads. The technology required to produce such a pressure membrane made of a flexible bladder with filamentary reinforcement is well within reach of current technology. Teflon-coated fabrics are used in architectural applications [21]; flexible pressure membrane were used in the Transhab space habitat [4]; and large, seamless Teflon bladders have been

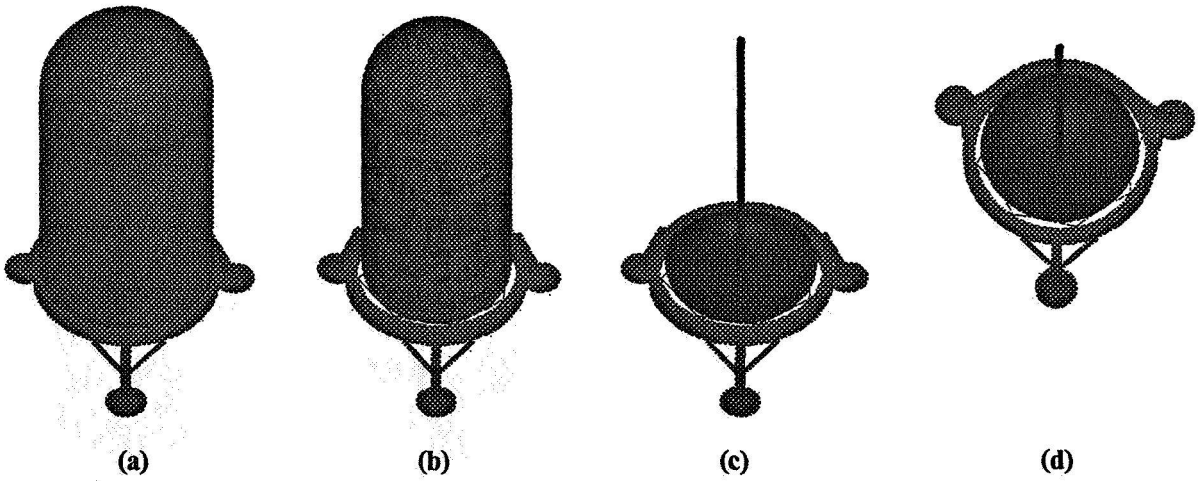

Figure 3 Schematic of the inflatable tank concept emphasizing (a) the flexible insulation membrane, (b) the pressure membrane, (c) the support structure including a rigid end cap, external support structure and legs, and (d) the suspension system (dark lines connecting the endcap to the external ring)

used as "positive expulsion bladders" in liquid fuel rockets [19,20]. For the Mars liquid oxygen tank bladder a 6 mil thick Teflon FEP bladder with an aluminum film embedded inside through a chemical vapor deposition (CVD) process is proposed. The mass loss due to permeability for this bladder is estimated to be on the order of 1 g/day (not including leaking at seals around the piping). Repeated folding and unfolding of the bladder is undesirable because it will degrade its impermeability. Further, because of the reduced flexibility of the material at cryogenic temperatures, it is undesirable to fold the material in the cryogenic state. Therefore, the tank must be inflated before cryogenic material is placed in the tank, and positive inflation must be maintained throughout its service life. There are various possible methods for reinforcing the bladder including fabric reinforcements, or more widely-distributed mesh or cable reinforcement schemes [4]. Due to the weakness of the bladder material at cryogenic temperatures, widely-spaced, discrete reinforcement bands will not be an effective solution. The best material to use for the reinforcement will be the flexible material compatible with the environment that has the highest specific strength. Advanced fibers are therefore superior to metal reinforcements such as stainless steel wire. Kevlar would be a logical choice for the reinforcement due to its high strength and excellent flexibility. However, it is not oxygen compatible, and thus, glass fiber reinforcement is recommended. Assuming that fibers are independently placed in the hoop and longitudinal directions average thicknesses of fibers in the hoop direction of 0.1 mm and in the longitudinal direction 0.05 mm are needed, for a total reinforcement thickness of about 0.15 mm. This is a typical thickness for a single, thin ply of fiberglass cloth. Similar quantities of material result from optimized placement of fibers using an off-axis, angle-ply arrangement. Although the diameter is rather large it would be beneficial to use a braided construction for the reinforcement in the cylinder to avoid joints in the hoop direction.

The total mass of one pressure membrane is about 38.7 kg (85 lb_m). To provide system redundancy, multiple bladder/reinforcement layers may be used, as in the Transhab design [4]. The weight penalty for including a redundant membrane is not very severe when the mass of other system components described below is considered. The inflatable tank concept is a pressure-stabilized structure. "Rigidizable" structure concepts [22] can potentially be used to make the pressure membrane rigid following inflation. This would help avoid problems with flexing of the bladder due to external loads such as wind, though care must be taken with regard to oxygen compatibility or the rigidizing agent.

For an insulation system compatible with the inflatable tank concept, the insulation will be contained within a double-walled flexible membrane. The insulating material is assumed to be "layered composite" type, with an approximate thickness of 25-40 mm (1 to 1½ inches), and a density of 52 kg/m^3 [11]. Sizing of the vacuum membrane walls will be determined based on permeability. Similar technology to that used for the pressure membrane bladder may be used for the vacuum membrane. Due to the double-walled construction and the need to fill the interior with vacuum insulation, it may not be possible to form the vacuum membrane using seamless construction, and considerable care will be necessary to form effective and durable joints for the vacuum membrane. The mass of the insulation is estimated to be 138 kg (304 lb_m). The vacuum membrane material is estimated to be

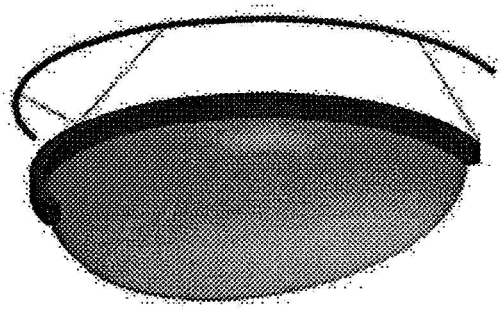

Figure 4 Ring girder support arrangement for lower endcap

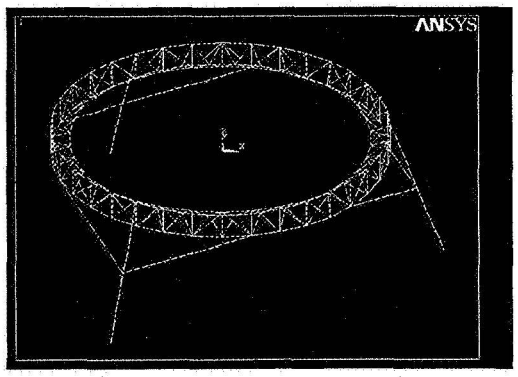

Figure 5 Truss structure for external support

about 40 kg (88 lb_m). Additional outer wall materials may be needed for impact protection, to resist abrasion from the Martian atmosphere, and to provide a reflective surface to limit radiation influx. Impact protection may be especially critical due to the requirement for vacuum insulation. Any impact that penetrates and causes leakage of the vacuum shell will effectively destroy the functionality of the tank. Because similar outer layers may be used for all tank concepts, detailed weight analysis is not made.

As discussed above, a composite strut suspension system is the most appropriate for the present application. The total mass of a six struts suspension system for the inflatable tank is small due to the tensile nature of the loading condition. The mass of the struts is estimated at 5.6 kg (12.4 lb_m), not including connections. The support structure is one of the most highly loaded components of the system. The pressure membrane alone is incapable of supporting concentrated loads such as are introduced through the suspension system or the structural legs. A rigid endcap will therefore be used to transfer load from the pressure membrane to the support structure. Although a rigid semimonocoque floor was considered for the lower endcap, a lighter alternative is to support the tank structure through a "ring girder" [23], as shown in Figure 4. This is a circumferential ring on the outside of the tank at the position of the junction between the lower endcap and the cylinder wall. A thin, metal lower end cap can be welded to this ring, and thus membrane stresses in the lower endcap will be transferred directly into this ring. A ring girder design that provides the necessary strength (assuming three vertical attachment points for the suspension system) is an aluminum hollow rectangular section with outside dimensions of 4×6 inches and a ¼ inch wall thickness. The mass of the ring of these dimensions is 81 kg (179 lb_m). Additional mass is required for the lower endcap, which can be fabricated at the minimum thickness required for a shallow ellipsoidal endcap. To accommodate the thickness of the suspension system, a "bulge" of extra insulation of about 20 cm (8 inches) thickness is required for the approximately ½ meter vertical height of the suspension system. This will result in extra insulation mass of about 52 kg (115 lb_m). An external support structure is needed to bear the load from the suspension system and pass it to the ground through the legs. Because the external support structure is outside the insulation space, the need for compactness is reduced, and a truss structure in the shape of a ring may be used. Estimation of the weight of such a structure for one possible configuration is based on the ANSYS model shown in Figure 5. The resulting structure, assuming graphite/epoxy composite members, has a mass of under 100kg, not including the joints. This analysis should be considered as preliminary as the suspension system configuration assumed for the model is different from what was ultimately selected and the truss configuration is not optimized. The total mass of the external support structure is estimated to be about 150kg.

Mass estimates for all of the system components for an inflatable Mars liquid oxygen storage tank are summarized in Table 1. The total mass of the tank not including legs, external impact protection, piping, or necessary systems such as vacuum pumps and cryocoolers is about 570 kg (1250 lb). The mass of the legs will be substantial, but the end result is likely to be a structure of less than one metric ton in mass.

5 TELESCOPING TANK DESIGN

A potential advantage of a telescoping arrangement for the Mars tank is the ability to use rigid structures. Minimum gage wall thickness can be used (with additional support necessary at the points of load application through the suspension system, as in the inflatable tank concept). However, extra rigidity may be needed to prevent damage of

Item	Mass	
	kg	lb_m
Pressure Membrane (2)	78	170
Insulation Membrane Walls	40	88
Insulation Material	190	419
Ring Girder and Cradle	100	220
Suspension Struts (6)	10	22
External Support Truss	150	330
Total (not including piping, legs, and mechanical systems)	568	1249

Table 1 Mass of components of inflatable cryogenic storage tank

the small thickness components during manufacture, flight and landing. Because design of the rigid inner vessel walls is conventional it will not be considered in detail. Rather, issues pertaining to joints, sealing, and integrating the vacuum insulation into the design will be explored. For the analysis here, it is assumed that the insulation is contained within a flexible "bag" which the telescoping structure will expand into, which simplifies the design of the joint.

Joints are the primary difficulty of a telescoping pressure tank. Not only must a mechanical joint be made between segments to restrain the longitudinal loads, the joints must also be sealed against leakage of the cryogen into the vacuum space. Locking rings operating on a principle similar to that used, for example, in autoclave doors may be used for this purpose, though external mechanism will be needed for actuation. An alternative means of clamping is through a shape memory alloy (SMA) locking ring proposed by Dr. Eric Thaxton. This concept uses the shape memory effect to make seals between segments in a cylindrical telescoping tank in a fashion similar to "Cryofit" fasteners, a commercial product used for joining high-pressure hydraulic tubing. A schematic of the concept is provided in Figure 6. The SMA locking ring is sized to be initially slightly larger than the telescoping segments it is intended to join. Upon heating above its transformation temperature the SMA locking ring experiences a phase change resulting in the reduction of its rest diameter below the diameter of the cylinder segments. Constraint provided by the cylinder structure produces clamping pressure between the segments. Because of the large diameter and thin walls of the cylinder segments, a back-up structure must be provided on the inside of the tank at the position of the SMA locking ring to avoid buckling. Preliminary sizing of a SMA locking ring for the present application is based on Nitinol material properties. However, due to the substantial amount of titanium in Nitinol it is questionable whether Nitinol alloys are oxygen compatible. Copper-based SMAs should be considered for this application [24]. A nominal design for a SMA locking ring has a cross-sectional area for the SMA ring of 422 mm^2 (0.65 in^2), which is sufficient to resist the longitudinal pressure loading through friction alone. An aluminum back-up ring with a W6×15 wide flange I-beam shape is sufficient to prevent buckling. This design results in a mass of 26 kg (57 lb_m) for the SMA ring and 75 kg (166 lb_m) for the backing ring. The system mass for one SMA joint is therefore 101 kg (220 lb_m), not including the mass of the mechanical stops or systems for activating the shape memory effect. While the SMA locking ring concept offers a simple joint design with few mechanical parts, there must be a system for activating the shape memory affect. Activation is initiated by heating the ring. The energy required for activation is between 1325 kJ and 2480 kJ, neglecting losses, which may be substantial.

Designing effective seals for the telescoping segments is a challenging problem. Dimensional tolerances in the large diameter, thin-walled cylinder will likely precluding forming effective O-ring seals around the hoop direction. Conventional static face-type seals could be used on the mechanical stops of telescoping tank segments, as illustrated in Figure 6. Pressure in the tank or residual pressure from deployment and clamping of the joints will compress these seals. If pressure alone is relied upon for sealing, loss of pressure in the tank, even temporarily, will produce failure of the seals. For this reason, either a positive locking mechanism for the tank or redundant seals must be used. The problem of sealing can be greatly simplified by the use of a flexible bladder to contain the cryogen inside a telescoping tank. Then, the mechanical joints will carry only the pressure loading and will not be depended upon for sealing (except as a backup). The same sort of bladder used for the inflatable tank concepts can be used in this application. If a SMA locking ring is used it will produce a sealing effect through metal-to-metal contact between the cylinder segments. The sealing principle is similar to that of metallic gaskets in which a soft metal is compressed between two harder flanges. For flat metallic gaskets, soft aluminum requires the lowest seating stress at 60–70 MPa (8800–10000 psi) [25]. Corrugated aluminum may allow seating stresses of as low as 1000 psi. Achieving such clamping pressures over the whole face of the proposed SMA locking ring system is problematical due to the structural stability of the structure. However, if relatively narrow cylindrical rings of metal gasket material are placed between the cylinder segments that are being joined, high clamping pressure in the gasket material is possible. For the nominal SMA locking ring design above, a gasket width of 2mm corresponds to an effective contact pressure in the gasket of 60 MPa (8800 psi). This width is small, and deformation effects may reduce the clamping pressure. Generating effective seals in the SMA ring joint may require larger and heavier components than in the baseline SMA joint design. An alternative is to use a flexible gasket material (Flouoroly 36, for example) between the cylinder segments. Keeping this gasket material in position and avoiding damage to it during tank extension will be a significant challenge.

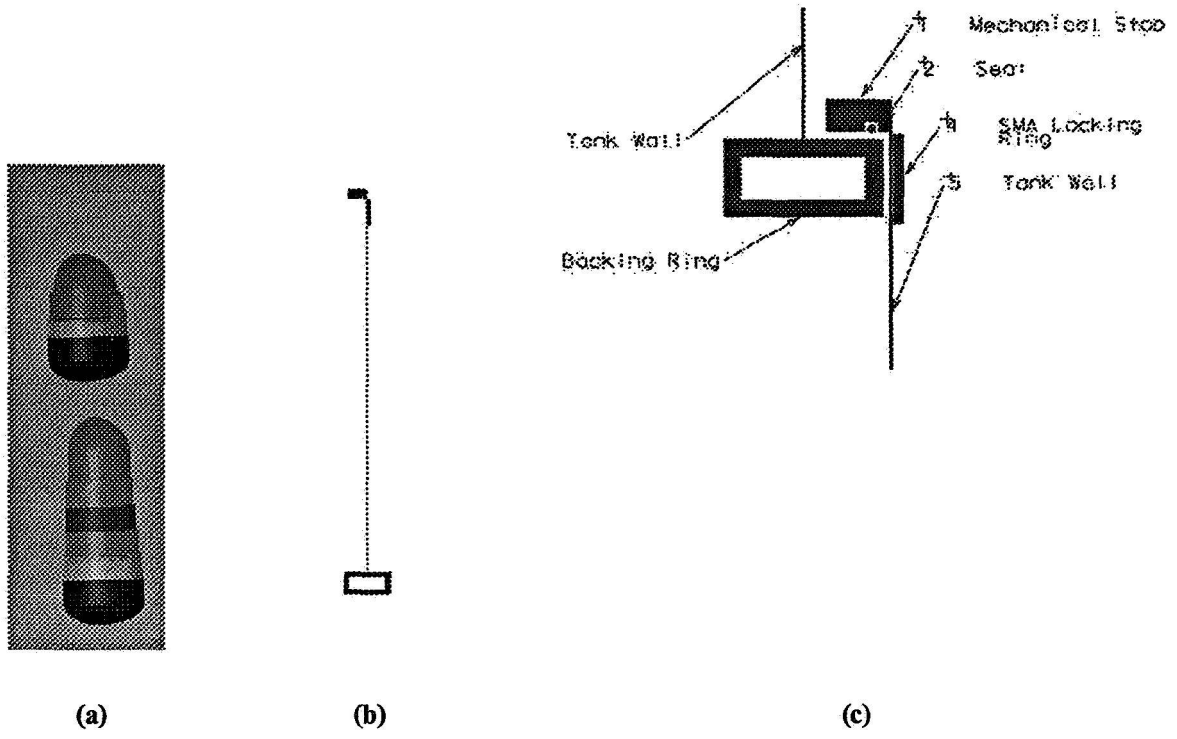

Figure 6 Schematic of telescoping tank concept with SMA locking ring joint (a) deployed and undeployed positions; (b) cross section of typical segment (c) detail of joint geometry

Deployment of the telescoping structure must be addressed if a telescoping tank structure is to be developed. Gas pressure alone will only be adequate for deployment purposes if a bladder is used inside the tank, because the other seal types are only effective following engagement. Locking rings, whether conventional mechanical systems or the SMA type will require proper positioning of the tank before they can be correctly engaged. Keeping the thin-walled tank segments properly shaped throughout the flight and landing environment such that the locking rings will be properly engaged is a substantial problem. The success of face seals on the mechanical back-up structure likewise depends on correct alignment during deployment, which is particularly challenging given the large diameter of the tank. Based on these concerns it is apparent that additional structure may be required to ensure correct deployment and positioning of the tank.

6 CONCLUSIONS

Long term storage of liquid oxygen on Mars can be effectively and efficiently developed based on existing technology. An inflatable tank concept using redundant fiber-reinforced Teflon FEP bladders to contain the cryogen is recommended. This is an efficient, lightweight option requiring no extra systems for deployment or sealing. The support structure is the highest mass portion of the structure. A ring girder support configuration supported externally by a truss structure and spacecraft legs is proposed for the support structure, though optimization of this structure can be used to develop a more efficient design. Prototype and development work in several areas is needed to ensure the success of such a design. Chief among the needs is for the demonstration of the durability of the proposed bladder design for the liquid oxygen environment, particularly with respect to permeability.

Telescoping tank concepts can be produced for the Mars liquid oxygen tank. However, the overhead associated with forming effective joints and extra weight associated with greater mass of the pressure wall segments, systems to maintain proper alignment of joints during deployment, and electrical or mechanical systems needed to engage joints represent inefficiency as compared with the inflatable tank concepts presented above. If telescoping design concepts are pursued, additional work in joint technology is needed, including development of oxygen compatible inflatable seals for sealing around the hoop direction; verification of the SMA locking ring concept; and evaluation of the sealing performance of a SMA locking ring.

Detail design work is needed before application of the design concepts in this report should proceed. Some fundamental choices should be addressed, including whether it would be more effective to use multiple smaller tanks rather than a single large tank, as proposed here. Also, while a cylindrical tank shape was considered in this report, the shape of the tank should be optimized based on specific mission requirements and launch vehicle specifications.

7 REFERENCES

1. Hoffman, S. J., and D. I. Kaplan, eds., 1997. *Human Exploration of Mars: The Reference Mission of the NASA Mars Exploration Study Team*, NASA-SP-6107.
2. Drake, B. G., and D. R. Cooke, Eds., 1998. *Reference Mission Version 3.0 Addendum to the Human Exploration of Mars: The Reference Mission of the NASA Mars Exploration Study Team*, NASA Exploration Office Advanced Development Office, EX13-98-036, June 1998.
3. Muller, 1999. Muller, P., and T. Durrant, "Cryogenic Propellant Liquefaction and Storage for a Precursor to a Human Mars Mission," *Cryogenics*, Vol. 39, pp. 1021-1028.
4. Cadogan 1998; Cadogan, D., J. Stein, and M. Grahne, 1998. "Inflatable Composite Habitat Structures for Lunar and Mars Exploration," *Proceedings of the 49th International Astronautical Congress*, Sept. 28-Oct. 2, 1998, Melbourne, Australia, IAA-98-IAA.13.2.04.
5. http://www.atlinc.com/pillowlit.pdf
6. Flanagan, D. T., and R. C. Hopkins, 1993. *Advanced Collapsible Tank for Liquid Containment*, NASA CR-188247, June 1993.
7. Cadogan D. P., and S. E. Scarborough, 2001. "Rigidizable Materials for use in Gossamer Space Inflatable Structures," *Proceedings of the 42nd AIAA/ASME/ASCE/AHS/ASC Structures, Structural Dynamics, and Materials Conference AIAA Gossamer Spacecraft Forum*, April 16-19, 2001, Seattle, WA.
8. Witcofsky, 1984. *Telescoping Space Station Modules*, NASA TM-86523.
9. Barron, R. F., 1985. *Cryogenic Systems*, 2nd ed., Oxford University Press, Oxford.
10. Anon., 1974. *Liquid Rocket Metal Tanks and Tank Components*, NASA SP-8088.
11. Hegab, H., 2001. *Thermal Design of a Collapsible Cryogenic Vessel*, NASA/ASEE SFFP Final Report, NASA Kennedy Space Center, to be published.
12. Alexander, M., Ed., 2001. *Mars Transportation Environment Definition Document*, NASA/TM-2001-210935, March 2001.
13. Flynn, T. M., 1997. *Cryogenic Engineering*, Marcel Dekker, Inc., New York.
14. Kittel, P., 1993. "Comparison of Dewar supports for space applications," *Cryogenics*, Vol. 33(4), pp. 429-434.
15. Reed, R. P., and M. Golda, 1997. "Cryogenic composite supports: a review of strap and strut properties," *Cryogenics*, Vol. 37(5), pp. 233-250.
16. Anon., 1996. *Safety Standard For Oxygen And Oxygen Systems*, NASA NSS-1740.15.
17. Hudson, G. C., 1998. "Roton Development and Flight Test Program," *Defense & Civil Space Programs Conference and Exhibit*, Huntsville, AL, Oct. 28-30, 1998, AIAA 98-5258.
18. Anon., 1999. "Lockheed Martin Receives Authority from NASA to Proceed on X-34 Composite Liquid Oxygen Tank," *Marshal STAR*, Oct. 21, 1999. http://www.msfc.nasa.gov/STAR/old_star/10-21-99.pdf
19. Petriello, J. V., 1968. "Modifications in Fluorocarbon Bladder Structures in Improving Flexibility and Impermeability," *Low Gravity Propellant Orientation and Expulsion, AIAA Lecture Series Vol. 6*, Los Angeles, CA, May 21-23, 1968, pp. 119-127.
20. Bazzarre, D. F., and J. Petriello, 1968. "Chemical Vapor Deposited Permeation Barriers in Teflon Expulsion Bladders," *Low Gravity Propellant Orientation and Expulsion, AIAA Lecture Series Vol. 6*, Los Angeles, CA, May 21-23, 1968, pp. 129-139.
21. Schock, H.-J., 1997. *Soft Shells*, Birkhäuser Verlag, Boston.
22. Freeland, R. E., G. D. Bilyeu, G. R. Veal and M. M. Mikulas, 1998. "Inflatable Deployable Space Structures Technology Summary," IAF-98-1.5.01.
23. Moss, D. R., 1987. *Pressure Vessel Design Manual*, Gulf Publishing Co., Houston.
24. Janocha, H., ed., 1999. *Adaptronics and Smart Structures*, Springer, Berlin.
25. Brink, 1993. Brink, R. V., D. E. Czernik, and Leslie A. Horve, 1993. *Handbook of Fluid Sealing*, McGraw-Hill, New York.

2001 NASA/ASEE SUMMER FACULTY FELLOWSHIP PROGRAM

JOHN F. KENNEDY SPACE CENTER
UNIVERSITY OF CENTRAL FLORIDA

INTEGRATED WORKFORCE PLANNING MODEL
A PROOF OF CONCEPT

Eranna K. Guruvadoo
Assistant Professor
Computer Science
Bethune-Cookman College

Louise Boyd
NASA/KSC

ABSTRACT

Recently, the Workforce and Diversity Management Office at KSC have launched a major initiative to develop and implement a competency/skill approach to Human Resource management. As the competency/skill dictionary is being elaborated, the need for a competency-based workforce-planning model is recognized. A proof of concept for such a model is presented using a multidimensional data model that can provide the data infracture necessary to drive intelligent decision support systems for workforce planing. The components of competency-driven workforce planning model are explained. The data model is presented and several schemas that would support the workforce-planning model are presented. Some directions and recommendations for future work are given

1. Introduction

Workforce planning simply defined as "getting the right number of people with the right skills, experiences, and competencies in the right jobs at the right time". As KSC redefines its mission and goals as a center for space innovation through the KSC Roadmap, the Workforce and Diversity Management Office has undertaken several initiatives to better support the Center's goals . One of the major tasks being undertaken is the deployment of a competency model that eventually will drive major HR (Human Resource) activities. Currently, the listing of the core competencies is being drawn. As the work progresses, the need for a Workforce Planning Model that integrates the competency dimension with other human resource dimensions is being envisioned.

This project presents a proof of concept for an integrated workforce-planning model that incorporate a competency-based approach to other Human Resource management (HRM). In particular, it examines the requirements for a competency-based approach to workforce planning, and the current data infrastructure and data requirements for workforce planning. To guide this project, a set of questions was drawn by the Workforce Planning Unit and was used as business drivers. These questions were used to identify the data infrastructure that would best drive intelligent decision support systems for workforce planning. A multidimensional data model is presented to support a competency-based approach to workforce planning. The model can provide guidelines to design and implement a data infracture that will drive desktop tools for workforce planning and other HR activities.

This paper is organized as follows: The remaining part of this section provides some background information and motivation for this project. Section 2 describes the components of a competency-based workforce-planning model. These components provide a context for identifying the data requirements for a workforce-planning model. Section 3 summarizes the existing databases, the current data support and the data handling for workforce planning processes, and the methods in use. Section 4 presents a multidimensional data model and several star schema models that integrate the HR dimensions required for workforce planning. Section 5 provides some discussion and recommendations for future work to implement an Integrated Workforce Planning System, and some concluding remarks are made.

1.1 Background.

NASA reorganization initiatives to better position KSC as a center for future space exploration has resulted into a matrix organizational structure with a more streamlined workforce. The mission and objectives of The Workforce and Diversity Management Office has been linked to KSC Roadmap Goal 4.0 - "Continually enhance core capabilities (people, facilities, equipment and systems) to meet NASA objectives and customers needs", and Objective 4.1A - "Develop and implement systems and approaches to attract, develop and retain a high quality, diverse workforce to meet current and future challenges".. The need for a framework to make HR decisions based on KSC mission, strategic plan, budgetary resources, and a pool of desired competencies, is greater than ever..

The Workforce and Diversity Office has undertaken several initiatives to implement KSC objectives. The office is in the process of elaborating the set of core competencies for KSC. Other initiatives include the design of a data warehouse that integrates data from various sources to support HR activities. A data model to capture KSC workforce competencies have been demonstrated, pending the completion of the competency listing. There is also an initiative to develop a center-wide knowledge management system.

2. Integrated Workforce Planning Model

2.1 Components

In reviewing literature on workforce model, it has been observed that there are great similarities in their contents although the terminology may vary. Essentially, all workforce-planning models consist of the following processes:

- Supply Analysis consists identifying present workforce competencies, analyzing staff demographics, and identifying employment trends. Competency analysis provides baseline data on the existing organization and present staff. Trend analysis provides both descriptive and forecasting models describing how turnover will affect the workforce in the absence of management action. Trend analysis is essential to the solution analysis phase defined below.
- Demand Analysis deals with measures of future activities and workloads, and describing the competency set needed by the workforce of the future. Demand analysis must take into account not only the workforce changes driven by changing work but also workforce changes driven by changing workload and changing work processes. Technology will continue to have an impact on how work is performed and must be considered in the demand analysis process.
- Gap analysis is the process of comparing information from the supply and demand analysis to identify the differences, the "gaps" " between the current organizational competencies and the competency set needed in the future workforce. The comparison requires the competency sets developed in the supply analysis and demand analysis phases to be comparable, not independently developed.
- Solution analysis is the process of developing HR plans, including hiring, training, and training, to close gaps in competencies and to reduce surplus competencies. Solution analysis must take into account employment trends.
- Evaluation involves a periodic and systems review of the workforce plan, reviewing mission and objectives to assure the plans remain valid by making adjustments as required by changes in mission, objective, and workforce competencies.

A data model to support workforce planning must capture the data requirements to support the processes described above.

3. Existing systems and supports for workforce planning

With limited access to the data sources, it has been extremely difficult to identify all HR related data in the databases and various data store. There was no data dictionary or proper documentation for the various databases. Therefore, the following characterization of the present systems and supports for workforce planning may not reflect the complete situation.

Currently, the Workforce Planning Unit draws it Data from the NPPS Database that holds HR related data, and from monthly file downloaded from the Labor System database containing FTE (Full Time Equivalent) hours of KSC employee on the different projects. The downloaded files are fed into Excel spreadsheet to generate monthly FTE reports by organizations and projects.

There is a set of pre-defined parametized queries or stored procedures that can be used to crank out subset of the NPPS database for further manual data processing to generate other HRM reports. The times spent on shifting through the data to satisfy some reports requirements are enormous. There is practically no decision support system or tools in place to facilitate data analysis, except for a few spreadsheet applications.

4. Proposed data model

In order to support a competency based integrated workforce planning model, the necessary data infrastructure has to established. The data architecture that can drive desktop decision support tools is presented.
It is based on a multidimensional data schema. The star schema transforms the de-normalized relational tables into a multidimensional space through the fact table. An example of a star schema is presented below. The OLAP services build hyper-cubes of pre-computed additive and semi-additive data and create access path to back-end data store, using highly sophisticated indexing scheme. The OLAP services allow browsing of multidimensional data at different levels of detail

4.1 A Star Schema for HR Transaction Data Mart

In order to perform trend analysis for workforce planning, HR historical data is required. Currently, the NPPS database holds some historical data but it does not capture all HR transactions, which are important for other reporting needs.
A star schema for an HR data mart that captures all HR transactions is presented below in Figure 4-1-1. An HR transaction can be any HR related event, such as a promotion, retirement, the starting date for a leave, change from full time status, etc. A set of complex HR profile of 100 or more attributes can be captured in an employee transaction dimension table to record every transaction performed on an employee record. This table is shown as the Emp_Trans_Dim table. The attributes with a plus sign indicate these attributes may consists of multiple fields. The month and organization dimensions are shown as Month Dim and the Org_Dim.

In the Emp_Trans_Dim table, there are two important attributes, Trans_End_Date and Last_trans_flag, that are crucial. The Trans_End_Date for each record is the date for the next transaction on that particular employee The Trans_End_Date together with Trans_Date/Time provide a span of time during which the employee description is exact. Last_Trans_Flag is used to indicate the last transaction made against an employee profile. This method allows the most current or final status of an employee to be retrieved. If a new transaction for that employee need to be recorded, this flag is set to false.

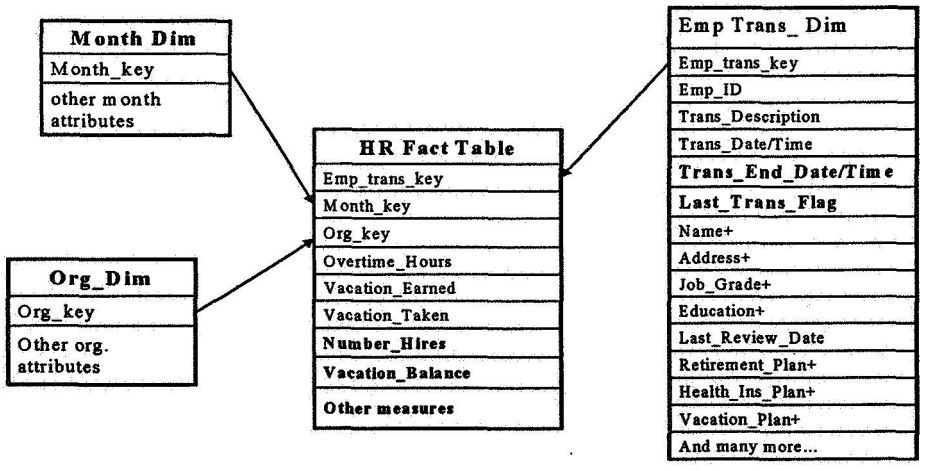

Table 4-1-1 HR Transaction Data Mart

The schema of the HR Transaction Data Mart can provide the data for supply analysis and many reporting needs. The schema addresses three fundamental type of queries:

1. Status report summaries on a monthly basis for all possible slices (& combinations) of data
2. 2.Detailed profiles on employee population at any point in time (snapshots)
3. –Every action taken on a particular employee with the correct transaction sequence in time

4.2. A Star Schema for FTE on Projects

Using multidimensional data modeling described above, a star schema is created for FTE on current projects at KSC. This schema integrates the required dimensions to support current HR monthly reporting requirements on FTE.

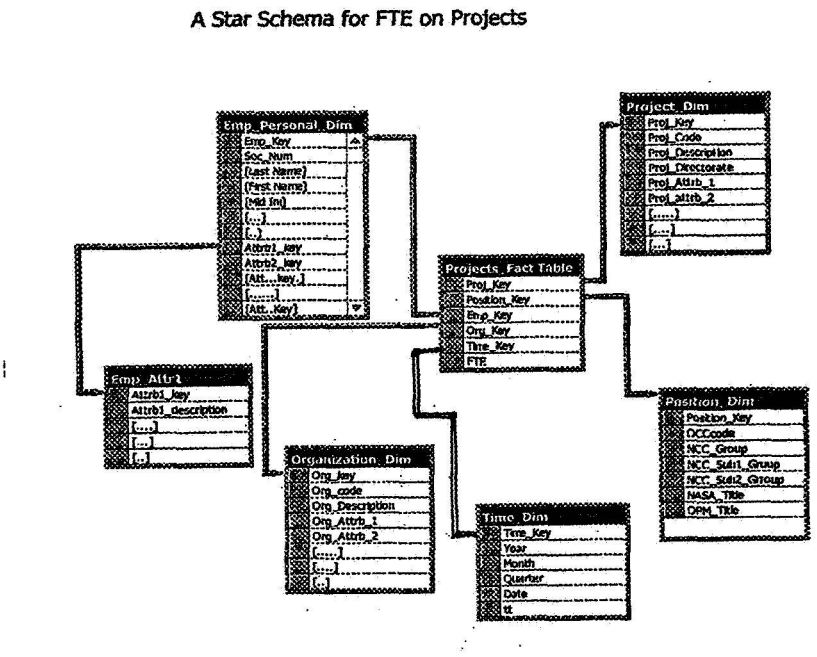

Figure 4-2-1 A Star Schema for FTE on Projects

4.3. Competency Modeling

The table below shows how the competency dictionary can be captured in a de-normalized table so that it be integrated into a star schema with other dimensions. This mapping is significantly different from the in-house model, which contained normalized tables with hierarchies – more appropriate for a transaction based operational systems. In the table below, the hierarchies have been collapsed. The first field, Comp_Key, is a system-generated key that uniquely identifies each row in the table. This representation

allows for subgroups within a field. The Tier_Item_Num field represents the item number in a particular Tier.

Comp_Key	Comp_ Code	Description	Subgroup	Tier_ Level	Tier_Item _Num	Comp_Item_Descr iption
1020	CRE	Cryogenic	Cryogenic Science	3	7	Demonstrate knowledge of low temp molecular ..
1020	CRE	Cryogenic	Cryogenic Technolog y	2	5	Demonstrate skills in handling low temp containers

Note: Hierarchies collapsed
Table de-normalized for performance
Typical for Dimension tables

Table 4-3-1 Competency Descriptions

4.3.1 Modeling Competency Gap with Job Profile

Competency clusters from the Competency Dictionary can be mapped into a table as shown below to capture each job profile. The Comp_Key is from the Competency Dictionary table shown above. The Job_Profile_Id is unique for each job as described by the NASA Classification Code or OPM Code. Again the Job_Profile_Key is a system-generated key that uniquely identifies each row. The Required_Comp field contains a scaled measure of the competency level required of a particular competency for a particular job. This field allows to capture the fact that different jobs may require the same competency but at different scale. The Priority_Indicator field is used to indicate the priority of a particular competency in a particular job profile. This field allows to create ranked competencies within a job profile, which is useful in matching algorithms to created weighed profile on employees or job applicants. The Skill_set_Id may be used to represent a set/additional skills descriptions to supplement the competency dictionary, which normally produces 80% fit for job profile. The skill_set_Id may be tied to a matching Training_set_Id to identify the relevant training. This model does not explore the training requirement further.

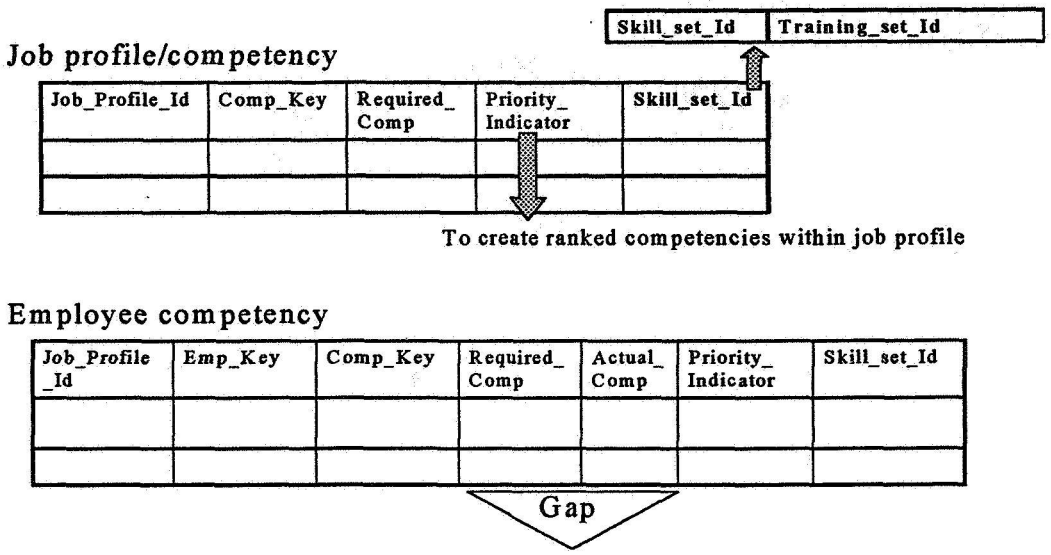

Figure 4-3-1-1 Capturing Competency Gaps

5.3.2. Measuring Competency Gap

The employee competency can be captured using the Employee Competency table shown above. This table contains all the fields of the job profile table; in addition the Emp_Key identifies each employee, and the Actual_Comp field holds the actual competency for the particular employee. The competency gap is a derived data from the two adjacent fields. .

5.4. A Competency Star Schema

Using the three de-normalized tables shown above, competency data can be captured in a very easily-understood form by the users; more importantly, it can be integrated into a star schema with other dimensions like employee, position, organization, projects, and other HR related dimensions as shown in the diagram below.

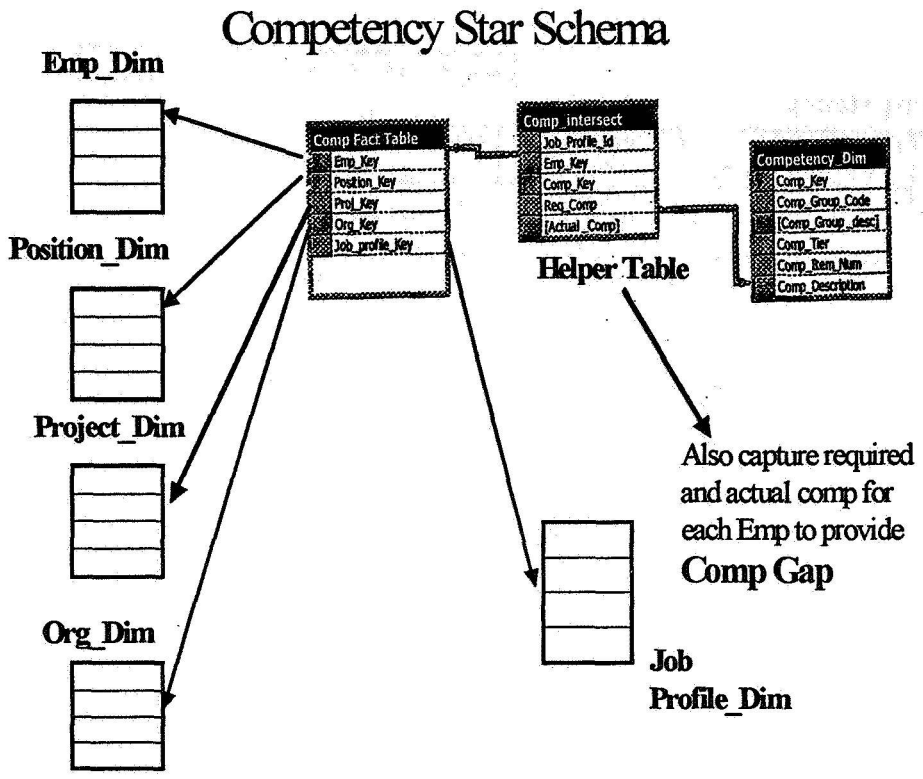

Figure 4-4-1 Competency Star Schema

The Competency Dimension is linked to the Competency Fact table using the Helper Table, which is the Employee Competency Table shown in the previous diagram. The helper allows the implementation of the many-to-many relationship between the Fact Table and the Competency Dimension.

The Competency Star Schema shown above is necessary to create an integrated data model for workforce planning. This schema provides all the data to drive desktop solutions to answer questions 1, 4 and 5 from the Appendix, A which were used as business drivers to guide this project.

5. Discussions/Recommendations for future work

Developing a proof of concept for an integrated workforce-planning model requires significant exploratory work, examining current systems and desirable systems. This section summarizes a development strategy for the design and implementation of the workforce planning model and some recommendations.

5.1 Current Data Warehouses

In examining the current data warehouse design containing corporate employees data and competency data, it is noted that the tables are normalized and some of them have hierarchical structure. A data warehouse is designed fundamentally different from operational databases, which are highly normalized to support transactions. Analytical processing often dictates that a

de-normalized approach be taken to gain access efficiency in order to perform online analytical processing. OLAP technology exploits the star schema structure, which usually generate thin and tall fact table containing the data of interest, to create highly efficient indexing scheme to support online processing. Thus, the existing design will have to be re-visited to ensure the desired characteristics

The most effective approach to the design and implementation of a workforce planning system is to use a system engineering approach to create the design process of a data warehouse through the development of a Meta data system. Meta data is the most crucial element in the effective management of data. A Meta data system provides a framework to define the data warehouse requirements, and can be used iterative ly during the life of the data warehouse to update and integrate new dimensions. Tracking Meta data from sources to data warehouse, to applications is a very important principle. The current data warehouse has no documentation of a Meta data system

5.2 Implementation and Development strategy

Key planning decisions include selecting an implementation strategy and a development methodology. A top down approach is preferable because the business requirements for the system can be identified clearly and used as drivers for the implementation of the data warehouse. However, it is being recognized that in most environment, the managers and users take some times to learn the capabilities, usefulness and values of a data warehouse as an OLAP resource. Then, it can be expected that the data warehouse will grow rapidly as more data is required for more applications. Given this situation, the development method preferred is the spiral method, which recognizes that requirements are not always clear or available when the sytem first implemented. The recommended steps of Requirement Analysis, Design, Integration, Verification and Maintenance should be followed iterative ly. Creating OLAP applications can be time consuming.

Developing the business objectives of the system can become difficult, as potential users cannot always describe the type of information desired out of the warehouse. In these situations, examining the current data and data analysis used may provide a starting point that can be further refined.

In identifying the requirements for the system, it is important to identify the owner's requirements, the architectural requirements, the developer' requirements as well as the end user requirements. Owner's requirements include identifying, beside cost, development duration, the impact of the users, their skills and the organization, and the risk involved. Important architectural requirements include functions and features to be offered, platform needed for implementation, standards and open interface to be used, and how much flexibility for enhancement is required. Developer's requirements are further elaborations of the architectural requirements, including deployment, connectivity, access and delivery methods, and client platform requirements. End users requirements include identifying how the functionality of the data warehouse fit the user daily workflow, query requirements; types of analysis performed, and reports requirements.

5.3 Conclusion

There are considerable advantages of using a competency-based approach to drive HR planning. A proof of concept presented. Competency-based approach to HRM and the components of a workforce-planning model are examined. A multidimensional data model that would provide the data infrastructure to support intelligent decision support applications for workforce planning is presented. Several modeling examples are provided a proof of concept for a competency-based workforce-planning model .

This project is an exploratory work for the design and implementation of a competency-based workforce-planning model. A formal design will require more exhaustive and detailed analysis of the requirements of such a system. The development of a workforce planning system is evolutionary. An initial iteration can produce a minimal system. An important consideration is to stay focus on methodology. This work provides the data architecture to launch a design and subsequent implementation.

References

Giovinazzo, William A. Object-Oriented Data Warehouse Design: Building a Star Schema. Upper Saddle River; NJ, Prentice Hall PTR: 2000.

Management of Skills and Manpower Planning for International Competitiveness. http://www.fba.nus.edu.sg/rsearch/pqrc/pqrcnw/CoreComp/pgManpower.htm

Building Successful Organizations: Workforce Planning in HHS. http://www.os.dhhs.gov/ohr/workforce/wfpguide.html

Kimball, Ralph, "*Human Resources Data Marts – Design guidelines for querying employee data*", DBMS, Feb 1998.

NASA Position Classification Handbook

Skill and Competency Management with BOTiC-Comp. http://www.botic.co.uk/compinfo.htm

Agosta, Lou. The Essential Guide to Data Warehousing. Upper Saddle River; NJ, Prentice Hall PTR: 2000.

Final Report

Surface Evaluation by XPS of High Performance Foams After Exposure to Oxygen Plasma

Dr. Michael D. Hampton

Introduction

This report will present the results of a study done during a 10-week summer faculty fellowship during the summer of 2001 working with Ms. Martha Williams of the Testbeds Group at Kennedy Space Center. The work was in a new area for this faculty and was both interesting and enjoyable.

An imide is a in which nitrogen is bonded directly to an R group and to two other R groups through carbonyls. The structure below is that of Kapton, a commercially available polyimide, and the imide groups in the repeating unit of the polymer are indicated by the dashed boxes.

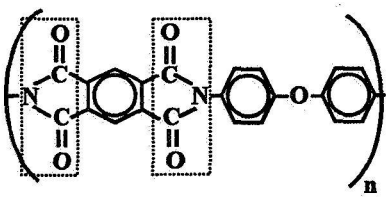

Polyimides have a number of properties that make them highly desirable materials for use on structures that are exposed to extreme conditions. They are strong, fire resistant, minimally outgasing, stable over a large temperature range, resistant to chemical attack, transparent to infrared and microwaves, and have a low density. One polyimide, solimide, commercially available as a foam, retains resiliency from –300°F to +500°F, is highly flame retardant, and decomposes with virtually no smoke or toxic byproduct formation. The density of this product is such that its use in place of fiberglass in the lower lobe of a 747 saves 400 lb. Shipboard applications have resulted in literally tons of weight reduction.

While polyimide films have been used in structures to be placed in low earth orbit (LEO) for many years, polyimide foams have found only minimal application in this realm. NASA Langley Research Center has developed new technology that allows for the processing of new polyimide foams. The resulting increased availability of these materials, along with their highly desirable properties, has prompted a study to determine the suitability of these materials for use in structures to be placed in LEO.

The atmosphere at LEO altitudes has a composition that is essentially the reverse of that in the troposphere, 20% N_2 and 80% O_2. Without the overlying atmosphere to filter short wavelength UV radiation (<243 nm), the molecular oxygen present is largely photodissociated to atomic oxygen (AO). Atomic oxygen is a highly reactive substance and thus is prone to rapidly oxidize materials exposed to it. Making the situation more extreme is the fact that structures in LEO are typically moving rapidly, as fast as 8 km/s, to maintain the orbit. Moving at that speed, it is typical for structures to collide with atomic oxygen with an energy of as much as 5 eV and to encounter 3×10^{24} oxygen atoms per cm^2 of surface area per second.

Before utilizing polyimide films in the aggressive environment of LEO, it is important to understand how they will perform. The purpose of this study was to study the interaction of atomic oxygen with these foams in order to determine their suitability for use in LEO applications. In the study, an oxygen plasma generator was utilized to produce an atmosphere of atomic oxygen that will simulate the atmosphere of LEO.

Experimental

The H, L. and C-series foams were supplied by NASA Langley Research Center. The foam samples supplied by Langley Research Center have labels in which the first letter indicates the series. Solimide was supplied by the manufacturer, Inspec foams, Inc. Kapton tape, Mystic 7362, was purchased from NASA federal stock. Kapton HN films, HN 100 (1 mil thick) and HN 200 (2 ml thick) were provided by the manufacturer.

Surface analysis of samples was done with a Kratos XSAM XPS/AES/ISS/SEM system. Foam samples were typically placed in the sample insertion chamber and allowed to pump down for 1-3 days before analysis. Film samples only required 2-3 hours to pump before analysis. Analyses were done with a Mg anode at 12 kV and 10 mA.

The oxygen plasma was generated with a SP1 Plasma Prep II plasma etcher. The Plasma Prep II was operated with an oxygen atmosphere at a feed pressure of 5 - 25 psi. The etcher was used at full power for cleaning sample pans and for the initial foam exposure. The second trial of atomic oxygen exposures was done at 25% power.

The effective atomic oxygen flux with the cavity of the etcher was determined, using the following procedure, at 100%, 50% and 25% power levels. This procedure was originally worked out by this researched and then was found to conform to that found in ASTM E 2089-00, "Standard Practices for Ground laboratory Atomic Oxygen Interaction Evaluation of Materials for Space Applications". Aluminum sample pans were cleaned by placing in the etcher at full power for 1 hour. Samples of Kapton tape, roughly 1-2cm square, were placed in cleaned aluminum samples pans, mastic side down, and weighed. Samples were then individually placed in the etcher and exposed to oxygen plasma for 30 min periods at the desired power level. After each 30 min period the samples were weighed. Determinations at each power level were run in triplicate. The effective atomic oxygen flux, F, was then calculated according to the following equation in which ΔM is the mass loss of the sample in grams, A is the sample surface area in the cm^2, E is the in-space erosion rate of Kapton, 3x10-24 g/O atom[1] and t is time in seconds.

$$F = \Delta M/(A\,E\,t)$$

The effective atomic oxygen flux determination was repeated using 4 samples of Kapton HN film mounted to the cleaned sample cups with a very small piece of carbon tape. The tape was situated such that the sample covered and protected it. The Kapton HN film samples were placed in the 4 positions within the etcher that were used for foam exposures and the flux determined as above.

For the initial trial of foam studies, samples were mounted to the tabs of a multisample tray from the XPS using carbon tape. Both survey and area scans were done on each sample with the XPS. Then the samples were removed from the XPS and the entire tray containing the samples was placed in the etcher and exposed to oxygen plasma at full power for 2 hr. Following the oxygen plasma exposure photos were taken and the remaining foams were analyzed again with XPS.

The next series of foam studies was done with the samples mounted to the tops of aluminum sample pans using carbon tape. The pans were previously cleaned in the etcher for 1 hr at full power. Samples were placed in reduced pressure, ~10-3 torr for 1 hr and then weighed. They were then placed in the etcher in groups of 4 and exposed to oxygen plasma at 35% power for 30 min increments. Samples were removed from the etcher and weighed, then placed back in the etcher and exposed to oxygen plasma again. This process was repeated until samples exhibited significant weight change. When significant weight change occurred, samples were placed in the XPS for surface analysis and then returned to the oxygen plasma treatment. When samples

---

[1] Obtained from: L. E. Bareiss, R. M. Payton, and H. A. Papazian, "Shuttle/Spacelab Contamination Environment and Effects Handbook", NASA Contractor Report 3993, pp 3-26, Sept., 1986.

were removed from the etcher for weighing or for XPS analysis, they were kept in a nitrogen atmosphere to exclude atmosphere oxygen and moisture.

One set of foams was analyzed for nitrate, sulfate, and carbonate ions before and after atomic oxygen exposure (full power, 1 hr). To do this analysis, samples were placed in a small amount of deionized water and placed in the sonicator for 5 min. The resulting extract was analyzed by ion chromatography for nitrate and sulfate ions. Separate portions of the extract were placed in centrifuge tubes and treated with barium nitrate solution to determine the presence of carbonate.

Results and Discussion

At the altitudes of low earth orbit (LEO), the concentration of gas is very low. The gas present at this altitude has a composition that is roughly the inverse of the atmosphere in the troposphere, 20% N_2 and 80% O_2. The absence of any overlying atmosphere allows short wavelength UV 9<240 nm) to split the majority of the molecular oxygen to individual atoms. This atomic oxygen is extremely reactive and will readily react with anything with which it collides. Structures in LEO are typically moving rapidly, as fast as 8 km/s, to maintain their orbit. At that velocity, these structures will encounter an atomic oxygen flux of 10^{15} oxygen atoms per second per square centimeter and collide with an impact energy of up to 5 eV. This collision energy accelerates the reaction of atomic oxygen with the structure materials and provide energy to drive additional reactions as well. The collision energy also allows atomic oxygen to more deeply penetrate materials and thus exert and even greater influence on the material.

In this study, an oxygen plasma etcher was used to generate an atmosphere that simulates that of LEO. This etcher utilizes radio frequency, 13.56 MHz, to excite an oxygen atmosphere at a pressure of 2-5 torr in to a plasma. This atmosphere will contain some undissociated oxygen molecules, oxygen ions, electrons, and oxygen atoms. For this work, the atmosphere was considered to consist of oxygen atoms only and the terms, oxygen plasma and atomic oxygen will be used synonymously.

In this study, foams based on four different chemistries were studied. One foam, Solimide, is a commercial product and its structure is proprietary. The other foams studied were produced by Langley research Center and they have the structures shown below. The structures are very similar but do have some important differences. Both the C and the L series foams have a carbonyl group between the two dianhydride groups while the H series foams have these groups bonded through and ether linkage. In the L series foams both benzene rings in the diether are linked through oxygen and both show para bonding. In the H series foams, the right most benzene ring is meta bonded. In the C series foams the two phenyl rings in the diether are linked through an SO_2 instead of a simple ether linkage. While these differences are small, they were expected to provide different reactions with atomic oxygen.

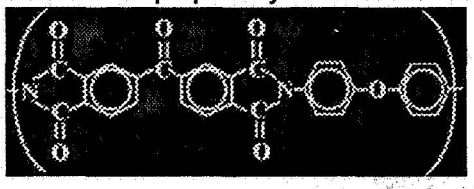

L

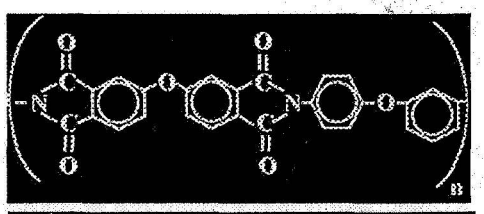

H

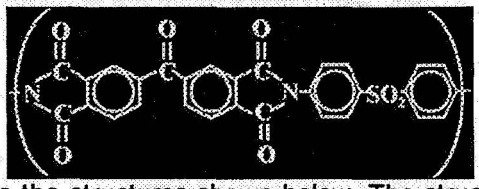

C

A significant amount of time in the first part of the fellowship period was devoted to helping the service engineer complete the installation of the XPS upgrade, work out bugs, and to learning the new system. Additional time was used to assemble, repair, and learn the oxygen plasma etcher. Once these tasks were accomplished, data gathering began.

For the initial trial, samples were prepared by cutting them from the larger foam pieces supplied with a razor blade. The samples were each approximately 1 mm thick and 1 cm on edge. They were mounted to the tabs of the XPS sample tray using carbon tape. For each sample, both survey and area scans were run. The sample tray was removed from the XPS and placed in the oxygen plasma etcher and exposed to oxygen plasma with the etcher set at full power for 2 hrs. Most surprisingly, when the sample tray was removed from the etcher, much greater than anticipated changes were observed in the foams. The sample tray that was originally coated with gold, showed a large visible decrease in the gold coating. The tray with the samples was placed back in t he XPS and the survey and area scans repeated.

Figure 1 shows the samples after the 2 hr, full power, oxygen plasma exposure, labeled B in the figure. Along with each of those samples in the figure, is a photo of a price of the original foam that was not exposed to plasma, labeled A in the figure. The figure also lists densities and surface areas of the samples for which those values were known.

The three L series samples show a definite relationship between density and oxygen plasma interaction. The L.5 foam was bleached from yellow to a gray color and only a small amount of material remained after oxygen plasma exposure. The L.H sample, with 10x the density of the L.5 sample showed a core of material remaining with the original color but reduced visual density surrounded by bleached and highly density-reduced material. The still higher density L8 sample showed a slight visible density reduction with the majority of the material remaining the original color and just a slight fringe of bleached material.

Two C series samples were exposed. The CL sample was just a typical foam and it showed total discoloration and a large amount of material loss after oxygen plasma exposure. The CL skin samples was the same foam but produced with a densified layer, the skin, that was oriented upwards. This skin largely protected the sample form the oxygen plasma. The skin showed some discoloration and material loss but largely remained intact. The foam underneath the skin was not affected by the plasma though the edges showed material loss where the foam was not protected by the skin.

The H series sample showed only slight discoloration and a small amount of material loss after oxygen plasma exposure. This was unexpected since this material was low density and had a large surface area.

The Solimide sample was totally decolorized and suffered a very large material loss after oxygen plasma exposure. This response was not totally unexpected, however, since the sample had a very low density and a large surface area.

The changes in the atomic percentages of C, N, and O in the surfaces of these samples, as determined by XPS, are plotted in Figure 2. Density and surface area are also plotted. Each sample showed a large increase in oxygen, a large decrease in carbon, and a small decrease in nitrogen concentration on the surface. For each of the samples, the decrease in the relative to the increase in oxygen is essentially the same and the nitrogen decrease is very small. There does not appear to be any correlation between these compositional changes and the surfaces are of the samples. The sample with the greatest density, the L8, showed the smallest visual changes after oxygen plasma exposure. This sample also showed the smallest oxygen increase and the smallest carbon decrease. In this trial, there also does not appear to be any link between the chemical structure of the foam and the interaction observed with atomic oxygen.

The changes in the binding energies of the C 1s, O 1s, and N 1s peaks in the XPS spectra of the samples after oxygen plasma exposure are shown in Figure 3. No correlation between the density or surface area and the binding energy shifts can be observed. This is as expected since the binding energy shifts indicate chemical changes. It is interesting that co correlation in these shifts and the chemistries of the foams can be detected either.

The first trial data indicate that there is indeed an interaction between oxygen plasma and the foams. The lower the density of the foam, the greater the bleaching and material loss upon exposure to the oxygen

plasma at full power. In this trial however, no relationship between the chemical structure of the foam and the interaction with atomic oxygen was observed.

The lack of structure-property correlation is not reasonable and is probably due to several experimental factors. After oxygen plasma exposure, many of the samples were found to contain silver and sulfur. Since only the C series and Solimide sample should contain sulfur and none has silver in their structure, there must be material transfer between the samples and the tray during oxygen plasma exposure. The effects of such a transfer are very difficult to predict. Also, the stability and homogeneity of the oxygen plasma within the etcher cavity were as yet unknown.

In order to characterize the atmosphere in the oxygen plasma etcher, studies were done with Kapton tape and Kapton HN films. The procedure was devised and utilized the Kapton tape samples. Then the standard procedure, ASTM E2089-00, was discovered. It is rewarding that the procedure devised was identical to that of the standard method with the exception of our use of Kapton tape instead of Kapton HN film. Thus, the determination was redone with Kapton HN film to verify the previous work with Kapton tape. The study done with the Kapton HN film was also done to determine the homogeneity of the plasma in the etcher cavity. This was accomplished by suing 4 samples simultaneously, each placed in one of the positions within the etcher caving where foams were placed for the exposure studies.

The parameter determined for the oxygen plasma generator was the effective atomic oxygen flux. This is the number of oxygen atoms striking a square centimeter of a surface per second assuming the same erosion rate as encountered in LEO. The effective atomic oxygen flux was determined for the etcher operating at full power, half power, and at 25% power. The results of these determinations are given below and plotted in Figure 4. The results indicate and the plots support the fact that the etcher is unstable at full power and provides much more reproducible results at 50 and 25% power levels. The plots indicate that, at 25% and 50% power levels, the effective atomic oxygen flux decreases with time but approaches a limiting value. Thus, the final value measured for each trial was taken as the limiting value.

effective atomic oxygen flux, 100% power = 5.10×10^{16} O atoms/cm^2 s
s = 2.81×10^{16} O atoms/cm^2 s

effective atomic oxygen flux, 50% power = 3.44×10^{16} O atoms/cm^2 s
s = 1.86×10^{16} O atoms/cm^2 s

effective atomic oxygen flux, 25% power = 2.16×10^{16} O atoms/cm^2 s
s = 1.20×10^{16} O atoms/cm^2 s

Figure 5 shows the data obtained from the Kapton HN samples. The data from this study corroborate well with those obtained from the Kapton tape studies, yielding an average effective atomic oxygen flux of approximately 2×10^{16} O atoms/cm^2 s. The effective atomic oxygen flux also appears to remain relatively constant throughout the etcher cavity.

Because the full power level of the etcher produces an unstable atmosphere that very rapidly attacks foam samples, a lower power was chosen for the next studies. The 25% power level was chosen because it produced the most reproducible environment and I had the lowest effective atomic oxygen flux to allow determination of changes with time in the foam samples.

The final part of the research done during this fellowship period was a more detailed study of the interaction of oxygen plasma with the foams. The was done by mounting samples on the bottoms of cleaned aluminum sample pans to allow for mass measurements and stable placement in the XPS. The etcher was used at 25% power to allow slower changes to the foams. Foams were placed in a reduced pressure environment to reduce the amount of absorbed moisture before initial weighing. After obtaining XPS survey and area data, they were exposed to oxygen plasma at 25% power for 30 min increments and weighed after each. When significant weight loss occurred, samples were re-analyzed with XPS, and then oxygen plasma exposure continued.

The mass loss data for foam samples during exposure to oxygen plasma at 25% power are shown in Figure 6. The carbon tape is particularly susceptible to the oxygen plasma. Thus, for this study, the carbon tape used to mount the samples was very small and placed up under the sample to protect it from mass loss. All of

the samples, except Solimide, showed only a small mass loss for the first hour of oxygen plasma exposure and then began a more rapid mass loss. Solimide resisted weight loss for only 30 min. The CL sample showed the greatest resistance to weight loss. This is the structure with the SO_2 linkage in the diamine and that structural group evidently provides added stability to the polymer in the presence of oxygen plasma.

Figure 7 shows the surface composition data for two samples as a function of oxygen plasma exposure time. Both samples show carbon losses and oxygen gains that mirror each other. However, the H series sample show greater carbon loss and oxygen gain than does the C series sample. The nitrogen content of the C series sample surface continually increases whereas that of the H series sample increases then drops again.

All of the foam samples exposed to oxygen plasma show huge increases of oxygen in the surfaces. The high vacuum of the XPS would cause loss of any oxygen that was just implanted and not bound in the samples. Thus, the oxygen shown to be present must be bound in some way. It was decided to determine if the oxygen plasma was causing oxidation of carbon to carbonate ion, the nitrogen to nitrate ion, and the sulfur to sulfate ion. This was accomplished by placing both virgin and samples that were exposed to 100% power oxygen plasma for 1 hr in separate flasks and sonicating for 5 min with a small amount of water. The aqueous extract of each sample was then analyzed with ion chromatography to determine the presence of sulfate and nitrate. A separate portion of each extract was also treated with aqueous barium nitrate to detect the presence of carbonate.

The following foams were extracted, HL, HLA, CL, Solimide, L8, and LH. The extracts from the unexposed samples showed no significant quantities of nitrate, sulfate, or carbonate for any of the samples. The CL sample showed a large amount of sulfate present after oxygen plasma exposure, indicating that the SO_2 linkage in the polymer backbone was oxidized. The extract from the exposed Slimmed sample also showed a significant amount, though far smaller than that of the CL sample, of sulfate ion. The exposed L8 extract showed a very small amount of sulfate, indicating a possible cross contamination in the etcher.

These studies indicated that the oxygen found in the surfaces of these samples is not in the form of nitrate or carbonate. Foams with structures containing sulfur do have a tendency to form sulfate and it is possible that this sulfate is part of the reason that the C series samples show the greatest resistance to oxygen plasma.

This summer faculty fellowship was highly successful and resulted in a large number of accomplishments. The upgrade and additional techniques were successfully completed on the XPS instrument. Many of the bugs from that installation were worked out and the software was learned. The oxygen plasma etcher was repaired, completed, set up, and characterized. Protocols for foam exposure and analysis were developed. Preliminary studies were done and finer studies begun on the interaction rates and mechanisms due to both physical and chemical parameters.

Most importantly, strong working relationships between this researcher and NASA colleagues have been established and reinforced. These relationships will last long into the future as the collaboration in research continues and grows.

Acknowledgements

The support of the NASA/ASEE Summer Faculty Fellowship program is deeply appreciated. The hard work of Dr. Ramon Hosler, Ms. Cassie Spears, Ms. Cassandra Black, and Mr. Gregg Buckingham to make the fellowship both happen and to be an enjoyable and rewarding experience are also greatly appreciated. My NASA colleague, Ms. Martha Williams was a true pleasure to work with. Thank you also to Dr. Orlando Melendez for his input as a colleague and friend. Mr. Wayne Marshall's help and expertise in doing the ion chromatography is greatly appreciated. Thank you also to the entire chemistry group for support, enthusiasm, professionalism, help and friendship.

List of Figures

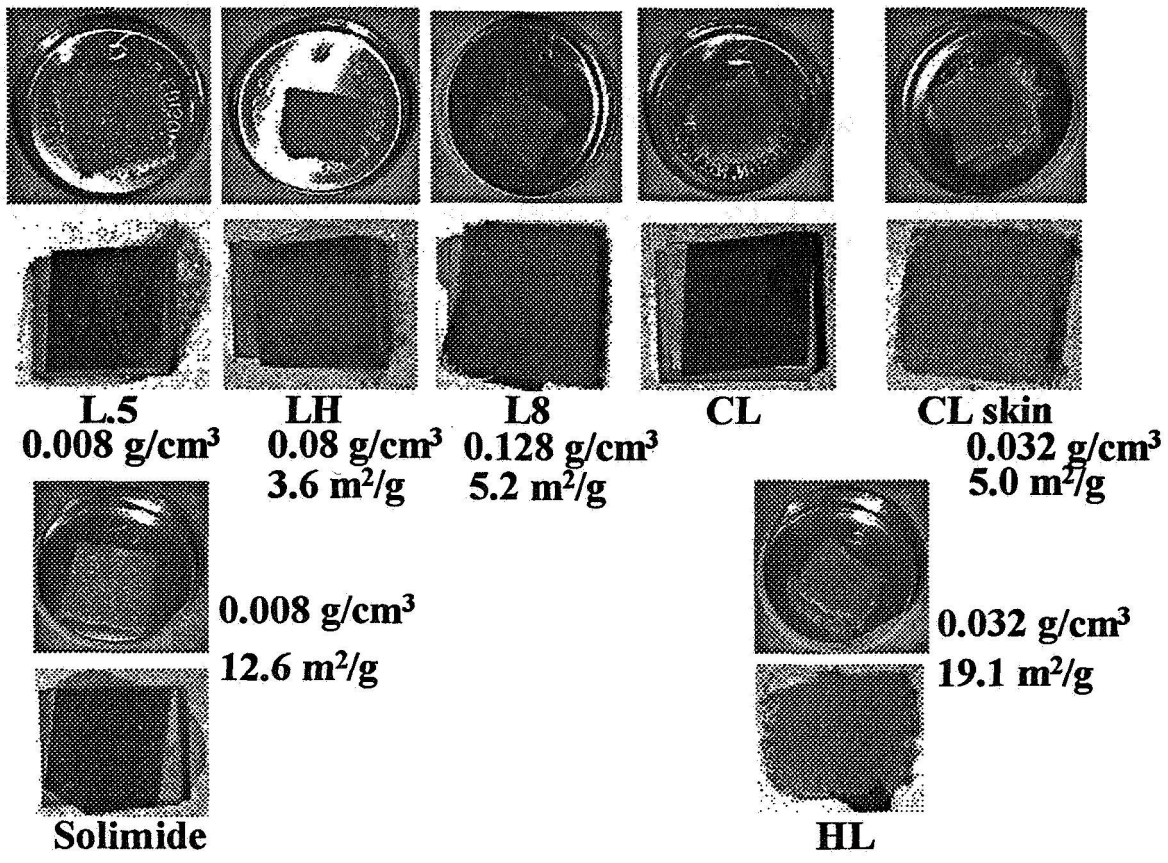

Figure 1. Foam samples from trial 1. A. unexposed samples. B. samples after exposure to oxygen plasma for 2 hr at full power. Density and surface area data included where available.

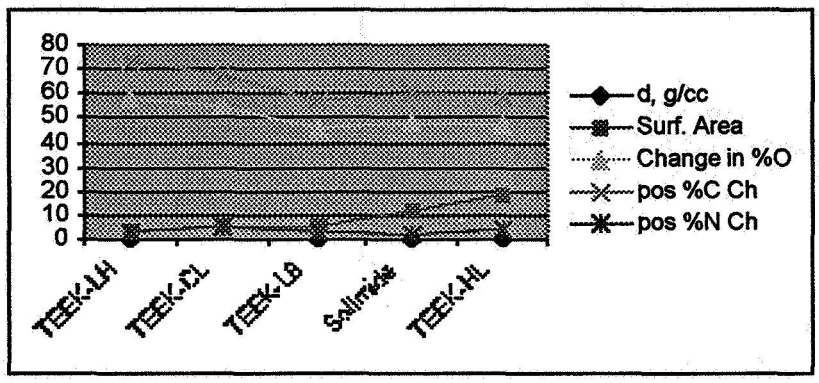

Figure 2. Surface composition change data for first trial samples before and after 2 hr, full power oxygen plasma exposure. The changes in C and N were negative because these elements were reduced in concentration after oxygen plasma exposure. For clarity, these values have been plotted as positive values.

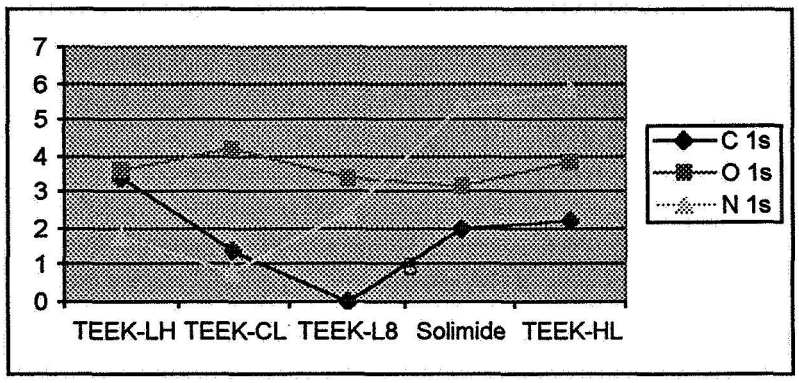

Figure 3. Plot of binding energy shift in C 1s, O1s, and N1s peaks after 2 hr, full power, oxygen plasma exposure for first trial samples. The y-axis binding energy change is in electronvolts.

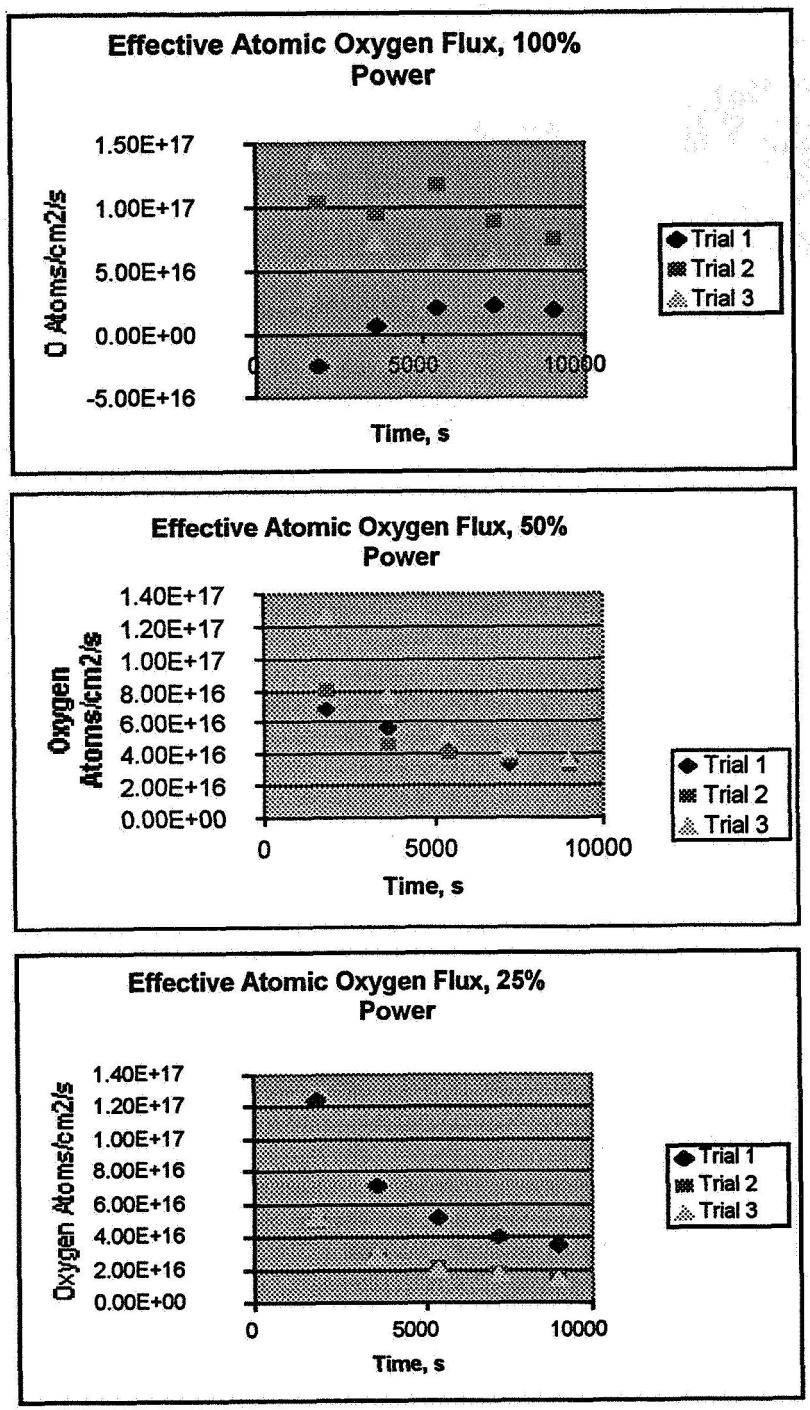

Figure 4. Effective atomic oxygen flux data for the three trials done at each power level using Kapton tape.

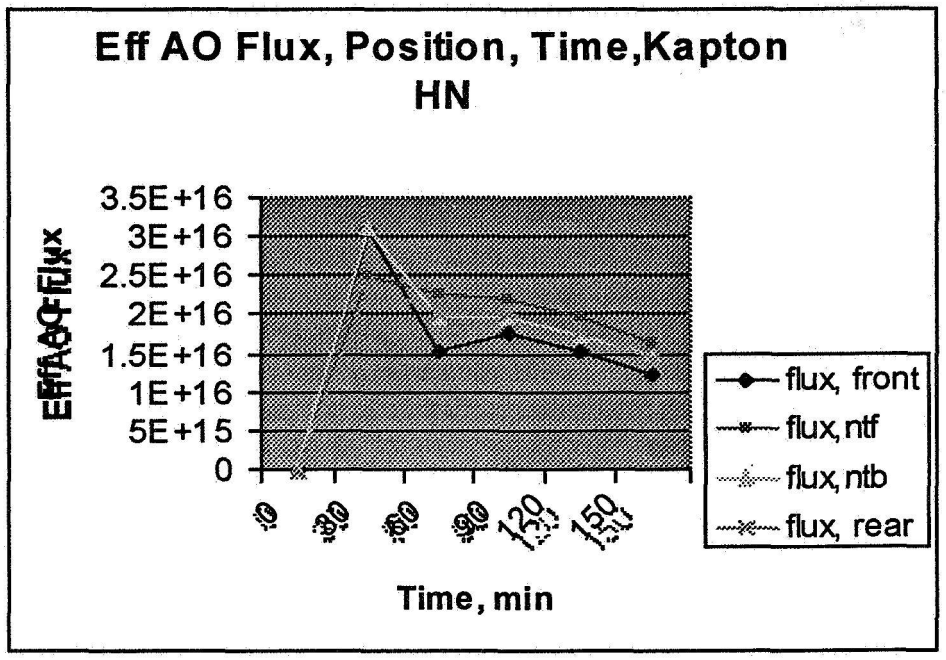

Figure 5. Effective atomic oxygen flux data obtained with Kapton HN film samples in 4 positions within the etcher cavity.

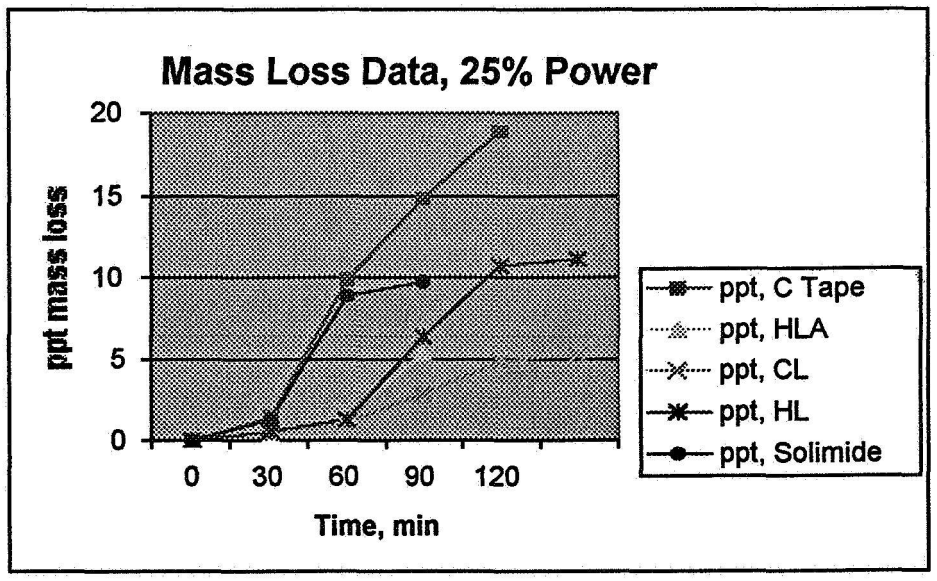

Figure 6. Mass loss data for samples exposed to oxygen plasma at 25% power. The y-axis is parts per thousand mass loss for clarity.

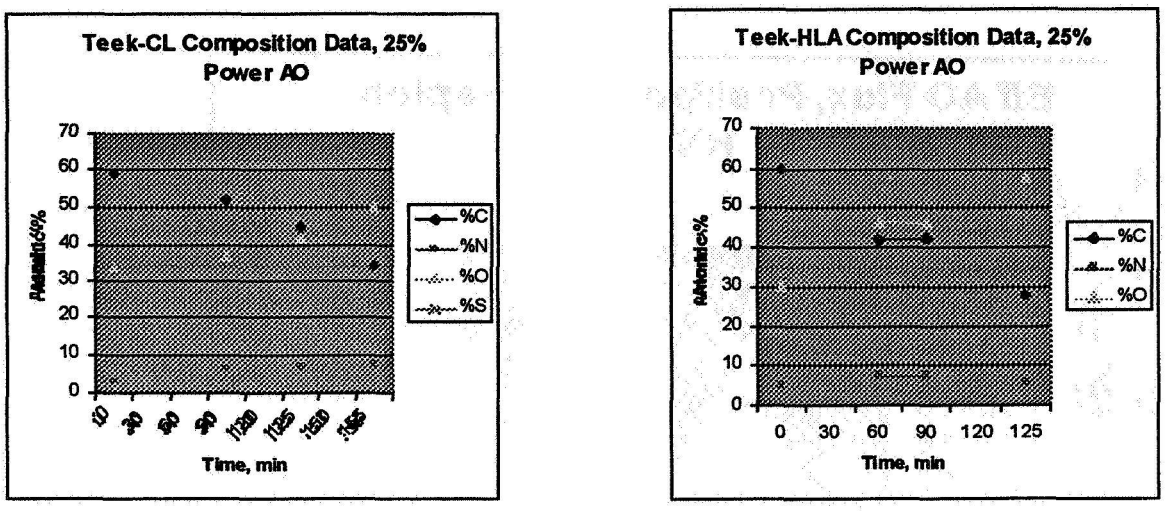

Figure 7. Surface composition data for C series sample and H series sample relative to oxygen plasma exposure time.

2001 NASA/ASEE SUMMER FACULTY FELLOWSHIP PROGRAM

JOHN F. KENNEDY SPACE CENTER
UNIVERSITY OF CENTRAL FLORIDA

THERMAL DESIGN OF A COLLAPSIBLE CRYOGENIC VESSEL

Hisham E. Hegab, Ph.D., P.E.
Associate Professor
Mechanical Engineering Program
Louisiana Tech University
KSC Colleague - Michael Lonergan, P.E.
Spaceport Engineering & Technology Directorate

ABSTRACT

Strategic planning for human exploration missions to Mars has conclusively identified in-situ resource utilization (ISRU) as an enabling technology. Most mission scenarios include an ISRU plant to produce propellants for ascent from Mars as well as the production of backup reserves of water, oxygen, and process gases. Current mission scenarios call for an ISRU plant to be deployed and then produce and store the required propellants and life support reserves before the arrival of the first human mission. Reliable cryogenic propellant liquefaction and storage technologies for extended period missions are especially critical. This report examines the cryogenic storage problem for liquid oxygen produced by an ISRU plant for a human mission scenario. The analysis examines various hardware configurations including insulation types, packaging techniques, and required cryocoolers to minimize the initial launch mass to low Earth orbit. Results of the analyses indicate that high vacuum insulation systems requiring vacuum pressures below one millitorr will be required to minimize the initial launch mass into low Earth orbit even though the temperature on the surface of Mars is much lower than Earth.

THERMAL DESIGN OF A COLLAPSIBLE CRYOGENIC VESSEL

Hisham E. Hegab, Ph.D., P.E.

1. INTRODUCTION

The current NASA mission plan for the first hum mission to Mars is based on an in-situ resource utilization (ISRU) approach where propellants will be produced using a production plant on the surface of Mars for the return ascent from the surface. This approach reduces the amount of propellants needed to be taken to Mars and ultimately reduced the overall mission cost. Making propellants on Mars requires liquefaction, storage, and transfer of cryogens on Mars. Cryogenic propellant liquefaction and storage technologies for extended periods of operation are especially crucial to a successful mission scenario. The current baseline for a human mission calls for a 500- to 600-day period of operation for propellant production and at least 700-days of continued storage capability. Trade-off studies are underway to examine various possible mission approaches. This report examines the cryogenic liquefaction and storage problem for a human mission to mars and proposes hardware configurations for a collapsible storage tank to be used for liquid oxygen storage. A collapsible design is being investigated for possible volume and mass reductions in the total system mass that is launched from Earth into low Earth orbit. The scheme of using a collapsible tank design is a derivative of inflatable habitat structures that were proposed in previous updates of the human reference mission. The use of these inflatable structures resulted in significant mass reductions. The mission costs depend principally on the initial mass to low Earth orbit (IMLEO) and will not be feasible if it becomes excessive. Thus, the selected criterion for evaluating mission options is the minimization of the IMLEO. For this analysis, the total storage system mass includes the mass of the insulation and required cryocoolers.

2. ASSUMPTIONS AND THERMAL ENVIRONMENT

The cryogen storage options evaluated in this report are based upon the Reference Mission of the NASA Mars Exploration Study Team [1] and its updated addendum [2] as well as recent papers examining cryogenic system requirements for a Mars mission scenarios [3,4]. The reference mission has several key attributes, including short transits for humans to and from Mars with long surface stays, and rendezvous on the Martian surface. Transit times are planned at less than 180 days, with surface stays over 500 days. The reference mission overview consists of two cargo mission launches and one crew transit launch. The first cargo mission will transport the Earth return vehicle for the crew into Mars orbit, and the second cargo mission, launched at the same time as the first one, will consist of a cargo lander with the propellant production plant, power systems, human habitat, and ascent vehicle. Approximately 26 months after the initial cargo mission launches, a human crew insertion mission is launched. After completion of the 500-day surface mission, the crew ascends to Mars orbit and rendezvous with the pre-deployed Earth return vehicle.

After deployment of the cargo lander on the Mars surface, in situ propellant production of methane and oxygen will commence. Current mission scenarios call for the propellant production of approximately 30,000 kg of oxygen and 8,500 kg of methane for the ascent vehicle. In addition, 4,500 kg of oxygen needs to be produced as a life support cache while the human crew is at Mars. Additional oxygen will likely be needed for EVAs and rover surface excursions [2,5] from the surface habitat. Based upon this information, it was decided to develop conceptual designs for a storage tank that could handle 50,000 kg of liquid oxygen. For the initial analysis of the various insulation systems investigated, a cylindrical shape with spherical end caps was selected for the tank. To hold the required 50,000 kg of liquid oxygen,

a tank approximately 3-m in diameter and 4.5-m long (cylindrical section length) is required. It was assumed the outer surface of the tank would be coated with a reflective material to reduce solar absorption and maximize radiative surface emission. A solar absorptivity and surface emissivity of 0.15 and 0.85, respectively, were assumed for the surface of the tank. Aluminized films are commercially available that provide these radiative properties. Table 1 summarizes the assumed parameters of the storage tank.

For this analysis, a storage pressure of 27.6 kPa (4 psia) was selected for the liquid oxygen. This pressure was selected for a companion study examining concepts for the structural design of the collapsible tank. At this selected storage pressure, the corresponding saturation temperature of the liquid oxygen is approximately 79 K. Selecting a higher storage pressure of approximately 155 kPa (22.5 psia) can increase the storage temperature to approximately 95 K, but this change was determined to produce little effect on the required insulation. However, the increase in storage pressure produces more significant increases in the structural requirements of the vessel; thus, increasing its mass so it was determined the lower storage pressure was preferable. In addition, the density of the liquid oxygen is slightly greater at the lower storage pressure, which helps to reduce the required size of the storage vessel.

Table 1. Summary of assumed tank parameters

Parameter	Assumption
Shape	Cylindrical with spherical end caps
Diameter	3 m
Length	4.5 m
α_s	0.15
ε	0.85

Table 2 provides the environmental conditions that were used to analyze the heat leak to the storage vessel. These conditions are essentially the same as those used by Mueller and Durrant [6] for the analysis of propellant liquefaction and storage for a precursor mission to demonstrate the ISRU technology. Environmental conditions for a typical Martian day, night, and dust storm are examined. Fig. 1 illustrates the differences in solar irradiance between Earth and Mars as described by the Mars Reference Mission addendum [2]. Solar irradiation at the surface of Mars is significantly lower than that at Earth's surface and is strongly influenced by the presence of dust storms. Other sources of Mars environmental conditions were also examined [6,7] and the conditions listed in Table 2 were deemed reasonable design conditions for analyzing the vessel. It should be noted the conditions listed in Table 2 are nominal conditions and significant variations from them are possible depending upon the chosen landing site and variations in local weather conditions. Thus, an insulation system based upon these design conditions would be expected to occasionally encounter conditions beyond their limits and would require a pressure relief system to prevent structural damage to the vessel. In the absence of designated landing site for the reference mission, these environmental conditions should provide an adequate analysis for the current level of this feasibility study.

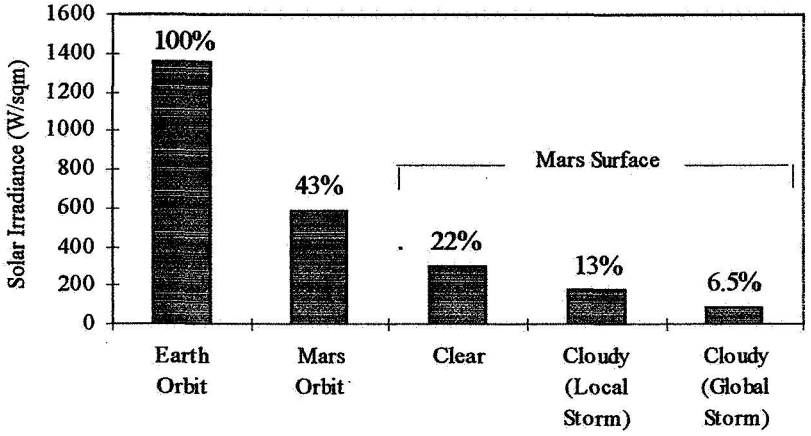

Figure 1. Earth and Mars solar irradiance comparison [2]

Table 2. Assumed Mars environment conditions

	Day	Night	Dust storm	Units
Average Solar irradiation	304	---	150	W/m^2
Atmosphere Temperature	230	190	210	K
Ground Temperature	220	195	200	K
Sky Temperature	170	130	200	K
Wind Speed	8	8	17	m/s

The insulation system design requirements are to obtain a near zero boil off rate for the stored liquid oxygen. To achieve this, cryocoolers will be required to re-liquefy any boil off from the storage tank due to heat leak. The additional mass of the cryocoolers is considered as part of the total insulation system mass but there is no mass penalty for the increased power needed for larger cryocoolers. For this analysis, it was assumed that the increase in cryocooler power requirements would have a negligible impact on the power system mass since the design reference mission calls for a nuclear power plant to support the human mission. Results from this study would need to be revised in the case of a solar power mission. The cryocooler efficiency was based upon the efficiency of a pulse tube cryocooler currently being developed for a Mars precursor mission [8]. This cryocooler is being specifically developed for liquefying oxygen on Mars and produces approximately 19 W of refrigeration for 222 W of input power ($COP_R = 0.086$). This performance is very high (~20% of Carnot efficiency) for a pulse tube cryocooler, but based upon the significant progress in improving cryocooler efficiencies in the last five years it is likely that cryocoolers used in a human mission to Mars would have similar or better efficiencies.

3. ANALYSIS APPROACH

Once the model assumptions and constraints were established, the analysis was developed to select the preferred insulation type, thickness required, and cryocooler capacity resulting in the minimum total insulation system mass (insulation mass + cryocooler mass + radiator mass). Several common cryogenic insulation types were considered including multilayer insulation (MLI), aerogel blankets, microspheres, opacified powder, perlite, and a new layered composite insulation (LCI) being developed at KSC. These various insulation types were evaluated at various ranges of ambient pressure ranging from high vacuum (<0.001 torr) to the atmospheric pressure on Mars (~7 torr). The apparent thermal conductivities and densities of the various insulation types at their respective pressures are provided in Table 3.

In order to estimate the insulation thickness and cryocooler capacity required an energy balance was conducted at the tank surface, which includes solar irradiance, radiation exchange with the environment, convection with the atmosphere, and conduction through the insulation as shown in Fig. 2. A simple one-dimensional, steady state heat transfer analysis was used. For simplicity, the tank was assumed to be cylindrical with spherical end caps. The structural design may require more of an egg shape to provide support to hold the weight of the liquid oxygen but would not significantly affect the results of this analysis.

Table 3. Insulation types examined

Insulation	Apparent k (mW/m-K)	Density (kg/m^3)	Vacuum Level*
MLI [9]	0.08	58	High
	2.68	58	Soft
Aerogel blanket [9]	0.55	125	High
	1.16	125	Soft
	4.97	125	Ambient
Layered Composite Insulation [9]	0.09	52	High
	1.23	52	Soft
	5.56	52	Ambient
Microspheres [10]	0.39	130	High
Opacified powder [10]	0.48	80	High
Perlite [11]	1.10	135	High
	2.50	135	Soft

* high vacuum ≈ 0.001 torr or less, soft vacuum ≈ 0.1 torr, ambient ≈ 7 torr

A model of the tank using three nodes to represent the surface temperature of the tank on the top hemisphere, the cylindrical side, and the bottom hemisphere was developed. Each surface node allows for convection and radiation to the atmosphere and absorption of direct solar irradiation. The three surface nodes are also linked to a single fixed temperature node representing the liquid oxygen temperature.

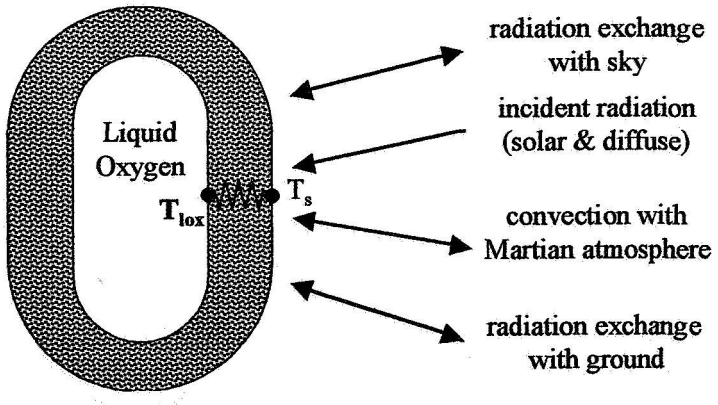

Figure 2. Energy balance schematic

In the following equations, the insulation properties (thermal conductivity and density) and boil off rate of the liquid oxygen are the inputs, and the desired outputs are the insulation system masses as well as other operating parameters such as tank surface temperature, heat leak, cryocooler power, etc.

$$\frac{T_{surf,i}-T_{lox}}{R_{ins,i}} = q_{solar,i} + \frac{T_{atm}-T_{surf,i}}{R_{conv,i}} + \frac{J_{surf,i}-\sigma T_{surf,i}^4}{\frac{1-\varepsilon}{\varepsilon A_i}} \quad \text{where} \quad i=1\ldots3 \tag{1}$$

$$\frac{J_{surf,i}-\sigma T_{surf,i}^4}{\frac{1-\varepsilon}{\varepsilon A_i}} = \frac{\sigma T_{sky}^4 - J_{surf,i}}{\frac{1}{A_i F_{i3}}} + \frac{\sigma T_g^4 - J_{surf,i}}{\frac{1}{A F_{i2}}} \quad \text{where} \quad i=1\ldots3 \tag{2}$$

$$R_{ins,1} = \frac{\ln\left[\frac{D/2+t_{ins}}{D/2}\right]}{2\pi k_{ins} L} \qquad R_{ins,2,3} = \frac{\frac{1}{D/2}-\frac{1}{D/2+t_{ins}}}{4\pi k_{ins}} \qquad R_{conv,i} = \frac{1}{h_{c,i}A_i} \quad \text{where } i=1\ldots3 \tag{3}$$

$$q_{solar,1} = \alpha_s \frac{A_1}{2} \qquad q_{solar,2} = \alpha_s A_2 \qquad q_{solar,3} = 0 \tag{4}$$

$$q_{leak} = \frac{T_{surf,1}-T_{lox}}{R_{ins,1}} + \frac{T_{surf,2}-T_{lox}}{R_{ins,2}} + \frac{T_{surf,3}-T_{lox}}{R_{ins,3}} \tag{5}$$

$$\dot{m}_{boiloff} = \frac{q_{leak}}{h_{fg}} \tag{6}$$

$$m_{insulation} = \rho_{ins} t_{ins} A \tag{7}$$

$$m_{cryocooler} = 0.9 \cdot \frac{171.85}{(T_{lox}-10)^{0.85}} \cdot q_{leak} \tag{8}$$

$$m_{radiator} = 0.05 P_{cryocooler} \tag{9}$$

$$P_{cryocooler} = \frac{q_{leak}}{0.2[T_{atm}-(T_{lox}-10)]} \tag{10}$$

$$m_{total} = m_{insulation} + m_{cryocooler} + m_{rad} \tag{11}$$

Eqs. (1) and (2) are energy balances at the tank surface for each of the three nodes. Variables for the three surface nodes are denoted by the subscript i, where $i = 1$ corresponds to the cylindrical side of the vessel, $i = 2$ corresponds to the top hemispherical cap, and $i = 3$ corresponds to the bottom hemispherical cap. The unknowns determined by these equations are the tank surface temperatures, $T_{surf,i}$, and the tank surface radiosities, $J_{surf,i}$. The insulation thermal resistance, $R_{ins,i}$, and convection thermal resistance, $R_{conv,i}$, in Eq. (1) are determined by Eq. (3) using one dimensional, steady state heat transfer equations. The convection coefficients, $h_{c,i}$, were determined using a Nusselt number correlations by Churchill and Bernstein for a cylinder in crossflow [12] and by Whitaker [12] for flow over a sphere for the selected atmospheric conditions. The view factors, F_{12} and F_{13}, are from the tank cylindrical surface to the ground and to the sky, respectively. They were determined using the geometry of the tank assuming no interference from other deployed equipment and both found to be 0.5 [13]. The top hemisphere node only exchanges radiation with the sky and similarly the bottom hemisphere node only exchanges radiation with the ground. Consequently, view factors F_{22} and F_{33} are zero and view factors F_{23} and F_{32} are one. The solar

irradiation for each surface node was determined using Eq. (4). It is assumed that half of the tank is exposed to the influx of solar irradiation such that the half of the cylindrical side surface area and the entire top hemispherical cap area are exposed. The heat leak, q_{leak}, into the liquid oxygen is calculated by Eq. (5). The boil off rate of the liquid oxygen is determined by Eq. (6), where the heat of vaporization, h_{fg}, was determined from the saturation pressure of the liquid oxygen. The individual insulation system masses are determined in Eqs. (7) – (9). Eq. (8) is an empirical correlation developed by Kittel et al. [4] that predicts cryocooler mass based upon commercially available cryocoolers. Eq. (9) is another empirical correlation that predicts the required radiator mass for the cryocooler [6]. Eq. (10) is used to estimate the cryocooler power assuming that it has a 20% Carnot efficiency [8]. Finally, the total insulation system mass is determined by Eq. (11).

4. RESULTS AND DISCUSSION

The results of the optimization of the various insulation systems for the nominal day environmental conditions are shown in Figs. 3 and 4. In Fig 3., the total insulation system mass is shown as a function of boil off rate of the liquid oxygen for the various insulation systems. In Fig. 4, the total insulation system mass is shown as a function of the insulation thickness. As expected, there is an optimal tradeoff between insulation mass and cryocooler mass. As the system insulation mass increases, the required cooler capacity, and consequently mass, decreases. Table 4 provides a summary of system parameters that minimize the total insulation system mass for each of the insulations for a nominal daytime environment on Mars. From examining the results, it is apparent that the high vacuum MLI and LCI systems provide the smallest total insulation system mass. Each offers almost the same IMLEO for the same insulating performance. It is also noted that the outer surface temperature of a well-insulated tank is essentially independent of the insulation type used and primarily depends on the external environment conditions and tank surface radiative properties. There is approximately an order of magnitude penalty in the total insulation system mass for using soft vacuum insulation systems compared to the high vacuum MLI and LCI. Soft vacuum or ambient pressure insulation systems would be desirable for their greater reliability and simplicity but would not likely be the best choice because of the significant mass penalty.

Table 4. Insulation system parameters for minimal IMLEO

Insulation	Vacuum level*	t_{ins} (cm)	Q_{leak} (W)	T_{surf} (K)	$P_{cryocooler}$ (W)	$m_{insulation}$ (kg)	$m_{cryocooler}+m_{rad}$ (kg)	m_{total} (kg)
MLI	High	3.6	31.1	217	361	146.3	149.2	295.6
	Soft	20.5	195.8	216	2267	840.6	937.9	1778.5
Aerogel blanket	High	6.3	121.6	216	1408	560.8	582.6	1142.4
	Soft	9.2	179.1	216	2075	812.3	858.2	1670.5
	Ambient	18.8	388.4	214	4498	1665.0	1861.0	3526.0
LCI	High	4.0	31.3	217	363	146.9	150.2	297.1
	Soft	14.7	122.2	216	1415	541.0	585.5	1126.5
	Ambient	31.0	280.0	215	3243	1142.0	1342.0	2484.0
Microspheres	High	5.2	103.9	216	1203	482.0	497.6	979.6
Opacified powder	High	7.4	91.4	216	1058	419.8	437.8	857.6
Perlite	High	8.6	180.8	216	2093	822.0	866.0	1688.0
	Soft	12.9	278.3	215	3223	1233.0	1333.0	2566.0

* high vacuum ≈ 0.001 torr or less, soft vacuum ≈ 0.1 torr, ambient ≈ 7 torr

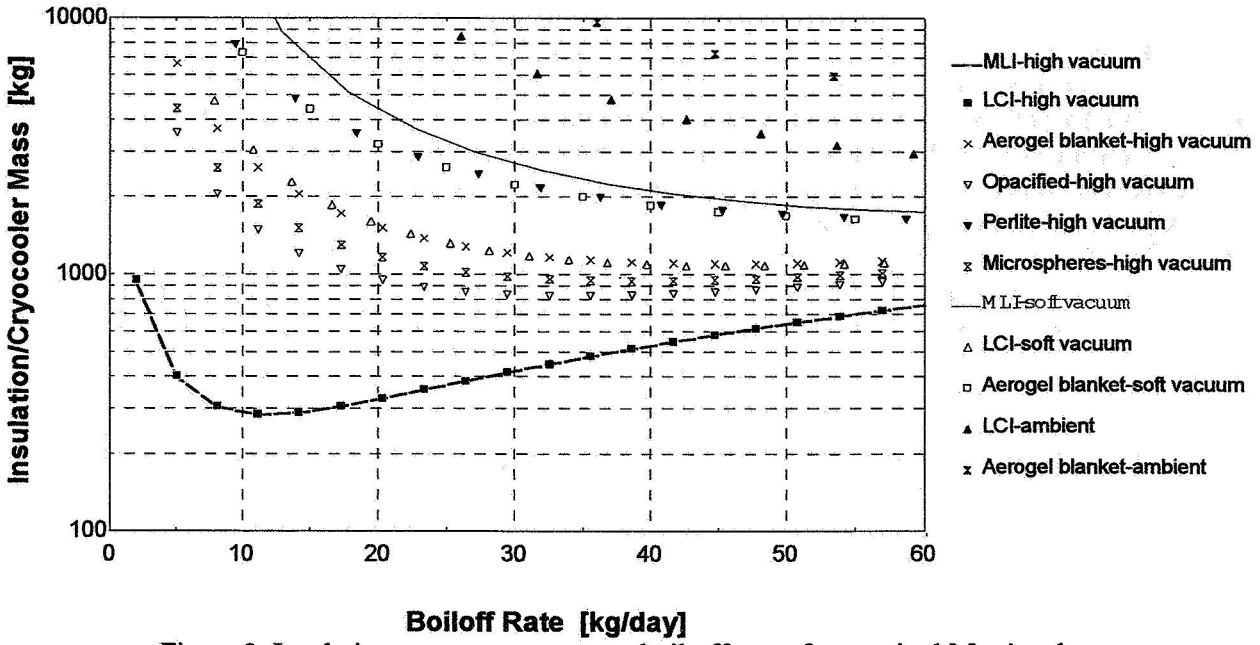

Figure 3. Insulation system mass versus boil off rates for nominal Martian day

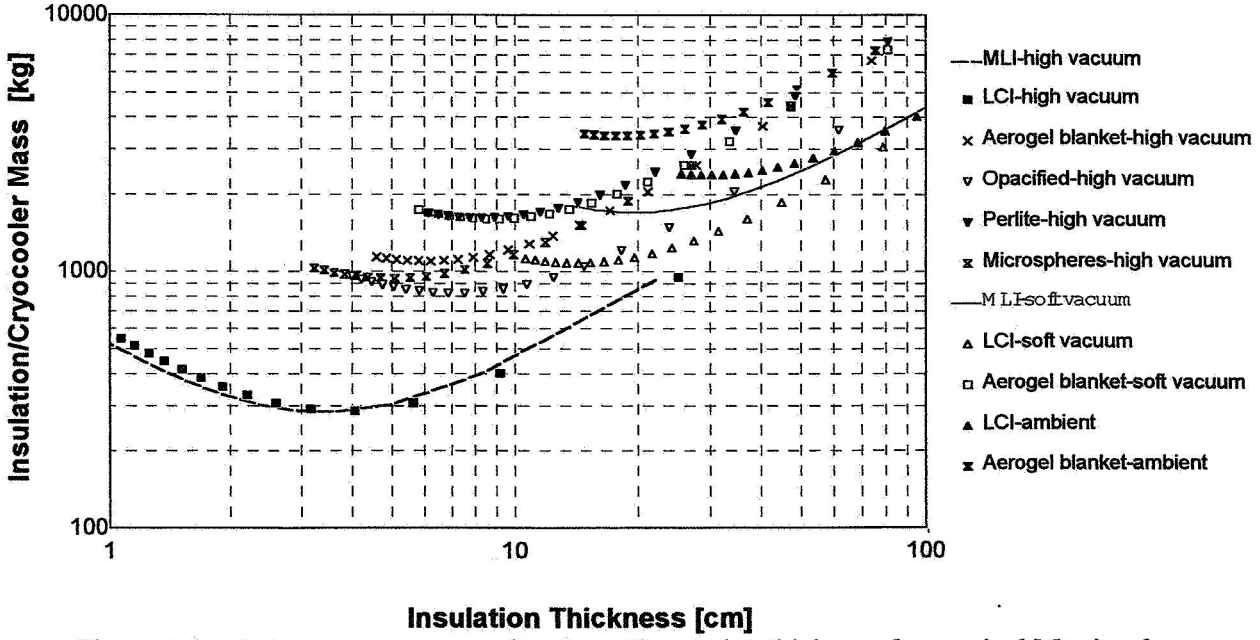

Figure 4. Insulation system mass as function of insulation thickness for nominal Martian day

Table 5 summarizes the operating conditions of the two insulation types with the lowest IMLEO, high vacuum MLI and LCI, for the three assumed nominal environmental conditions. Both insulations perform essentially the same since they have almost the same densities and thermal conductivities. Consequently, other factors such as reliability, installation, and packaging should be considered when selecting between the two. For a collapsible storage vessel design, reliability and packaging issues would likely be disadvantages for using MLI. MLI is highly anisotropic so its performance can be severely degraded by edge effects in its installation. In addition, its thermal performance is easily degraded by compression loading effects, which are a likely loading condition for a collapsible structure since a rigid

outer vessel wall is not desirable in a collapsible design. While it is anticipated that the layered composite insulation would be susceptible to these disadvantages as well it is difficult to calculate approximately how it would perform because of the lack of experimental data on it. Thermal performance under slight compressive loads is needed as well as experiments on edge effects associated with packaging it in vacuum-sealed polymer sheets.

Table 5. Summary of operating conditions for high vacuum MLI and LCI

Parameter	3.6 cm of MLI-high vacuum			4.0 cm of LCI-high vacuum		
	Day	Night	Dust storm	Day	Night	Dust storm
Q_{leak} (W)	31.1	22.2	29.1	31.4	22.3	29.3
$m_{boiloff}$ (kg/day)	12.1	8.6	11.3	12.1	8.6	11.4
T_{surf} (K)	217	177	208	217	177	208

Packaging of any selected insulation type is a significant issue for a collapsible design. It is envisioned that vacuum insulation panel technologies would be used for packaging LCI or MLI. Typical vacuum insulation panels consist of three components as shown in Fig. 5. The core material is the selected insulation such as LCI. The barrier/envelope may consist of a metal foil or polymer and serves to protect the insulation from permeation and possibly as a radiative shield. The most suitable choice for this application would most likely be a polymer with thin layer of metal vapor deposited on it. Using metal foils for the barrier provides a heat conduction path around the insulation so very thin layers are required to limit the heat leak. Getters and desiccants are typically used to maintain the vacuum level in the insulation panel. There are a number of commercial developers of this technology and vacuum levels below 0.003 torr have been maintained for more than two years in laboratory testing. Selection and design of the envelope, getters, and desiccants is a complicated matter and must be matched to the selected insulation as well as the external operating environment and desired vacuum level. Further studies on designing a vacuum insulation package for this application would be needed to be able to predict heat leaks due to edge effects as well as predict the thermal performance of the system over an extended period of operation.

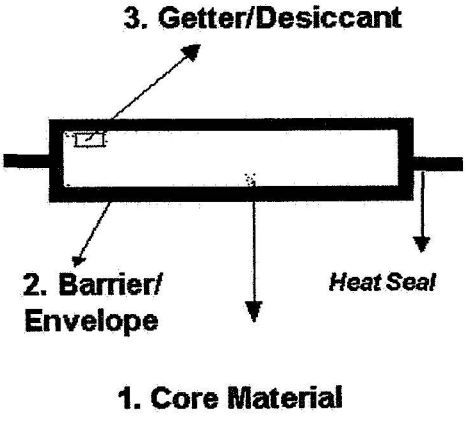

Figure 5. Components of a vacuum insulation panel

5. CONCLUSIONS

Based upon the analysis results, the surface temperature of a cryogenic storage vessel on Mars is primarily determined by solar irradiation, surface radiative properties, and convection with the atmosphere. For a properly insulated tank, the surface temperature of the tank is essentially independent of the insulation selected. The optimal insulation systems that minimize the initial launch mass to low Earth orbit are high vacuum systems using MLI or a layered composite insulation being developed at KSC. These insulations combined with a cryocooler system could achieve near zero boil-off rates with a total insulation system mass of approximately 300 kg. The corresponding heat leak into the storage tank and required cryocooler power are approximately 30 W and 360 W, respectively. The analysis assumes that there is no mass penalty for the cryocooler power. A solar powered human mission scenario would present significant complications to the cryogenic liquefaction and storage problem and may produce different results for the optimal insulation parameters. Vacuum insulation panel technology could be used to develop a packaging system for the insulation such that it could be integrated into a collapsible design, but the design of such a system would need to be tailored to the expected environmental conditions on Mars.

ACKNOWLEDGEMENTS

I would like to express my sincere appreciation to my NASA-KSC colleague Mike Lonergan for sponsoring me on this project. I would also like to thank Ray Hosler, Cassie Spears, and Greg Buckingham for their efforts in supporting the Summer Faculty Fellowship Program at KSC. Many thanks to everyone who helped to make this summer an enjoyable and interesting experience.

REFERENCES

[1] Hoffman, S. J., Kaplan, D. I., editors, Human Exploration of Mars: The Reference Mission of the NASA Mars Exploration Study Team, Johnson Space Center, July 1997.

[2] Drake, B., editor, Reference Mission 3.0 Addendum to the Human Exploration of Mars: The Reference Mission of the NASA Mars Exploration Study Team, Johnson Space Center, June, 1998.

[3] Salerno, L. J., and Kittel, P., Cryogenics and the human exploration of Mars, *Cryogenics*, 39, 1999, p. 381-388.

[4] Kittel, P., Salerno, L. J., and Plachta, D.W., Cryocoolers for Human and Robotic Missions to Mars, *Cryocoolers 10*, Kluwer Academic/Plenum Publishers, 1999, pp. 815-821.

[5] Sridhar, K. R., Finn, J. E., and Kliss, M. H., In-Situ Resource Utilization Technologies for Mars Life Support Systems, *Adv. Space Res.*, vol. 25, no. 2, 2000, pp 249-255.

[6] Mueller, P., and Durrant, T., Cryogenic propellant liquefaction and storage for a precursor to a human Mars mission, *Cryogenics*, 39, 1999, pp. 1021-1028.

[7] Environment of Mars, NASA-TM 100470, October 1988.

[8] Marquardt, E. D., Radebaugh, R., Pulse Tube Oxygen Liquefier, *Adv. Cryogenic Engineering*, vol. 45, 2000, pp. 457-464.

[9] Augustynowicz, S. D., and Fesmire, J. E., Cryogenic Insulation System for Soft Vacuum, KSC-00408 Report, 1999, pp. 1-7.

[10] Barron, R. F., *Cryogenic Systems, 2nd Ed.*, 1985, pp. 391-396.

[11] Barron, R. F., Cryogenic Heat Transfer, 1999, pp. 29-33.

[12] Incropera, F. P. and DeWitt, D. P., *Introduction to Heat Transfer, 3rd Ed.*, 1996, p. 345-349.

[13] Rea, S. N., Rapid Method for Determining Concentric Cylinder Radiation View Factors, *AIAA Journal*, 13, 8, August 1975, pp. 1122-1123.

2001 NASA/ASEE SUMMER FACULTY FELLOWSHIP PROGRAM

JOHN F. KENNEDY SPACE CENTER
UNIVERSITY OF CENTRAL FLORIDA

EVALUATION OF ELECTROCHEMICAL METHODS FOR ELECTROLYTE CHARACTERIZATION

Robert H. Heidersbach
Professor of Materials Engineering and Department Chair
California Polytechnic State University
KSC Colleague: Luz Marina Calle

ABSTRACT

This report documents summer research efforts in an attempt to develop an electrochemical method of characterizing electrolytes. The ultimate objective of the characterization would be to determine the composition and corrosivity of Martian soil. Results are presented using potentiodynamic scans, Tafel extrapolations, and resistivity tests in a variety of water-based electrolytes.

EVALUATION OF ELECTROCHEMICAL METHODS FOR ELECTROLYTE CHARACTERIZATION

Robert H. Heidersbach

1. INTRODUCTION

Purpose of this project: This report documents the summer research efforts in an attempt to develop an electrochemical method of characterizing electrolytes. This summer's project had as its objectives the following tasks:

Design experiments to be done at KSC, then at an Arizona test site, and ultimately on a Mars mission in 2007 or later.

Validate that the experiments are relevant and reproducible.

Identify limitations and uses for the experiments developed.

The ultimate objective of the characterization would be to determine the composition and corrosivity of electrolytes, including Martian soil. Results are presented using potentiodynamic scans, Tafel extrapolations, and resistivity tests in a variety of water-based electrolytes.

The summer efforts are part of a multi-year project to develop electrochemical characterization techniques for a variety of NASA-related uses. Work will continue at Kennedy Space Center after the summer project.

Mars: The composition and other characteristics of Martian soil are controversial and not well documented. A number of probes have been sent to Mars, and the results have been publicized [1-3], but the interpretation of the data remains controversial. They can be summarized by stating that Mars has a variable climate with temperatures that range from very cold near the poles to temperatures that get above the freezing point of water during the day near the equator. This is summarized in Figure 1, adopted from a recent National Geographic article on Mars.

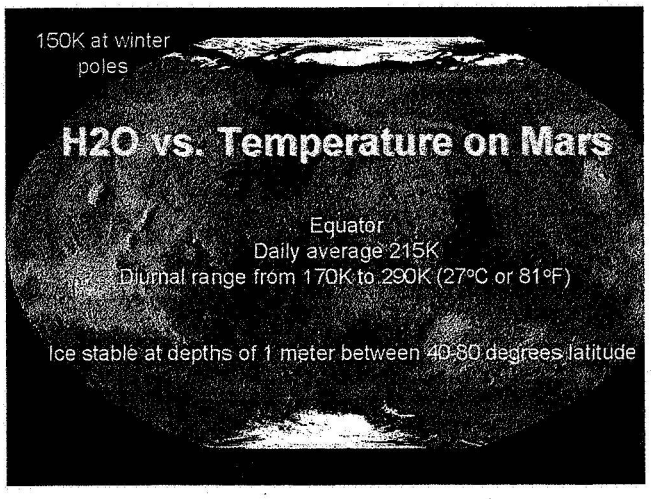

Figure 1: Temperatures and water on Mars [4].

While most of Mars is very cold and dry, it will be necessary to create habitats with moisture and warmer temperatures if manned missions ever go to Mars. The Mars Surveyor missions in the 1990's showed that Martian soil is ionic and will leach ions into any available water. Recent reports indicate that there may be natural brines on or near the surface. These brines would be corrosive at the temperatures where humans would function (approximately 25°C).

Table 1: Atmospheres on Earth and Mars [5]

	Earth	Mars
Pressure	760 mm Hg	7 mm Hg
N_2	78%	2.7%
CO_2	0.033%	95.3%
Ar	0.93%	1.6%
O_2	21%	0.13%

The atmospheres on Earth and Mars are also very different. Table 1 shows that the Earth's atmosphere is primarily inert nitrogen and argon, whereas Mars has an atmosphere that is mostly carbon dioxide at a very low pressure. Experience on earth indicates that most corrosion and other chemical activity arises from the levels of dissolved atmospheric oxygen in electrolytes such as condensation, surface water, and soils. The presence of carbon dioxide serves to make waters corrosive on earth (Figure 2), unless there are also substantial amounts of dissolved metallic ions. If this happens, then scales can form which will cover metal surfaces and retard corrosion (Figure 3). This scale is normally somewhat protective and leads to the general conclusion that "hard" waters (those having high calcium or magnesium contents) are generally less corrosive than "soft" waters that have lower concentrations of these dissolved metals.

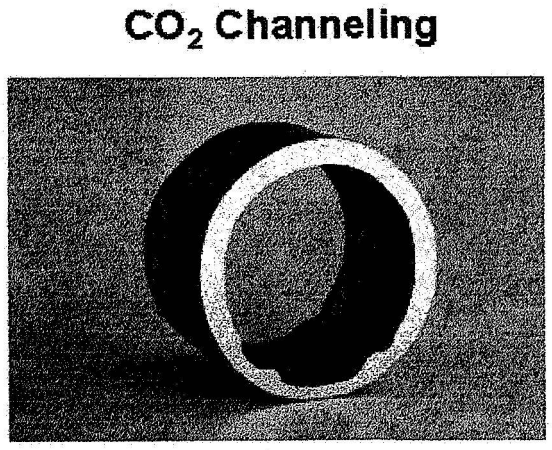

Figure 2: CO_2 channeling caused by high dissolved gases in unbuffered condensate soft water. [6]

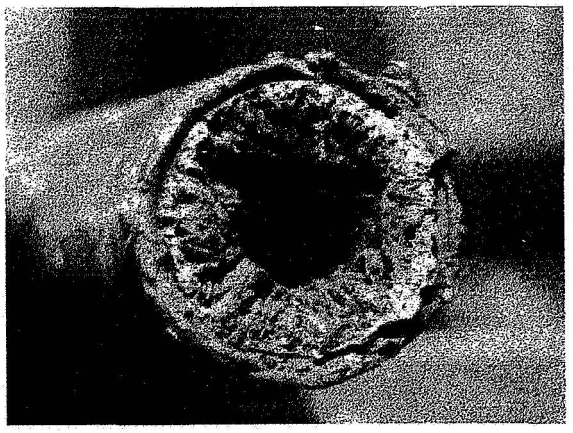

Figure 3: Calcium carbonate scale caused by high mineral content in in hard water.

The effects of dissolved oxygen in water cause most corrosion on earth. Dissolved CO_2 is a secondary effect that leads to corrosion, but only if a reducible species such as dissolved oxygen is also available to promote corrosion. On Mars, the presence of CO_2 will insure that the pH and mineral scale formation on metal surfaces will tend to be different than on earth,

but the limited amount of atmospheric oxygen should make any brines that form less corrosive than they would be on the earth's surface.

Electrochemical characterization of soil and electrolytes: Pipelines and other structures exposed to soil on earth will corrode depending on a number of variables. The most important variables are recognized to be the conductivity of the soil, its compaction (permeability to moisture and air), and moisture content. Figure 4 shows the relationship between soil corrosivity and soil resistivity on earth. In general, low resistivity soils are more corrosive than high resistivity soils.

Characterization of the corrosivity of Martian soil should also depend on the conductivity of the soil. The NASA Kennedy Space Center already has a group working on the effects of conductive Martian soils on the reliability of equipment sent to Mars [8], and joint efforts are underway between the Electromagnetic Physics Laboratory and the Corrosion Technology Testbed groups. It is an obvious step to include conductivity measurements in the program at some time in the future.

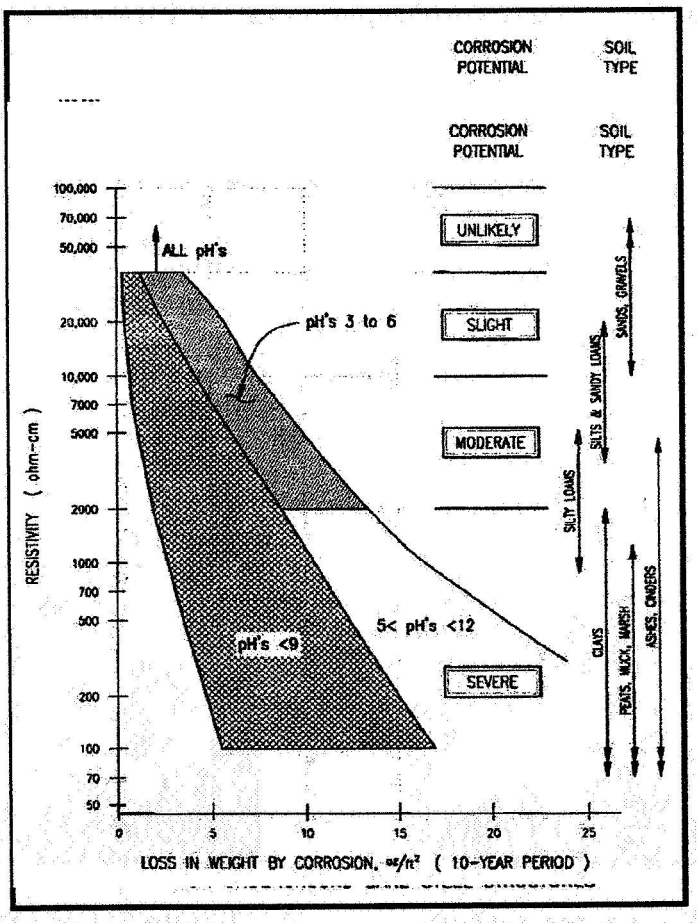

Figure 4: The effects of soil resistivity on soil corrosivity [7]

2. Experimental procedures

Background efforts: The incentive for this summer's work is a collaborative effort between NASA's Kennedy Space Center and the Jet Propulsion Laboratory (JPL) in Pasadena, California. The original idea on this project was to use a series of electrodes fabricated for a Mars mission to characterize Martian soil. JPL has experience in developing similar electrodes [9], and the electrode arrangement being developed by JPL is shown in Figure 5. The eight sensors labeled "galvanic cell array" in Figure 5 are the electrodes being fabricated for the Kennedy Space Center and will be used for electrochemical experiments designed to characterize electrolytes such as Martian soil.

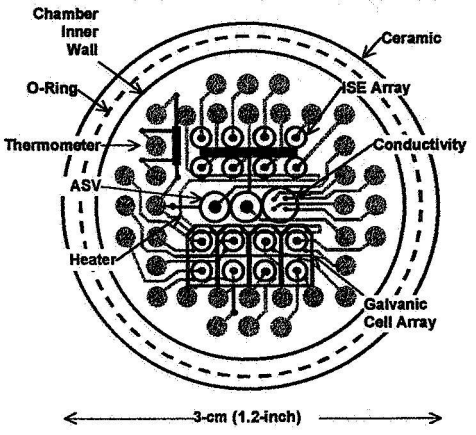

Figure 5: Mars soil characterization electrode schematic.

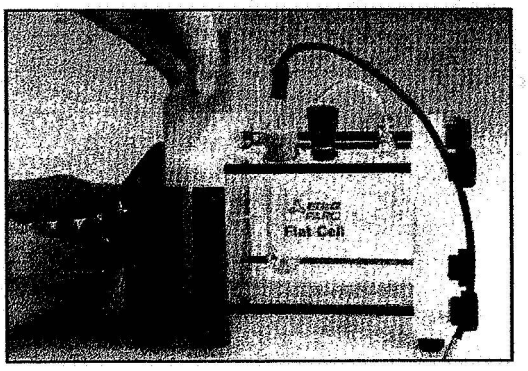

Figure 6: Electrochemical cell used for potentiodynamic scans

Potentiodynamic experiments: The original ideas that started this research were based on the results of a Master's thesis [10] cited in a standard corrosion textbook [11]. The idea was to use potentiodynamic scans of various metals to characterize electrolytes. Figure 6 shows a standard electrochemical cell used for this type of experiment.

Cells of this type are routinely used for corrosion electrochemistry tests around the world, and they can be purchased from a variety of commercial suppliers.

Conductivity experiments: Electrolyte conductivity is one of the controlling parameters that

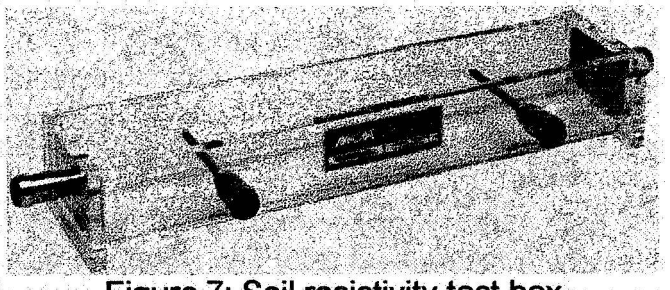

Figure 7: Soil resistivity test box

control corrosion. The test box shown in Figure 7 is one standard apparatus used for measuring resistivity. A test box similar to the one shown in Figure 7 was purchased for the purpose of the resistivity measurements conducted on this project.

Electrochemical control apparatus: The potentiodynamic scans measured in this project used a variety of potentiostats, and resistivity was determined using a standard resistivity meter. These instruments are commonly used in electrochemical testing [11] and will not be discussed in this report.

3. RESULTS

Potentiodynamic scans: Figure 8 shows representative potentiodynamic scans made using

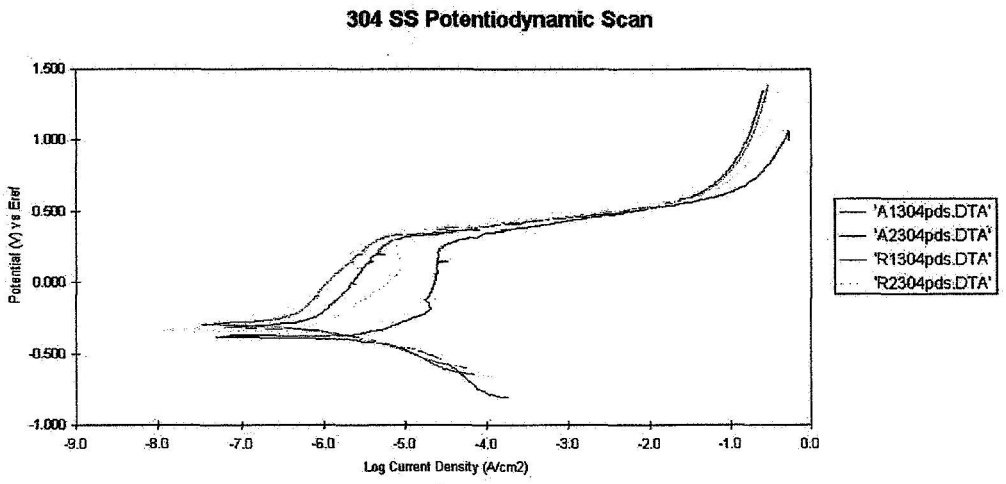

Figure 8: Typical potentiodynamic scans obtained at the KSC corrosion laboratory

a laboratory potentiostat and following standard electrochemical procedures. The four scans shown in Figure 8 represent supposedly replicate experiments performed on the same piece of 304 stainless steel by two different electrochemists. Other potentiodynamic scans were performed in a variety of one-normal acid and base electrolytes using both 304 stainless steel and carbon steel samples.

The conclusions from this work were that the potentiodynamic scan technique could not be used to characterize electrolytes. While open circuit (rest or "corrosion") potentials could be reproduced within approximately 50 mv, the current densities were not reproducible. Thus these scans could not be used to predict corrosion rates or to identify electrolytes. A careful check of the electrochemical literature [12-17] shows that, since current density is highly dependent on potential, electrolyte resistivity, reduction reactions, and other parameters, electrochemical currents are unlikely to be useful for identifying or characterizing electrolytes.

Resistivity measurements: One of the more common methods of characterizing environments for their corrosivity is resistivity measurement. [18] The resistivity of 1 Normal solutions of the same electrolytes that were used for the potentiodynamic tests were determined using a resistivity "soil box" shown in Figure 7. While soil boxes are normally used for soil electrolytes, they can be used for liquids as well. Figure 9 compares the resistivity of diluted NaOH as measured by two different electrochemists using the same soil box and compares

these measurements with the results obtained using a single probe electrode meter.

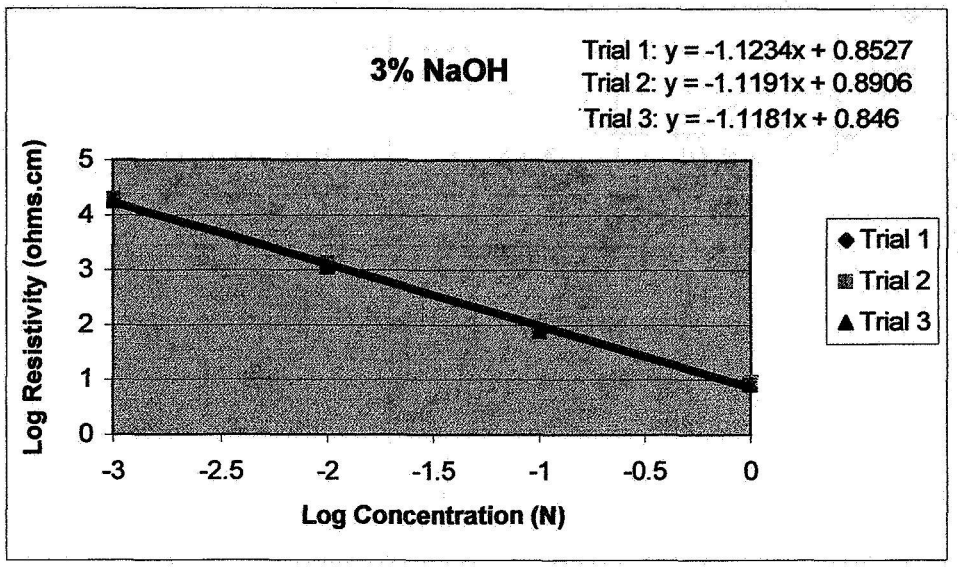

Figure 9: Results of resistivity measurements by two different electrochemists using a "soil box" compared with the resistivity determined by a single probe resistivity meter

The results of this work showed that resistivity is far more reproducible than potentiodynamic scanning and does not vary from experimenter to experimenter. Resisitivity can also be duplicated using several standard resistivity techniques.

While resistivity measurements can be used to compare the corrosivity of various electrolyes, it is not specific to any given electrolyte and cannot be used to identify electrolytes. Any electrolyte with the same ionic concentration can be expected to show the same conductivity. The reason for the different conductivities for one normal electrolytes shown in Figure 9 is because the salts in these electrolytes have slightly different solubilities. This effect would be more apparent if divalent metallic salts (e.g., salts of calcium or magnesium) had been included in the experimental program.

Soil collection: Because the conductivities of various soils can be used to determine their relative corrosivities, a series of soils were collected from locations in Florida, Georgia, and South Carolina. Time restraints prevented the resistivities of these soils from being tested, but they were supplied to the KSC corrosion personnel for use in the future.

Tafel extrapolation: An examination of the "open circuit" or "corrosion" potentials obtained with the potentiodynamic scans (e.g., Figure 8) suggested that concentrating on the regions near the open circuit potentials would produce more reproducible data.

Table 2 shows that the Tafel slopes (Beta C and Beta A in Table 2) [13, 16] obtained using the standard potentiodynamic scan technique are not reproducible. A review of the literature suggested that if the potentials tested were limited to those nearer the open circuit potential, less damage to the sample might occur during testing, and the slopes, or at least the open circuit potentials, should be more reproducible. Figure 10 confirms this supposition.

Table 2: Tafel slope data from potentiodynamic scans

Trial	Electrochemist 1, trial 1	Electrochemist 1, trial 2	Electrochemist 2, trial 1	Electrochemist 2, trial 2
Environment	3.5% NaCl	3.5% NaCl	3.5% NaCl	3.5% NaCl
Ecorr (mV)	-403.5	-471.2	-414.6	-468.6
Icorr (A/cm2)	3.83E-06	3.50E-O6	6.61E-06	5.29E-07
BetaC (mV/decade)	72.9	43.2	84.9	11.9
Beta A (mV/decade)	34.9	33.7	34	14.5
Rp (ohm-cm2)	2.68E+03	2.35E+03	1.60E+03	5.36E+03
Corrosion rate (mm/yr)	0.044	0.041	0.077	0.006

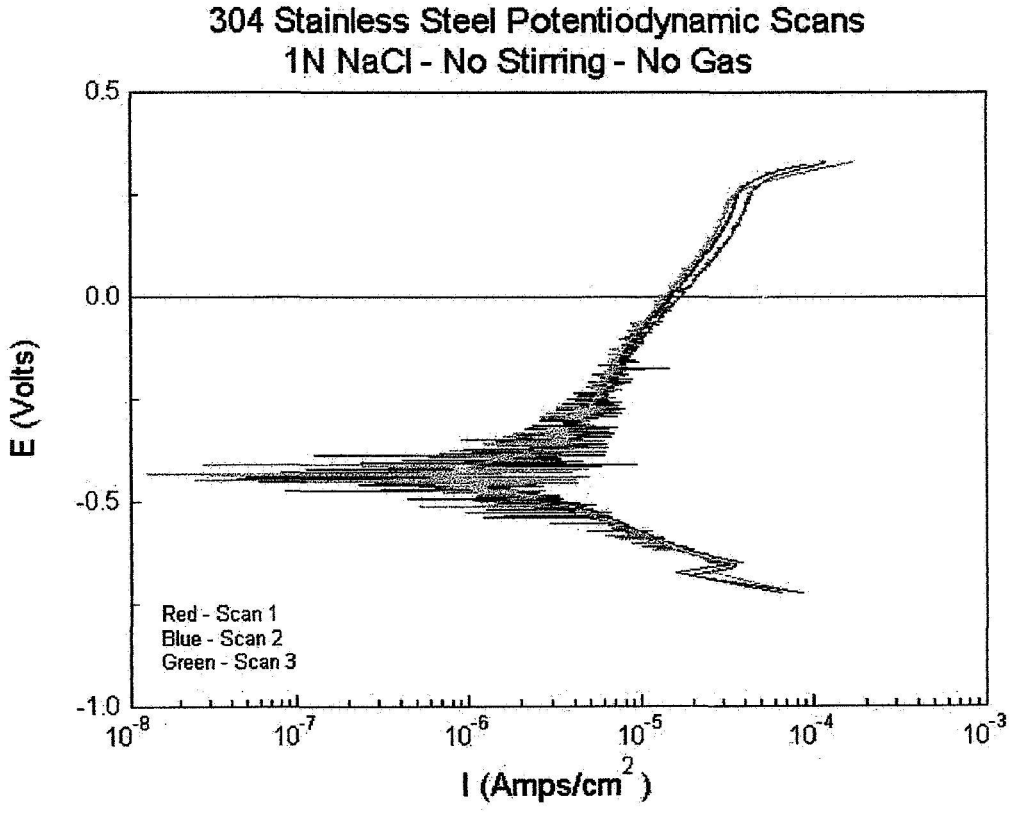

Figure 10: Reproducibility of open circuit potentials and Tafel extrapolation currents for 304 stainless steel in NaCl

A series of tests in various electrolytes was conducted using 304 stainless steel samples. The complete results of these tests have been provided to the NASA Kennedy Space Center colleagues. The results of this work conducted in August 2001 were that the potentials seem reproducible with approximately 50 mv, but the current data is noisy. This experimental noise could be due to metal/environment interactions, or it could be due to instrumental settings. This experimental approach seems worthy of continuing work.

when the potentials are limited to less than 100 mv from the open circuit potential

4. CONCLUSIONS

The purpose of this work was to determine an electrochemical means of characterizing electrolytes.

Potentiodynamic scans using techniques suggested by the work of Bennett at the University of Connecticut [10] did not yield useful results. The suggestion that this kind of experiment would prove useful in characterizing electrolytes [11] could not be confirmed.

Resistivity measurements were shown to be very reproducible. This would prove useful information for characterizing the corrosivity of electrolytes. Unfortunately, resistivity determinations cannot be used to identify the chemicals in an electrolyte.

Preliminary results indicate that further efforts on potentiodynamic experiments near the open circuit potential may prove useful in characterizing electrolytes. This may produce useful Tafel slope information that would be characteristic of various electrolytes. This work was not completed, but a complete set of the data necessary for continuation of this work has been provided to NASA Kennedy Space Center Corrosion Test Bed group.

5. ACKNOWLEDGEMENTS

Amanda Runciman, a summer student fellow from Cal Poly, and Ruby Vinje, Dynacs Inc., performed the laboratory experiments described in this report. Dr. Luz Marina Calle was the NASA colleague whose original ideas started this project. She also obtained funding for its continuation. We thank her for her insight, ideas, and thoughtful contributions and encouragement. Louis McDowell is the NASA researcher most responsible for the continuing vitality of the Corrosion Test Bed efforts at Kennedy Space Center, and we thank him for his foresight and determination in keeping Kennedy Space Center as a major source of government expertise in corrosion research, engineering, and testing. Joe Curran from Dynacs insured that support was available whenever necessary. This work could not have been done without all of their help.

6. REFERENCES

[1] Allen, C.C., and J.L. Conca, "Weathering Of Basaltic Rocks Under Cold, Arid Conditions - Antarctica and Mars," Proceedings of Lunar and Planetary Science, 21, 711-717, 1991.

[2] S. Clifford and T. Parker, "The evolution of the Martian Hydrosphere: Implications for the Fate of a Primordial Ocean and the Current State of the Northern Plains," www.lpi.usra.edu/meetings/geomars2001/eleclogo.jpg

[3] G. Landis and P. Jenkins, "DUST ON MARS: Materials Adherence Experiment Results From Mars Pathfinder," Proceedings of the 26th IEEE Photovoltaic Specialists Conference - 1997, IEEE, NJ, 1997, pp. 865-869. ISBN 0-7803-3767-0. http://powerweb.grc.nasa.gov/pvsee/publications/mars/Dust_97.html

[4] National Geographic Map of Mars Using MGS MOLA and MOC Data, http://ltpwww.gsfc.nasa.gov/tharsis/ngs.html

[5] Jet Propulsion Laboratory, "Mars environmental compatibility assessment," http://mars.jpl.nasa.gov/2001/lander/meca/science.htm#Corrosion

[6] R. Heidersbach, Carbon dioxide channeling, http://www.mate.calpoly.edu/mate425/powerpoint/forms/img164.gif

[7] M. Romanoff , "Underground Corrosion" (National Bureau of Standards Circular 579, April 1957), reprinted in 1989 by NACE, Houston.

[8] Kennedy Space Center Electromagnetic Physics Laboratory, http://empl.ksc.nasa.gov/index2.htm

[9] M. Buehler, S. Kounaves, D. Martin, S. West, and G. Kuhlman, "Designing a Water-Quality Monitor with Ion Selective Electrodes, 2001 IEEE Aerospace Conference Proceedings, Big Sky, Montana (March 2001).

[10] D. Bennett, "The Application of Electrode Kinetics to Galvanic Corrosion: I. The Use of Polarization Curves for Predicting Galvanic Corrosion, II. The Galvanogram," MS Thesis, University of Connecticut, 1973.

[11] D. Jones, Principles and Prevention of Corrosion, Macmillan, New York, 1992

[12] M. Fontana, "Corrosion Engineering," McGraw-Hill, New York, 1986.

[13] H. Hack, "Galvanic Corrosion Test Methods," NACE International, Houston, 1993, pp. 7-10.

[14] H. Hack, private communication, July 2001.

[15] F. Mansfeld, "Don't be afraid of electrochemical techniques, but use them with care," Corrosion, 1998, pp. 856-868.

[16] J. Scully, "Electrochemical methods for laboratory corrosion testing," Corrosion Testing and Evaluation: Silver anniversary volume, ASTM STP 1000, R. Baboian and S. Dean, editors, American Society for Testing Materials, Philadelphia, 1990. pp. 351-378.

[17] W. S. Tait, "Increase your confidence in corrosion test data," Materials Performance, March 2001, pp. 58-61.

[18] "Standard method of Field Measurement of Soil Resistivity Using the Wenner Four-Electrode Method," ASTM G 57-95(a).

[19] Mars Environmental Compatibility Assessment (MECA) Science, http://mars.jpl.nasa.gov/2001/lander/meca/science.htm#Corrosion

JOHN F. KENNEDY SPACE CENTER
UNIVERSITY OF CENTRAL FLORIDA

Methodology Development for Assessment of Spaceport Technology Returns and Risks

Prafulla Joglekar
Lindback Professor of Operations Management
La Salle University, Philadelphia, PA 19141
Tel: (215) 951 1036 E-mail: Joglekar@lasalle.edu

Edgar Zapata
Spaceport Technology Development Office (YA-C)

Executive Summary

As part of Kennedy Space Center's (KSC's) challenge to open the space frontier, new spaceport technologies must be developed, matured and successfully transitioned to operational systems. R&D investment decisions can be considered from multiple perspectives. Near, mid and far term technology horizons must be understood. Because a multitude of technology investment opportunities are available, we must identify choices that promise the greatest likelihood of significant lifecycle benefits. At the same time, the costs and risks of any choice must be well understood and balanced against its potential returns. The problem is not one of simply rank-ordering projects in terms of their desirability. KSC wants to determine a portfolio of projects that simultaneously satisfies multiple goals, such as getting the biggest bang for the buck, supporting projects that may be too risky for private funding, staying within annual budget cycles without foregoing the requirements of a long term technology vision, and ensuring the development of a diversity of technologies that support the variety of operational functions involved in space transportation.

This work aims to assist in the development of methods and techniques that support strategic technology investment decisions and ease the process of determining an optimal portfolio of spaceport R&D investments. Available literature on risks and returns to R&D is reviewed and most useful pieces are brought to the attention of the Spaceport Technology Development Office (STDO). KSC's current project management procedures are reviewed. It is found that the "one size fits all" nature of KSC's existing procedures and project selection criteria is not conducive to prudent decision-making. Directions for improving KSC's procedures and criteria are outlined. With help of a contractor, STDO is currently developing a tool, named Change Management Analysis Tool (CMAT)/ Portfolio Analysis Tool (PAT), to assist KSC's R&D portfolio determination. A critical review of CMAT/PAT is undertaken. Directions for the improvement of this tool are provided. STDO and KSC intend to follow up on many, if not all, of the recommendations provided.

Methodology Development for Assessment of Spaceport Technology Returns and Risks

Prafulla Joglekar

1. INTRODUCTION

As part of Kennedy Space Center's (KSC's) challenge to open the space frontier, new spaceport technologies must be developed, matured and successfully transitioned to operational systems. R&D investment decisions can be considered from multiple perspectives. Near, mid and far term technology horizons must be understood. Because a multitude of technology investment opportunities are available, we must identify choices that promise the greatest likelihood of significant lifecycle benefits. At the same time, the costs and risks of any choice must be well understood and balanced against its potential returns. The problem is not one of simply rank-ordering projects in terms of their desirability. KSC wants to determine a portfolio of projects that simultaneously satisfies multiple goals, including getting the biggest bang for the buck, supporting projects that may be too risky for private funding, staying within annual budget cycles without ignoring the requirements of a long term technology vision, and ensuring the development of a diversity of technologies that support the variety of operational functions involved in space transportation.

This work aims to assist in the development of methods and techniques that support strategic technology investment decisions and ease the process of determining an optimal portfolio of spaceport R&D investments. Towards that goal, this summer, I pursued three different paths. First, I reviewed available literature on risks and returns to R&D. My findings and recommendations from this review are summarized in Section 2. Second, I reviewed KSC's current project management procedures in terms of their ability to support prudent R&D project selection. The findings from that review are summarized in Section 3. Third, I undertook a critical review of a tool, named Change Management Analysis Tool (CMAT)/ Portfolio Analysis Tool (PAT), currently being developed by Knowledge Based Systems, Inc. (KBSI) under a contract from KSC. My findings and recommendations from that review are summarized in Section 4. The final section summarizes the recommendations from all three paths of my activity.

2. A REVIEW OF RELEVANT LITERATURE

I identified, gathered, browsed through numerous books and articles on such topics as:

- Technology Management [1], [5], [12], [13], [16]
- R&D Project Selection [2], [4], [9], [11]
- Cost-Benefit Analysis [6], [7], [8], [10], [15]
- Analysis of Public Decisions [3], [14]
- Risk Assessment and Decision Making [2], [4], [9], [11], [13] and
- Measuring Technology Investment Payoffs [2], [3], [5], [10], [11], [13], [15].

Several pieces in the general R&D literature had references to space transportation R&D. However, I could not locate a single piece that was exclusively devoted to spaceport R&D project selection. Although more focused on industry rather than government, the available *literature is vast*. I have limited the references only to the works that may be most useful to STDO/ KSC. I would recommend that project selection decision-makers at KSC/ STDO should familiarize themselves with at least one or two works in each of the topic areas listed above.

Although there are a few reports of successful practical applications, most of the literature is *theoretical*. On the other hand, as most personnel at KSC (a science focused organization) would agree, there is nothing more practical than a good theory. The literature that I have cited is *conceptually very rich and quite applicable* to KSC's project development and portfolio selection problem.

In particular, *Martino[11] and Brandenburg [2]* seem most relevant, for the following reasons:

- ✓ KSC has been using *scoring models* in all kinds of decision areas for quite some time now. These books provide a better understanding of theoretical underpinnings of scoring models and explain proper ways of developing scoring schemes.
- ✓ Martino ([11], Ch. 5) presents a *mathematical programming (constrained optimization) model* that may be most applicable to KSC's R&D portfolio selection problem since it is best suited to deal with *the multiplicity of goals KSC wants to accomplish*, such as:
  - Fund projects with the *greatest likely benefits*,
  - Fund projects *too risky* for private investment,
  - Fund projects that are *adequately diverse* in terms of:
    - the Spaceport Technology Development Initiative (STDI) areas supported
    - the TRL levels they seek to accomplish
    - risky and not-so-risky projects
    - old (on-going) projects and new projects Comply with the annual budget cycles and still have a long-term perspective on the technologies funded,
  - Provide well-structured justification for growth in KSC's R&D budget in competition with NASA's traditional R&D centers,
  - Within each Spaceport Transportation Development Initiative (STDI) area, ensure that available KSC employees and contractor/ university personnel can meet the FTE requirements of funded projects.

  A constrained optimization model also allows one to accommodate constraints such as:

  - Maximum budget to be spent, year by year
  - Maximum funds to be spent on projects in specific functional areas (e.g., fluid systems, or command and control, etc.)
  - Minimum % of total spending to go to specific STDI
  - Maximum number of projects to be funded

  Finally, through a properly done sensitivity analysis, a constrained optimization model can give us valuable information about the robustness of an optimal solution and about the impact of relaxing certain constraints or changing certain objectives.

3. A REVIEW OF KSC'S PROJECT MANAGEMENT PROCEDURES

On KSC's internal website, I located numerous documents that describe KSC's "authorized" procedures, practices, and data requirements for R&D project formulation, review, selection and management. Below is a partial list of those documents.

- KDP-KSC-P-2764 Program/ Project Management Process
- KDP-KSC-P-2755 Initial Project Formulation
- KDP-F-5002 Research Project Plan
- KDP-KSC-P-2602 Project Approval

- KDP-P-1453 KSC Independent Assessment Process
- KDP-P-5016 SE&T Project Management Process

A careful study of these documents suggests that KSC is interested in using a *systematic and uniform process for managing all R&D projects*. While this approach helps seemingly "fair and equitable" practice of such administrative functions as budget administration, project documentation, and auditing, I believe its "one size fits all" nature is *not conducive to prudent project/ portfolio selection. Uniformity* requires that the process, the data requirements, and the compliance expectations must be *simple enough* to be not too onerous on small projects. Perhaps, that is why the only project selection guidance that KSC procedures provide is a "Feasibility Check List" (KDP-KSC-P-2755).

Although components of returns, costs, and risks are mentioned, the "Feasibility Check List" provides is *no guidance on the metrics* to be used. Even familiar issues of cost/ benefit measurement [e.g., valuation of (a) facility costs, (b) KSC FTEs, (c) multi-year cash flows] are not addressed. The only prescribed feasibility *criterion* seems to be *availability of adequate funding*. KSC procedures do not address issues of

(a) Comparing costs and benefits that may be in different units of measurement,
(b) Minimum expected return on investment,
(c) Establishing the desirability of one project over another
(d) Assessing synergies between different projects.

Thus, even decisions about large-scale projects involving millions of dollars of investment must be based on the limited data and guidance the required Feasibility Check List provides.

I recommend that *KSC should develop different processes and criteria for small, medium, and large projects*. Particularly for selection among large projects, provide better metrics of benefits and costs, some guidance on how to resolve classical cost benefit analysis issues, how to establish relative desirability among projects, and how to seek an optimal portfolio of projects.

4. A CRITIQUE OF CMAT/ PAT

CMAT/PAT is still evolving. This critique is based on CMAT/PAT documents here should be taken not as a "judgment" of CMAT but as *an aid to further development of the tool.*

With the primary goal of assisting the Strategic Planning Process at KSC, CMAT promises to:

–*Use Fuzzy Logic* to generate strategy ideas, to predict strategic performance, and to provide strategic decision support.
–*Adapt Markovitz' Portfolio Theory* for strategic decision analysis in support of a well rounded, balanced R&D portfolio selection.
–*Analyze the risks* (i.e., the *variance* of the returns) of individual R&D projects as well as that of a portfolio of projects by using "multiple managerial inputs."
–*Use system simulation* to provide predictive analysis of STC change evolution and the "gap" between KSC's technology targets and projected accomplishments.

Roadblocks in the attainment of CMAT/ PAT Objectives

While CMAT's goals are extremely worthy, *they may not be actually attained* due to:

I. Inadequacy of available data.

II. Ambiguous, overlapping, internally inconsistent, and incomplete definitions of required data and metrics.
III. Lack of work on the specification of a good data collection process.
IV. Lack of work on the promised decision support models.*Inadequacy of Data*

Although the CMAT project is already in Phase II, the documents I have examined do not outline precisely what data KBSI would need to build its Fuzzy Logic engine, its System Simulation model, or its Portfolio Analysis Tool and precisely how KBSI would go about collecting the necessary data.

Instead, as requirements of the CMAT/ PAT project KBSI has accepted to

(a) Use existing NASA data sources and systems, and

(b) Minimize new data entry ("minimally intrusive").

Now, I appreciate why Spaceport Technology Development Office (STDO) may have imposed these requirements. Scientists and researchers are typically more interested in satisfying their curiosity and investigating interesting phenomena rather than thinking about potential costs, benefits, and risks of their research. They hate to comply with existing data collection processes and will surely find any additional data requirements as burdensome. Secondly, NASA's engineering/scientific culture emphasizes expertise within well-defined, narrow fields. This culture underestimates the true value of a well-designed, broad information system that supports organizational learning and improved decision-making. Third, even if new data requirements are defined, STDO personnel may have to estimate and enter those data themselves since they have no authority to enforce project managers' compliance with the new requirements.

Unfortunately, *existing NASA data sources and systems are woefully inadequate* for the kind of analysis CMAT aims at. For instance, to develop its "Fuzzy Rules" CMAT would require current and targeted ratings (Low, Medium or High) on such factors as "Design and Engineering Capability," "Science Enabling Capability," "Safety," or "Virtual Collaboration." CMAT would not only need such rating data (albeit "fuzzy") over several years, it would also need data on the correlations between the ratings of various factors. Similarly, PAT's portfolio variance analysis requires either "multiple managerial input" or other means of capturing the standard deviation of projected benefits of individual R&D projects, as well as the co-variances of benefits from different projects (i.e., data on the synergies between projects). NASA's existing data systems have not been collecting such data.

Poor Data Definitions

CMAT's Definition of "Return," as an example,

- Does not value possible one-time benefits of an R&D
- Does not value knowledge contributed by a failed project
- Does not specify how to account for time value of money multi-year benefit flows
- Differs from NASA's standard list of benefits on KDP-KSC-F-2755
- Is subject to several different interpretations and hence vulnerable to intentional or unintentional fudging
- Does not allow for negative rating any of the criteria
- Does not specify the process of arriving at the weights for different criteria

Similarly, CMAT's Definition of "Risk"

- Attempts to use an approach that is logically unacceptable, namely to take a weighted average of
  (a) costs to TRL9,
  (b) probability of technical success, and
  (c) the degree of collaboration.

  I do not know if "Cost to TRL 9" would necessarily increase or decrease a project's probability of failure. However, it is reasonable to assume high levels of "Collaboration" may reduce that probability. However, to capture that relationship I would not use a weighted average approach.
- Is inconsistent with CMAT's definition of "return." CMAT defines returns in terms of "benefits to NASA if the project is successfully implemented," CMAT should not simultaneously say that "Risk as defined here is more from a technology standpoint rather than from an operational standpoint." To be consistent, either the definition of risk or the definition of returns must be modified.

CMAT has not clearly defined "cost" yet. But it must soon confront classical cost measurement issues such as:

- Valuation of existing/ new facilities necessary for the project
- Valuation of NASA FTEs
- Valuation of multi-year costs (that may or may not be incurred) while approving a single year's funding
- Time value of money

Lack of Specification of a Good Data Collection Process

In addition to providing clear and sound data definitions, *KBSI needs to outline a data collection process* that is not too burdensome on the project managers and yet is capable of capturing relevant data with adequate accuracy in a timely manner. Among other things, *the process should specify:*

- Who is to provide what data to whom at what time?
- Who is to verify the reliability, validity, and/or accuracy of the data?
- In the case of subjective ratings, who is to be considered an expert? Who would ensure that the expert is not biased; and how?
- Who has the authority to enter or modify a project's status data (e.g., funded/ rejected, successful/ unsuccessful, actual benefits generated, costs incurred, etc.)?
- Who would have the responsibility to maintain the database over the years?
- How will the data be statistically analyzed to obtain historic success rates, average benefits, costs, etc? And, how will that statistics be used to update CMAT (including its data collection process) and improve KSC's portfolio selection methodology in the future.

In designing the data collection process, an important principle to keep in mind is that *the costs of data collection must be justified by the benefits resulting from the collected data.* Thus, for projects involving relatively small investment, the data requirements must be considerably simpler and smaller than the data requirements for projects involving millions of dollars of investment.

At the same time, it should be realized that, in the long run, *the benefits of informed decision-making and management practices resulting from the data collected using a properly designed process often outweigh the costs of that process.* Particularly in the R&D context, it should be realized that as a project proponent prepares to provide the data required by a well-designed decision-making system, often, he/she is forced to improve the very design of the project so as to make it more acceptable in terms of the organization's decision criteria. Often, such *improved project designs themselves pay for the costs of the data collection system.*

Lack of Work on Decision Support Models

At present, CMAT does not provide a clear and sound method of recommending an "optimal" portfolio of projects. It only attempts to show the costs, risk and returns of a given portfolio, and the diversity that portfolio reflects in terms of TRL levels or STDI area, etc. In other words, at present CMAT is simply a presentation software.

While this presentation software is non-intrusive and supportive, *it would not prove to be practical decision support tool.* An analyst using CMAT would have to input each possible portfolio, print its results and then manually compare all the printed results to identify the most preferred portfolio. The trouble is that if one wanted to select a portfolio consisting of 10 out of 40 projects, there are over 800 million possible alternatives!

Personally, I would recommend the use of a *generic constrained optimization model* (such as the one described by Martino, 1995, Ch. 5) *adapted separately to two sets of projects*

Set 1: Those with beginning TRL 1 to 3 and ending TRL ≤ 4 (applied research)

Set 2: Those with beginning TRL 4 to 6 and ending TRL ≤ 7 (development)

In my vision, the project selection criteria and the data requirements for Set 1 projects would be far simpler than those for Set 2 projects.

In short, while CMAT's stated goals are laudable, they are unlikely to be attained unless both NASA and KBSI work at removing the four major roadblocks identified above. Otherwise, with all the charts and diagrams it can produce, CMAT would prove to be an impressive presentation software. However, it would hardly be worthy of being called, "Change Management Analysis Tool."

5. CONCLUSION/ RECOMMENDATIONS

KSC should recognize that the "one size fits all" nature of its current project management procedures is not conducive to prudent R&D portfolio selection. KSC must work on suitably modifying those procedures and the criteria used for project selection.

KSC should also recognize

(a) The inadequacy of its existing data sources and systems, and

(b) The true value of a properly designed data collection system for R&D projects

and remove the requirement on CMAT to use only exiting data sources and systems.

KBSI and KSC should together come up with data definitions that are clear, theoretically sound, internally consistent, and complete.

In consultation with KSC/ STDO, KBSI should outline a data collection process that is not too burdensome on the project managers and yet is capable of capturing relevant data with adequate

accuracy in a timely manner. The designed process must ensure that the costs of data collection are justified by the benefits resulting from the collected data. This calculus should recognize

(a) The long term the benefits of informed decision-making and management practices, and

(b) The benefits of improved project designs

resulting from a properly designed data collection system.

If KSC truly desires to bring about a strategic change in its R&D endeavors, the Center must be willing to change its data culture. This includes giving adequate authority to STDO to be able to collect the necessary data. The concern for not overwhelming researchers and developers with demanding data requirements must be balanced against organizational need to make informed decisions in support of its strategic goals.

Finally, KBSI should develop and validate theoretically sound yet practical models that will truly support KSC's decision-making, be it in the area of project portfolio selection, or predicting strategic performance, or identifying technology gap. KSC should work towards a full realization of CMAT's stated goals by using such rigorous models.

I am pleased to note that STDO/ KSC intend to follow up on many, if not all, of my recommendations.

ACKNOWLEDGEMENTS

This summer, I have benefited from my close association with four STDO colleagues, Edgar Zapata, Carey McCleskey, Russ Rhodes, and Tim Barth, whose contributions to my research have been mutually complimentary. Together, Edgar, Carey, Russ, and Tim make a great team and I am thankful to them for making me a part of their team.

I also want to express my thanks to Dr. Ray Hosler and Cassie Spears of UCF and Greg Buckingham of NASA, who made sure that my summer was not only educational and comfortable but also enjoyable.

REFERENCES:

1. Allen, Gene and Jarman, Rick (1999) Collaborative R&D: Manufacturing's New Tool, Wiley, New York, NY.
2. Brandenburg, Richard (1964) Research and Development Project Selection: A Descriptive Analysis of R and D Management Decision Processes, University Microfilms Inc., Ann Arbor, MI.
3. Chase, Samuel B. ((1968) Problems in Public Expenditure Analysis, The Brookings Institution, Washington, DC.
4. Chicken, John, C. (1994) Managing Risks and Decisions in Major Projects, Chapman and Hall, New York, NY.
5. George Mason University (1998) Performance Metrics for R&D Organizations, Proceedings of a Workshop jointly sponsored by GMU and NASA, Arlington, VA.
6. Gross, A. (1976) Is cost-benefit analysis beneficial? Is cost-effectiveness analysis effective? The Heller School for Advanced Studies in Social Welfare, Brandeis University, Distributed by the National Technical Information Service (NTIS).

7. Joglekar, P. (1984) Cost-benefit studies of health care programs: choosing methods for desired results. Evaluation and the Health Professions, 7(3), 285-303.

8. Joglekar, P. (1994) "Applying Costs, Risks, and Values Evaluation (CRAVE) Methodology to Engineering Support Request (ESR) Prioritization," in L. Anderson, E. Hosler, and W. Camp (Eds.) NASA/ASEE Summer Faculty Fellowship Program, Contractor Report No. CR-197448, Kennedy Space Center, FL., October 1994, pp. 263-311.

9. Koller, Glenn, R. (1999) Risk Assessment and Decision Making in Business and Industry, CRC Press, Boca Raton, FL.

10. Levin, H. (1975) Cost-effectiveness analysis in evaluation research. In Guttentag, H., & Struening, E. (eds.) Handbook of evaluation research, Vol. 2. Beverly Hills, CA: Sage.

11. Martino, Joseph P. (1995) Research and Development Project Selection, Wiley, New York, NY.

12. Miller, William & Morris, Langdon (1999) 4th Generation R&D: Managing Knowledge, Technology, and Innovation, Wiley, New York, NY.

13. Noori, Hamid &Radford, Russell W. (1990) Readings and Cases in the Management of New Technology, Prentice Hall, Englewood Cliffs, NJ.

14. Quade, E. (1975) Analysis for public decisions. New York, NY: Rand Corporation.

15. Rothenberg, J. (1975) Cost-benefit analysis: A methodological exposition. In Guttentag, H., & Struening, E. (eds.) Handbook of evaluation research, Vol. 2. Beverly Hills, CA: Sage.

16. Szakonyi, Robert (1999) Technology Management 1999, Auerbach, New York, NY.

2001 NASA/ASEE SUMMER FACULTY FELLOWSHIP PROGRAM

JOHN F. KENNEDY SPACE CENTER
UNIVERSITY OF CENTRAL FLORIDA

ANALYSIS OF VOLATILE ORGANIC COMPOUNDS IN A CONTROLLED ENVIRONMENT: ETHYLENE GAS MEASUREMENT STUDIES ON RADISH

Suk Bin Kong, Ph.D.
Associate Professor of Chemistry
University of the Incarnate Word
Raymond Wheeler, Ph.D.
Kennedy Space Center

ABSTRACT

Volatile organic compound(VOC), ethylene gas, was characterized and quantified by GC/FID. 20-50 ppb levels were detected during the growth stages of radish. SPME could be a good analytical tool for the purpose. Low temperature trapping method using dry ice/diethyl ether and liquid nitrogen bath was recommended for the sampling process for GC/PID and GC/MS analysis.

ANALYSIS OF VOLATILE ORGANIC COMPOUNDS IN A CONTROLLED ENVIRONMENT: ETHYLEN GAS MEASUREMENT STUDIES ON RADISH

Suk Bin Kong, Ph.D.
Associate Professor of Chemistry
University of the Incarnate Word
Raymond Wheeler, Ph.D.
Kennedy Space Center

1. INTRODUCTION

Volatile organic compound(VOC), ethylene gas, was characterized and quantified by Gas Chromatograpny-Flame Ionization Detector (GC/FID). Radish was grown in a controlled environment. . Raising plants in a closed environment could be one of the challenges in space. In such a system, the possibilities present for some VOCs to reach levels that could lead to poor plant growth. Ethylene level of 20-50 ppb was detected during the growth stages of radish. For all tests, the materials used for the experiment (e,g, vinyl tubing, plastic cups, and epoxy resins) were not significant sources for ethylene but needed to be addressed. Methods using GC/MS, GC/PID, GC/FID and SPME(solid phase microextraction) to measure the VOCs have been studied from planting to harvest, under controlled environmental atmosphere.

2. Experimental Methods

1). Planting the seeds.

Cherry Bell Radish was purchased from W. Atlee Burpee & Co., Warminster, PA. The radish has a round shape, smoth, redi color, white flesh and ready 22 days after seeding to harvest. It was recommended to sow in average stone-free soil in early to late spring and again in late summer. In Deep South, Gulf and Pacific Coast areas, sow from fall to early spring. In rows 6" or more apart, sow seeds evenly and cover with ½" of fine soil. Firm lightly. Keep soil most. Seedlings emerge in 7-10 days depending on soil and weather conditions. It thrives in cool weather. Recommended to jake succe3ssive plantings every 2 weeks until late spring then again a moth before frost.

six seeds were placed in a Oasis foam (medium growing foam) saturated with Hoggland's solution in a 3x3 " magenta (outside covered with black electrical masking tape) container. There are 6 duplications and a control.

2). **Ethylene studies**

The schedule for the experiement is as follow:

June 29th.	Plant seed.	
July 6th.	1st thinning.	7 days after.
9th.	Dry weight check after 72 hours.	
July 13th.	2nd thinning.	14 days after.
16th.	Dry weight check after 72 hours.	
July 20th.	Harvest.	21 days after.
23rd.	Dry weight check after 72 hours.	

3. **Method for Ethylene**

In a Percival chamber, 3 radish jars were placed. The chamber is supplied with lights, 3000 ppm of Carbon dioxide gas. Humidity is controlled. The plants were transferred in a bell jar every day for ethylene studies. The air samples were collected 1, 2, and 3 hours interval. The plants were moved out of the bell jar after sampling. There was a control pot with the same conditions without seed.
Ethylene gas sample was collected with syringe.

Gas chromatography-Flame Ionization Detector(GC/FID) was used to measure the emission rate. Gas chromatography-Mass Spectrometer (GC/MS), Gas chromatography-Photoionization Detector (GC/PID) and Solid Phase Microextraction (SPME) sampling techniques were also investigated.

Figure 1. Bell jar and cooling system inside of the growth chamber.

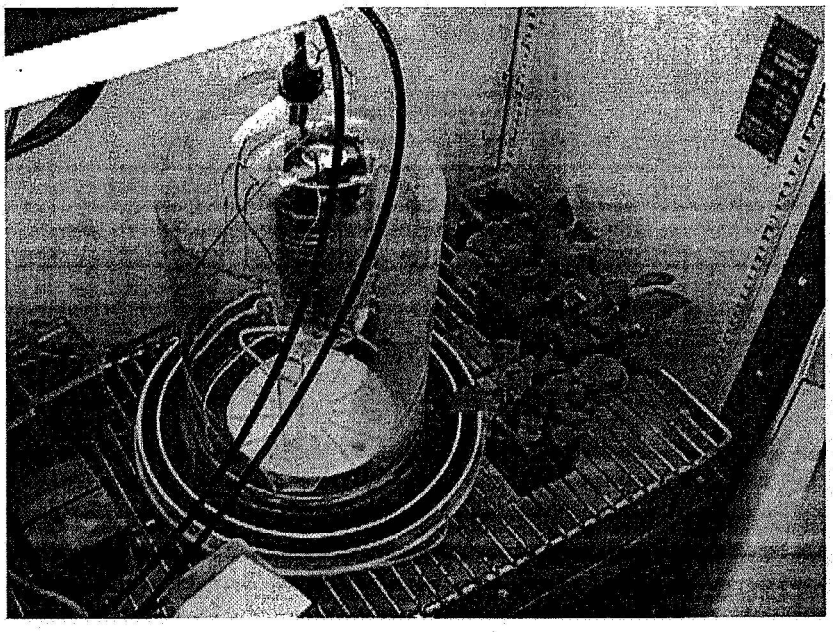

Figure 2. Plant growth after 20 days.

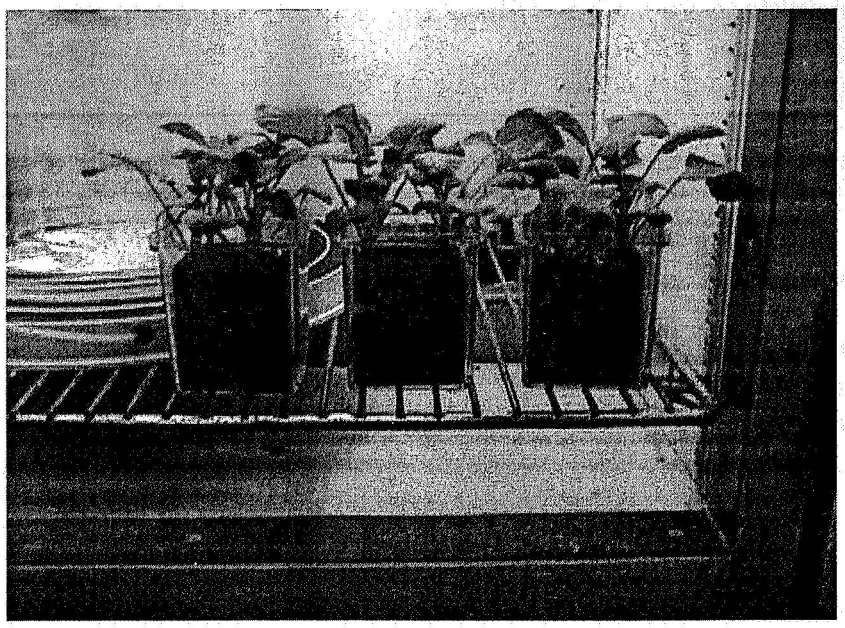

Figure 3. Leaf area measurement.

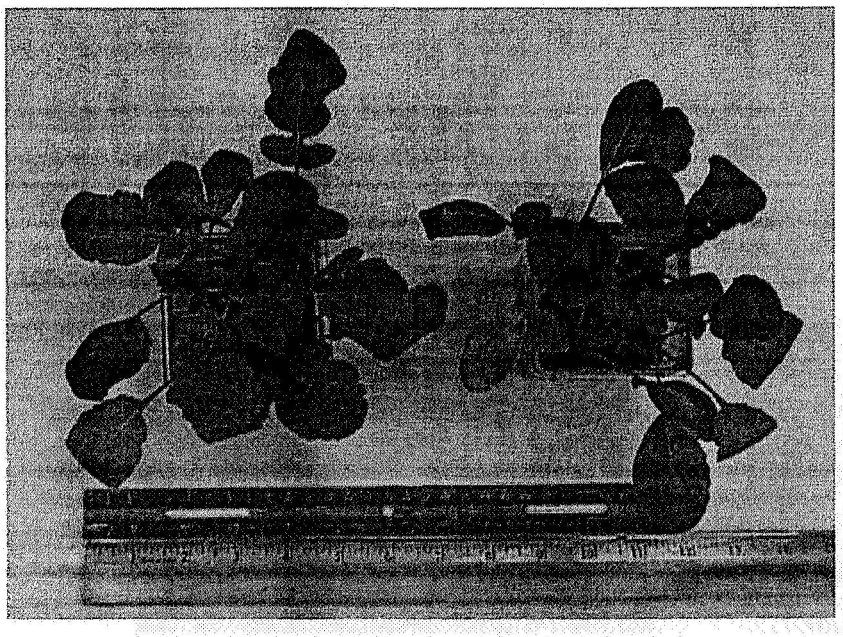

4. Results

Ethylene gas emission rate was measured with Gas Chromatography-Flame Ionization Detector (GC-FID).

Detectable Limits = 3(Noise): signal
Noise = 0.058825
Detectable Limits (PPB) = 11.80

Analysis Date	Sample Date	Sample File Name	Ethylene	% SD	Peak Area
7/11/01	7/6/01	control	28.392		0.436
7/11/01	7/6/01	control	11.596		0.191
7/11/01	7/6/01	1 hour	32.004		0.489
7/11/01	7/6/01	1 hour	21.400		0.334
7/11/01	7/6/01	2 hours	14.201		0.229
7/11/01	7/6/01	2 hours	12.842		0.209
7/11/01	7/6/01	3 hours	13.003	0.83%	0.212
7/11/01	7/6/01	3 hours	13.173		0.214
7/11/01	7/9/01	control	17.492		0.277
7/11/01	7/9/01	control	14.750		0.237
7/11/01	7/9/01	1 hour	22.908	0.60%	0.356
7/11/01	7/9/01	1 hour	22.702		0.353
7/11/01	7/9/01	2 hours	21.537	1.47%	0.336
7/11/01	7/9/01	2 hours	21.057		0.329
7/11/01	7/9/01	3 hours	29.900	0.15%	0.458
7/11/01	7/9/01	3 hours	29.832		0.457

Result. Continued.

Detectable Limits = 3(Noise): signal
Noise = 0.058825
Detectable Limits (PPB) = 11.80

Analysis Date	Sample Date	Sample File Name	PPB Ethylene	% SD	Peak Area
7/16/01	7/10/01	control	24.622	1.99%	0.381
7/16/01	7/10/01	control	23.888		0.370
7/16/01	7/10/01	1 hour	27.021	0.00%	0.416
7/16/01	7/10/01	1 hour	27.021		0.416
7/16/01	7/10/01	2 hours	27.844	0.50%	0.428
7/16/01	7/10/01	2 hours	27.638		0.425
7/16/01	7/10/01	3 hours	34.631	1.88%	0.527
7/16/01	7/10/01	3 hours	33.671		0.513
7/16/01	7/11/01	control	39.292	0.00%	0.595
7/16/01	7/11/01	control	39.292		0.595
7/16/01	7/11/01	1 hour	46.354	0.61%	0.698
7/16/01	7/11/01	1 hour	45.942		0.692
7/16/01	7/11/01	2 hours	42.096	0.23%	0.636
7/16/01	7/11/01	2 hours	42.240		0.638
7/16/01	7/11/01	3 hours	39.704	#DIV/0!	0.601
7/16/01	7/11/01	3 hours	<2.51		
7/17/01	7/13/01	control	36.345	0.77%	0.552
7/17/01	7/13/01	control	36.756		0.558
7/17/01	7/13/01	1 hour	33.260		0.507
7/17/01	7/13/01	1 hour	32.300		0.493
7/17/01	7/13/01	2 hours	38.744	0.48%	0.587
7/17/01	7/13/01	2 hours	38.470		0.583
7/17/01	7/13/01	3 hours	42.446	0.11%	0.641
7/17/01	7/13/01	3 hours	42.377		0.640

Figure 3. Calibration curve.

Ethylene Analysis

06/19/01
BPS MVT
Barbara Peterson: Organic Analytical Lab
Data Reference: Chem/Orbitac/BPS MVT

Ethylene Analysis

			Standards	PPB Ethylene	Peak Area	Response Factor	
			4/17/01	25	0.374	66.8548	
				50	0.760	65.7485	
				60	0.910	65.9424	
				100	1.471	67.9610	
HP 6890	GC/FID			Continuing Calibration			
FID	350	Degrees Centigrade		100	1.456	99.0%	07/03/01
FID-O2	100	mL/Minute Oxygen		100	1.474	100.2%	07/05/01
FID-H2	32	mL/Minute Hydrogen		100	1.460	99.2%	07/06/01
Oven	20(@10->54(1.6)	Degrees Centigrade		100	1.460	100.6%	07/09/01
Carrier	6.6	mL/Minute Helium		100	1.457	99.0%	07/11/01
				100	1.460	99.3%	07/14/01
				100	1.475	100.3%	07/16/01
				100	1.466	99.7%	07/17/01

Rt	4.159	minutes
Run Time	5	minutes
Column	0.54mm X 30M HP Plot Q	

Regression	25-100 PPB
Constant	-1.497
Std Err of Y Est	1.084
R Squared	0.99960
No. of Observations	4
X Coefficient(s)	68.555

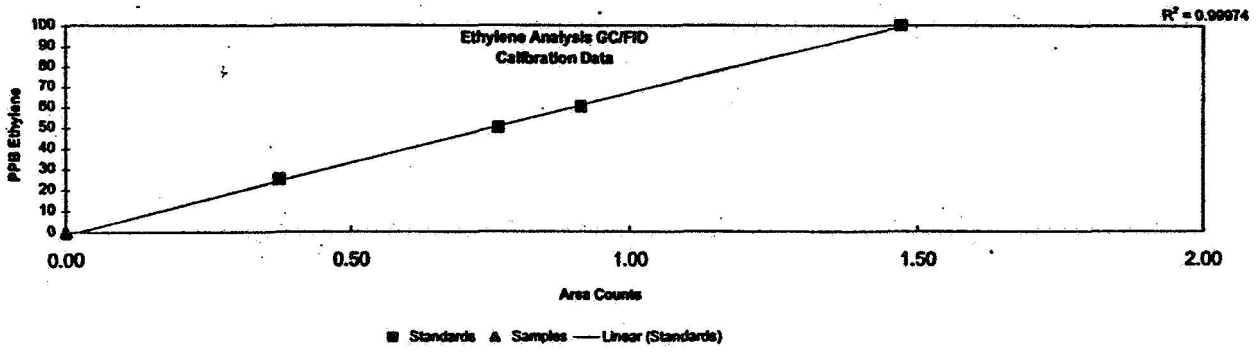

5. **Conclusions**

1. Well Calibrated Photovac (GC/Photo Ionization Detector) or GC equipped with Flame Ionization Detector (FID) could be more useful to detect ethylene gas in the chamber if a longer GC column is used or temperature programmed.
2. Solid Phase Microextraction (SPME) applied to GC/MS will be an interesting sampling device to try if quantification and calibration are not that time consuming. The present gas sampling method needs to be improved.
3. Sample concentration process is recommended.
4. Trapping the gas in low temperature with diethyl dry ice bath and liquid nitrogen could separate the ethylene gas from carbon dioxide and nitrogen. It can produce better spectra minimizing the interferences resulting a good GC/PID and GC/MS resolution.
5. Further studies on this subject are necessary.

6. **References**

Batten, J.H., Stutte, G. W., and Wheeler, R. M. (1995). Effect of crop development on biogenic emissions from plant populations grown in closed plant growth chambers, Phytochemistry, Vol. 39, No. 5, pp 1351 – 1357.

Batten, J. H., Stutte, G. W., and Wheller, R. M. (1996). Volatile Organic Compounds detected in the atmosphere of NASA's Biomass Production Chamber, Adv. Space Res. Vol. 18, N0. 4/5, pp 189-192.

Charron, S. S., Cantliffe, D. J., Wheeler, R. M., Manukian, A., and Heath, R. R. (1996). A system and methodology for measuring volatile organic compounds produced by hydroponic lettuce in a controlled environment, J. Amer. Soc. Hort. Sci. 121 (3): 483-487.

Stutte, G. W., and Wheeler, R. M. (1996). Accumulation and effect of volatile organic compounds in closed life support systems. Presentation at 31st Scientific Assembly of COSPAR, The University of Birmingham, England.

Acknowledgements

The author wished to thank Drs, Gary Stutte, Barbara Peterson, Lanfang Levine, Greg Goins, Jay Garland, Vadim Rygalov, Kathleen Daumer and Ignacio Eraso, Dynamac Corporation, and Dr. Raymond Wheeler, National Aeronautic and Space Administration Biological and Life Support, Kennedy Space Center, FL 32899, U.S.A for the time, energy and efforts that helped my tour of duty. The author also would like to thank the summer university faculty program officers and staff members and researchers at Kennedy Space Center, NASA and University of Central Florida.

2001 NASA/ASEE SUMMER FACULTY FELLOWSHIP PROGRAM

JOHN F. KENNEDY SPACE CENTER
UNIVERSITY OF CENTRAL FLORIDA

Signal Characterization for TDRSS Support of Range Safety

Sam Kozaitis
Associate Professor
Department of Electrical and Computer Engineering
Florida Institute of Technology, Melbourne, FL 32901

KSC Colleague: Richard Nelson, Advanced Range Technologies Manager/YA-E6

ABSTRACT

This work involves the analysis of signal attenuation using the NASA Tracking and Data Relay Satellite/Space Network to provide range safety and flight termination system support for expendable launch vehicles and the space shuttle. We found that at least one of the two operational TDRSS satellites could provide flight termination operating at about 250bps. Lowering the data rate could provide a larger link margin. The other satellite's signal would be attenuated below an acceptable link margin due to rocket exhaust. Lowering the data rate could provide a larger link margin.

1.0 Introduction

One of the most critical range services is that of evaluating real-time tracking and telemetry data to provide command sequences for range safety. This work involves the analysis of the communication system used for the NASA Tracking and Data Relay Satellite/Space Network (TDRSS) to provide range safety and flight termination system support for expendable launch vehicles and the space shuttle. The concept and feasibility study of this approach can be found in Ref. 1. The range safety idea can be expanded to include critical communication for vehicles from launch, orbit, and reentry.

The current method for providing range safety commands for US ranges requires ground-based antenna systems to maintain a UHF link with vehicles. Currently the Eastern range (ER), and the Western range (WR) rely on multiple ground stations to support the command destruct system. The range operations control centers (ROCCs), one at the WR, and one at the ER evaluate real-time tracking and telemetry data and provide command sequences for range safety. Some of these stations reside in foreign locations, with the associated rules, regulations, and logistics issues. New concepts for providing range safety have been investigated because of the costs associated with maintaining antenna systems, ground station horizon coverage limitations, and UHF frequency band crowding.

The TDRSS system has been considered to support range safety. The space portion of TDRSS fleet consists of several satellites in geosynchronous orbit, and can provide hemispheric coverage for the ER and WR. The ground segment is located near Las Cruces, NM with a remote terminal Guam. Use of the TDRSS would eliminate downrange stations and provide "seamless" coverage between launch-head (local) and space-based communications. The TDRSS/SN would provide maximum coverage for all potential launch trajectories, and provide centralized control.

Space-based ranges may provide a more flexible, robust and technologically advanced solution. They offer increased reliability and global coverage augmenting or eliminating ground-based tracking systems currently used. In addition, modern and future communication systems are often based on digital spread-spectrum communication modulation. Spread-spectrum is a modulation technique that separates signals by codes and transmits different signals in the same time and frequency space. It provides an inherent degree of immunity to noise and jamming. We examined some of the issues involved in converting to a modern space-based network from an analog ground-based network. These include, data rate, link margin, and effect of rocket exhaust on signal transmission.

2.0 NASA Tracking and Data Relay Satellite/Space Network (TDRSS)

The TDRSS system is a communication signal relay system that provides tracking and data acquisition services between low earth orbiting spacecraft and NASA/customer control data processing facilities.[2,3] The system is capable of transmitting to and receiving data from customer spacecraft's over at least 85% of a customer's orbit. The TDRSS system consists of several satellites in geosynchronous orbits, a dedicated ground station, and remote station. Two satellites form the nominal operational TDRSS service at 41°W, and 174° W longitudes. The other satellites in the constellation provide ready backup in the event of a failure to an operational spacecraft and, in some specialized cases,

resources for target of opportunity activities. A third satellite operates at 285°W with limited service with a ground station in Guam that could possibly provide global coverage.

The TDRSS ground segment is located near Las Cruces, New Mexico and consists of two functionally identical ground terminals known collectively as the White Sands Complex. Customer forwarded data is uplinked from the ground segment to the TDRS, and from the TDRS to the customer spacecraft. Customer return data is downlinked from the customer spacecraft via the TDRS to the ground segment and then on to the customer designated data collection location.

The TDRSS offers several services that are summarized in Table 1. Forward service is defined as the communication path that generally originates at the customer control center and is routed through the TDRSS to the customer spacecraft. Return service is defined as the communication path that originates at the customer spacecraft and is routed through the TDRSS back to the customer control center or other customer-specified destination. Single access service, is a dedicated customer service utilizing the steerable single access antennas. Single access services support higher forward and return customer data rates. Services are available within a specified range of S or Ku band frequencies unlike the multiple access service that is fixed frequency. Multiple access service is a shared capability from which up to five return services can be run simultaneously. The multiple access service are more readily available than the single access service however they support lower forward and return data rates.

	FREQUENCY	SERVICE	MAX. DATA RATE	SERVICES PER TDRS
SINGLE ACCESS S-BAND	2020.4 MHz - 2123.3 MHz	FORWARD	300 k bps	2
	2200 MHz - 2300 MHz	RETURN	6 Mbps	2
K-BAND	13.747 GHz - 13.802 GHz	FORWARD	25 Mbps	2
	14.887 GHz - 15.119 GHz	RETURN	300 Mbps	2
MULTIPLE ACCESS S-BAND	2103.1 MHz - 2109.7 MHz	FORWARD	10 k bps	1
	2284.5 MHz - 2290.5 MHz	RETURN	100 k bps	5*

* GROUND STATION LIMITED

Table 1 Services of TDRSS system

TDRSS supports the following modulation schemes: bi-phase shift keying (BPSK), qudrature phase shift keying (QPSK) and staggered qudrature phase shift keying (SQPSK). Data formats supported are non-return to zero and Bi-Ø - Level (BiØ-L), also known as Manchester.

3.0 TDRSS communication

The TDRSS system uses a digital spread spectrum method of communication. Spread spectrum describes a modulation technique that transmits in the same time and frequency space as other signals, but the signals are separated by codes.[4] Spread spectrum modulation provides, a resistance to jamming, allows multiple users to access the same channel, and, signals can be transmitted at low power. Basically, the spread spectrum system transmits a signal over a frequency much wider than the minimum bandwidth required to send the signal. The fundamental premise is that, in channels with narrowband noise, increasing the transmitted signal bandwidth results in an increased probability that the received information will be correct. If total signal power is interpreted as the area under the spectral density curve then signals with equivalent total power may have either a large signal power concentrated in a small bandwidth or a small signal power spread over a large bandwidth. Then at the receiving end, the signal is de-spread.

The process gain (Gp) is what actually provides increased system performance without requiring a high SNR. This is described as,

$$G_p = BW/R, \tag{1}$$

where, BW = RF bandwidth, and R = data rate in bits/second. The baseband signal is spread out over the full bandwidth. Then at the receiving end, the signal is de-spread by the same amount by a correlation with a desired signal generated by the spreading technique. When the received signal is matched to the desired signal the baseband signal is retrieved.

Direct sequence spread spectrum (DSSS) is probably the most widely recognized form of spread spectrum. The DSSS process is performed by multiplying an RF carrier and a binary pseudo-noise (PN) digital signal. First the PN code is modulated onto the information signal using one of several modulation techniques (e.g. BPSK, QPSK, etc). Then, a mixer is used to multiply the RF carrier and PN modulated information signal as shown in Fig. 1. This process causes the RF signal to be replaced with a very wide bandwidth signal with the spectral equivalent of a noise signal. The signals generated with this technique appear as noise in the frequency domain. The wide bandwidth provided by the PN code allows the signal power to drop below the noise threshold without loss of information.

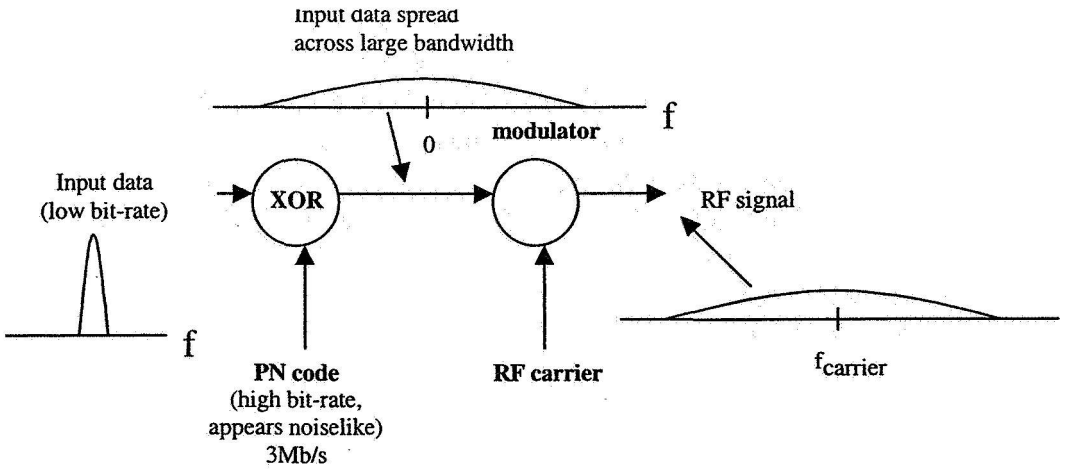

Figure 1 Schematic diagram of DSSS transmitter

The demodulation process consists of multiplying the incoming RF signal with the same PN code used in the transmitter as shown in Fig. 2. Using the same PN code in the receiver as in the transmitter despreads the bandwidth of the received signal to that of the input to the transmitter. Otherwise, the input to the demodulator will have a large bandwidth and appear noise-like. The resulting signal is then demodulated, and the bits recovered using a correlation process. Signals encoded with different PN codes will generally not interfere because the codes are usually chosen to be uncorrelated.

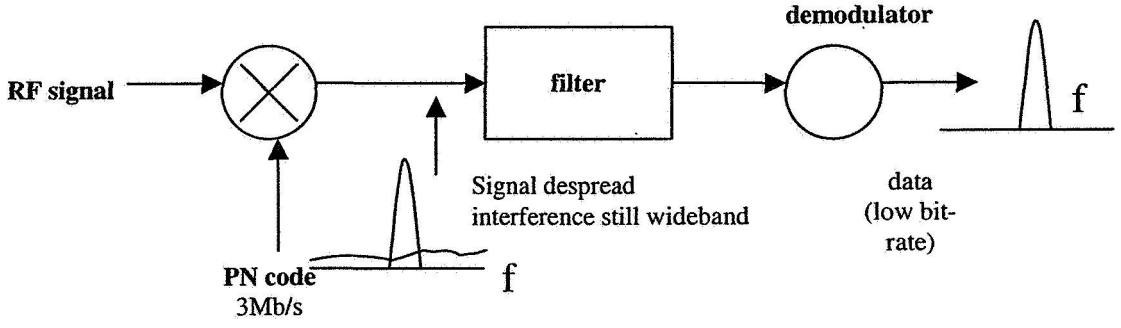

Figure 2 Schematic diagram of a DSSS receiver

A detailed link budget analysis of the TDRSS - vehicle (forward) link has been previously performed.[1] The link margin can be written as,

$$M_L = E_b/N_{o(\text{rec})} + G_p - E_b/N_{o(req)} - PL, \quad (2)$$

where each parameter in Eq. (2) is measured in decibels. The value of PL was taken to be 1.0dB, and the value of $E_b/N_{c(rec)}$ = -21.4dB from the analysis. The value of BW is 6MHz for TDRSS, which gives G_p = 43.8dB at 250bps. The value of $E_b/N_{o(req)}$ depends on the bit-error rate (BER) that can be tolerated and the type of modulation used and are usually widely available. We considered binary phase shift keying (BPSK) modulation in our study which is commonly used and available with TDRSS, and a BER = 10^{-5}. A common practice is the use of convolutional encoding of data with a ½ code, Viterbi decoding with a constraint length of 7, and a 32-bit path memory, which gives $E_b/N_{o(req)}$ = 5.1dB. The results show that the static link margin to be 16.2dB at 2106.4 MHz, at a data rate of 250bps. Note that the convolutional encoding used here increases the amount of data transmitted by a factor of two.

Different values for data rates and $E_b/N_{o(req)}$, will give different values of M_L. We showed the link margin as a function of bit-rate in Fig. 3. for a constant value of $E_b/N_{o(req)}$ = 5.1dB. The results show how the link margin is increased by decreasing the bit-rate. For larger values of $E_b/N_{o(req)}$, the data is shifted down by the difference between the two values, and similarly for smaller values of $E_b/N_{o(req)}$.

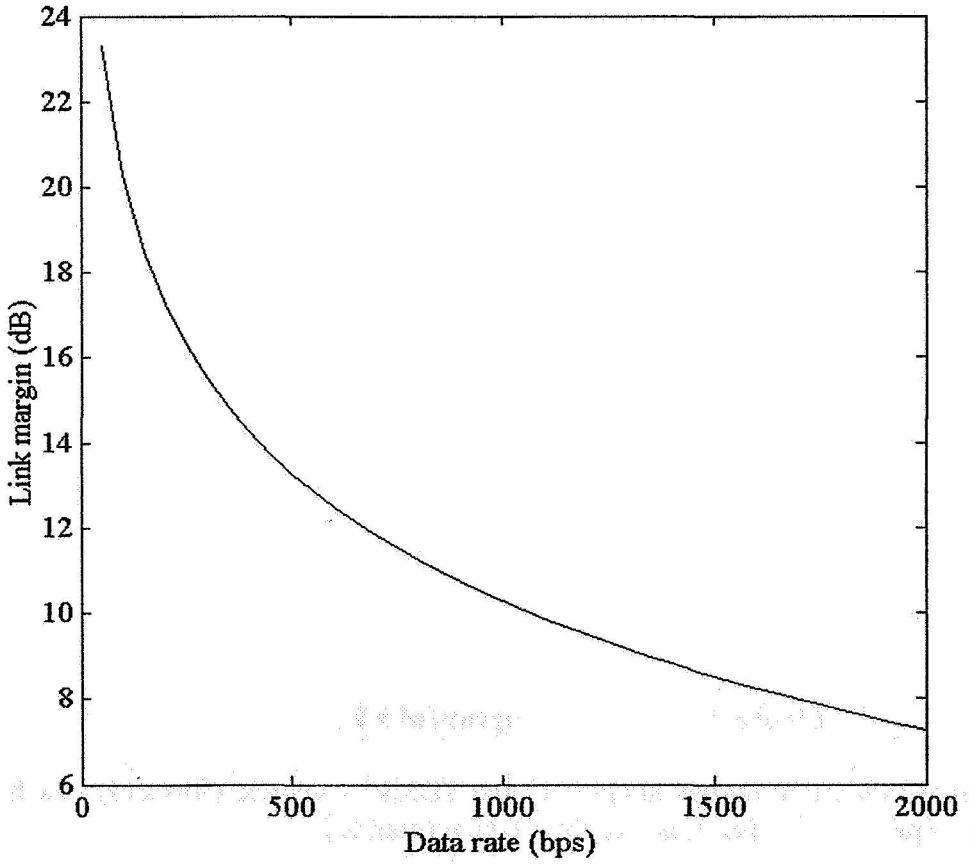

Figure 3 Link margin as a function of data rate for $E_b/N_{o(req)}$ = 5.1dB.

4.0 High-alphabet encoding

Currently, flight termination is provided by an analog FM system. Messages are encoded using a series of tones in what is known as a high-alphabet scheme. There are 7 tones plus 1 pilot tone. The pilot tone is not used in the alphabet. Each character consists of two tones. Because the tones are sequence independent, the number of characters in the alphabet is

$$7^2 - \sum_{i=1}^{7} i = 21. \tag{3}$$

Each message consists of 11 characters. Because the message is sequence dependent, there are $21^{11} = 3.5 \times 10^{14}$ possible messages. A message is transmitted in 111.4mS, and the start between two messages is 180mS, for a rate of 5.5 messages/sec.

We considered implementing the high-alphabet system digitally to be equivalent in terms of the number of possible messages. Considering the number of messages, $\log_2(3.5 \times 10^{14}) \approx 50$ bits are needed to represent all messages. If each character is represented by five bits, then, each message would consist of 5 bits/character x 11 characters = 55 bits. Therefore, approximately 55 bits can be used to replace the high-alphabet method in a digital system to have the equivalent number of messages. Note that the number of bits do not include any dead spaces or headers between characters or messages.

Another way to implement the current high-alphabet system is to digitize the analog signal. The tone frequencies range from 7.35kHz to 13.65kHz. Therefore, to properly digitize the signal, a sampling frequency greater than 27kHz must be used. At this sampling rate, digitizing a message for 111.4ms results in $0.1114 \times 27000 \approx 3000$ bits.

5.0 Effect of rocket exhaust on communication signals

Rocket exhaust has been known for some time to have significant effect on communication to and from launch vehicles. This is primarily because rockets generate exhaust plasma clouds containing a high density of free electrons.[5,6] It has been found that the attenuation of a microwave signal by rocket exhaust plasma can be modeled as a diffraction problem, where the exhaust plasma is replaced by a diffracting object.[7,8] This model has shown to be useful, but it is only valid for relatively small angles from the vehicle axis. An improved model would allow for the effects of scattering at larger angles. Such an approach would allow the modeling of both diffraction and multipath fading.

We considered a conducting sphere to model an exhaust plume to include the effects of reflection at larger angles than those typically used with diffraction. It has been shown that the scattered (diffracted) field in the forward direction of an obstacle does not depend on the detailed shape of the obstacle.[9] This phenomenon has been observed experimentally with a scale model of a rocket.[7] Therefore, the scattering by a sphere in the forward direction is a typical diffraction pattern and our approach is consistent with

previous results with respect to diffraction. The diffracted field due to rocket exhaust has been previously described.[8] In addition, general solution describing the scattered field from a sphere at all points in space has also been described in detail.[10]

We used the flight trajectory from a launch vehicle to find the angle (α) involved between a launch vehicle at the TDRSS satellites measured along the vehicle axis from the front of the vehicle. The flight trajectory was from a Space Shuttle mission, STS-103 on 12/20/90 from Kennedy Space Center, Fl on a 90 degree launch azimuth. To establish the link margin as a function of time, we needed to calculate the attenuation as a function of angle. For small values of α, the attenuation will be due to multipath effects due to reflection from the plume, and for large values of α will be due to diffraction. In terms of multipath effects we considered the average symbol energy-to-interference ratio of 1, and the phase to be uniformly distributed. In this case it can be shown that an additional 3dB if required by the degraded channel to achieve the same performance as an unfaded channel.[11] At larger angles, attenuation will be due to diffraction. Using the same geometry as in Ref. 8, we used the lower envelope of the diffraction of the plume. These results are shown in Fig. 4 as the attenuation of link margin as a function of α.

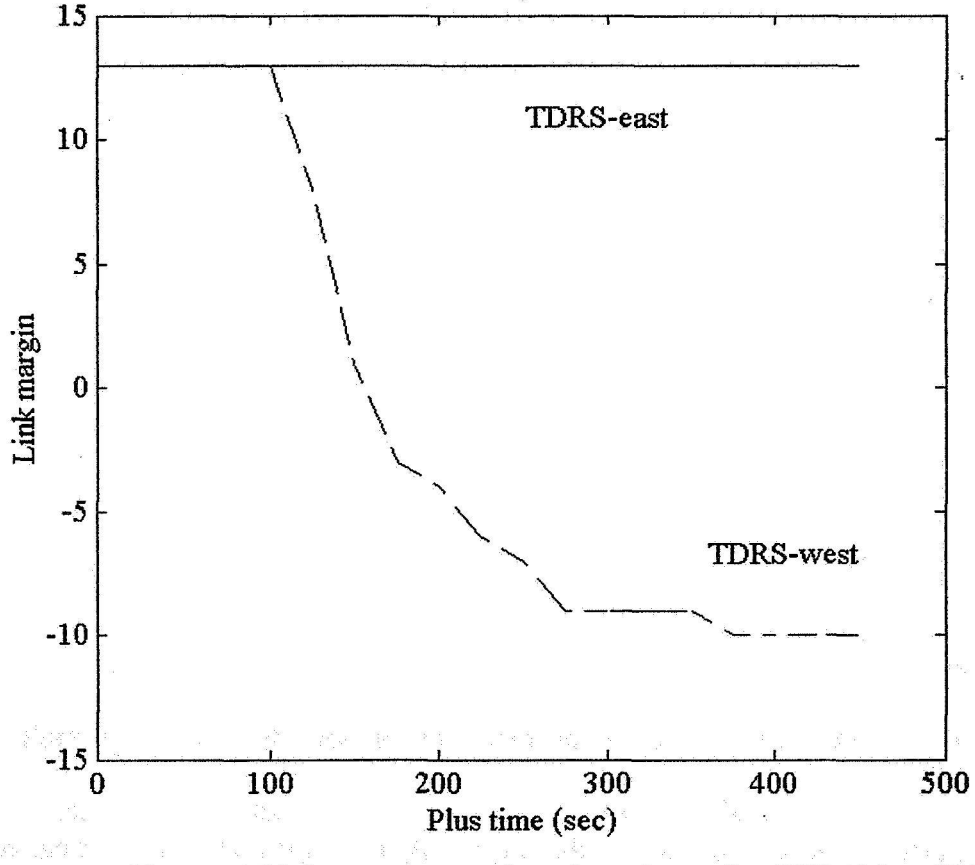

Figure 4 Link margin as a function of time for STS-103 at 250bps.

6.0 Conclusion

We found that a flight termination method using the digital spread-spectrum system available with the TDRSS system can meet the requirements for bit-rate and link margin. Bit-rates in the vicinity of 100-250 bps seem to the most probable with link margins in the vicinity of 13 dB. We found that at least one of the two operational TDRSS satellites could provide flight termination operating at about 250bps. Lowering the data rate could provide a larger link margin. The other satellite's signal would be attenuated below an acceptable link margin due to rocket exhaust.

7.0 References

1. J. A. Smith, T. Sobchak, and J. Walker, "NASA space network (SN) support for range safety: Concept and feasibility study," *NASA doc. 450-RSOPSCON-SN* (May 1998)

2. Brandel, D. L., Watson, W. A., and Weinberg, A., "NASA's Advanced Tracking and Data Relay Satellite System for the Years 2000 and Beyond," *Proc. of the IEEE* , Vol. 78, No. 7, 1990, pp. 1141-1151.

3. "TDRSS Training Manual," Revision C, PCN-1, *NASA doc. JSC-ATS-TDRSS 21002* (June 1999).

4. Sklar, B., *Digital Communications, Fundamentals and Applications*, PTR Prentice Hall:New Jersey, 1988.

5. Smoot, L. D., "Causes of Ionization in Rocket Exhausts," *Journal of Spacecraft and Rockets*, Vol. 12, No. 3, March 1975, pp. 179-183.

6. Simmons, F. S., *Rocket Exhaust Plume Phenomenology*, The Aerospace Press, El Segundo, CA, 2000.

7. Golden, K. E., Taylor, E. C., and Vincete, F. A., "Diffraction by Rocket Exhausts," *IEEE Trans. Anten. And Prop.*, Vol. AP-16, No. 5, 1968, pp. 614-616.

8. Senol, A. J., and Romine, G. L., "Three-Dimensional Refraction/Diffraction of Electromagnetic Waves Through Rocket Exhaust Plumes," *Journal of Spacecraft and Rockets*, Vol. 23, No. 1, Jan.-Feb. 1986, pp. 39-46.

9. Jackson, J. D., *Classical Electrodynamics*, John Wiley & Sons: New York, 1975, p.448.

10. Born, M., and Wolf, W., *Princples of Optics*, 5th ed., Permagon Press:Oxford, 1975, p. 644.

11. Viterbi, A. J., CDMA: Principles of Spread Spectrum Communication, Addison-Wesley:MA, 1995, p.96.

2001 NASA/ASEE SUMMER FACULTY FELLOWSHIP PROGRAM

JOHN F. KENNEDY SPACE CENTER
UNIVERSITY OF CENTRAL FLORIDA

Intelligent Systems for Self-Healing Electronics

Carl D. Latino Ph.D.
Associate Professor
Electrical and Computer Engineering Department
Oklahoma State University

ABSTRACT

For long duration missions it is imperative to be able to monitor and record critical information. The data acquisition systems used must therefore be fault tolerant. This usually meant having redundant copies of critical channels. Since each channel usually consists of various components, the parts count, cost, weight and complexity of the system could be very high. The Advanced Data Acquisition System (ADAS) has been developed as a proof of concept. The purpose was to demonstrate an architecture where individual spare parts can replace defective ones to repair a channel. By so doing entire channels do not need replication. This reduces the need of total redundancy and reduces the parts count. This has the added feature that in addition to spare parts, good components of a failed channel can be used as spares in another channel. In addition to reducing parts count and cost, this configuration, with an intelligent decision maker, can improve the reliability of the overall system. Another unique feature of ADAS is that it uses reconfigurable analog filters. These components can be programmed, by the smart system to meet the specific needs of the part they are to replace. This way one part can serve as spare for many different components. The hardware was built and now serves as a platform for developing intelligent algorithms. Another related project was a wireless data acquisition system. I was invited to participate in the meetings and issue suggestions. A brief description of this system will also be included.

Intelligent Systems for Self-Healing Electronics

Carl D. Latino Ph.D.

1. INTRODUCTION

The objectives of the summer 2001 project entailed the development of a self-healing system. Such a system is intended for cases where repair or replacement of failed parts is not possible, cost effective or practical. In space flight, for example, data collection is critical and must be taken regularly. If a data acquisition system fails, critical data could be lost endangering the mission or even risking lives. Generally this problem is dealt with by inclusion of redundant systems. This approach results in increased weight, cost and system complexity. Furthermore, if a single component fails, an entire sub-system may become unusable. The objective of this summer's project was to help in the development of an intelligent system capable of reconfiguring itself to switch out defective components and switch in good replacements. The system, as designed, includes flexible analog components manufactured by Lattice Semiconductor Corporation. These unique parts contain discrete analog components that can be configured into a broad range of filters and amplifiers. With this flexibility, one component can serve as the spare for a broad range of parts. To make the system intelligent, it is necessary to have all the necessary hardware on board and controlled by an embedded computer with appropriate software. The system is part of the ADAS (Advanced Data Acquisition Systems) objective. The prototype system consists of a central processor capable of performing the decisions and other processing duties, components and a means for interconnecting the components. The data acquisition system that was built consisted of the following components:

Switching matrix [1] – This is a programmable x-y matrix which can interconnect analog signals for system reconfiguration. The actual parts used were Mitel MT8806 and permitted the programmable connection of 4 rows (columns) and 8 columns (rows). The matrix consists of thirty-two switches corresponding to the cross points. These switches are closed by writing a logic "1"at the appropriate address and opened by writing a "0".

Programmable filters [2]– These devices, manufactured by Lattice Semiconductor Corporation are programmable by writing digital data to the device. The basic building block is an instrumentation amplifier with programmable gains and feedback. There are several such blocks per integrated circuit. Programming is performed by serially loading a binary file into the device. For more detail refer to ispPAC documentation. The device can be reprogrammed while in the circuit.

Digital to Analog Converter [3]– D to A converters are used to change digital data to analog signals.

Sample and Hold – These components are used in conjunction with Analog to Digital Converters to stabilize the input while the Analog to Digital converter digitizes the sample.

2. THE ADAS SYSTEM

The prototype system was designed by NASA and printed circuit boards built. The system architecture is described in the NASA document[4]. The printed circuit boards were manufactured and populated but needed to be tested. Since the assembled system was available for only two weeks, the prime objectives were to ensure the board was defect free and that all the components interacted correctly. The system was designed to allow analog signals to be read in, routed to appropriate components and output to the desired locations. Among the many duties, the processor calibrates the data paths, analyzes the received data and decides on how and when to reconfigure the system. The intelligence necessary to perform these functions have not yet been developed. The initial tasks required making a few corrections to the hardware and generating the software needed to ensure that all components interfaced correctly. At this writing, the components were individually tested and communications between all parts were verified. A voltage reference component did not operate as expected. It later turned out that the part was unsuitable and a different part will be needed. Other than this, the system operated correctly. Accomplishing these goals was a large step in the direction of demonstrating the capabilities of a working system. Future goals include the incorporation of software to analyze the incoming data for alarm conditions or to determine if component aging or failure is a possibility. The analysis of incoming data might be done using intelligent algorithms such as Neural Nets and other tools. This would evaluate the health of the device being measured as well as monitoring its own health. The system was designed capable of injecting known signals at desired inputs, routing these signals in a variety of paths for the purpose of locating possible system defects. The type of problems that this system will be asked to deal with include broken paths, degrading components and evaluation of the components being sensed. These are issues that are just now being addressed. Other topics to be addressed include search algorithms for faulty path detection and fault location. Knowing this, selection of alternate paths must be determined. This problem is further complicated when multiple paths must all be working. Other topics of importance include the development of models, which based on component reliability cost and other factors, suggest necessary redundancy.

3. SYSTEM RELIABILITY

Cost analysis of Advanced Data Acquisition System.

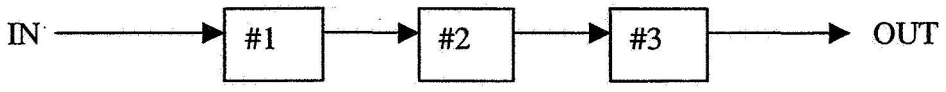

Fig. 1 Single Channel Single Path

To ensure that a sensor system is functioning, all components in the data path must be working. I.e. If a sensor system consists of three components operating in series, all must

be working for the system to work. If probability of failure for the components is p1, p2 and p3, (where 0< pi <1 for i = 1,2 or 3) the probability that the system works is:

P(system works) = (1-p1)*(1-p2)*(1-p3)

That is, the system works, if each of the three components works.

To ensure that the data is collected, an identical redundant system might be employed as shown in Fig. 2.

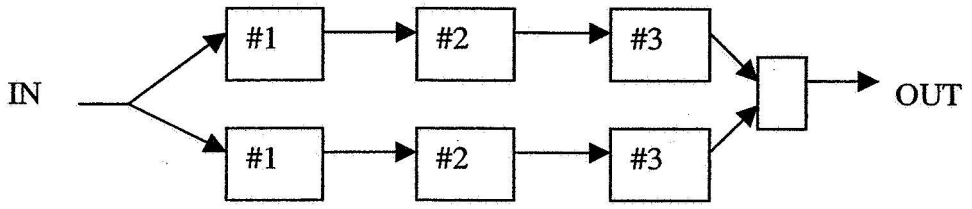

Fig. 2 Single Channel Double Path

If the redundant system has the same reliability as the original, the probability of the overall redundant system working is:

P(redundant works) = 1-(1-P(system1 works))*(1-P(system2 works))

This basically states that the system will work if the redundant systems have not both failed. The increased reliability comes at a cost in that twice as many components are needed and additionally a means of deciding which of the systems to operate. Neglecting, for the moment, the means of deciding and assuming the switching component won't fail, let's see what benefit is realized by this redundancy.

Example: If failure probabilities are: p1=0.1, p2=0.15 and p3=0.3

P(system works) = 0.9*0.95*0.7 = 0.598

P(redundant works) = 1-(1-0.598)*(1-0.598) = 0.8387978

This increases reliability by about 40% while increasing cost by about 100%.

Another possibility is that of making the individual components interchangeable. That is, that each of the three components can be switched in and out as shown below:

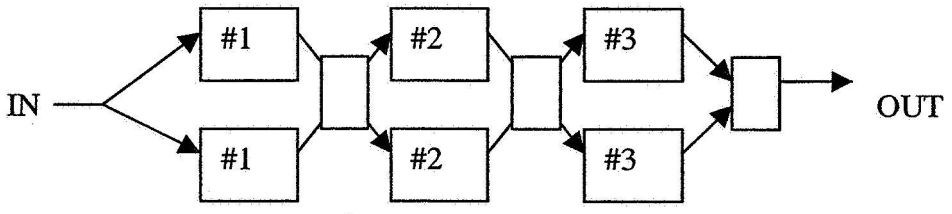

Fig. 2 Single Channel Changeable Parts

The cost is further increased, but so is the reliability. This system works if at least one of each of the redundant components is working.

P(switched works) = ((1-p1^n1)* (1-p2^n2)* (1-p3^n3)).

Where ni (i = 1,2 or 3) is the number of redundant sub components. If ni = 2 for all i, then:

P(switched works) = ((1-0.1^2)* (1-0.15^ 2)* (1-0.3^2)) =
(1-0.01)*(1-0.0225)*(1-0.09) = 0.8806297

This further increases reliability (by about 47% over original) but requires greater complexity. This is in the form of switching components, which could also fail, as well as require more intelligence to decide on the switching arrangement. An advantage of such a system is that higher redundancy can be applied to most critical components only incrementally increasing the cost of the overall system. Using the above as an example, since device 3 is most prone to failure, what happens if three copies of it are used (instead of just two).

P(switched new works) = ((1-0.1^2)* (1-0.15^ 2)* (1-0.3^3)) =
(1-0.01)*(1-0.0225)*(1-0.027) = 0.9415964

This represents a sizeable increase in reliability (increase over original of about 57%, and an increase over redundant by about 7%) with a marginal increase in cost. To make an intelligent decision, it is necessary to decide factors such as component cost, system weight, importance of the data etc.

Another way of looking at the problem is that probability of the system working must be at least some value x. If x = 0.9 and there is no redundancy, then (1-p1)*(1-p2)*(1-p3) must exceed 0.9. If all pi are equal, (1-pi)^3 < 0.9, therefore (1-pi) = 0.9^(1/3) = 0.965489 and pi = 0.034511. This is the ideal case and in reality, there is a "weak link" which makes the numbers look worse. That is, if one component is more prone to failure, the overall system performance is affected mostly by this component. In general, if a signal must traverse three components, the most favorable situation is where the probability of successfully traversing each of the three component is the same. Roughly speaking, if a component is more apt to fail, then it must exist in greater number. As a simple example, if p1 = 0.1, p2 = 0.2 and p3 = 0.3, and there are n copies of unit 1, how many copies of units 2 and 3 are needed for an optimal system?

Example:
Let n = 2, with the above error probabilities. What is the probability of a working system?
Answer:
If there are two copies of unit #1, the probability that it works is:
(1-0.1^2) = 0.99
To get the same probability for unit #2 want (1-0.2^k) >= 0.99.
If k=3 then (1-0.2^3) = 0.992
Similarly for unit #3, will need about three of those.
(1-0.3^m) >= 0.99 if m=4, (1-0.3^4) = 1-0.0081 = 0.9919

A system thus configured would have a probability of success of:

0.99*0.992*0.9919 = 0.9741251

If each of the different units cost the same, is there a better way of configuring the system as to increase reliability or reducing cost?

Removing one of the two units #1 will drop the reliability to:

$$P(1,3,4) = ((1-0.1^1)* (1-0.2^ 3)* (1-0.3^4)) = 0.9*0.992*0.9919 = 0.8855683$$

Removing one of the three units #2 will drop the reliability to:

$$P(2,2,4) = ((1-0.1^2)* (1-0.2^ 2)* (1-0.3^4)) = 0.99*0.96*0.9919 = 0.9427017$$

Removing one of the four units #3 will drop the reliability to:

$$P(1,3,4) = ((1-0.1^2)* (1-0.2^ 3)* (1-0.3^3)) = 0.99*0.992*0.973 = 0.9555638$$

As expected, the more reliable system has the greatest effect on reliability. That is, removing a reliable component will have a greater effect on reliability than removing a less reliable component. Now for the second part of the test, seeing if the removed component is replaced by one of the other units, i.e. remove one of 4 units #3, and replace it with one unit #2.

$$P(2,4,3) = ((1-0.1^2)* (1-0.2^ 4)* (1-0.3^3)) = 0.99*0.9984*0.973 = 0.9617287$$

This is a lower probability of success than the P(2,3,4) configuration. Other combinations using a total of 9 components will be lower than 0.9617287. This illustrates (but does not prove) that for a given cost, the best configuration balances the reliability of each leg.

Another comparison worth considering is how many times must a path be made redundant to have the same reliability shown above? The probability of a non redundant path working is: $P(1,1,1) = (1-0.1)*(1-0.2)*(1-0.3) = 0.504$

Two such parallel paths have reliability P(2 paths) = $1-(1-P(1,1,1))^2 = 1-(1-0.504)^2$ = 0.753984. This requires six components.

Three such parallel paths have reliability P(3 paths) = $1-(1-P(1,1,1))^3 = 1-0.496^3$ = 0.8779761. This requires nine components.

Four parallel paths have reliability P(4 paths) = $1- 0.496^4 = 0.9394762$. In spite of the fact that twelve components are used, the reliability is only 0.9394762. This is compared to the probability of 0.9741251 utilizing only nine units for the ADAS system.

In order to operate the system it is necessary to adopt an efficient way of selecting the paths. For example, if there are 2, 3 and 4 elements in each level, there are 2*3*4 = 24 possible paths. The following simple algorithm illustrates an exhaustive search. This will find all possible good paths. Are there better methods? Probably yes.

```
For i = 1 to 2
        For j = 1 to 3
                For k = 1 to 4
                        Is Path ijk valid?
                                Yes?  Then
                                Add ijk as valid path.
                                No?   Continue
                Next k
        Next j
Next I
No valid path
END
```

If multiple channel and thus separate paths are needed, the algorithm becomes more complex. This is so, since each path must use unique components. The advantage of multiple paths is that it takes only a few redundant components to handle a relatively large number of paths. If the number of spares is insufficient to deal with the faults, shutting down the least critical data paths and using some of those parts for spares may allow the overall system to function albeit at a somewhat reduced rate. It may also be possible to collect data at reduced rate by different data through the same channel, but multiplexed in time.

4. CONCLUSIONS

The circuit which was constructed represents a platform on which reconfigurable, intelligent systems may be evaluated and tested. Our objective was assembling such a system for the purpose of demonstrating its potential. The complexity and cost of such a system is relatively high but it has many advantages. In order for it to be feasible, however, the system must demonstrate tangible benefits. When a series of components must all work for a system to work, it is reasonable to replicate the least reliable ones in order to increase reliability while optimizing usage of resources. Some of the objectives were to demonstrate that parts count could be reduced, reducing power requirements and increasing overall reliability. To realize this, some statistical data should be taken and component redundancy should relate to these numbers in order to attain desirable results. This way, the more critical or least reliable components would be replicated in the proper amount to attain overall system reliability. Cost may also be a factor to consider. To help in the determination of level of redundancy and degree of reliability, a model should be developed with this problem in mind. Armed with this model, the user could make estimates of resource needs based on various factors such as component reliability, parts cost, number of needed channels etc. As the number of channels increases, the benefits of this type of system become more pronounced. With ADAS, a few redundant components can support a large number of channels. In addition to the normal spares, good parts of a failed channel can also be used. In extreme cases, the least critical

channels can be disabled or use one channel to collect data from several different components. The possibilities are many. Another issue of great importance is that although the ADAS developed has redundant systems, it has been designed with a single processor. This single failure point can invalidate many of the advantages of the system. Replicating the central processor, however, is a more difficult problem than simply producing another copy. This problem is an important issue to address in order to make the system optimally reliable.

5. A POSSIBLE WIRELESS COMMUNICATIONS PROTOCOL

The following is a brief, high level description of how the Base Station and Sensor Stations might communicate in order to maximize data throughput and minimize lost data. Depending on the hardware design, frequency bandwidths, power requirements and other limitations, such a system may or may not be practical. It however illustrates a means whereby each Sensor Station is identical with every other with the single exception of station number.

There is one Base Station (BS) and multiple Sensor Stations (SSi) where i is the number of the station. Assume there are N stations numbered 1, 2, 3, ... N.

Normal Operations (All stations can receive from and transmit to BS)

BS tells SSi to broadcast its data.
BS goes into listen mode and receives the data from SSi
At the same time all other stations SSj (j><I) receive the data
Each station purges all old data not requested by BS
This is repeated for all values of i from 1 to N

Example (Normal operation):
BS goes into Transmit Mode, all SSi in Receive Mode
BS tells SS1 to send its data and goes into Receive Mode
SS1 goes into Transmit Mode, sends its data and returns to Receive Mode
All SSi (i<>1) and BS receive the data
BS goes into Transmit Mode
BS tells SS2 to send its data and goes into Receive Mode
SS2 goes into Transmit Mode, sends its data, all SS1 data is purged (since BS already received it). SS2 returns to Receive Mode.
Process repeats. ...

Lost stations (One, or more SSi can hear, but cannot communicate directly with BS)

BS broadcasts for SSi to broadcast its data.
BS goes into listen mode but fails to receives the data from SSi

At the same time all other stations SSj (j<>I) listen for and some receive the data
Station SSi is added to the list of requested stations (at BS)
BS broadcasts for SSk to broadcast its data and that of lost stations
SSk broadcasts all requested data that it has
At the same time all other stations receive the data they do not already have and add it to their memory. Data not requested is purged from memory.
BS updates its request list and repeats the process.

Example: One BS, 4 SS. Assume SS2 can broadcast to 1 and 4 but not to BS or SS3. Assume also that SS2 cannot hear BS.

Operation:
BS broadcasts for SS1 to send data from a Request list (at first this only contains SS1).
All stations hear request except SS2.
SS1 broadcasts its data. BS and all stations hear and record data.
BS broadcasts for SS2 to send data. All stations that hear purge the SS1 data stored internally.
BS does not get response from SS2 adds SS2 to request list
BS broadcasts for SS3 to send data from the Request list (that now contains SS2 and SS3). All stations hear request except SS2.
SS3 only has its data (not that of SS2) and sends only that.
All listening devices add SS3 data to their memory
BS hears SS3 data and removes SS3 from request list.
BS broadcasts to SS4 for data (SS2 and SS4 are on the list)

6. FUTURE PROJECTS

The ADAS project, initiated by NASA and continued during the summer 2001 revealed the need for several issues to be addressed. To turn the prototype into a fully functional system, many critical issues need to be addressed. Among these is the need for redundancy in the imbedded processor. Since the processor, in the present system, is a single point of failure, its failure could make the entire system non-functional. Selecting the processors and duties to be performed by each is still an open problem. Another very interesting and important problem is that of intelligent software. Intelligence can be subdivided into the operational and evaluational. The operational controls the switching and reprogramming of the components while the evaluational determines the health of the system as well as that of the parameter being sensed. Health evaluation can be performed with Neural Networks and other intelligent means. Neural Networks have been successfully applied to the evaluation of the Gaseous Hydrogen Flow Control Valve. With Neural Networks, the ADAS could not only collect data but catalog system degradation over time. Another very useful tool would be a model. This could take cost, component reliability and other factors into account for deciding how many components are needed and where. All of the afore mentioned seem like ideal student projects which can be undertaken at The Oklahoma State University.

7. REFERENCES

[1] Mitel MT8806 8X4 Analog Switch array

[2] Lattice Semiconductor ispPAC

[3] Analog Devices AD5541 %volt Serial-Input Voltage-Output 16 bit DAC

[4] Intelligent Sensors & Instrumentation Advanced Data Acquisition Technologies Design Architecture Document. NASA internal document, January 2001

8. ACKNOWLEDGEMENTS

The work undertaken this summer was of great educational benefit to me. I hope that I contributed positively to the development of an intelligent data acquisition system of the future. Many people made the summer not only productive but very enjoyable. Whenever I needed answers or resources, there was always someone there to provide help and support. In mentioning the few I am sure I will be omitting the many who have made this summer very special for me. I hope I will be forgiven for not having mentioned you by name. My deepest thanks to Jose Perotti, my NASA Colleague. The fine talents of Bradley Burns and Tony Eckhoff, of Dynacs, Dr. Carlos Mata and Angel Lucena, of NASA and others helped bring the system to its present level. Without this support there would be many more unsolved problems than there are today. Dr. Ramon Hosler and Cassie Spears worked very hard to make the summer truly enjoyable for all the faculty and their families and guests. Their professionalism and friendship will long be remembered. Good luck and fondest wishes to Dr. Hosler on his retirement.

2001 NASA/ASEE SUMMER FACULTY FELLOWSHIP PROGRAM

JOHN F. KENNEDY SPACE CENTER
UNIVERSITY OF CENTRAL FLORIDA

A STUDY OF THE ELECTROSTATIC INTERACTION BETWEEN INSULATORS AND MARTIAN/LUNAR SOIL SIMULANTS

James G. Mantovani
Assistant Professor
Florida Institute of Technology
Department of Physics and Space Sciences
150 West University Boulevard
Melbourne, FL 32901

KSC Colleague: Carlos I. Calle

ABSTRACT

Using our previous experience with the Mars Environmental Compatibility Assessment (MECA) electrometer, we have designed a new type of aerodynamic electrometer. The goal of the research was to measure the buildup of electrostatic surface charge on a stationary cylindrical insulator after windborne granular particles have collided with the insulator surface in a simulated dust storm. The experiments are performed inside a vacuum chamber. This allows the atmospheric composition and pressure to be controlled in order to simulate the atmospheric conditions near the equator on the Martian surface. An impeller fan was used to propel the dust particles at a cylindrically shaped insulator under low vacuum conditions. We tested the new electrometer in a 10 mbar CO_2 atmosphere by exposing two types of cylindrical insulators, Teflon (1.9 cm diameter) and Fiberglass (2.5 cm diameter), to a variety of windborne granular particulate materials. The granular materials tested were JSC Mars-1 simulant, which is a mixture of coarse and fine (<5μm diameter) particle sizes, and some of the major mineral constituents of the Martian soil. The minerals included Ottawa sand (SiO_2), iron oxide (Fe_2O_3), aluminum oxide (Al_2O_3) and magnesium oxide (MgO). We also constructed a MECA-like electrometer that contained an insulator capped planar electrode for measuring the amount of electrostatic charge produced by rubbing an insulator surface over Martian and lunar soil simulants. The results of this study indicate that it is possible to detect triboelectric charging of insulator surfaces by windborne Martian soil simulant, and by individual mineral constituents of the soil simulant. We have also found that Teflon and Fiberglass insulator surfaces respond in different ways by developing opposite polarity surface charge, which decays at different rates after the particle impacts cease.

A STUDY OF THE ELECTROSTATIC INTERACTION BETWEEN INSULATORS AND MARTIAN/LUNAR SOIL SIMULANTS

James G. Mantovani

1. INTRODUCTION

When spacecraft, landers, and the spacesuits of future astronauts come into contact with either the lunar or Martian soil, it is believed that triboelectric charge generation on their man-made material surfaces may result in potentially disastrous situations. The absolute lack of humidity on the lunar surface, and the extremely arid conditions on the Martian surface have raised concerns that electrostatic charge buildup will not be dissipated easily. If triboelectrically generated charge cannot be dissipated or avoided, then dust will accumulate on charged surfaces and electrostatic discharge may destroy electronic components. Solar panels and thermal radiators that accumulate dust over time will have decreasing efficiency. Moving parts, such as joints in spacesuits, will also be affected as soil accumulation inhibits their motion.

There are two mechanisms by which a surface can become triboelectrically charged. The first method is through frictional contact by rubbing the surface over the soil. The second is through collisions between windborne dust particles and a surface. Although the second method of charge generation is not possible on the moon, dust storms occur on a frequent basis on Mars. Major Martian dust storms are easily visible from Earth, and satellites orbiting Mars have also observed the occurrence of so-called dust devils that can drive soil high into the atmosphere.

The Mars Environmental Compatibility Assessment (MECA) electrometer was designed jointly by the Jet Propulsion Laboratory and Kennedy Space Center to be a flight instrument on a 2001 unmanned Mars lander mission [1, 2], which was later cancelled. The MECA electrometer was designed primarily to characterize the electrostatic interaction between insulating materials and the Martian soil by rubbing the insulators simultaneously over the soil. The five insulators chosen for the MECA Electrometer were Fiberglass/Epoxy (G10), a Polycarbonate (Lexan™), Polytetraflouroethylene (Teflon™), Rulon J™, and Polymethylmethacrylate (Lucite™, also called PMMA). The MECA electrometer also contained an ion gauge for detecting charged particles in the Martian atmosphere, and an electric field sensor for detecting the local electric field on an object's surface.

Our research goal last year [3] involved testing and evaluating the MECA electrometer and its four types of onboard measurement sensors: (1) a triboelectric sensor array, (2) an ion gauge (charged particle sensor), and (3) a local electric field sensor. These goals were accomplished by (1) bringing the MECA electrometer into physical contact with Martian and lunar soil simulants [4, 5], (2) using a weak alpha particle source to create atmospheric ions under low vacuum conditions, and (3) applying a known voltage to a metal plate above the electric field sensor.

In 2001, our summer research evolved into measuring the effect of windborne dust particles on insulator surfaces. Martian dust storms were simulated in a vacuum chamber using an impeller

fan to propel dust particles at an insulator-capped electrometer. The electrometer sensor was embedded below the surface of a cylindrically shaped insulator. The insulator target had a cylindrical shape for aerodynamic reasons. Less turbulence would be created as wind encounters a cylinder. Hence, windborne dust particles would more likely impact the windward side of the cylinder in head-on collisions at higher speeds than they would under more turbulent conditions, thus maximizing the triboelectric charge they can produce.

The experiments and data taken using our new electrometer are described and presented in the following sections. We conclude with a discussion of the results of the experiments, and present conclusions about the new electrometer.

2. EXPERIMENTAL

In this section, we describe the design and development of the new aerodynamic electrometer. We also present data taken with the electrometer under conditions that attempt to simulate a Martian dust storm.

2.1 Design of the Aerodynamic Electrometer

The purpose of this research was to measure the amount of electric charge that is generated triboelectrically when windborne dust particles strike an insulator surface. A cylindrical geometry was chosen for the design of the electrometer based on its aerodynamic shape. When wind encounters a cylinder under non-turbulent conditions, the atmospheric molecules in the wind will follow streamlines around the cylinder. Any turbulence that might occur would be found on the side opposite the windward face of the cylinder. By contrast, a planar surface that is perpendicular to the wind will create turbulence everywhere over the surface. Any turbulence at the surface is likely to diminish the effect of an impact between a windborne dust particle and the surface. For these reasons, a cylindrical shape was chosen for the electrometer in order to maximize the chances for a windborne dust particle to make an impact with the electrometer. In addition, it was expected that an aerodynamic design would more likely produce consistent and reproducible results.

Dust particles that are carried by the wind will also tend to follow the streamlines unless the streamlines begin bending too sharply around an obstacle such as a cylinder. Since the dust particles are much more massive than the atmospheric molecules, there is high probability that they will cross streamlines due to their momentum and strike the cylinder's surface. This is especially true for particles that are on a head-on collision with the cylinder.

When a dust particle makes contact with the cylindrical insulator's surface, electric charge can be transferred between the two materials even if both are originally neutral. The physical reason for this is well known from solid state physics. Charge transfer is necessary in order for the two dissimilar materials to reach equilibrium. If the two materials that are brought into contact have different Fermi energies, then electrons will try to move from the material with the higher Fermi energy to the other material in order to equalize their Fermi energies.

2.2 Experimental Procedure

Figure 1 shows the aerodynamic cylindrical electrometer system that was constructed to perform the experiments. A dc power supply (not shown) is normally attached below the electrometer's electronics housing.

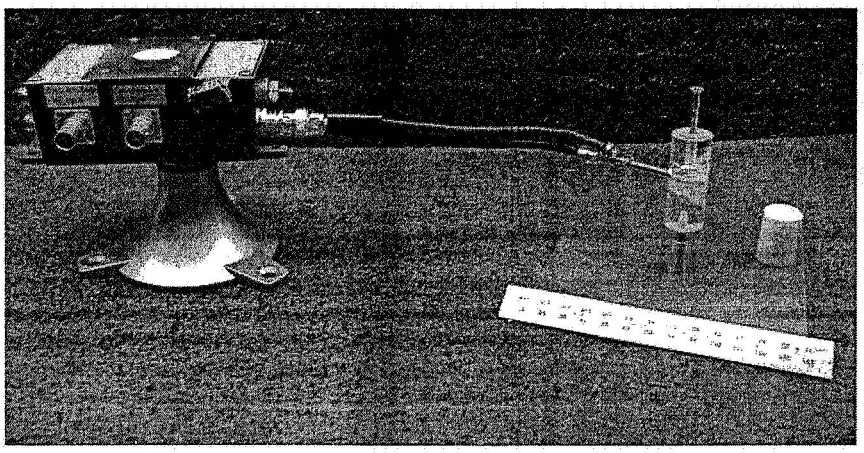

Figure 1. Lucite and Teflon cylinders are shown on the right. An electric field sensor probe is embedded in the Lucite cylinder to within 0.1 inches of the surface. A planar Teflon-capped electrode is mounted on the top of the electronics housing shown on the left. The BNC connectors attached to the respective outputs of the cylindrical and planar electrometers are shown together on the housing, An external dc power supply (+/-5V and +12V) is contained in a separate housing, but is not shown.

Figure 2 shows the cylindrical electrometer placed in the vacuum chamber along with the dust impeller fan that was used to propel dust particles towards the cylinder. A fixed volume of granular material is placed on the aluminum foil that covers an audio speaker. The speaker is used to force the dust to move in a vertical direction above the foil so that the wind that is generated by the impeller fan can carry the particles to the cylinder. The atmosphere within the chamber consists of carbon dioxide at a pressure of 10 mbar. Before an experiment is performed, the chamber is first evacuated to <5 mbar and then backfilled with carbon dioxide to over 133 mbar. The chamber is pumped down again and backfilled with CO_2 once more before being pumped down to a final pressure of 10 mbar CO_2.

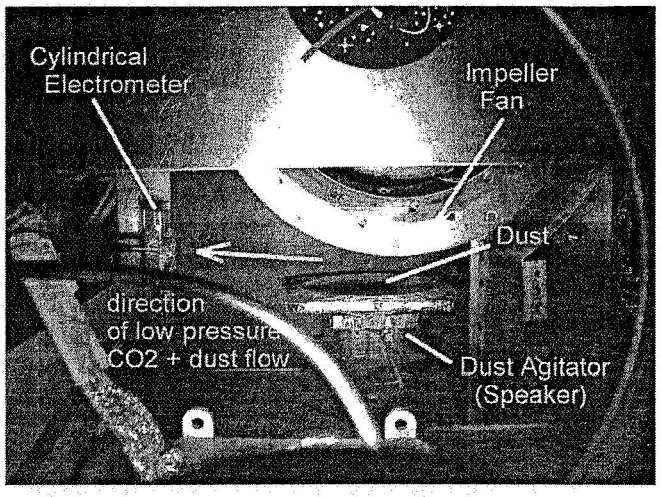

Figure 2. The cylindrical electrometer and dust impeller apparatus shown in the small vacuum chamber where experiments were performed.

When the impeller fan is turned on and the Martian soil simulant is propelled towards a Teflon cylinder, the dust coverage on the windward face of the Teflon surface is shown as in Figure 3. The electrometer probe is able to measure the residual charge at a location near the middle of the cylinder and below the dust-covered side of the Teflon cylinder.

The cylindrical insulator is removed from the electrometer probe for cleaning. Dust from a previous experiment is partially removed from the insulator surface using compressed air, followed by rinsing the insulator with alcohol and using compressed air to dry the surface.

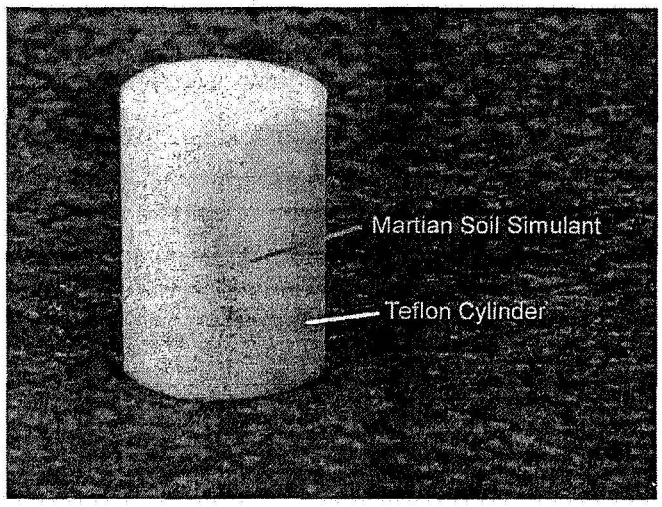

Figure 3. Windward side of a Teflon cylinder that was partially coated with Martian soil simulant. The soil was blown at the cylinder in a vacuum chamber by an impeller at 10 mbar CO_2 pressure.

A dry-vac is used to vacuum up any loose dust that is present on objects located in the vacuum chamber and on the chamber walls prior to conducting an experiment.

2.3 Data

A Lecroy Waverunner Digital Storage Oscilloscope (DSO) model LT364L (500MHz, 1GS/sec, 4 channels) was used to collect the data. A DSO probe type PP006 (10 MW, 12 pF, 500 MHz, 10:1) was used to pick up the output voltage coming from the cylindrical electrometer located in the vacuum chamber. The DSO was configured using Channel 1 to monitor the electrometer output signal, and with Channel A providing a filtered view of Channel 1 using the DSO's "Enhanced Resolution Filtering" mode.

Data was stored on a removable hard drive on the DSO after each experiment that could be later downloaded to a networked PC. Data was saved in ASCII format, which allowed the data to be easily imported into Microsoft Excel. The data shown in Figure 4 was generated in this manner.

Figure 4 shows data that was taken by the aerodynamic electrometer in the vacuum chamber at 10 mbar CO_2 pressure using the impeller fan to propel granular materials at Teflon and Fiberglass cylinders in separate experiments. The experiments were performed using Martian soil simulant (<5μm diameter particles), and three of the mineral constituents of the Martian soil: Fe_2O_3, SiO_2, and MgO. It should be noted that only the change in voltage is important over the course of a particular experiment. The zero voltage level is arbitrary for that reason, and the Teflon/Fiberglass data could be shifted in each graph so that the data for the two materials could be overlaid. However, the voltage offset for the electrometer circuit was approximately 20 mV. The electrometer circuit gain is based on resistor components, and was set at 0.25 pC/mV.

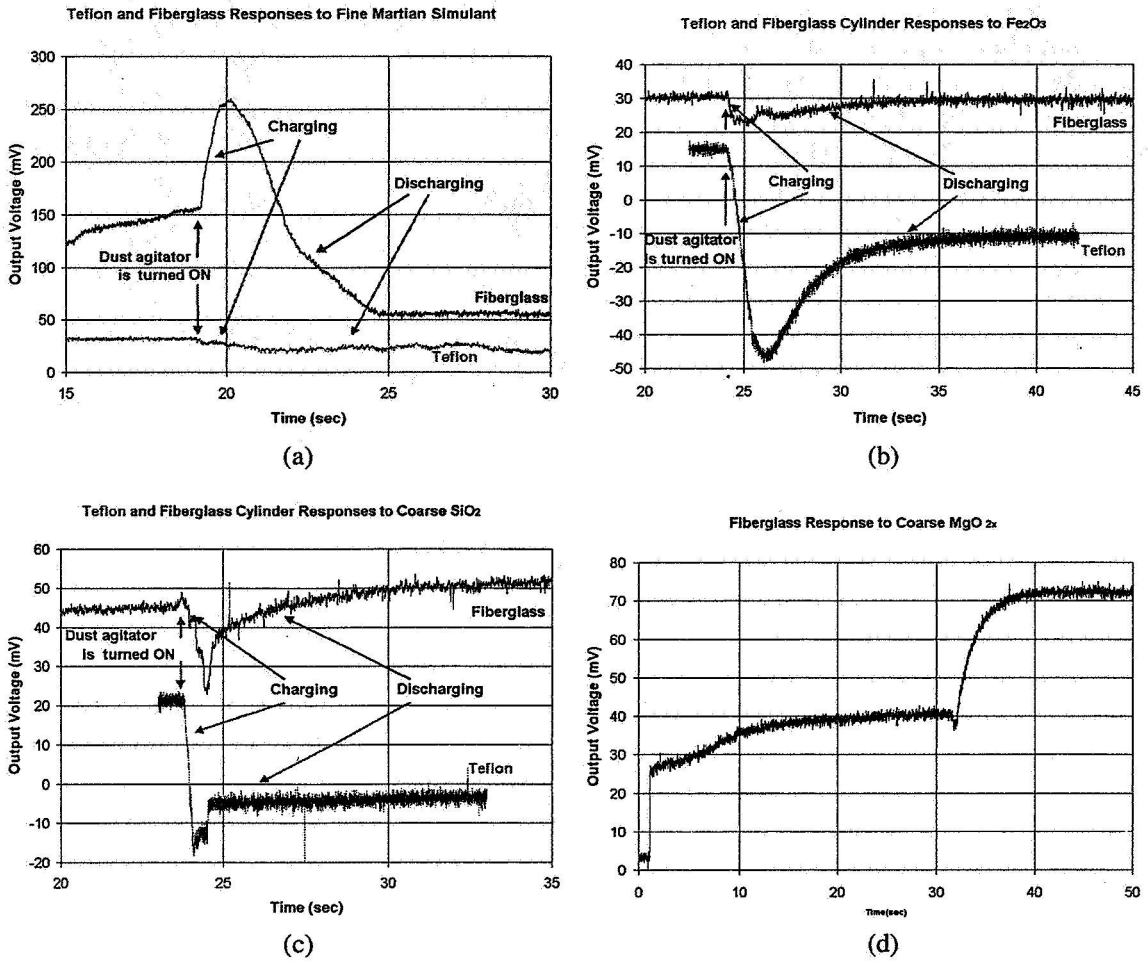

Figure 4. Electrometer output voltage response versus time for Teflon and Fiberglass being struck by windborne granular materials. The materials used were (a) fine (<5 μm) Martian soil simulant, (b) Fe_2O_3 (17 μm), (c) coarse SiO_2. The response of Fiberglass to MgO is shown in (d). The electrometer output voltage is related to the amount of surface charge according to the conversion factor 0.25 pC/mV.

3 DISCUSSION

The data presented in Figures 4 (a), (b), and (c) clearly show that a Teflon cylinder will respond in a different manner to a given type of windborne granular material than does a Fiberglass cylinder. This observation has favorable implications for the possibility of modifying our design by combining individual cylindrical electrometers into a single multisensor electrometer that can be used to identify the mineral composition of windborne dust particles. The amount and polarity of surface charge produced on a cylindrical material's surface might generate a signature that is characteristic of the interaction between the cylindrical material and the type of incident dust particle. For example, Fiberglass charged to (-8mV)x(0.25pC/mV)=(-2pC) in response to the windborne iron oxide (Fe_2O_3) before this charge began to decay through leakage across the

surface, whereas the Teflon cylinder charged to (-62mV)x(0.25pC/mV)=(-15.5pC). Furthermore, the charge decay rates for Fiberglass and Teflon are not the same. In contrast to iron oxide, some materials, such as magnesium oxide (MgO), cause Fiberglass to charge positively. These different responses provide encouragement that a multisensor approach to mineral determination is possible. Additional experiments are clearly needed in which many more types of cylindrical insulators are used in addition to Fiberglass and Teflon, and other mineral compositions are used.

The present electrometer is limited by having to perform separate experiments for different types of cylinders. Ideally, an array of electrometer sensors that are attached to different types of cylindrical materials would allow their simultaneous responses to the same windborne particles to be studied. Thus, a follow-up to this research would be to construct a multisensor electrometer based on the cylindrical geometry that was utilized here.

One of the complicating factors associated with the method of charge measurement used here is that the windward side of the cylindrical insulator may accumulate a layer of granular materials on it (see Figure 3). The apparent reason for this is that the presence of a charged surface can allow an incident particle to be attracted to the surface, and to adhere to the surface. Further investigations are needed to understand the effect of the presence of a dust layer on the insulator surface on the measurement of charge by the electrometer sensor.

4 CONCLUSIONS

This research has demonstrated that a cylindrically shaped electrometer can be developed to measure the amount of electrostatic charge produced when windborne dust particles collide with the surface of an insulator. We were able to conduct experiments under controlled atmospheric conditions in a small vacuum chamber using a high-speed impeller fan to produce the windborne dust particles.

The cylindrical electrometer and its associated circuitry were constructed at NASA KSC during the summer 2001 research, and initial data was taken. The sensitivity of the electrometer is 0.25 pC/mV, but the sensitivity can be adjusted by changing resistors in the circuit that we built. The cylindrical electrometer was tested using Teflon and Fiberglass cylinders. The dust particle composition consisted of JSC Mars-1 simulant, which is a mixture of coarse and fine (<5μm diameter) particle sizes, as well as some of the major mineral constituents of the Martian soil. These other materials included Ottawa sand (SiO_2), iron oxide (Fe_2O_3), aluminum oxide (Al_2O_3) and magnesium oxide (MgO). An atmosphere consisting of carbon dioxide at 10 mbar was used in the vacuum chamber to simulate the Martian atmosphere. The atmospheric temperature was not controlled, and remained at ambient room temperature.

The data taken by the cylindrical electrometer shows that Teflon and Fiberglass cylinders charge differently when exposed to the same type of windborne granular material under similar pressure conditions and atmospheric composition. With further testing of the instrumentation using other types of cylinder materials, it is believed that a cylindrical multisensor can be constructed that will provide simultaneous measurements of charge by the different sensors. This approach may

make it possible for a multisensor electrometer to identify the mineral composition of the windborne granular particles by a unique electrostatic charging signature that multisensor output produces in response to the dust particles that collide with it. The next step that we intend to pursue in this research is to construct a prototype multisensor cylindrical electrometer.

ACKNOWLEDGMENTS

I would like to thank Dr. Carlos Calle for inviting me to work with him on this project, and for all of the assistance and support he provided during my stay at NASA Kennedy Space Center. I would also like to thank Dr. Charles Buhler, Andrew Nowicki, and Ellen Groop for their assistance during the course of the research. Finally, I would like to thank Dr. Ray Hosler and Cassie Spears of the Univ. of Central Florida for organizing the summer faculty program at KSC.

REFERENCES

[1] M. Buehler, L.-J. Cheng, O. Orient, M. Thelen, R. Gompf, J. Bayliss, J.Rauwerdink, "MECA Electrometer: Initial Calibration Experiments", Inst. Phys. Conf., Ser. No. 163, pp. 189-196, Proceedings of the 10th Int. Conf., Cambridge, 28-31 March 1999.

[2] M.G. Buehler, et al., "From Order to Flight in Eighteen Months: The MECA/Electrometer Case Study", IEEE Aerospace Conference, March 2000.

[3] J.G. Mantovani, "Evaluation of the Performance of the Mars Environmental Compatibility Assessment Electrometer", 2000 NASA/ASEE Summer Faculty Fellowship Program Final Report, July 2000.

[4] C.C. Allen, et al., "Martian Regolith Simulant JSC MARS-1", Lunar and Planetary Science Conference XXIV, Houston, TX, 1998.

[5] D.S. McKay, et al., "JSC-1: A New Lunar Regolith Simulant", Lunar and Planetary Science Conference XXIV, Houston, TX, 1998.

2001 NASA/ASEE SUMMER FACULTY FELLOWSHIP PROGRAM

JOHN F. KENNEDY SPACE CENTER
UNIVERSITY OF CENTRAL FLORIDA

CONTROL FOR NOx EMISSIONS FROM COMBUSTION SOURCES

Maria E. Pozo de Fernandez, Ph.D.
Assistant Professor
Department of Chemical Engineering
Florida Institute of Technology

Michelle M. Collins, Ph.D., P.E., Q.E.P.
NASA-KSC
Environmental Program Office

ABSTRACT

The Environmental Program Office at the Kennedy Space Center is interested in finding solutions and to promote R&D that could contribute to solve the problems of air, soil and groundwater contamination. This study is undertaken as part of NASA's environmental stewardship program. The objective of this study involves the removal of nitrogen oxides from the flue gases of the boilers at KSC using hydrogen peroxide. Phases 1 and 2 of this study have shown the potential of this process to be used as an alternative to the current methods of treatment used in the power industry.

This report summarizes the research done during the 10-week summer program. During this period, support has been given to implement the modifications suggested for Phase 3 of the project, which focus on oxidation reactions carried at lower to medium temperatures using UV lights as a source for the hydrogen peroxide dissociation and the effect on the NO conversion.

CONTROL FOR NOx EMISSIONS FROM COMBUSTION SOURCES

Maria E. Pozo de Fernandez, Ph.D.

1. Introduction

NASA launches the Space Shuttle from a 149,000-acre Wildlife refuge. NASA is committed to Environmental Stewardship and has explicitly stated this commitment in the NASA Strategic Plan. Nitrogen Oxide (NOx) emissions are a primary criteria pollutant regulated by the USEPA. The Kennedy Space Center is permitted to emit approximately 60 tons of NOx annually under their Title V air permit. NASA is pursuing R&D to minimize the detrimental environmental effects of KSC operations on the environment. This study is undertaken as part of NASA's environmental stewardship program.

This study involves the removal of nitrogen oxides from the flue gases of the boilers at KSC. The primary focus of the research is the conversion of NOx to nitrogen acids for the purpose of scrubbing them from the gas stream. NO is virtually non-soluble and NO_2 is only slightly soluble; however, nitrogen acids (HNO_2 and HNO_3) are highly soluble and can be removed via scrubbing.

Phase 1 of this study was completed in December 1998 and consisted of oxidation of the NOx at high temperatures (~930 °F). Phase 2 focused on oxidation at lower temperatures utilizing an ultraviolet (UV) light source. Key to the success of this study was the redesign, operation and optimization of the scrubber operation. The redesign included the following: 1. Conversion from batch to continuous reservoir flow. 2. Lower temperatures in the scrubber recirculation system. 3. Continuous and Batch caustic feed. 4. Providing for sampling and analysis in-line. 5. Increase recirculation flow rate.

Phase 3A started in January 2000 and concluded in March 2001. This phase focused on the oxidation at low temperatures utilizing a microwave source. Laboratory experiments have shown that microwaves promote the conversion of H_2O_2 into hydroxyl radicals, thus helping the desired NO to NO_2 conversion. Also, a new configuration to connect the flue gas pipe from the convection section at the boiler to the inlet gas port at the reactor was designed and built.

Phase 3B started in March 2001. For this phase a UV light unit with 2 lights replaced the microwave unit. The difference of this experimental setting than the one used in phase 2 is that the hydrogen peroxide was exposed to the UV lights prior entering the reaction chamber. This report summarizes the research done during the 10-week program at NASA-KSC.

2. Background

Laboratory studies have demonstrated that hydrogen peroxide (H_2O_2) when injected under proper conditions into hot gases of the exhaust stream it oxidizes nitric oxide (NO) into NO_2, HNO_2 and HNO_3. The formation of nitrogen acids allows for more inexpensive methods of post treatment for nitrogen removal, such as, scrubbing. Sulfur dioxide can also be added to the combustion source to simulate the exhaust of an industrial power plant.

The primary reactions that are expected to occur during this process are as follows:

$$H_2O_2 \Rightarrow 2\,OH \quad [2.1]$$

$$NO_2 + SO_2 \Rightarrow NO + SO_3 \quad [2.2]$$

Hydroxyl-Radical Reactions:

$$H_2O_2 + OH \Rightarrow HO_2 + H_2O \quad [2.3]$$

$$NO + OH \Rightarrow NO_2 + H \quad [2.4]$$

$$NO + OH \Rightarrow HNO_2 \quad [2.5]$$

$$NO_2 + OH \Rightarrow HNO_3 \quad [2.6]$$

$$SO_2 + H_2O + OH \Rightarrow HSO_3{\bullet}H_2O \quad [2.7]$$

Hydroperoxyl-Radical Reactions:

$$NO + HO_2 \Rightarrow HNO_3 \quad [2.8]$$

$$NO_2 + HO_2 \Rightarrow HO_2NO_2 \quad [2.9]$$

$$SO_2 + HO_2 \Rightarrow SO_3 + OH \quad [2.10]$$

To demonstrate the viability of such process in an industrial setting, researchers at NASA-KSC and the University of Central Florida (UCF) joint efforts to implement this process from a laboratory scale to a pilot plant scale. The experimental setting is located at the KSC Central Heat Plant (CHP). This study is part of Phase III of the BES Project. Highlights of Phase I and Phase II results are given below.

BES Phase 1: Phase 1 of this project was performed on a 35 mmBTUH natural gas boiler. The fuel used in the boiler consists mainly of methane and varying amounts of ethane, propane, butane, a sulfur-containing mercaptan added to natural gas, and inerts, such as, nitrogen, carbon dioxide and helium. When burning natural gas the major pollutant in the exhaust gases is mainly NOx. The percentage of NOx presence depends on the temperature of the combustion chamber as well on the fuel/oxygen ratio.

Part of the flue gas was diverted to the experimental apparatus consisting of different sections: Injection Zone, Reaction Zone, Quenching and Scrubbing. At the Injection Zone hydrogen peroxide (H_2O_2) was injected to the system. NO and SO_2 was added to the exhaust gases to simulate the composition of a flue gas from an industrial power plant. Once passed the Injection Zone the mixture of flue gas, NO, SO_2 and (H_2O_2) went through an auxiliary gas burner to bring the slipstream gases to the desired reaction temperature. From this point, the gases went through the Reaction Zone, where the conversion of NO to NOx and nitric acids took place. The Reaction Zone consisted of a 12-inch diameter, 8-ft long stainless steel pipe, having sampling ports and thermocouples

distributed along its length. Reactions were carried out up to 500 °C. The reaction products and by-products passed then through the Quenching system, where water was added to cool off the gas mixture before entering the Scrubbing System. The scrubber was a packed column consisted of an 8-ft tall acrylic column with a 6-ft bed depth. 1-inch Hyflow 25-7 polypropylene rings were used as packing material. The scrubber had a 30x60x30 inch^3 reservoir, a 1¼ - inch PVC recirculation line with a Hayward diaphragm valve, a by-pass valve, a ½ HP submersible pump and reservoir drain and sampling port. Sodium bicarbonate was used to control the pH of the fluid at the reservoir.

Figure 2.1 shows the process schematics for Phase 1. A Data Acquisition System (DAQ) using LabView software from National Instruments was used to obtain instant readings of the key parameters in the process. Figure 2.2 shows the schematics of the experimental system as the computer monitor displays it.

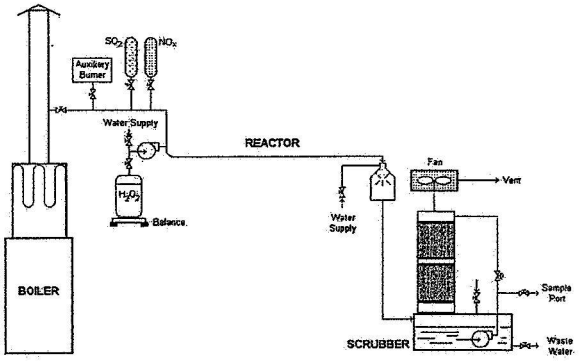

Figure 2.1. Process Schematics (Phase I)

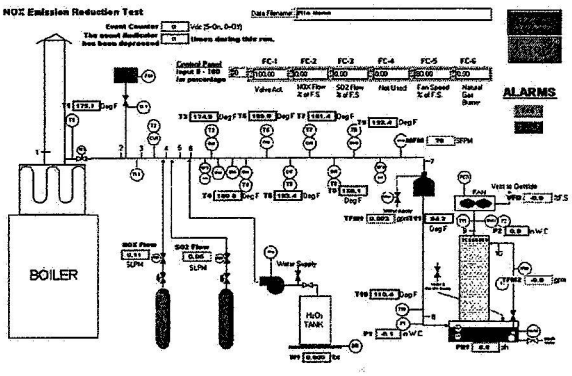

Figure 2.2. LabView Diagram (Phase I)

Several runs were made with this experimental configuration changing the following variables: Reaction temperature, NO, SO_2 and H_2O_2 concentration, NO/H_2O_2 ratio, SO_2/H_2O_2 ratio and residence time. The results obtained during Phase 1 were encouraging but some modifications were required in order for the system to perform to the optimum expected values. The conversion from NO to NOx worked very well, getting conversions greater than 96% for NO/ H_2O_2 ratios of 1:1. Conversion from NO_2 to nitric acids was not as high as expected. Operating the reactor at high temperatures and having the surface of the stainless steel reactor without any type of coating could have been part of the problem. The removal of the nitric acids by the scrubber was not as efficient as expected. The scrubbing system was never optimized for the kind of removal required by the process. The submersible pump provided was under-specified, since the rates of liquid flow recommended for optimal scrubbing operation were never achieved. The implementation of these modifications led to Phase 2 of the project.

BES Phase 2: Based on the results obtained during Phase I, several modifications were proposed for Phase 2 of the project. The sections to be re-designed were the Reaction Zone and the Scrubbing System. The reaction zone pipe (12" diameter, 8' long SS pipe) was coated with a boron-nitride paint to prevent the release of iron during the reaction. The paint selected was high temperature ceramic boron nitride paint from Carborundum. UV lights were used as a heat source to carry the reaction at lower temperatures.

Scrubbing System: The scrubber used during Phase 1 of the project was designed and manufactured by Rauschert Industries, Inc. Based on the parameters supplied, they estimated the size, material, packing material, optimum gas and liquid rate within the column and the operation temperature. The packing material selected by the vendor was 1-inch Hyflow 25-7 polypropylene rings. This packing material is proprietary, meaning that its characteristics and hydraulic behavior can not be found in the open literature. Once the vendor specified the unit, he recommended 500 scfm for the gas rate and 35 gpm for the liquid rate. Since the recirculation pump provided with the unit was under-specified the maximum liquid flow achieved was approximately 15 gpm, which proved to be too low for the scrubber operation.

The scrubber was re-designed for continuous operation having inlet, outlet and recirculation lines. Fresh water was introduced in the system through the inlet line. Two Hayward diaphragm valves control the flow through the outlet line and the recirculation line in the system. Mass flowmeters hooked up to the DAQ provided accurate flow measurement at the inlet, outlet and recirculation lines. Liquid recirculation was provided through a new 1-HP pump, able to deliver 35 gpm if desired. A continuous and batch caustic feed was also added to the system. The submersible pump at the reservoir provided continuous mixing of the tank fluid and the caustic solution added to the tank. Figure 2.3 shows the process schematics of Phase 2 and Figure 2.4. shows the scrubber with the modifications.

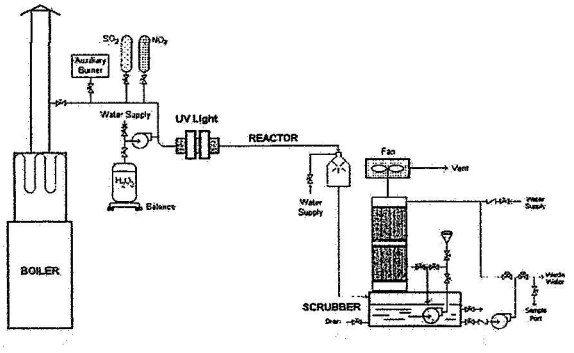

Figure 2.3. Process Schematics (Phase 2)

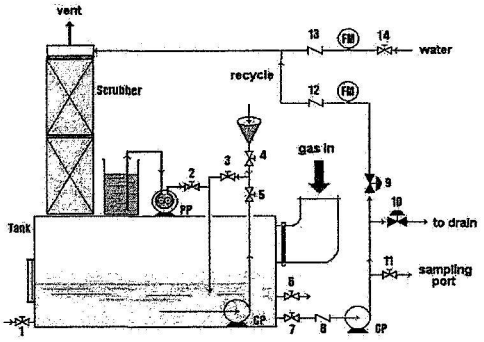

Figure 2.4. Scrubber Modifications

Many tests were performed during Phase 2 of the project. The parameters varied included: the reaction temperature (350, 400 and 450 °F), the injection point location, the

NO_2/H_2O_2 ratio, and SO_2/H_2O_2 ratio, the pH of the scrubber reservoir solution and the recycle flow at the scrubber.

The Phase 2 data showed that the use of UV lights was slightly to moderately effective in oxidizing NO to NO_2 at low to moderate temperatures. The improvements in the scrubber re-design provided a better temperature control and the capability to perform steady state operations.

BES Phase 3A: Laboratory experiments have shown that microwaves promote the conversion of H_2O_2 into hydroxyl radicals, thus helping the desired NO to NO_2 conversion. In Phase 3A of the project, a microwave source replaced the UV lights unit. The microwave commercial unit was built by one of the industrial partners of this project.

A new configuration to connect the flue gas pipe from the convection section at the boiler to the inlet gas port at the reactor was designed and built. The streams coming from the convection section and the radiation section at the boiler were mixed to obtain the desired working temperature at the reactor. Tests were conducted having the microwave unit in two configurations: parallel (Figure 2.5a) and perpendicular (Figure 2.5b) to the inlet flue gas. The schematic diagram of the process for Phase 3A is presented below.

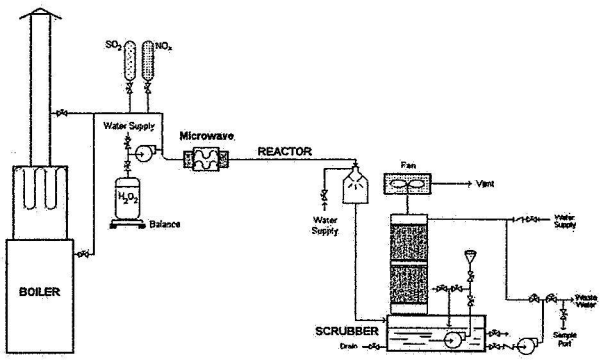

Figure 2.5a. Schematic Diagram (Phase 3A)

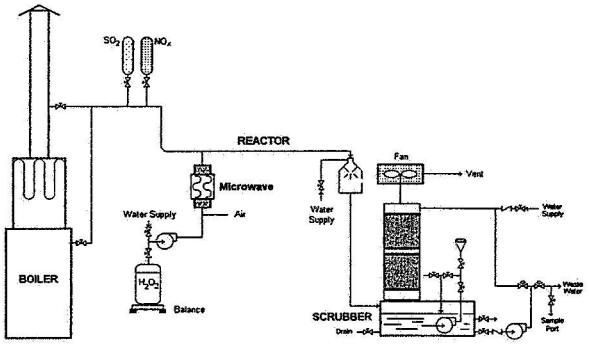

Figure 2.5b. Schematic Diagram (Phase 3A)

3. Experimental

For Phase 3B, UV lights were placed where the microwave unit was. In this case, the stream of hydrogen peroxide and the gas inlet stream were perpendicular to each other. The purpose of studying this configuration was to find out the capabilities of the UV lights to initiate the H_2O_2 dissociation without being affected by the flue gas stream as it happened in Phase 2 (see figure 2.3)

First the injection nozzle for the hydrogen peroxide was heated using heating tape; placed inside a PVC pipe and later inside the UV light chamber. Only a small part of the whole

injection nozzle was exposed to the UV lights. In this configuration the results were not as good as expected. In a second attempt, the injection nozzle was placed directly inside the UV light chamber without being covered, exposing the hydrogen peroxide directly to the UV lights.

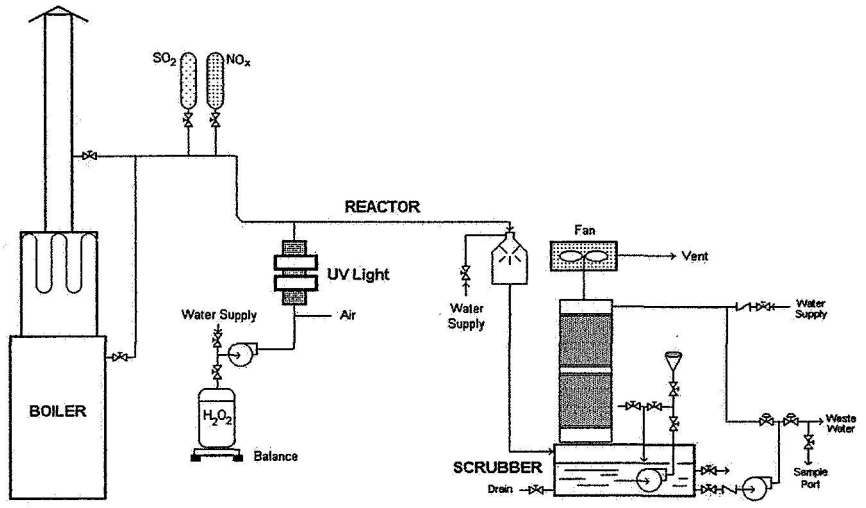

Figure 3.1. Schematic Diagram (Phase 3B)

Based on the results obtained during Phase I, it was determined that the conversion of NO to NO_x was favorable at high temperatures. To check whether or not the UV lights had an effect in the NO conversion reaction, the experiments were performed using no lights, using only 1 light and using 2 lights. The experiments were carried out at three reaction temperatures: 186, 340 and 580 °F. A total of 43 experimental runs were performed and the average of the experimental results obtained at each temperature are presented in the following table.

Table 3.1. Experimental Results (Average Values) for Phase 3B.

Run	T (°F)	T (°C)	# UV Lamps	NO Conversion %	NO_x conversion %
1	186	85.5	0	1.1	0.0
2	186	85.5	1	1.9	0.0
3	186	85.5	2	2.5	2.2
4	340	171.1	0	0.2	0.0
5	340	171.1	1	6.5	1.9
6	340	171.1	2	8.2	2.4
7	580	304.4	0	33.9	15.4
8	580	304.4	1	42.6	20.4
9	580	304.4	2	55.4	26.5

A graph of percentage conversion versus temperature for NO and NO_x were obtained and it is shown in figure 3.2. It can be observed that the trendline of the data at different temperatures for both NO and NO_x conversion follow an exponential behavior. It is observed also, that the % conversion for NO and NO_x increases with temperature and with the number of UV lights used.

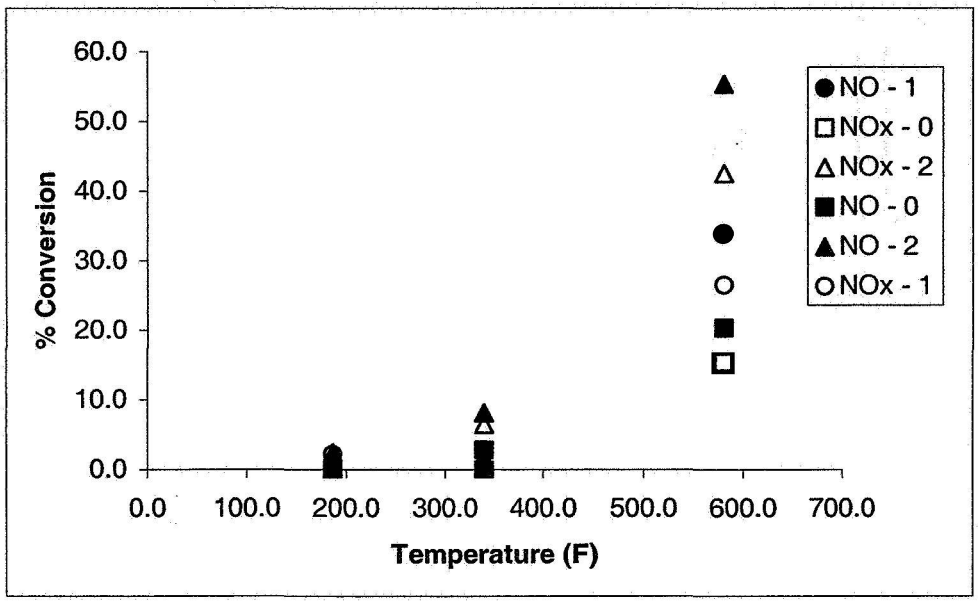

Figure 3.2. Percentage Conversion versus Temperature

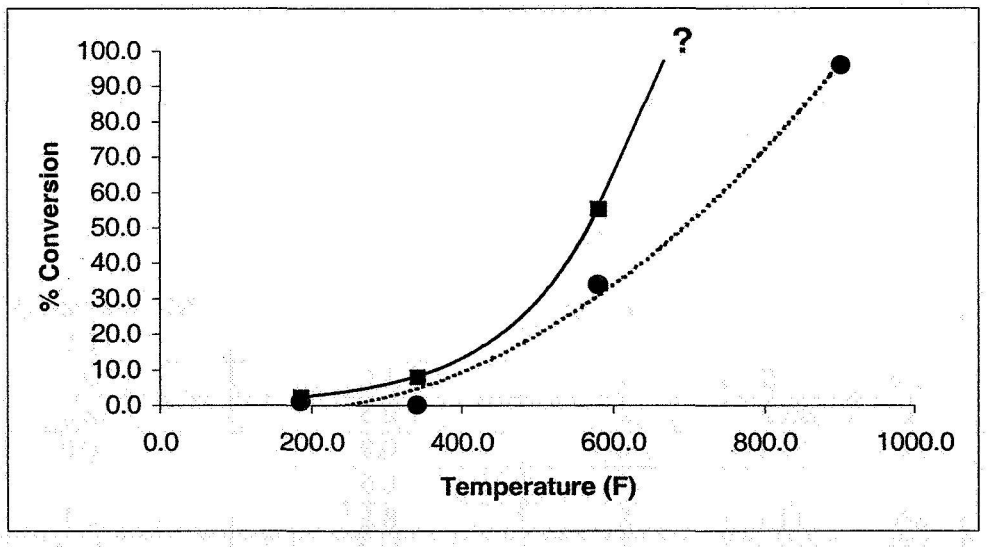

Figure 3.3. Percentage Conversion NO versus Temperature
Legend: --■-- 2 UV lights --●-- No lights

To compare the effect of the UV lights in the reaction, a second graph was obtained using the data for NO. The % conversion data for NO was plotted versus the temperature using the experimental data for "no lights" and for "2 UV lights" as it is shown in figure 3.3. The "no lights" data (--●--) shows the temperature dependence of the reaction. At higher temperatures the % conversion increases. The value for the % conversion for the data point at 900 °F was obtained from previous results at Phase I.

The experimental results for "2 UV Lights" (--■--) for the % conversion for NO versus temperature were plotted in the same graph. The data shows that at the same temperature the % conversion increases when the UV lights are used. From the results it is observed that the presence of the UV lights increases the % conversion. Since there were no experiments done with this configuration at temperatures higher than 580 °F, it will be recommended to check whether or not the exponential trendline continues at higher temperatures values than the ones used in this investigation.

4. Summary

This experimental work has shown the impact of using UV lights as precursors for the dissociation of hydrogen peroxide (H_2O_2). The dissociation of the peroxide and the production of OH radicals is the key in the process to oxidize nitric oxide (NO) into NO_2, HNO_2 and HNO_3.

The experiments were carried out at three different temperatures and from the results it can be concluded that the dissociation of H_2O_2 in the presence of UV lights favors the formation of the OH radicals, and subsequently the conversion of NO. The best results were obtained at higher temperatures.

5. References

[1] Collins, M. M. (1998) Ph.D. Dissertation. University of Central Florida.

[2] Collins, J. G. (1999) M.S. Thesis. University of Central Florida.

[3] Coulson, J. M. and J. F. Richardson (1991) *Chemical Engineering*, Volume 2, Pergamon Press, USA.

[4] McCabe, W. L.; J. C. Smith and P. Harriot (1985) Unit Operations in Chemical Engineering, 4th Edition, McGraw-Hill, Inc., USA.

[5] Orioles, J. J. (1999) M.S. Thesis. University of Central Florida.

6. Acknowledgments

I would like to thank my NASA colleagues Dr. Michelle M. Collins and Tracey Fredrickson for providing the opportunity to work in this project. Special thanks to the members of the BES Group: Dr. Chris Clausen, Dr. C. David Cooper, and the UCF

graduate students for their help and support. My sincere appreciation to the personnel of the Central Heat Plant, especially the CHP Foreman George Broyles and Tom Petelle. Without their help, support and expertise it would have been impossible to accomplish the tasks of this project. Special thanks to Hector Delgado and Maxime Cherry for providing a friendly working environment. Special thanks to Dr. Ramon Hosler, Gregg Buckingham and Cassie Spears from the NASA/ASEE Summer Program for all their efforts. This has been a great research experience.

2001 NASA/ASEE SUMMER FACULTY FELLOWSHIP PROGRAM

JOHN F. KENNEDY SPACE CENTER
UNIVERSITY OF CENTRAL FLORIDA

FLUID DYNAMICS OF A PRESSURE REDUCING INLET

JOHN M. RUSSELL
Associate Professor, Aerospace Engineering
Florida Institute of Technology
NASA colleague: FREDERICK W. ADAMS, YA-D2

ABSTRACT

Instruments for the monitoring of hazardous gases in and near the space shuttle collect sample gas at pressures on the order of one atmosphere and analyze their properties in an ultra-high vacuum by means of a quadrupole-mass-spectrometer partial pressure tranducer. Sampling systems for such devices normally produce the required pressure reduction through combinations of vacuum pumps, fluid Tees and flow restrictors (*e.g.* orifices, sintered metal frits or capillaries). The present work presents an analytical model of the fluid dynamics of such a pressure reduction system which enables the calculation of the pressure in the receiver vessal in terms of system parameters known from the specifications for a given system (*e.g.* rated pumping speeds of the pumping hardware and the diameters of two orifices situated in two branches of a fluid Tee). The resulting formulas will expedite the fine tuning of instruments now under development and the design of later generations of such devices.

FLUID DYNAMICS OF A PRESSURE REDUCING INLET

JOHN M. RUSSELL

1. FLOW GEOMETRY; OBJECTIVE

Figure 1.1 is a schematic diagram of a fluid Tee.

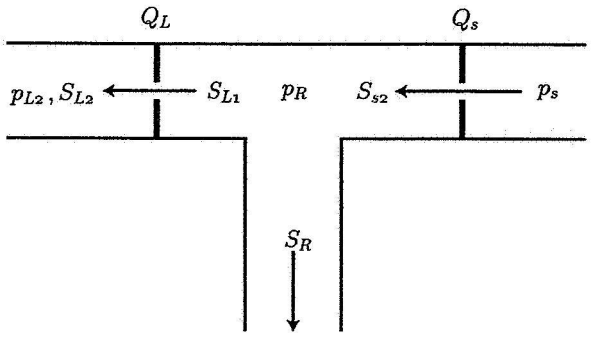

Fig. 1.1

The top left branch of the Tee discharges into an ultra high vacuum envelope containing a partial pressure transducer (*e.g.* a Quadrupole Mass Spectrometer gas analyzer). The volumetric throughput through the partial pressure transducer is presumed to be given by the rated pumping speed, S_{L2}, of a high-vacuum pump of turbomolecular type. The bottom branch of the Tee discharges into a low-vacuum foreline pump (*e.g.* of scroller type). The top left and top right branches of the Tee each contain an orifice of prescribed diameter.

As the arrows indicate, the Tee has one inlet and two outlets. In keeping with the notation conventions in vacuum literature, I have denoted *volumetric rate of transport of gas across a cross section* by the symbol S. The symbol p denotes local *gas pressure* and the symbol $Q := pS$ denotes the *pressure volume throughput* of gas at a given cross section. The numerical subscripts 1 and 2 denote conditions on the upstream and the downstream sides of an orifice, respectively. The letter subscripts S, L and R denote *supply*, *leak*, and *roughing* (pump) respectively.

The objective of the present discussion will be *to show how one may calculate the two outlet pressures, namely p_R and p_{L2} from various constants of the system.* The be specific, the constants of the system consist of the members of the following list:

$$S_{L2}\ ,\ S_R\ ,\ T_s\ ,\ T_L\ ,\ d_s\ ,\ d_L\ ,,\ k\ ,\ m\ ,\ \gamma\ ,\ p_s \tag{1.1}$$

in which (for example):

S_{L2}=pumping speed at the inlet to a high-vacuum turbopump (Alcatel model ATH30+):
$\begin{cases} 20 \text{ L/s} & \text{for } He, \\ 30 \text{ L/s} & \text{for } N_2, \end{cases}$

S_R=pumping speed at the inlet of a Dry Scroll type roughing pump (Varian model TriScroll 300):
8.8 ft^3/min (or 4.15314 L/s),

T_s=temperature of the supply gas upstream of the top right orifice in Fig. 1.1:
295.15 °K (22 °C),

T_L=temperature of the gas in the Tee between the two orifices in Fig. 1.1:
295.15 °K (22 °C),

d_s=diameter of the top right orifice in Fig. 1.1:
0.009 in,

d_L=diameter of the top left orifice in Fig. 1.1:
0.002 in,

k=BOLTZMANN constant:
1.38066×10^{-23} J/°K,

m=mass of an individual gas particle:
$\begin{cases} 4.0026 \text{ amu} & \text{for } He, \\ 28.0134 \text{ amu} & \text{for } N_2, \end{cases}$
in which the notation 'amu' stands for *atomic mass unit* (1 amu=1.66054×10^{-27} kg),

γ=ratio, c_p/c_v, of specific-heat-at-constant-pressure to specific-heat-at-constant-volume of the gas:
$\begin{cases} 1.667 & \text{for } He, \\ 1.4 & \text{for } N_2, \end{cases}$

p_s=pressure of the supply line (upstream of the top right orifice in Fig. 1.1):
400 Torr.

2. APPLICATIONS OF THE LAW OF CONSERVATION OF MASS

In order make the following analytical solution self contained I will preface it with a discussion of the consequences of the law of conservation of mass and the equation of state of an ideal gas as they apply to the present problem. Recall, first, that one may write the equation of state of an ideal gas in the form (*cf.* CHAPMAN AND COWLING, 1970, p38)[1]

$$p = nkT\ , \tag{2.1}$$

in which n is the *number density of particles*, k (as stated above) is the BOLTZMANN constant and T is the absolute temperature. Let V denote the volume of a given sample of gas. If one multiplies both sides

of (2.1) by V and writes $nV := N$ for the *number of particles in the sample*, one gets

$$pV = NkT\,. \tag{2.2}$$

If (as above) m is the mass of a single particle in the sample then $Nm := M$ is the *total mass of the gas in the sample*. If one writes $N = M/m$ in (2.2) one gets

$$pV = M\frac{k}{m}T\,. \tag{2.3}$$

Consider a steady-state process. Then a special case of (2.3) is

$$p\Delta V = \Delta M\frac{k}{m}T\,, \tag{2.4}$$

in which ΔV and ΔM are the values of of volume and mass of a small sample of gas transported across a fixed cross section during the time interval Δt. If one divides (2.4) by Δt one gets

$$p\frac{\Delta V}{\Delta t} = \frac{\Delta M}{\Delta t}\frac{k}{m}T\,. \tag{2.5}$$

If one passes to the limit $\Delta t \to 0$ one may write, in turn

$$\lim_{\Delta t\to 0}\left(\frac{\Delta V}{\Delta t}\right) := S\,,$$

in which S, as above, is the volumetric throughput across the generic cross section and

$$\lim_{\Delta t\to 0}\left(\frac{\Delta M}{\Delta t}\right) := \dot{M}\,,$$

in which $\dot{M}$ is the corresponding *mass throughput* across the same cross section. Equation (2.5) thus becomes, in the limit $\Delta t \to 0$,

$$pS = \dot{M}\frac{k}{m}T\,, \tag{2.6}$$

Let the subscripts $(\,)_1$ and $(\,)_2$ refer to any two distinct cross sections of conduit between which there are no brances (or leaks). I have already introduced the assumption that the flow is steady in time. Then the law of conservation of mass requires that

$$\dot{M}_1 = \dot{M}_2\,. \tag{2.7}$$

If one eliminates $\dot{M}$ from the left and right members by means of (2.6) one gets

$$\left(\frac{pS}{(k/m)T}\right)_1 = \left(\frac{pS}{(k/m)T}\right)_2\,. \tag{2.8}$$

In many vacuum applications, the changes in absolute temperature, T, along the conduit between two cross sections is small compared to, say, the average value over that interval. In that case, one may take

$$T_1 \approx T_2 \tag{2.9}$$

in (2.8). In the mean time, the factor k is a universal physical constant and m is constant for a given gas mixture. One may thus simplify (2.8) by cancelling the common factor $(k/m)T$ in the right and left members to obtain

$$(pS)_1 = (pS)_2 := Q\,. \tag{2.10}$$

The symbol Q thus denotes a parameter that is constant between any two distinct cross sections of conduit provided there are no branches or leaks in between. This model (which is subject to the uniform temperature assumption) may be quite accurate even though the individual factors, p and S, contributing to the product $Q = pS$ undergo large changes (*e.g.* p may decrease by a factor 10^{-3} while S increases by the factor 10^3).

Now suppose that there is a branch in a conduit. Then in steady flow the law of conservation of mass requires that the net flow of mass into the branch be balanced by the net outflow from it, *i.e.*

$$\sum \dot{M}_{\text{in}} = \sum \dot{M}_{\text{out}}\,.$$

One may, as before, eliminate $\dot{M}$ by means of (2.6) to get

$$\sum\left(\frac{pS}{(k/m)T}\right)_{\text{in}} = \sum\left(\frac{pS}{(k/m)T}\right)_{\text{out}}\,. \tag{2.11}$$

The uniform temperature assumption, (2.9), enables one to cancel T from the left and right members and k/m cancels for the same reasons as before. Thus,

$$\sum (pS)_{\text{in}} = \sum (pS)_{\text{out}}\,. \tag{2.12}$$

In the particular example of the flow in the fluid Tee shown in Fig. 1.1 equation (2.12) implies that

$$p_R S_{s2} = p_R S_R + p_R S_{L1}\,.$$

If one cancels the common factor p_R one gets

$$S_{s2} = S_R + S_{L1}\,. \tag{2.13}$$

3. ON THE FLOW THROUGH THE ORIFICES

I will restrict attention in the present problem to the case in which the pressure, p_R, is less than half of the pressure on the upstream side of the supply orifice. In the case when the flow through the supply orifice in the regime of *continuum* gas flow the conditions are such that the gas speed at the throat of the orifice just attains the speed of sound. According the equations of Gasdynamics (*cf.* LIEPMANN & ROSHKO, 1957, §§2.10 and 5.3)[2] one may derive the following equation for Q_s

$$Q_s = p_s \pi \frac{d_s^2}{4} \sqrt{\frac{kT_s}{m}} \left(\frac{2\gamma}{\gamma+1}\right)^{1/2} \left(\frac{2}{\gamma+1}\right)^{1/(\gamma-1)} . \tag{3.1}$$

Here, d_s is the diameter of the supply orifice, γ is the ratio of specific heats c_p/c_v of the gas (namely 1.6667 for a monotomic gas or 1.4 for a diatomic one). Equation (3.1) is compatible with the equations in LIEPMANN & ROSHKO[2] (though none of the equations they write is equivalent to an explicit solution for Q). One may find equation (3.1) as written above in O'HANLON, 1989, p29[3].

I will further restrict attention to the case when flow through the left orifice in Fig. 1.1 is in the regime of *free molecule flow* (as opposed to contiuum flow). One may then relate the pressure-volume throughput, Q_L, though that orifice to the difference between the pressures on the two sides and to the *conductivity*, C_L defined by

$$C_L = \frac{Q_L}{p_R - p_{L2}} . \tag{3.2}$$

The kinetic theory of gases (*cf.* JEANS, 1940, pp 58–60)[4] furnishes an estimate of the rate of effusion of a gas through a circular hole in a plate subject to the assumptions that the fluid is in the regime of free-molecular flow and the remote pressure in the receiver vessal is a perfect vacuum. If one adjusts this formula to allow for nonzero (but unequal) pressures on the two sides of the hole one can arrange the result into a formula having the structure of (3.2) with the conductivity, C_L, given by

$$C_L = \frac{d_L^2}{4} \sqrt{\frac{\pi k T_L}{2m}} , \tag{3.3}$$

(see also O'HANLON, 1989, equations 2.2 and 3.19) [3].

4. ALGEBRAIC SOLUTION FOR THE OUTLET PRESSURES

As stated in §1 above suppose that the parameters listed in (1.1) are given and that the two pressures p_R and p_{L2} are sought. One begins by noting that all of the terms in the right member of equation (3.3) are in the list (1.1) of given data. Thus, *the conductivity, C_L, of the orifice in the top left of Fig. 1.1 is known.*

Note that the reciprocal of (3.2) is

$$\frac{1}{C_L} = \frac{p_R - p_{L2}}{Q_L} = \frac{p_R}{Q_L} - \frac{p_{L2}}{Q_L} \tag{4.1}$$

But the general identity $Q := pS$ implies that $p = Q/S$. In particular, $p_R = Q_L/S_{L1}$ and $p_{L2} = Q_L/S_{L2}$. The outermost equality in (4.1) thus becomes

$$\frac{1}{C_L} = \frac{Q_L}{S_{L1}} \frac{1}{Q_L} - \frac{Q_L}{S_{L2}} \frac{1}{Q_L}$$

or

$$\frac{1}{C_L} = \frac{1}{S_{L1}} - \frac{1}{S_{L2}} \tag{4.2}$$

after simplification. One may arrange this result in the equivalent form

$$\frac{1}{S_{L1}} = \frac{1}{C_L} + \frac{1}{S_{L2}} .$$

The reciprocal of this equation is

$$S_{L1} = \frac{1}{\frac{1}{C_L} + \frac{1}{S_{L2}}} .$$

If one multiplies the right member by $1 = C_L/C_L$ one gets

$$S_{L1} = \frac{C_L}{1 + \frac{C_L}{S_{L2}}} . \tag{4.3}$$

Now (2.13) asserts that $S_{s2} = S_R + S_{L1}$. One concludes from (4.3) that

$$S_{s2} = S_R + \frac{C_L}{1 + \frac{C_L}{S_{L2}}} = S_R \left[1 + \frac{\frac{C_L}{S_R}}{1 + \frac{C_L}{S_{L2}}} \right] ,$$

or

$$S_{s2} = S_R \left[\frac{1 + \frac{C_L}{S_{L2}} + \frac{C_L}{S_R}}{1 + \frac{C_L}{S_{L2}}} \right] . \qquad (4.4)$$

Recall that the general identity $Q := pS$ implies that $p = Q/S$. In particular, $p_R = Q_s/S_{s2}$. If one eliminates S_{s2} from the identity $p_R = Q_s/S_{s2}$ by means of (4.4) one gets

$$p_R = \frac{Q_s}{S_R} \left[\frac{1 + \frac{C_L}{S_{L2}}}{1 + \frac{C_L}{S_{L2}} + \frac{C_L}{S_R}} \right] \qquad (4.5)$$

To calculate the pressure, p_{L2}, downstream of the top left orifice in Fig. 1.1 one applies equation (2.10) at two stations of the top left branch of the Tee, namely stations upstream and downstream of the top left orifice. The result is

$$p_{L2} S_{L2} = Q_L = p_R S_{L1} . \qquad (4.6)$$

If one divides through by S_{L2} the outermost equality becomes

$$p_{L2} = \frac{S_{L1}}{S_{L2}} p_R .$$

If one eliminates S_{L1} from this identity by means of (4.3) one gets

$$p_{L2} = \frac{1}{S_{L2}} \left(\frac{C_L}{1 + \frac{C_L}{S_{L2}}} \right) p_R$$

or

$$p_{L2} = \left(\frac{\frac{C_L}{S_{L2}}}{1 + \frac{C_L}{S_{L2}}} \right) p_R .$$

If one eliminates p_R by means of (4.5) one gets

$$p_{L2} = \left(\frac{\frac{C_L}{S_{L2}}}{1 + \frac{C_L}{S_{L2}}} \right) \frac{Q_s}{S_R} \left[\frac{1 + \frac{C_L}{S_{L2}}}{1 + \frac{C_L}{S_{L2}} + \frac{C_L}{S_R}} \right] .$$

or

$$p_{L2} = \frac{C_L}{S_{L2}} \frac{Q_s}{S_R} \frac{1}{\left(1 + \frac{C_L}{S_{L2}} + \frac{C_L}{S_R} \right)} . \qquad (4.7)$$

In summary, equations (4.5) and (4.7) [with Q_s and C_L determined by (3.1) and (3.3), respectively] fulfill the stated purpose of finding the two outlet pressures in terms of the given data listed in (1.1) above.

Having taken the trouble to calculate p_R, one may as well write down the corresponding formula for the leak rate into the analyzer cell, namely the pressure-volume throughput, Q_L, though the top left orifice in Fig. 1.1. Thus, from (4.6), we have $Q_L = p_{L2} S_{L2}$ so (4.7) implies that

$$Q_L = \frac{C_L}{S_R} \frac{Q_s}{\left(1 + \frac{C_L}{S_{L2}} + \frac{C_L}{S_R} \right)} , \qquad (4.8)$$

5. NUMERICAL EXAMPLE

If one carries out an appropriate set of unit conversions, then equation (3.1) yields, under the foregoing assumptions, the following values for the pressure-volume throughput, Q_s, into the Tee from the supply line:

$$Q_s = \begin{cases} 12.2744 \ \text{atm(cm)}^3/\text{s} & \text{for } He, \\ 4.37454 \ \text{atm(cm)}^3/\text{s} & \text{for } N_2. \end{cases} \qquad (5.1)$$

Similarly, equation (3.3) yields, under the foregoing assumptions, the following values for the conductivity C_L, of the top left orifice in Fig 1:

$$C_L = \begin{cases} 0.633135 \ (\text{cm})^3/\text{s} & \text{for } He, \\ 0.239323 \ (\text{cm})^3/\text{s} & \text{for } N_2. \end{cases} \qquad (5.2)$$

Continuing in the same vein equation (4.7) yields, under the foregoing assumptions, the following values for the pressure, p_{L2}, downstream of the top left orifice in Fig. 1.1 (*i.e.* into the analyzer cell):

$$p_{L2} = \begin{cases} 7.11469 \times 10^{-5} \ \text{Torr} & \text{for } He, \\ 6.39054 \times 10^{-6} \ \text{Torr} & \text{for } N_2. \end{cases} \qquad (5.3)$$

Likewise equation (4.5) yields, under the foregoing assumptions, the following values for the pressure, p_R, in the interior of the Tee in Fig. 1.1 (*i.e.* into the input port of the roughing pump):

$$p_R = \begin{cases} 2.24752 \ \text{Torr} & \text{for } He, \\ 0.801084 \ \text{Torr} & \text{for } N_2. \end{cases} \qquad (5.4)$$

Finally, equation (4.8) yields, under the foregoing assumptions, the following values for the

pressure-volume throughput, Q_L, through the top left orifice of the Tee in Fig. 1.1 (this quantity represents the leak rate into the analyzer cell) :

$$Q_L = \begin{cases} 1.87085 \times 10^{-3} \text{ atm(cm)}^3/\text{s} & \text{for } He, \\ 2.52064 \times 10^{-4} \text{ atm(cm)}^3/\text{s} & \text{for } N_2. \end{cases} \tag{5.5}$$

6. DESIGN CHARTS

I have presented several of the more useful results in §4 so as to isolate, wherever possible, expressions such as

$$1 + \frac{C_L}{S_{L_2}} \tag{6.1}$$

or

$$1 + \frac{C_L}{S_R} \,. \tag{6.2}$$

Note from the numerical examples of §5 that C_L is typically of the order of one $(\text{cm})^3/\text{sec}$ or smaller while S_{L_2} is of the order of tens of L/s. Thus, C_L/S_{L_2} is typically of the order of 10^{-4} and thus small compared to one in the present examples. Furthermore, S_R is on the order of a few L/s, so C_L/S_R is again small compared to one in the present examples. To an engineering approximation one may thus approximate expressions such as (6.1) and (6.2) by one.

When one makes an approximation of the sort described in the last paragraph, one finds that the pressure p_R in the intermediate space between the two orifices in Fig. 1.1 is effectively independent of the diameter d_{L_2} of the orifice in the to left branch of the Tee and of the pumping speed S_{L_2} of the pump downstream of it. In other words, *to an engineering approximation* (with an error on the order of one tenth of one percent) *the pressure p_R depends upon only the pumping speed S_R of the foreline pump and the diameter d_s of the supply orifice.*

I have applied the algorithm described in the last section to a set of input parameters significantly larger than the one summarized in §1 above. Expecting that the results for p_R to be effectively independent of d_{L_2} and S_{L_2} I arbitrarily took the values of those parameters to be their nominal ones for the present version of the HGS2000 system (*cf.* §1 above) while retaining the accurate versions of the equations of §4 (*i.e. not* approximating expressions such as (6.1) and (6.2) by one). The result of such a set of calculations is shown in Fig. 6.1 nearby.

In order not to limit the results needlessly, I carried out a calculation of the *ratio* p_{L_2}/p_R as a function of the parameters S_{L_2} and d_L. Figures 6.1 and 6.2 thus enable one to estimate the value of, say, p_{L_2} as a function of the *four* variables

$$S_R \quad , \quad d_s \quad , \quad S_{L_2} \quad , \quad d_L$$

in terms of data presented in just two sets of log-log plots.

7. RECOMMENDATIONS

It may happen that a mass-spectrometer gas analyzer that features a two-orifice pressure-reduction inlet may perform well for a given set of orifice diameter when Nitrogen is the background gas but less well when Helium is in the background. Adjustment of the orifice sizes may improve the performance of the system when Helium is the background gas but have the unintended consequence of degrading the performance when Nitrogen is again in the background.

One engineering approach that may enable one to get the best of both worlds is to incorporate two distinct pairs of orifices of which only one is active for a given background gas (the inactive pair being isolated by electronically controlled valves). I would thus recommend the consideration of such an option should it happen that there is no combination of orifice sizes that leads to satisfactory performance of the HGS2000 system for both a Nitrogen and a Helium background.

I have not discussed the application of the design charts 6.1 and 6.2 to the estimation of the partial pressures of trace gases in a background. I will simply assert that the charts in Fig. 6.2 were constructed under the assumption that the flow through the second orifice (in the top left branch of Fig. 1.1) is in the free-molecule flow regime. They should thus apply with equal validity when p_R represents the *partial* pressure of a tracer gas. The present model of the flow through first, orifice, by contrast, presumes that the flow there is in the continuum flow regime. The value of the effective molecular weight (and the ratio γ of specific heats) of fluid through it must, therefore be that of the background gas.

8. ACKNOWLEDGEMENTS

This summer is the eighth in which I have worked as a NASA/ASEE Summer Faculty Research Fellow and the sixth in which RIC ADAMS has been my

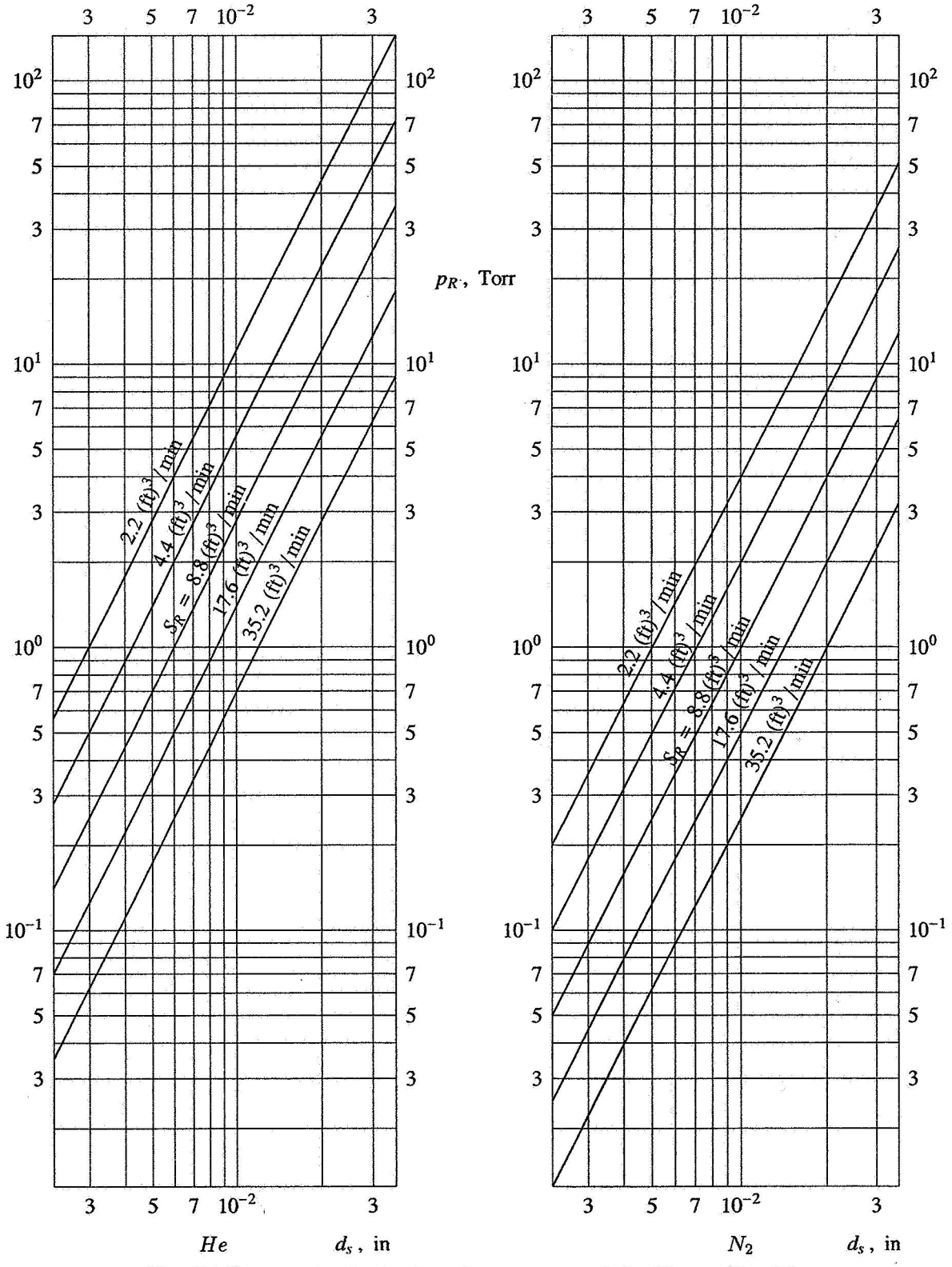

Fig. 6.1 Pressure in the intermediate portion of the Tee in Fig. 1.1.

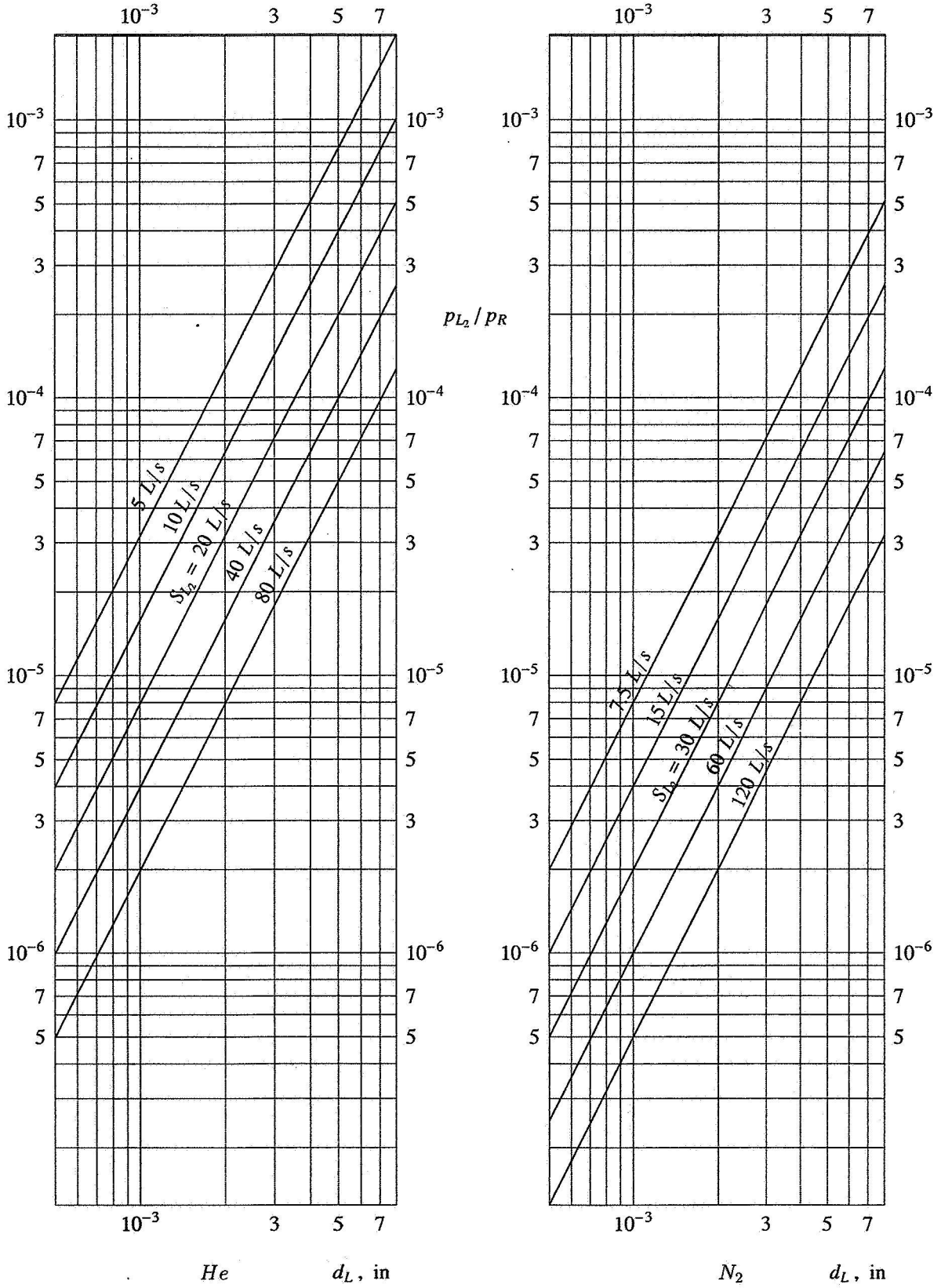

Fig. 6.2 Pressure downstream of the second (*i.e.* top left) orifice in the Tee in Fig. 1.1.

NASA colleague. I am, as so many times before, indebted to him for suggesting the present problem and providing much material and moral support. I am also indebted to his NASA supervisor, BILL HELMS, to his NASA colleague DUKE FOLLESTEIN, to Drs. TIM GRIFFEN and RICHARD ARKIN and Mr. GUY NAYLOR of DYNACS and, of course, to Dr. RAY HOSLER and CASSIE SPEARS of the Unviersity of Central Florida for their able administration of the Summer Faculty Fellow Program.

REFERENCES

[1] CHAPMAN, S. & COWLING, T.G. *The mathematical theory of non-uniform gases.* Third edition, Cambridge University Press, 1970

[2] LIEPMANN, H.W. & ROSHKO, A. *Elements of gasdynamics.* John Wiles & Sons, 1957.

[3] O'HANLON, JOHN F. *A user's guide to vacuum technology.* Second edition, Wiley-Interscience, 1989.

[4] JEANS, SIR JAMES *An introduction to the kinetic theory of gases.* Cambridge, 1940.

2001 NASA/ASEE Summer Faculty Fellowship Program
John F. Kennedy Space Center
University of Central Florida

Electronic Nose
Evaluation of Kamina prototype unit

Nathan Schattke
Research Associate
Illinois Institute of Technology
For Rebecca Young NASA/KSC

Abstract

The Kamina, Sam and Cyranose electronic nose systems were evaluated and partially trained. Much work was performed on the Kamina as it has the ability to respond to low (less than 10 ppb) concentrations of hydrazine compounds.

We were able to tell the difference between Hydrazine (Hz) and Monomethylhydrazine (MMH) in standard clean humid air. We were able to detect MMH in reduced pressure (1/3 atm) at about 250 ppb, however the training set was to far from the real situation to be useful now.

Various engineering and usability aspects of both the noses was noted, especially the software. One serious physical engineering flaw was remedied in the Kamina system. A gas flow manifold was created for the Sam system.

Different chips were evaluated for the Kamina system. It is still unclear if they can be exchanged without retraining the software.

The Sam Detect commercial unit was evaluated for solvent detection and evaluation. It was able to successfully identify some solvents.

The Cyranose was observed and evaluated for two days. It has the ability to detect gasses in the 100 parts per million level but not the 10 parts per billion level. It is very sensitive to humidity changes; there is software to partially handle this.

Introduction

The electronic nose idea is that several sensors when working together can give much more information than the individual sensors not networked. Multiply or exponentize instead of add. There are advantages and disadvantages with this much information. Such as, you have to calibrate much more upfront and much less in the future. You may also be able to calibrate on a general system then use that information to make all future calibrations for new sensors or components take much less time and money. Information from the electronic nose includes qualitative and quantitative elements and since it runs through a versatile analysis machine the direction of analysis can be performed several ways simultaneously. But in some packages the information can only be looked at one way thus allowing you to have only quantitative or qualitative but not both. As you can see the above explanation in not limited to chemical sensors, the idea would give even better service if other types of sensors were added to the matrix. The methods used for information analysis are perfectly applicable to the following sensors as well as all types of chemical sensors: pressure, temperature, positional, sonic, radar, sonar. The electronic nose doesn't really care what form its signal comes in. One interesting aspect of the Kamina nose system is the analog change between sensors. This causes the system to change as a whole, leaving the difference between the sensor elements as the indicating information. This may have positive effects on calibration and component replacement.

Electronic Nose Basics

If the above was a bit much for you, here is a primer on the electronic nose.
An electronic nose mimics the animal nose by doing three things: Sampling-Sniffing; Sensing-Smelling; Evaluating-Thinking. Sampling is very important; the signals from the sensors are different if gas flows over them for 15 seconds rather than 10 or if the gas flows past the sensors at 100 milliliters per minute or 200. In the animal nose we have physical control over how hard we sniff and how much goes through the mouth or nose. The brain takes that into account when it thinks about the signal. I have yet to see an electronic nose training set take advantage of sniffing deep or shallow. Many electronic nose systems spend a lot of money and build complicated equipment so that the gas with the smell in it comes to the sensors in easy to understand packets. For instance the operator may set up a series of jars with rubber lids, heat them to be warm, stick two needles in, push special clean gas in through one and take gas out

through the other. Other systems use less exacting methods such as: a fan to pull air over the sensor, diffusion, or a manifold and pressurized gas. This has disadvantages because the nose has to be trained to recognize all the different atmospheric conditions it could be exposed to (and you get many more with the open air than with jars). The sensors react differently to 10 ppb of Hydrazine at 70 F and 30 RH (relative humidity) or 70 F and 5 RH.
Sensing by the human nose is performed by more than a million different sensing cells, made up of over 1000 types of cells. These are spread throughout the complicated nasal passages. Signals from these sensors go to nerves. Sensing by the electronic nose as a general idea is that some change is produced on the sensor that causes or changes a signal to the computer. This can be a change in the capacitance of a catalytic surface, change in the resistance from a catalytic surface or sensitive plastic, change in the color of a catalyst at the end or on the side of a fiber optic cable, change in the frequency of a coated crystal, or increase of electrons from a fuel cell type sensor. All these types and more can be added to the system and tuned to detect the possible gasses of question. Note that this type of thing can work for liquids just as easy by using sensors that react in a liquid environment, thus giving you an electronic tongue.

Evaluating by the animal nose is both instinctive and learned. The action of pheromones on our behavior is an example of instinct. Most of what we know about the smells around us are learned. Evaluating by the electronic nose is very different. Each sensor will have a standard normal signal. Then the gas of interest will change some of the normal signals. These changes are compared to previously known samples and the results reported. One way to think about this is to imagine each sensor as an axis on a graph. If you had three sensors you would have a three-dimensional graph. As you trained the system with one chemical the three sensors would each react a certain amount. Then with another chemical they would each react in another way. So if you put a ball in the graph at the first chemical and another ball at the second they should be in different places. If they are not then the sensors chosen probably do not differentiate these two chemicals enough. This is overcome by having many sensors (10-100). Now with many sensors you have that many dimensions. As you can imagine visualizing and using 100 dimensional space is rather difficult. Practically the signals are normalized to the difference from the average or a fraction of initial signal then a plane is cut through all the dimensions that shows the best change between the areas of the different gasses in two dimensions.

Equipment and Results

The chemical applications laboratory at KSC is a large five-hood lab on the second floor of the O&C building. Two of the hoods have Kintek diffusion type gas generators. Samples of liquid are placed in special containers that have a part that will let the vapor diffuse through. These are in turn placed in an oven of very carefully controlled temperature. Inert gas is passed over the containers picking up a small amount of the vapor from the liquid. As long as there is some liquid in the container, the temperature and gas flow rate are constant the concentration of the exit vapor will remain the same. This "mother" gas can be further diluted with any gas or with a Miller-Nelson unit which produces air of known temperature, flow rate, and humidity. These

tools can accurately, quickly, and repeatedly deliver nine different types of vapors delivered to the noses.

The Kamina electronic nose is composed of a sensor chip, data acquisition and control, and computer control and analysis software.
The sensor chip is made with lines of conductor material interspaced with lines of semiconductor material (tin oxide, SnO2). These are in the X-axis. In the Y-axis are heat platens and silicone oxide (glass) covering. The heat (from underneath) is uneven so that the segments on one edge are hotter than the other edge. The glass covering is thicker on one edge than the other. This gives 38 segments each a little different from the next all of them showing the same surface to the gas stream. The chip is held up on four posts of ceramic material.

The data acquisition and control starts with the connection to the individual segments. It is performed by very fine (thinner than 0.001") gold (soft) wires attached to the chip then to the holder. These wires span through the air and are not insulated or kept separate except by bending. Although these wire should not be touched in the normal course of operation they are easily bumped which can cause shorting and a loss of signal. The other side of the gold wire is connected to the surface of a much larger chip holder with pins leading down and away from the sensing surface. This chip is plugged into a holder. This holder is plugged into another chip holder. This holder is soldered onto a small printed circuit board (PCB). This PCB has pins leading down to connect with a socket on the next PCB. This pin and socket connection was found to be a major cause of noise in the system from uneven pressure on the connections. In my opinion this connection system is too complicated and prone to failure. Training the nose requires that the signals be steady day to day. This bad connection was causing a different type of signal depending on how much the inner board was warping. Connected to the lower PCB are two data acquisition and control PCB's with electronics on them. The connection here has no faults. At the bottom of the module are two multipin sockets, one for data, and the other for power. The power module is a separate box that must be less than 18" away. The ribbon connectors are of a low cost and quality at times leading to a noisy signal.

The computer control and analysis software is supplied by Kamina. There are two ways to analyze the data, early transition detection (ETD) and resistance detection. ETD was used exclusively because it has an initial reference value that the signal is compared to. This allows the change in signal to be compared to the others no matter what level you start at. Some of the variables that can be modified in the Kamina program are:

Signal homogenization by logarithm- this allows vastly different signal changes to be treated as if they were not very different.

Signal Normalization by 1- Resistance 2- Resistance divided by Reference or 3- Reference divided by Resistance – this changes the difference from normal to be analyzed two different ways or just taking the resistance signal strait.

Median Normalization by divide by median- this gives you a stable baseline to reference all different measurements to.

Signal Filters by Time Series or Sensor Array- this option was not explored by this researcher.

Principal Component Analysis (PCA)- This is a very strong tool for this type of data analysis. It analysis the data to find the parts (components) of the data set that mostly (principally) cause the differences. The variables for this are number of principal components (up to 12 have been used) and weather or not to scale by standard deviation.

Linear Discrimination Analysis (LDA)- This is the final analysis tool used by this researcher. This analysis tool cuts the best plane through the dimensions and shows a two dimensional graph of the best fit to that.

SIMCA- this option was not used by this researcher. As explained by Susan Rose-Pehrsson this is similar to LDA in that it cuts a plane through the many dimensions but instead of being a strait plane it is a planer surface that can be bent. This could show differences better.

Neural Net- this option was not used by this researcher. I understand there is much difference between versions of this type of program. This could be a good or a bad one.

The best options for analyzing data for difference of chemicals HZ, air, and MMH was: No Logarithm, Reference divided by Resistance, divide by median, PCA w/ standard deviation and 12 components, LDA w/ 12 components. These settings and a good model on a stable sensor system were effective for determining the difference between MMH and Hz.

Lower Pressure tests

From May 31st to June 8th several tests were performed on the Kamina system at lower pressures in a bell Jar. Note that this was before the new chips were in and the board pull away problem was fixed. It is expected that if the experiment were to be performed today it would be more sensitive and accurate for detection of hydrazine compounds. Even with these limitations the group was able to successfully detect hydrazine compounds at 1/3 to ¼ atmosphere.

The equipment used was bell jar prepared by Paul Yocum of Dynacs. This chamber has as serial and 115 volt pass-throughs. The power supply and sensing head of the Kamina was placed inside. Another pass-through was a 1/4 " line with a ball valve. And the last was a ¾" pump down hose to a roughing pump (standard high quality lab roughing type with oil).

In practice the system was pumped down to 150 torr (0.20 atm), the Kamina responded. Then five minutes later (the standardization of the timing was Bill Buttners' idea) 4.0 liters of gas was introduced through the ¼" line. This raised the pressure to about 250 torr (0.32 atm). Then

five minutes later another 4.0 liters of gas was introduced. This raised the system to 350 torr (0.46 atm).

Tests were initially performed with air, the change from 760 to 150 torr was noticeable, and the change from 150 to 250 and 250 to 350 was insignificant. With MMH the system reacted clear and strong. The system concentration of 280 ppb MMH was the lowest tested. LDA plots were prepared and clear separation was established between 760 torr air, 150 torr air, 281 ppb MMH, 407 ppb MMH, 1286 ppb MMH, 1863 ppb MMH.

This experiment has been planed to change. The system will be modified to allow constant flow of gas to better simulate the changes expected.

Engineering the Kamina

The system produced by Kamina was a generalized system designed for burnt wire detection. It had a head with a small (1 ½" dia.) fan pulling air across the sensing area. The other side from the fan was a Teflon membrane, this had to be removed for hydrazine detection it can degrade the signal by as much as 2 ppm.

A new manifold was received June 19th made with glass as the main material in contact with the gas. A small amount of inside edge of a Viton gasket between the glass manifold and the chip holder surface was open to the gas, it is expected that this would not significantly effect the signal. The sensor chip holder surface is made of an epoxy coated metal surface. The volume of the glass manifold is relatively small at about 15 ml of volume over the chip. There is no disturbance in the manifold area above the chip, this could lead to an uneven and unpredictable flow over the sensing surface. The flow of gas should be disturbed in the sensing area for good mixing. The glass manifold was held in place with two half circles that were screwed down onto a ring. The half circles overlapped the glass manifold and pushed it down. At flow rates of 2 liters per minute this system can afford some leakage. If lower flow rates were preferred then a, low durometer closed cell silicon foam, would be preferable.

On July 13th the Kamina was repaired. The two PC boards that plugged into each other at the top were being pressed together unevenly. Bill Buttner, Steve Parks and Tim Hodge helped design a pin system to hold the two other corners in place. It worked; the random easily changing noise was eliminated.

The complete system for getting gasses onto the sensing surface and away and connecting to the electronics would have to be completely redesigned in order to travel to space and be usable. The present system is too fragile and prone to failure.

The software is good in that it measures the difference from the base on segments in order to determine the gas in question. Generating the rule set to check against could much easier, see the Cyranose software system. Currently effective models or rule sets are a shotgun approach of

trying all sorts of different analysis tools. Much of this could be generated and checked by the program.

A problem of 3.2 mega ohms exists for all four chips and both manifolds. The system responds to a gas signal by lowering resistance for the segments. The median of all the resistances is reported on a graph in the main part of the program. When this median reaches 3.2 Mohm it will stay at that level for a while or for a very long time, depending on how far down the final signal will go. This is probably an intermediate hardware translation problem centered around the 32768 or 2^15 bit level transition. The data at this level is suspect.

The Sam Detect system was only used for a short time. Several areas of improvement should be explored. The filters over the sensors are sintered metal, this will catalytically react with some materials including hydrazine and cause it not to be detected. These should be removable. The system resets apparently at random. This should be either well automated during training or manually switchable. No manifold was available, a fine one was fabricated by the Dynacs group of Bill Buttner, Tim Hodge, Steve Parks, and Paul Yocum. The inside of this was Teflon.

Interchangeability

Four chips were evaluated with the Kamina system. The hardware was not working well enough to determine if they could be interchanged. From the data so far and visual observations this is not likely. The fabrication process leaves many differences between the different chips. The observed, after burn in, polar charts showed much different patterns. Further work needs to be performed. Future work should focus on reproducibility of sensors. This would assist the space exploration by allowing a signature of an unknown gas to be received and later analyzed on earth. Such a system could greatly help with medical diagnosis on long missions.

Conclusion

The ability to successfully detect hydrazine compounds in the 5 ppb range is a great success that cannot be understated. Tin Oxide sensors all alone cannot do the job. The current electrochemical sensors are the best available and yet are still not stable enough, being particularly susceptible to CO2, a common element of human breath.

Use in the airlock of the ISS or shuttle is promising for Hz leak detection. This chip concept is very strong. The change in signal with time is easily handled and controlled. The sensitivity stays rather high. The range of chemicals available for detection is high but perhaps skewed towards the hydrocarbons. If this tool were to be used with medical diagnosis a predigestor or filament may be desirable. Use in the airlock of the ISS or shuttle is promising for Hz leak detection.

This concept of changing sensors a small amount across the array of an electronic nose that Kamina has introduced should be expanded to perform better. Of use to NASA would be a small

integrated nose system that has radio or IR communication to and from a computer, has the sampling system with: pump, flow path, calibration standards, sensors, filters, and data collection all on one platform. Even more useful but also much more complicated would be a heterogeneous sensor system of resistive and other types of sensors.

2001 NASA/ASEE SUMMER FACULTY FELLOWHIP PROGRAM

JOHN F. KENNEDY SPACE CENTER
UNIVERSITY OF CENTRAL FLORIDA

KSC HISTORY PROJECT

Lee Snaples
Assistant Professor
Department of History
Tarrant County College
Dr. Shannon Roberts

ABSTRACT

The project is a joint endeavor between Dr. Henry Dethloff and myself and is producing a number of products related to KSC history. This report is a summary of those projects. First, there is an overview monograph covering KSC history. Second, there is a chapter outline for an eventual book-length history. Third, there is monograph on safety at KSC. Finally, there is a web page and database dedicated to the KSC oral history project.

KSC HISTORY PROJECT

Lee Snaples

Introduction

The Kennedy Space Center was created in 1962 to support the mission to the Moon proposed by President John F. Kennedy. For the next forty years, KSC served as the primary NASA launch facility and the only place in the western hemisphere where people have left the friendly confines of Earth's atmosphere for outer space. The Apollo program focused national attention on the center and brought it great accolades in 1969 when Neil Armstrong and Buzz Aldrin became the first men to walk on the Moon. More than one hundred shuttle missions have followed up this success and helped establish a permanent station in space. KSC has become the focus of NASA operations and public attention, to the average person KSC is NASA.

With the approach of the 40th anniversary in 2002, senior officials at KSC became concerned about preserving the center's history. KSC is the only NASA center without an official history. To rectify this situation, KSC has set aside money for a complete history of the center, a three-year project. Henry Dethloff and I, as Summer Fellows, were asked to prepare a number of preliminary projects not only for immediate dissemination but also for use in the eventual manuscript. These projects included, an article-length overview history of the center, an article-length overview of safety at KSC, a chapter outline of the history manuscript, a number of oral history interviews, and development of a database and web page to support the oral history work.

KSC Overview

Cape Canaveral, a protrusion of land from the Florida peninsula into the Atlantic first encountered by European explorers about 1500, became a milepost and a way station for the European discovery and exploration of the New World. Half a century later the Cape resumed that role as a milepost and a way station in the new age of Off-World planetary discoveries and the exploration of space. "Space," commented Kennedy space Center's first center Director, Kurt Debus, perhaps reflecting on the common heritage of the New World explorers and those engaged in space and planetary exploration, "is not something new. It's part of the total environment, and we've been looking for the total environment ever since we looked out of caves at the stars." Ponce de Leon, who explored the area around Cape Canaveral in 1513, and multitudes of aerospace engineers, scientists, technicians, administrators, businesses, and their associates throughout the old world and the new, through NASA, the National Aeronautics and Space Administration, share a common bond in the continuing exploration of the total human environment.

First organized in December 1959 as the Launch Operations Directorate under the authority of the Marshall Space Flight Center located in Huntsville, Alabama, NASA's John F. Kennedy Space Center became the Launch Operations Center at Cape Canaveral on March 7, 1962. Twelve years earlier, in July 1950, an Army rocket team launched the first long-range missile, utilizing a refined version of a German World War II era V-2 rocket and a second-stage American WAC (Without Any Control)-Corporal rocket from Cape Canaveral. By the close of the decade American space vehicles, fired from the Cape, had taken the United States through the threshold of space. Just as Cape Canaveral was geographically situated to mark the way for the European exploration of the Americas, so the Kennedy Space Center is strategically situated

at the apex of NASA's programs for the exploration and development of space. Earth and Space sciences and aerospace technology, new ideas, and new products, are incubated in the intricately-meshed management teams of NASA Centers and Laboratories, and in the laboratories and offices of their contractors from industry and academia. Those ideas, the space flight vehicles and missions, the Earth and Space science laboratories, and their accompanying designs, innovations, and inventions are then "hatched" or tried and tested, as it were, under the management and direction of Kennedy Space Center. "Liftoff," at KSC is the most important and visible milestone in NASA space program development.

The history of Kennedy Space Center revisits the story of the inception of an American space program and the creation of NASA, and provides a new understanding of those remarkable events. It examines for the first time the unique relationship between KSC and the other NASA centers, and between KSC and other agencies engaged in space related activities, including the Department of Defense, the Army, the Air Force, and the Navy. This is the story, for the most part, of the men and women who managed the fantastically complicated send-offs of the launch vehicles and payloads designed and manufactured by American, and indeed, by the developing international aero-space, science, engineering, and space exploration community–and made them work.

It is the story of the Atlantic Missile Range and early experiments with long-range missiles, and of American successes and failures in early piloted flight. It is the history of Apollo and the lunar landings, now more than a quarter-century past. The narrative focuses heavily on the new, post-Apollo, Space Transportation System which, since the first flight of the Shuttle in April 1981, by the turn of the 21st Century had flown over 100 missions in space.

KSC too, is integral to the inception and development of the International Space Station, which promises to give not just Americans but the people of Earth a more permanent presence in space–that "extended environment of Earth"–well into the new millennium. KSC is NASA's lead center for the acquisition and management of Expendable Launch Vehicle launch services, so essential to the maintenance of a continuing off-world presence.

And because Kennedy Space Center has been so omnipresent in the total story of NASA and space exploration, it, perhaps more so than other NASA Centers has been in the focus of the national (and global) media and press. That has created unique management problems, situations, and opportunities at KSC. A "public" presence has affected its history more so than that of other NASA facilities. External and public relations, a stress on safety, and on accommodating and educating the media, NASA's "customers," and the general public, have been an integral part of KSC's history. As Cape Canaveral became a milepost, a way station in the European exploration of the New World five hundred years earlier, Cape Canaveral's Kennedy Space Center has become within the past half-century our stepping stone, a literal launch pad, a way station in the exploration of space. Liftoff is the most critical event in the history of space exploration.

Chapter Outline

Chapter I. Cape Canaveral
- A. The Cape and the Exploration of the New World
- B. The Army and the Atlantic Missile Range
- C. Kurt Debus
- D. NASA/Huntsville and the Launch Operations Directorate

Chapter II. The Launch Operations Center
- A. Space Program Development and Needs
- B. Organizing the Launch Operations Center
- C. Center Design: Engineering/Community/Environment/Labor
    - 1. Land Acquisition/National Wildlife Refuge

D. The Space Task Group: Projects Mercury and Gemini
1. Mercury: Alan Shepard/John Glen
1. Gemini: 4 and 7/6 missions

Chapter III. The Apollo Lunar Program
A. President John F. Kennedy
B. Engineering for Lunar Launches
C. New Construction/Expansion
D. Designing for Lunar Launch
1. Overview: KSC and Launch Complex 34, 37, and 39

Chapter IV. The Flight of Apollo
A. Apollo Missions to Apollo 17 (1972): Overview
B. KSC and Center Interface/interactions
C. AS 204/ Safety and the Human Factor
D. Focus: KSC and Apollo 8, 10, 11, 17

Chapter V. Post Apollo
A. Skylab
B. Apollo-Soyuz
C. Lee R. Scherer: Review/Redirection/KSC Plans and Programs
D. KSC And the Changing Dimensions of Space Exploration

Chapter VI. A Space Transportation System
A. The Case for a Reusable Space Vehicle
1. The ELV and the Shuttle
B. Shuttle Design and Development
C. Re-Engineering KSC's Launch facilities and operations
1. Richard G. Smith
D. Conversion: Launch Complex 39
1. VAB/Crawler/Mobile Launcher
1. Orbiter Processing Facility/Shuttle Landing Facility
2. Launch Processing System

Chapter VII. The Shuttle Takes Flight
A.STS-1 through STS-51L: Overview of STS History to 1990
1. Focus on: STS-1, STS-5, STS-41
B. Challenger (STS-51L)
C. In the Aftermath of Challenger
1. Forrest S. McCartney/KSC Reforms and Reorganization
2. The Safety Factor
D. A NASA Reappraisal/RIFs
1. The KSC/Canaveral Community

Chapter VIII. Living and Working in Space
A. Earth and Planetary Sciences and Investigations
1. Payloads and Payload Specialists
B. STS-26>35
C. Hubble/Remote Manipulation Arm/Spacelab Module
D. The Growing Public Presence at KSC

1. KSC/NASA/Public Education and the Media

Chapter IX. Countdown

A. KSC/STS in the Nineties [Overview of 50 flights]

B. A Changing Dynamics in Space

1. Capt. Robert L. Crippen, 1992-1995

2. Jay Honeycutt, 1995-1997

C. Earth and Planetary Science Missions

1. Focus on STS-41; STS-71

D. Mir Missions/ESA/Japan/Canada

Chapter X. KSC and The Internationalization of Space Exploration

A. Reflections on the Cold War

B. Global Communications Systems

C. MIR Missions

D. European Space Agency/ESA/Japan/Italy/Canada/China/The Americas

Chapter XI. The International Space Station

A. Conceptual Development

B. Political and Financial Evaluations

C. The Contractors'Payloads/Assembly

D. Mission Plans and Projections

Chapter XII. . The Role of the Expendable Launch Vehicle

A. A Brief History of ELV Since 1960

B. Reusable vs. Expendable

1. Cost considerations and evaluations

C. NASA Plans and Projects for the ELV

D. KSC: Lead Center for ELV Launch and Payload Processing

Chapter XIII. Into the 21st Century

A. Space Spinoffs/Technology/Inventions

1. KSC and Privatized/Commercial Space Initiatives

B. KSC and the Space Congresses

C. Roy Bridges/KSC Spaceport Master Plan

1. STS 20th Anniversary/Reflections

2. Space Experiment Research and Processing Laboratory

D. KSC: A Roadmap to Space Exploration

Oral History Program

Extensive interviews were conducted with the following people for the purpose of documenting their careers and experiences for posterity. This material will eventually be used for the full history text and for other projects.

- Bobby Bruckner: Manager of both payload processing and expendable launch vehicles.

- Terry Greenfield: KSC engineer since 1950s, present at Explorer 1 launch through present shuttle launches.
- Hugh Harris: Former Director of Public Affairs.
- Lisa Malone: First female voice of countdown at KSC.
- Forrest McCartney: KSC Center Director 1987-1991, responsible for the return to flight following Challenger accident.
- George Page: Test Director for Apollo 1 and Launch Director for STS-1.
- Alan Parrish: Arrived at KSC as an engineer in 1964, rose to Associate Director before retiring.
- Ike Rigell: KSC engineer since early 1960s, present for most major launches.
- Robert Sieck: Launch Director for the majority of STS missions, more than 70.
- Richard 'Dick' Smith: KSC Center Director 1979-1986, director during Challenger.
- Lee Solid: Former Vice-President and General Manager of Rockwell International's Florida operations.
- John Straiton: Oversaw development of International Space Station at KSC.
- Gene Thomas: Launch Director for Challenger, later the first Director of Safety.

Safety

The task of placing a human being into the vacuum of space is, by its very nature, a dangerous endeavor that demands extreme dedication to the question of safety. Even the simplest launch vehicle contains millions of parts and the failure of even one of these parts can have potentially catastrophic consequences. The cost of failure is measured not only dollars but also in the infinitely more valuable commodity of human life. Therefore the people who work on the United States' space program have developed a deep appreciation for the need to insure the utmost safety in every task.

Their constant vigilance has greatly reduced the number of accidents, making NASA one of the safest agencies in the United States government. Unfortunately, completely accident free operations remain an ongoing quest for NASA rather than an accomplished goal. Periodic accidents are a constant reminder of the danger inherent in space exploration and the ground

tasks necessary to support such an operation. This paper explores the development of safety policy and procedures at the Kennedy Space Center over the course of its forty-year history.

As the focal point of America's space program, the Kennedy Space Center has increased interest in insuring safety at the facility. The center is synonymous with NASA in the public mind and the national media focuses more coverage on KSC than any other NASA installation. Therefore accidents that occur at KSC attract more attention than similar incidences occurring at other NASA centers or private industry. The most remembered NASA failures, Apollo 1, Apollo 13, and Challenger, are irrevocably linked to KSC in the nation's collective memory.

Each of these accidents, and a number of lesser-known ones, has led directly to changes in policy, procedure, and even the bureaucratic structure at KSC. These changes have been designed to minimize the number and impact of accidents at KSC. While inherently reactive in nature, these accident-induced reviews are only part of the ongoing effort directed at making operations at KSC as safe as possible. Safety remains a prime consideration in all design work for both launch equipment and ground facilities. KSC requires all employees to undergo extensive safety training. Finally, in 1997 KSC Center Director Roy Bridges Jr. took the proactive step of committing the center's administration to the safety philosophy of the world's safest corporation, DuPont

Database & Web Page

Designed to complement the oral history program, both a database and web page are being developed by Dynex to in place by the end of the summer. The web page is based upon those at Ellis Island and will serve several purposes. First, it will allow KSC current employees and retirees, both NASA and contractor, to volunteer for the oral history project. They will enter

their pertinent biographical and contact information. Then they will be offered the opportunity to recount some of their favorite/most memorable moments at KSC. The Public Affairs Office will use selected accounts on the KSC web page to encourage more participation in the KSC history project.

Information collected via the web page or interviews will be entered into a database. The database will offer historians and other interested parties the ability to search oral history transcripts for pertinent information. It will also allow them to contact those individuals who have entered information on the web page but have yet to be interviewed. Searchable information include years worked, projects, positions, and contractor. Eventually this database may become a tremendous asset to historians working on a wide variety of topics at the center and throughout NASA.

Conclusion

As a total, this work lays the groundwork for a much larger project, a complete history of the forty years of launching space vehicles from the John F. Kennedy Space Center. From KSC, the first American orbited the Moon. From KSC, human beings first left our home and traveled to another celestial body. From KSC, more than one hundred flights of the Space Shuttle have lifted off. KSC exists as the focus of everything NASA does, yesterday, today, and for the foreseeable future. It is imperative that the history of this great place not be lost and thanks to the efforts of Center Director Roy Bridges, Director of External Relations JoAnn Morgan, and others there is now an ongoing project to preserve this past.

2001 NASA/ASEE SUMMER FACULTY FELLOWSHIP PROGRAM

JOHN F. KENNEDY SPACE CENTER
UNIVERSITY OF CENTRAL FLORIDA

OPERATION, MODELING AND ANALYSIS OF THE REVERSE WATER GAS SHIFT PROCESS

Dr. Jonathan E. Whitlow
Associate Professor
Department of Chemical Engineering
Florida Institute of Technology

NASA COLLEAGUE: Clyde Parrish

ABSTRACT

The Reverse Water Gas Shift process is a candidate technology for water and oxygen production on Mars under the In-Situ Propellant Production project. This report focuses on the operation and analysis of the Reverse Water Gas Shift (RWGS) process, which has been constructed at Kennedy Space Center. A summary of results from the initial operation of the RWGS process along with an analysis of these results is included in this report. In addition an evaluation of a material balance model developed from the work performed previously under the summer program is included along with recommendations for further experimental work.

1. INTRODUCTION

The human exploration of Mars will require the utilization of resources present in the Martian environment in order to minimize the payload mass imported from Earth. Reverse Water Gas Shift (RWGS), which reacts carbon dioxide and hydrogen to form water and carbon monoxide, when coupled with water electrolysis is a candidate technology for oxygen production on Mars. The use of the RWGS process for In-Situ Propellant Production, (ISPP) was originally studied by Pioneer Astronautics, who determined the RWGS process to be a viable candidate for oxygen production. [1-2]

An RWGS prototype system has been constructed and modified at Kennedy Space Center (KSC) over the past 18 months. While some experimental runs were made on the RWGS system at the end of the year 2000, it was not until July 2001 that successful operation of the process was made with no system leaks. Although the operating time has been limited, several conclusions on the RWGS operation have been made and problem areas identified as discussed in this report. An overview of the process components for RWGS is given below followed by a discussion of the results obtained from operation of the system. An evaluation of the validity of a material balance simulation model for the RWGS process developed under this research program in 1999[3] is then presented and followed by a recommendation for further experimental modifications and development.

2. AN OVERVIEW OF THE REVERSE WATER GAS SHIFT PROCESS

RWGS uses carbon dioxide and hydrogen as reactants to produce oxygen and carbon monoxide with a copper on alumina catalyst. Prior to operating the RWGS system the copper catalyst, which is produced from copper oxide reduction, must be conditioned to insure no oxygen is present in the system. Operating temperatures for processes on Mars are constrained and in general designs are not being considered which exceed 500 Celsius. At such temperatures, the RWGS reaction equilibrium is limited and does not favor the production of water. Thus in order to improve the overall conversion a separation step is required to allow the non reacted hydrogen and carbon dioxide to be recycled. This is achieved by passing the exit gases to a condenser to remove most of the water and then to a hollow fiber polymeric membrane, which preferentially permeates hydrogen and carbon dioxide. From the membrane, the reactants can be recycled while the byproduct carbon monoxide can be vented. The water produced is stored in a vessel and used as feed to an electrolysis unit, which produces oxygen as product and hydrogen, which can also be recycled to the reaction process. The RWGS process flow schematic with instrumentation labels is presented in Figure 1 below.

3. RWGS OPERATION AND RESULTS

The sensors and valves indicated in Figure 1 are referred to for this description of the RWGS operation The RWGS process is started up by energizing the heater HR2 and passing a small amount of hydrogen (typically 0.1 slpm), through the system from flow controller FC1 or FC2.

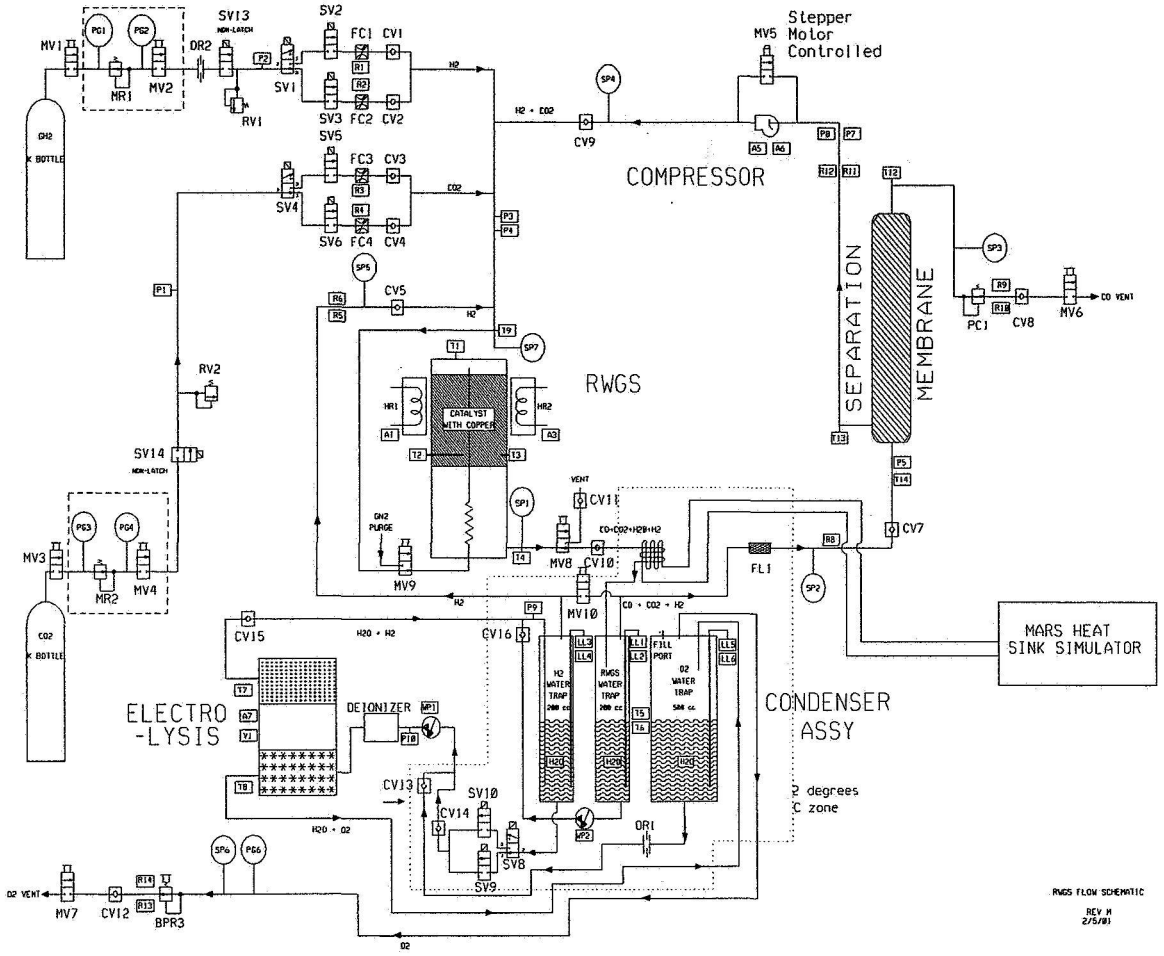

Figure 1 RWGS Process Flow Schematic

(Solenoid valves SV2 & SV3) The hydrogen exiting the system is monitored using R9 & R10 through the CO vent as the system pressure is regulated between 30 and 60 psia with pressure controller PC1. During the start up the recycle compressor is started and the pressure and flow are monitored through P8 and R12 respectively. (Measurements P7 and R11 are not working)

It takes approximately 1 ½ hours to heat and stabilize the reactor catalytic bed to 375-380 Centigrade based on temperature probe T2. A proportional only temperature controller is used to aid in achieving this temperature, however it uses T3 as the control variable, which typically operates about 35 to 40 degrees cooler that T2 as shown in Figure 2 below. This indirect method of controlling the reactor temperature hinders the operation and the time to reach a desired steady state due to the manual intervention required.

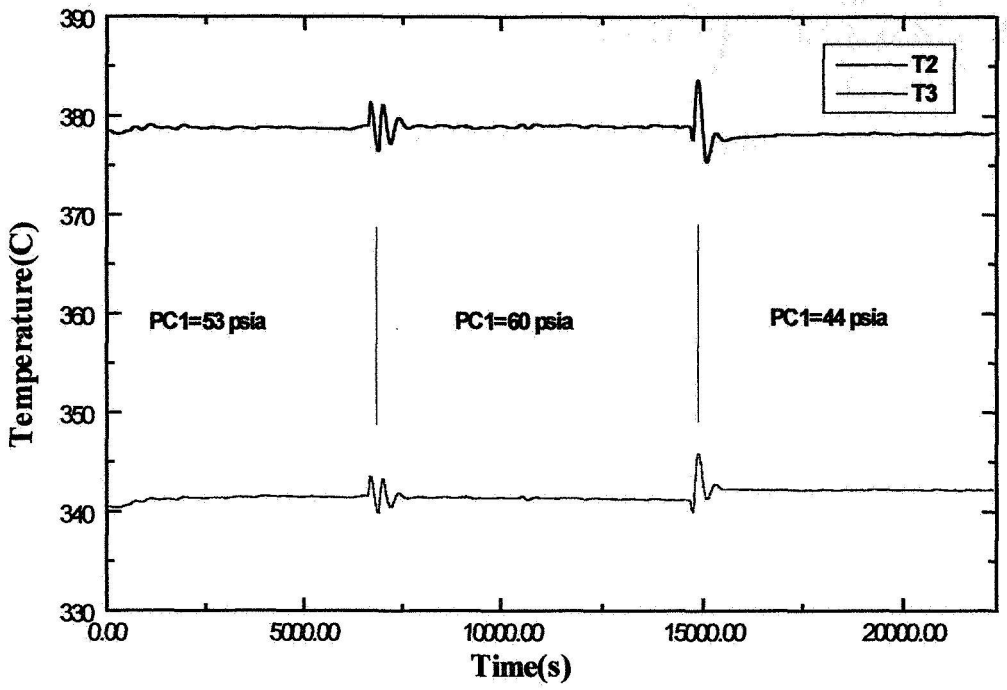

Figure 2 RWGS Reactor Temperatures during July 19th Operation

Once temperature T2 exceeds 300 Centigrade, the carbon dioxide flow can be introduced through flow controller FC3 or FC4. It was found that waiting until the reaction temperature is closer to the desired temperature reduces the start up time since less gas is being heated and the endothermic reaction is not started. At this point the water electrolysis can be started if desired assuming sufficient water of low conductivity is available in the system. The water is pumped to the electrolysis unit using WP1 after passing through an ion exchange bed to purify the water. This is a problem area as the exchange resin appears to become saturated after (~15 hours of operation) and requires new or regenerated resin.

Another problem with the use of electrolysis in conjunction with the RWGS process is related to the control of the system. The largest disturbance is introduced through the water level control system. When the electrolysis unit is running, the hydrogen water trap LL1 is continuously receiving a water input thus requiring periodic removal. The water is removed by opening solenoid valve SV10 whenever the level approaches full. When the valve opens the RWGS sees a sudden drop in pressure, which in turn disturbs the flows and temperatures in the system A similar disturbance occurs when the RWGS water receiver LL3 is drained after significant water production. Another potential problem with electrolysis is the difficulty in maintaining a constant source of hydrogen production, since the efficiency of the process is dependent on other process variables such as temperature, which are not automatically controlled.

The RWGS system was operated successfully on 7 different occasions each using a steady state

reactor temperature near 379 Celsius. The electrolysis unit was operated the first 3 occasions where recycled hydrogen and oxygen were produced. Due to the disturbances discussed above however, a sufficient steady state operation could not be achieved and the experimental runs were for the next 4 occasions focused on RWGS only with no electrolysis. The 4th run was successful in achieving steady state, however problems with the composition analysis limited the usefulness of the data. The best data was obtained during the runs of July 18, 19 and 27th.

Table 1 presents a summary of average operating conditions for the runs of July 18, 19 and 27th. It was found from the runs that the overall conversion based on hydrogen, increased with system pressure and consequently increased membrane pressure drop. The conversion also increased with lower feed rates to the system. It can also be observed from Table 1 that the ratio of product flow R9 to H_2 feed decreases as conversion increases since one mole should leave the system for every 2 moles of reacted feed assuming all of the water is removed at the condenser.

Steady state operation was closely approached for each of the runs outlined in Table 1 in terms of reactor temperature as previously shown in Figure 2 and product flow as shown by Figure 3. It can be observed from Figure 4 however, that longer operating times are needed before the recycle and membrane feed reach steady state at the higher system pressures.

Table 1 RWGS July 18, 19 & 27 Operating Summary

Experimental Run	Feed Flow	mem ΔP	P5 Port 2	P8 Port 4	Overall Conversion	R9/H2 Feed Ratio	T2	T3	T5
7/18/01 9:30-10:55	2.0	35.94	52.65	16.71	97.37	1.0146	379.06	342.11	5.67
7/18/01 1:15-3:45	2.0	36.71	52.60	15.90	98.66	1.0175	378.80	344.10	5.61
7/18/01 4:00-5:25	2.4	34.68	52.76	18.08	95.04	1.0828	379.82	342.81	5.62
7/19/01 1:15-12:00	2.6	39.42	59.69	20.27	79.46	1.1508	378.97	341.42	5.88
7/19/01 12:30-1:55	2.6	39.42	59.69	20.27	93.09	1.0570	378.97	341.42	5.88
7/19/01 2:15-4:20	2.6	27.11	44.08	16.97	94.62	1.2870	378.19	342.23	5.75
7/27/01 12:30-1:35	2.20	34.73	52.63	17.90	96.37	1.0559	378.77	344.15	5.46
7/27/01 3:20-5:05	2.20	42.06	59.40	17.34	99.34	1.0079	378.18	344.92	5.83

Table 2 provides a summary of mass balance results obtained from July 18th. A similar table was generated for the other 2 days however could not be included due to space restrictions. An overall mass balance error between 2 and 7 % was observed over the 3 days of operation. After compensating for this error by adding the difference to the flow into the membrane, a component mass balance was performed and the resulting error are also presented in the tables. The analysis was performed using a gas chromatograph with a thermal conductivity detector for the CO and CO_2 and a helium ionization detector for the H_2.

Table 2 July 18th RWGS Mass Balance Summary

Date	Port	Time	%H2	%CO2	%CO
7/18/01	3	9:30	2.48	2.97	94.55
7/18/01	3	9:50	2.70	2.83	94.47
7/18/01	2	10:10	70.85	22.67	6.49
7/18/01	2	10:25	70.08	23.17	6.75
7/18/01	4	10:40	71.91	24.50	3.58
7/18/01	7	10:55	69.83	26.71	3.47

Port 2 Flow	Port 3 Flow	Port 4 Flow	Port 7 Flow	Feed Flow		
30.608	1.022	30.541	32.541	2.000	slpm	0.96 MB Error (slpm)
1.2517	0.0418	1.2489	1.3307	0.0818	gmole/min	3.12 %Error
28.784	1.015	28.595	30.595	2.000	CO2 adjusted	0.83 Adjusted CO2 Error
1.1771	0.0415	1.1694	1.2511	0.0818	gmole/min	2.87 %Error

Comp. Bal.	H2	CO2	CO	
In 2	20.864	6.786	1.960	Overall Balance Error
Out 3	0.026	0.029	0.959	Added to port 2
Out 4	20.564	7.007	1.024	
Error	0.273	-0.250	-0.023	

Date	Port	Time	%H2	%CO2	%CO
7/18/01	3	1:15	1.16	1.44	97.41
7/18/01	3	1:40	1.90	1.22	96.88
7/18/01	3	2:00	0.89	1.25	97.86
7/18/01	2	2:10	63.79	28.16	8.05
7/18/01	2	2:20	63.47	28.61	7.92
7/18/01	4	2:35	66.26	29.41	4.33
7/18/01	4	2:45	65.67	29.82	4.51
7/18/01	7	3:00	64.46	31.45	4.10
7/18/01	7	3:10	63.84	31.95	4.21
7/18/01	7	3:20	63.59	32.18	4.23
7/18/01	3	3:35	1.34	1.44	97.22
7/18/01	3	3:45	1.20	1.42	97.38

Port 2 Flow	Port 3 Flow	Port 4 Flow	Port 7 Flow	Feed Flow		
27.723	1.018	27.612	29.612	2.000	slpm	0.91 MB Error (slpm)
1.1337	0.0416	1.1291	1.2109	0.0818	gmole/min	3.27 %Error
25.677	1.014	25.486	27.486	2.000	CO2 adjusted	0.82 Adjusted CO2 Error
1.0500	0.0415	1.0422	1.1240	0.0818	gmole/min	3.20 %Error

Comp. Bal.	H2	CO2	CO	
In 2	16.861	7.522	2.116	Overall Balance Error
Out 3	0.013	0.013	0.988	Added to port 2
Out 4	16.812	7.547	1.126	
Error	0.036	-0.038	0.002	

Date	Port	Time	%H2	%CO2	%CO
7/18/01	3	4:00	4.30	5.69	90.01
7/18/01	3	4:15	5.00	6.19	88.81
7/18/01	2	4:25	71.02	23.65	5.33
7/18/01	2	4:35	72.42	22.36	5.22
7/18/01	4	4:50	76.68	21.43	1.89
7/18/01	4	5:00	77.27	20.80	1.93
7/18/01	7	5:15	75.76	22.55	1.69
7/18/01	7	5:25	75.75	22.57	1.67

Port 2 Flow	Port 3 Flow	Port 4 Flow	Port 7 Flow	Feed Flow		
35.880	1.299	36.021	38.421	2.400	slpm	1.44 MB Error (slpm)
1.4672	0.0531	1.4730	1.5712	0.0981	gmole/min	4.02 %Error
33.734	1.279	34.043	36.443	2.400	CO2 adjusted	1.59 Adjusted CO2 Error
1.3795	0.0523	1.3922	1.4903	0.0981	gmole/min	4.71 %Error

Comp. Bal.	H2	CO2	CO	
In 2	25.333	8.126	1.864	Overall Balance Error
Out 3	0.059	0.076	1.144	Added to port 2
Out 4	26.205	7.189	0.650	
Error	-0.932	0.861	0.071	

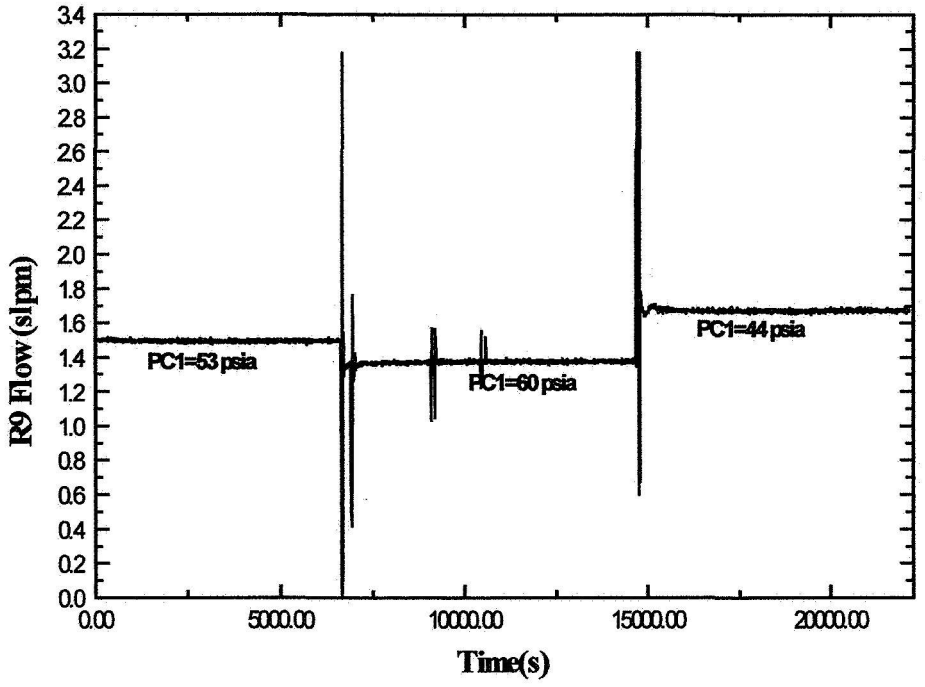

Figure 3 Product Flow R9 (CO Vent) for July 19th Operation

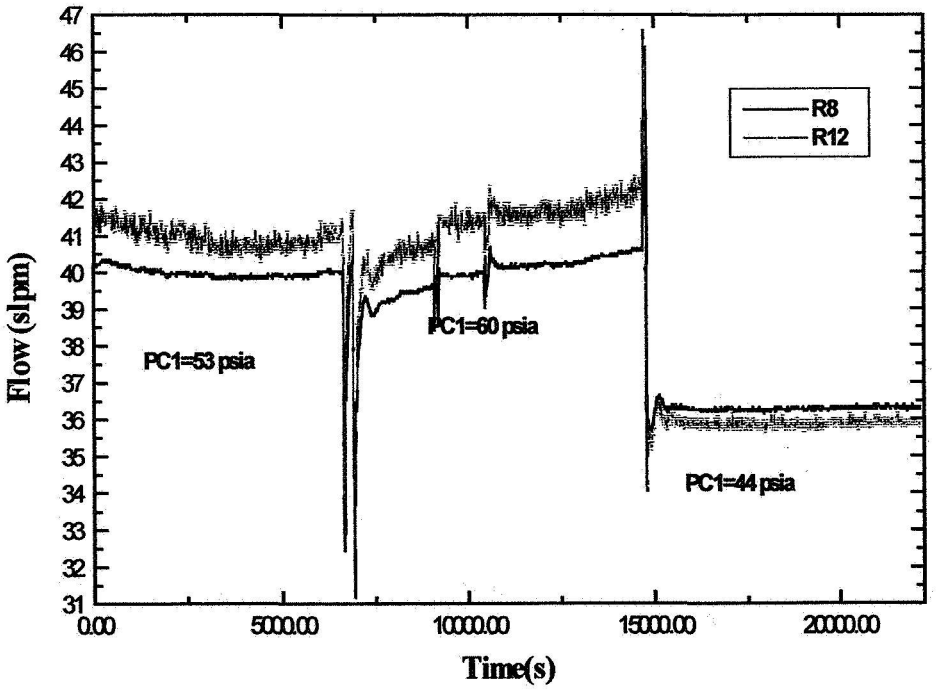

Figure 4 Recycle Flow R12 and Membrane Feed Flow R8 for July 19th Operation

4. RWGS Model Description

A brief description of the equations used to model the RWGS system is provided in this section. The RWGS material balance solution was implemented by programming in MATLAB code. A more detailed description of the modeling equations and associated theory can be found in the 1999 NASA/ASEE Summer Faculty Program Research Report [3]. The chemical equilibrium constant K for this reaction is given as a function of temperature by the expression: [4]
Fro products and reactants and in terms of conversion of a limiting reactant by the expression:

$$K = e^{13.148 \frac{5639.5}{T} 1.077 \ln T 5.44 \times 10^{4} T + 1.125 \times 10^{7} T^{2} + \frac{49170}{T^{2}}} \quad (1)$$

$$K = \frac{[CO]\,[H_2O]}{[CO_2]\,[H_2]} = \frac{(\Theta_{CO} + x_{eq})\,(\Theta_{H_2O} + x_{eq})}{(\Theta_{CO_2} - x_{eq})\,(1 - x_{eq})} \quad (2)$$

The values of Θ_{CO}, Θ_{H2O}, Θ_{CO2} represent the molar ratios of those components to the limiting reactant (assumed to be hydrogen) in the inlet stream to the reactor. The limiting reactant is based m thermodynamic considerations, the value of K can is related to the concentrations of the on the total feed to the reactor, (recycle stream + fresh feed) instead of the fresh feed to the reactor. If carbon dioxide were the limiting reactant, equation 2 would need to be modified to reflect this. Given a reaction temperature, the value of K can be determined from equation 1 and the equilibrium conversion determined by solving equation 2, which is a quadratic in x_{eq}. The equilibrium conversion is the maximum conversion, which can be achieved, in a single pass through the reactor.

The exit gases from the reactor are sent to a condenser where most of the water is removed. For modeling purposes, the compositions of the liquid and vapor streams leaving the condenser are determined by employing Raoult's Law to determine the amount of water in the vapor phase and Henry's Law to determine the solubility and hence concentration of the gasses dissolved in the condensed phase.

The gases leaving the condenser are fed into a hollow fiber polymeric membrane which separates the components of a gas mixture based on a given components permeability to the polymer. The membrane operates in a countercurrent fashion, and is modeled based on a 1998 publication, [4] which depicts the membrane as an N stage process as shown in Figure 5. Here, $L_{,k}$ and $x_{j,k}$ are the total molar flow and mole fraction of component j in the feed/reject leaving stage k, while $V_{,k}$ and $y_{j,k}$ are the total molar flow and mole fraction of j in the permeate leaving stage k. For each stage the mass transferred of a component j on a given stage $m_{j,k}$ is given by the permeability coefficient of that component times the difference in partial pressures in component j across the membrane. For N stages, a system of N nonlinear simultaneous equations is yielded for each component j requiring an iterative solution.

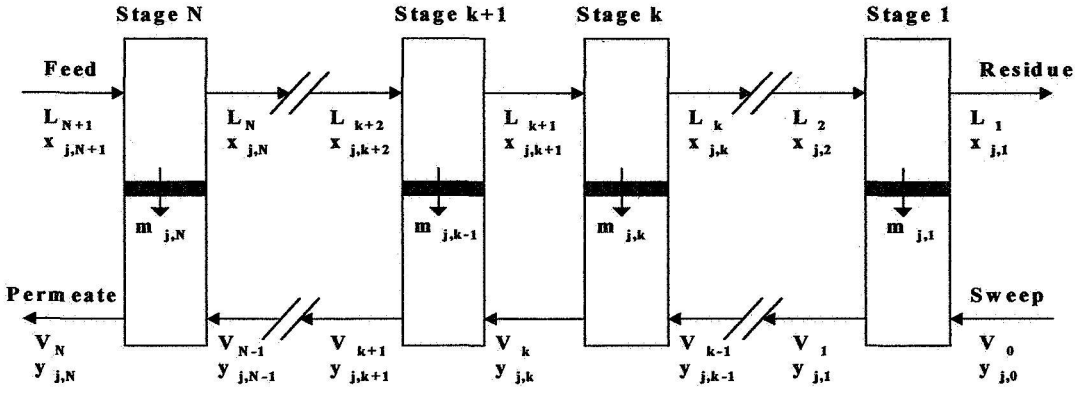

Figure 5 Flow Diagram for an N Stage Counter-Current Membrane

After the membrane equations have been solved, the permeate component molar flow rates are compared to those assumed initially in the recycle stream and adjusted using the Wegstein algorithm until overall convergence is achieved. Due to time constraints, only the model of the membrane was evaluated for validity. The errors in the component mass balances resulting from the operating data were corrected prior to input into the membrane model. This was done by adding or subtracting the required difference needed for mass balance closure to the component entering the membrane. The permeability coefficients in the membrane model for each component (excluding water) were refined based on a set of operating data on July 18th such that the prediction error was zero for the set. The table presented below, shows the model prediction for permeate and reject for all the operating runs of July 18, 19 and 27th. While it can be observed that the model predicts well especially in face of the errors in the mass balance, it could be further refined with additional data.

5. CONCLUSIONS

Successful operation of the RWGS system was achieved during July 2001 confirming RWGS as a potential technology for water production on Mars. Various operational and analysis problems have been identified to aid in further system development. The model developed in Matlab for the RWGS system was validated for the membrane and found to have good predictive capabilities. Further testing of the system is needed to better develop the understanding of the RWGS process including the examination of the influence of the reactor temperature and the hydrogen to carbon dioxide feed ratios.

6. ACKNOWLEDGMENTS

I would like to express my sincere gratitude to Bill Larson & Clyde Parrish for their effort, which has given me the opportunity to be involved in the development of knowledge to aid in the exploration of Mars. I would also like to thank Jan Surma and Curtis Ihlefeld for their technical assistance on this project.

Table 3 Comparison of Experimental Values and Model Predictions for July 18, 19 & 27

7/18/01 9:30-10:55	Calculated H2	Actual H2	Absolute Difference	Calculated CO2	Actual CO2	Absolute Difference	Calculated CO	Actual CO	Absolute Difference
Feed	20.591	20.864	0.273	7.036	6.786	0.25	1.983	1.96	0.023
Permeate	20.552	20.564	0.012	7.008	7.007	0.001	0.952	1.024	0.072
Reject	0.039	0.026	0.013	0.028	0.029	0.001	1.031	0.959	0.072
7/18/01 1:15-3:45									
Feed	16.825	16.861	0.036	7.56	7.522	0.038	2.114	2.116	0.002
Permeate	16.812	16.812	0	7.547	7.547	0	1.126	1.126	0
Reject	0.013	0.013	0	0.013	0.013	0	0.988	0.988	0
7/18/01 4:00-5:25									
Feed	26.265	25.333	0.932	7.265	8.126	0.861	1.793	1.864	0.071
Permeate	26.058	26.205	0.147	7.162	7.189	0.027	0.64	0.65	0.01
Reject	0.207	0.059	0.148	0.103	0.076	0.027	1.153	1.144	0.009
7/19/01 1:15-12:00									
Feed	30.748	30.555	0.193	7.984	8.07	0.086	1.537	1.644	0.107
Permeate	30.011	30.48	0.469	7.681	7.801	0.12	0.3831	0.541	0.1579
Reject	0.737	0.267	0.47	0.303	0.184	0.119	1.154	0.996	0.158
7/19/01 12:30-1:55									
Feed	29.552	29.428	0.124	8.605	8.696	0.091	2.028	2.047	0.019
Permeate	29.324	29.463	0.139	8.486	8.523	0.037	0.723	0.834	0.111
Reject	0.228	0.09	0.138	0.119	0.082	0.037	1.305	1.194	0.111
7/27/01 12:30-1:35									
Feed	25.603	25.099	0.504	7.035	7.332	0.297	1.986	1.779	0.207
Permeate	25.515	25.563	0.048	6.987	6.96	0.027	0.753	0.747	0.006
Reject	0.088	0.04	0.048	0.048	0.076	0.028	1.026	1.032	0.006
7/27/01 3:20-5:05									
Feed	16.507	17.248	0.741	8.921	8.323	0.598	2.47	2.327	0.143
Permeate	16.43	16.5	0.07	8.843	8.909	0.066	1.032	1.384	0.352
Reject	0.077	0.007	0.07	0.078	0.012	0.066	1.438	1.086	0.352

7. REFERENCES

[1] Zubrin R., Kito, T. and B. Frankie, "Report on the Construction of a Mars Methanol In-Situ Propellant Production Unit", NASA Contract NAS9-97082, Sept., 1997.

[2] Frankie, B. and R. Zubrin, "Mars Reverse Water Gas Shift Unit Design Manual", Delivered to Dynacs Engineering and The Embedded Technology Development Group, June 30, 1999.

[3] Whitlow, J.E., "Modeling and Analysis of the Reverse Water Gas Shift Process for In-Situ Propellant Production", NASA/ASEE Summer Faculty Program Research Report, NASA CR-1999-208586, 1999.

[4] Bissett, L. "Equilibrium Constants for Shift Reactions", Chemical Engineering, October 24, 1977.

[5] Coker, D.T. , Freeman, B.D. and G.K. Fleming, "Modeling Multicomponent Gas Separation Using Hollow-Fiber Membrane Contactors, AICHE Journal, V. 44 , N 6, June 1998.

REPORT DOCUMENTATION PAGE

Form Approved
OMB No. 0704-0188

1. AGENCY USE ONLY *(Leave blank)*	2. REPORT DATE	3. REPORT TYPE AND DATES COVERED
	October 2001	Contractor Report - Summer 2001

4. TITLE AND SUBTITLE

2001 Research Reports
NASA/ASEE Summer Faculty Fellowship Program

5. FUNDING NUMBERS

NASA Grant
NAG10-299

6. AUTHOR(S)

See attached list

7. PERFORMING ORGANIZATION NAME(S) AND ADDRESS(ES)

University of Central Florida
Orlando, Florida 32816-2450
John F. Kennedy Space Center
Kennedy Space Center, Florida 32899

8. PERFORMING ORGANIZATION REPORT NUMBER

NASA CR-2001-210265

9. SPONSORING / MONITORING AGENCY NAME(S) AND ADDRESS(ES)

National Aeronautics and Space Administration
Washington, D.C. 20546

10. SPONSORING / MONITORING AGENCY REPORT NUMBER

11. SUPPLEMENTARY NOTES

12a. DISTRIBUTION / AVAILABILITY STATEMENT

Unclassified - Unlimited
Subject Category 99

12b. DISTRIBUTION CODE

13. ABSTRACT *(Maximum 200 words)*

This document is a collection of technical reports on research conducted by the participants in the 2001 NASA/ASEE Summer Faculty Fellowship Program at the Kennedy Space Center (KSC). This was the 17th year that a NASA/ASEE program has been conducted at KSC. The 2001 program was administered by the University of Central Florida (UCF) in cooperation with KSC. The program was operated under the auspices of the American Society for Engineering Education (ASEE) with sponsorship and funding from the Education Division, NASA Headquarters, Washington, D.C., and KSC. The KSC Program was one of nine such Aeronautics and Space Research Programs funded by NASA in 2001. The KSC Faculty Fellows spent ten weeks working with NASA scientists and engineers on research of mutual interest to the university faculty member and the NASA colleague. The editors of this document were responsible for selecting appropriately qualified faculty to address some of the many research areas of current interest to NASA/KSC. The NASA/ASEE program is intended to be a two-year program to allow in-depth research by the university faculty member.

14. SUBJECT TERMS	15. NUMBER OF PAGES
Research and Technology	205
	16. PRICE CODE

17. SECURITY CLASSIFICATION OF REPORT	18. SECURITY CLASSIFICATION OF THIS PAGE	19. SECURITY CLASSIFICATION OF ABSTRACT	20. LIMITATION OF ABSTRACT
Unclassified	Unclassified	Unclassified	UL